IL
NUOVO CIMENTO
ORGANO DELLA SOCIETÀ ITALIANA DI FISICA
SOTTO GLI AUSPICI DEL CONSIGLIO NAZIONALE DELLE RICERCHE

VOL. XVIII, N. 6 *Serie decima* 16 Dicembre 1960

Equilibrium Thermodynamic Properties of a Vacancy in a F.C.C. Lattice with Central Interaction (*).

G. F. NARDELLI

Centro Studi Nucleari, Gruppo di Fisica dello Stato Solido - Ispra

A. REPANAI CHIAROTTI

Istituto di Fisica dell'Università - Milano
Istituto Nazionale di Fisica Nucleare - Sezione di Milano

(ricevuto il 20 Aprile 1960)

Summary. — The influence of a vacant lattice site on the thermodynamic equilibrium properties of crystals is investigated at various temperatures ranging from zero to the melting point. The change of vibrational properties are evaluated by means of an Einstein model. The study of the elastic relaxation is extended to a vibrating lattice, and the vibrational free energy is evaluated taking into account the displacement field. The « image forces » due to the vacancy are discussed including the cubic tensors in the expression of the potential energy. Numerical results are reported for crystals of inert gases.

1. – Introduction.

In recent years, the study of the equilibrium properties of localized defects has been essentially developed along two directions: some authors (1) study

(*) Research supported in part by the Comitato per la Fisica del Consiglio Nazionale delle Ricerche.

(1) H. B. HUNTINGTON: *Acta Metall.*, **2**, 554 (1954); H. KANZAKI: *Journ. Phys. Chem. Solids*, **2**, 24 (1957); L. TEWORDT: *Phys. Rev.*, **109**, 61 (1958).

the elastic displacement around a point defect and calculate the so-called « relaxation energy » and the volume change, assuming a static lattice; at the same time, the study of the effects of defects on the vibrational properties of crystals in the unrelaxed lattice has been developed using several methods based on the « force constant model » (2). The effect of the elastic relaxation on the vibrational entropy was studied by HUNTINGTON, SHIRN and WAJDA (3) using the approximation of a continuous elastic medium.

This paper extends the study of the elastic displacement to a vibrating lattice, and presents an evaluation of the vibrational free energy, taking into account the displacement field. The method is applied to a vacant lattice point in a f.c.c. lattice. The method given by KANZAKI (1) for evaluating the displacement field, entirely based on the discrete nature of the lattice, is shown to be valid also for a vibrating lattice, provided we take into account the vibrational field in discussing the boundary conditions. The changes in the force constants, and the external forces, equivalent to the introduction of the defect, are evaluated assuming a two-body central interaction. This interaction is encountered for example in crystals of inert gases. The detailed calculations will later be applied to a vacancy in solid argon.

In a subsequent paper we shall further extend this method to evaluate the activation free energy for the migration of vacancies (4). By comparing the theoretical values with the experimental data in crystals of inert gases, one might obtain some indication of the validity of the « rate processes » model for crystal diffusion.

2. – Method of calculation.

In the following we shall consider a « cyclic cell » of an infinite lattice, having a volume V_0 equal to the entire volume of the actual crystal, and containing $(N-1)$ atoms plus a vacant lattice site far from the boundary walls.

By introducing « periodic boundary conditions », we may study the microscopic states of the system, without consider explicitly surface effects.

Referring to a co-ordinate system originating at the vacant lattice point, let $\boldsymbol{R}_l$ be an arbitrary position vector of the nuclei, $\boldsymbol{R}_l^{(0)}$ the position vector

(2) I. M. LIFSHITZ: *Suppl. Nuovo Cimento*, **3**, 716 (1956); G. W. MONTROLL and R. B. POTTS: *Phys. Rev.*, **100**, 525 (1955); J. MAHANTY, A. A. MARADUDIN and G. H. WEISS: *Progr. Theor. Phys.*, **20**, 369 (1958).

(3) H. B. HUNTINGTON, G. A. SHIRN and E. S. WAJDA: *Phys. Rev.*, **99**, 1085 (1955).

(4) Preliminary results have been communicated at the Conference of the Italian Physical Society, Palermo, 1958 (R. FIESCHI, G. NARDELLI and A. REPANAI: *Suppl. Nuovo Cimento*, **3**, 463 (1959)).

of the l-th lattice points for the perfect crystal, and $\boldsymbol{u}_l = \boldsymbol{R}_l - \boldsymbol{R}_l^{(0)}$ the displacement from the lattice points. The potential energy for the system including $(N-1)$ atoms and a vacancy at the origin site may be written

$$\Phi = \tfrac{1}{2} \sum_{l}^{(N)} \sum_{l'}{}' \varphi(|\boldsymbol{R}_{l'} - \boldsymbol{R}_l|) - \sum_{l \neq 0} \varphi(|\boldsymbol{R}_l|) \tag{1}$$

if one supposes to add and remove the interaction energy of an extra-atom at the origin site.

The potential energy (1) may be expanded in powers of the displacements from the perfect lattice positions $\boldsymbol{R}_l^{(0)}$, in the following manner:

$$\begin{aligned} \Phi = {} & \tfrac{1}{2} \sum_{l}^{(N)} \sum_{l'}{}' \varphi(|\boldsymbol{R}_{l'}^{(0)} - \boldsymbol{R}_l^{(0)}|) - \sum_{l \neq 0} \varphi(|\boldsymbol{R}_l^{(0)}|) + \\ & + \tfrac{1}{2} \sum_{l \neq 0}^{(N)} \sum_{l' \neq 0} \boldsymbol{A}(ll') : \boldsymbol{u}_l \boldsymbol{u}_{l'} + \frac{1}{6} \sum_{l \neq 0}^{(N)} \sum_{l', l'' \neq 0} \boldsymbol{B}(ll'l'') \vdots \boldsymbol{u}_l \boldsymbol{u}_{l'} \boldsymbol{u}_{l''} + \dots \\ & \dots + \sum_{l \neq 0} \boldsymbol{f}_l \cdot \boldsymbol{u}_l - \tfrac{1}{2} \sum_{l \neq 0} \nabla_l^{(2)} \varphi(l) : \boldsymbol{u}_l \boldsymbol{u}_l - \frac{1}{6} \sum_{l \neq 0} \nabla_l^{(3)} \varphi(l) \vdots \boldsymbol{u}_l \boldsymbol{u}_l \boldsymbol{u}_l - \dots , \end{aligned} \tag{2}$$

where $\boldsymbol{A}(ll')$ are the coupling tensors (second order tensors in xyz co-ordinates) between the nuclei in the perfect crystal, $\boldsymbol{B}(ll'l'')$ are the anharmonic cubic tensors of the expansion for the perfect crystal, and we have by definition

$$\begin{aligned} \boldsymbol{f}_l & \equiv - \nabla_l \varphi(l) = - [\nabla \varphi(|\boldsymbol{R}|)]_{\boldsymbol{R} = \boldsymbol{R}_l^{(0)}} , \\ \nabla^{(2)} \varphi(l) & \equiv [\nabla \nabla \varphi(|\boldsymbol{R}|)]_{\boldsymbol{R} = \boldsymbol{R}_l^{(0)}} , \quad \text{etc.} \end{aligned}$$

The linear terms in the expansion (2) are due to the presence of the imperfection: their coefficients $\boldsymbol{f}_l$ may be regarded as external forces applied to the lattice points around the defect.

Under conditions of thermodynamic equilibrium each nucleus oscillates through a new equilibrium position $\tilde{\boldsymbol{R}}_l^{(0)} = \boldsymbol{R}_l^{(0)} + \boldsymbol{\xi}_l$, where $\boldsymbol{\xi}_l$ is the elastic displacement caused by the imperfection. The potential energy Φ may be expanded in powers of the displacements $\boldsymbol{u}_l'$ from the new equilibrium positions: this expansion may be deduced from (2), setting $\boldsymbol{u}_l = \boldsymbol{u}_l' + \boldsymbol{\xi}_l$:

$$\begin{aligned} \Phi = {} & - \frac{N}{2} \sum_{l}^{(N)} \sum_{l'}{}' \varphi(|\boldsymbol{R}_{l'}^{(0)} - \boldsymbol{R}_l^{(0)}|) - \sum_{l \neq 0} \varphi(|\boldsymbol{R}_l^{(0)}|) + \frac{1}{2} \sum_{l \neq 0}^{(N)} \sum_{l' \neq 0} \boldsymbol{A}(ll') : \boldsymbol{\xi}_l \boldsymbol{\xi}_l + \dots \\ & \dots + \sum_{l \neq 0} \boldsymbol{f}_l \cdot \boldsymbol{\xi}_l - \frac{1}{2} \sum_{l \neq 0} \boldsymbol{\xi}_l \boldsymbol{\xi}_l : \nabla_l^{(2)} \varphi(l) - \dots + \sum_{l \neq 0}^{(N)} \Big\{ \sum_{l' \neq 0} \boldsymbol{A}(ll') \cdot \boldsymbol{\xi}_{l'} + \boldsymbol{f}_l - \boldsymbol{\xi}_l \cdot \nabla_l^{(2)} \varphi(l) + \dots \Big\} \boldsymbol{u}_{l'}' + \\ & + \frac{1}{2} \sum_{l \neq 0}^{(N)} \sum_{l' \neq 0} \Big\{ \boldsymbol{A}(ll') - \delta_{ll'} \nabla_l^{(2)} \varphi(l) + \sum_{l'' \neq 0} \boldsymbol{B}(ll'l'') \cdot \boldsymbol{\xi}_{l''} - \sum_{l'' \neq 0} \delta_{ll'} \delta_{ll''} \nabla_l^{(3)} \varphi(l) \cdot \boldsymbol{\xi}_{l''} + \dots \Big\} : \boldsymbol{u}_l' \boldsymbol{u}_{l'}' + \\ & + \frac{1}{6} \sum_{l \neq 0}^{(N)} \sum_{l \neq 0} \sum_{l' \neq 0} \Big\{ \boldsymbol{B}(ll'l'') - \delta_{ll'} \delta_{ll''} \nabla_l^{(3)} \varphi(l) + \dots \Big\} \vdots \boldsymbol{u}_l' \boldsymbol{u}_{l'}' \boldsymbol{u}_{l''}' + \dots . \end{aligned}$$

The condition of equilibrium in the relaxed crystal is obtained when all the $(N-1)$ coefficients of the linear terms are equal to zero in the above expansion; from these $(N-1)$ vectorial equations with $(N-1)$ unknown vectors, $\boldsymbol{\xi}_l$, one deduces the displacement field in the imperfect cyclic cell. Knowing the displacement field one may calculate any coefficient of the expansion (3); in particular we are interested in the elastic energy due to the deformation as well as in the dynamical matrix elements of an imperfect cyclic cell.

2·1. *Displacement field inside the cyclic cell.* – If the elastic displacement is so small that we can neglect the powers beyond the first order, the conditions of equilibrium inside the cyclic cell are:

$$\{\sum_{l'} [\boldsymbol{A}(ll') - \delta_{ll'}\nabla_l^{(2)}\varphi(l)]\cdot\boldsymbol{\xi}_{l'} + \boldsymbol{f}_l = 0\} \qquad (l = 0, 1, ..., N) \tag{4}$$

with the additional condition $\boldsymbol{\xi}_{l=0} = 0$.

By solving the system (4) we shall be able to find a solution for the displacement field in the unit cyclic cell for any lattice constant.

In a more compact form (4) is written:

$$[\boldsymbol{A} + \delta\boldsymbol{A}]\cdot[\boldsymbol{\xi}] = -[\boldsymbol{f}]\,, \tag{5}$$

where $[\delta\boldsymbol{A}]$ is the perturbation matrix, whose elements are

$$\delta\boldsymbol{A}(ll') = -\sum_{j\neq 0}^{(J)} \delta_{lj}\delta_{l'j}\nabla_j^{(2)}\varphi(j)\ ;$$

by $\sum_{j\neq 0}^{(J)}$ we mean the summation over a suitable set (J) of lattice points around the defect (the extension of this set will be discussed later); $[\boldsymbol{\xi}]$ and $[\boldsymbol{f}]$ are one-column matrices, $\delta_{lj}\delta_{l'j}$ are the Kronecker symbols.

The exact solution of (5) is:

$$[\boldsymbol{\xi}] = -[I + \boldsymbol{A}^{-1}\cdot\delta\boldsymbol{A}]^{-1}\cdot[\boldsymbol{A}]^{-1}\cdot[\boldsymbol{f}]\,.$$

The matrix $[I+\boldsymbol{A}^{-1}\cdot\delta\boldsymbol{A}]^{-1}$ may be expanded in terms of Taylor series. If this expansion is convergent, the displacement field is given by

$$[\boldsymbol{\xi}] = -\sum_{n=0}^{(\infty)} (-1)^n[\boldsymbol{A}^{-1}\cdot\delta\boldsymbol{A}]^{(n)}\cdot[\boldsymbol{A}]^{-1}\cdot[\boldsymbol{f}] = -\{[I]-[\boldsymbol{A}]^{-1}\cdot[\delta\boldsymbol{A}]+...\}\cdot[\boldsymbol{A}]^{-1}[\boldsymbol{f}]. \tag{6}$$

For the numerical evaluation of this series, the elements of the inverse matrix

$$\boldsymbol{A}^{-1}(l,l') \equiv \frac{\Omega}{(2\pi)^3}\int_{(B.Z)}[\boldsymbol{V}(\boldsymbol{k})]^{-1}\exp\left[-i\boldsymbol{k}\cdot(\boldsymbol{R}_l^{(0)}-\boldsymbol{R}_{l'}^{(0)})\right]\mathrm{d}^{(3)}\boldsymbol{k}\,,$$

must be known: $[\boldsymbol{V}(\boldsymbol{k})]$ is a 3×3 matrix, whose elements are the « coupling coefficients » $V_{\alpha\beta}(\boldsymbol{k})$ between the elastic waves having wave vector $\boldsymbol{k}$; Ω is the atomic volume, and the integration is over the first Brillouin zone ([5,2]).

KANZAKI ([1]) used the elastic equations (4) to find the displacement field in a static lattice. By solving them with a successive approximation method he found an expression for the displacement field equal to the series (6); his « second approximation » is equivalent to ignoring the terms beyond the second order in this expansion. KANZAKI calculated the elements of the product of the inverse matrix $[\boldsymbol{A}]^{-1}$ times the force vector $[\boldsymbol{f}]$ for a monoatomic f.c.c. lattice; $[\boldsymbol{A}]^{-1}$ was evaluated assuming a purely central interaction with twelve first nearest neighbours and a Hooke's force constant of central type. This seems to be a satisfactory approximation for the van der Waals crystals. Kanzaki's numerical results for the relaxation field are dimensionless; since the elastic field equations (4) for a vibrating cyclic cell are found to be the same as for a static one, we shall use Kanzaki's numerical results for calculating the displacement field at any temperature, taking the correspondent lattice constants $a(T)$ for the perfect crystal.

The influence of nuclear vibrations will be considered in discussing boundary conditions.

2·2. *Relaxation energy for a cyclic cell.* – For a cyclic cell the relaxation energy ΔU_{elast} due to the displacement field ξ is given by

$$\Delta U_{\text{elast}} = \tfrac{1}{2}[\xi]^{\dagger}\cdot[\boldsymbol{A}+\delta\boldsymbol{A}]\cdot[\xi] + [\xi]^{\dagger}\cdot[\boldsymbol{f}]\ (*)\,.$$

Using the elastic field equation (4) and the expression (6) for the displacement field, we have

$$\Delta U_{\text{elast}} = +\tfrac{1}{2}[\xi]^{\dagger}\cdot[\boldsymbol{f}] = -\tfrac{1}{2}[\boldsymbol{f}-\boldsymbol{A}^{-1}\cdot\delta\boldsymbol{A}\cdot\boldsymbol{f}+\ldots]^{\dagger}\cdot[\boldsymbol{A}]^{-1}\cdot[\boldsymbol{f}] =$$
$$= -\tfrac{1}{2}\{[\boldsymbol{f}]^{\dagger}\cdot[\boldsymbol{A}]^{-1}\cdot[\boldsymbol{f}]-[\boldsymbol{f}]^{\dagger}\cdot[\boldsymbol{A}]^{-1}\cdot[\delta\boldsymbol{A}]\cdot[\boldsymbol{A}]^{-1}\cdot[\boldsymbol{f}]+\ldots\}.$$

The terms in the expansion correspond to the different orders of approximation in the displacement field.

([5]) M. BORN and K. HUANG: *Dynamical Theory of Crystal Lattices* (Oxford, 1954).
(*) By $[\ldots]^{\dagger}$ we mean the adjoint to $[\ldots]$.

2·3. *Vibrational Helmholtz free energy of an imperfect cyclic cell.* – Here we consider the vibrational problem of the imperfect cyclic cell in the harmonic approximation. Neglecting the powers of ξ_l higher than the first, the effective potential for the harmonic motion of $(N-1)$ nuclei in the cyclic cell containing a vacancy at the origin, can be expressed as follows:

$$\Psi_v = \tfrac{1}{2} \sum_{l \neq 0}^{(N)} \sum_{l' \neq 0} \{ \boldsymbol{A}(ll') + \delta \boldsymbol{A}(ll') + \sum_{l'' \neq 0} (\boldsymbol{B}(ll'l'') + \delta \boldsymbol{B}(ll'l'')) \cdot \xi_{l''} \} : \boldsymbol{u}_l \boldsymbol{u}_{l'} ,$$

where $\delta \boldsymbol{A}(ll')$ and $\delta \boldsymbol{B}(ll'l'')$ are the perturbation tensors arising from the failure of the interatomic bond around the defect.

The problem of determining the frequencies of the normal modes of an imperfect lattice, requires a sufficiently simple model of a crystal lattice, so that the elements of the inverse matrix $[A - Mz^2 I]^{-1}$ can be readily obtained. Unfortunately, the calculation of the inverse matrix is very difficult, because of the coupling between the x, y, z components of the nuclear displacements. As a possible approximation, in finding the vibrational free energy change due to the defect, we employ an Einstein model. The reliability of this model will be discussed in the last section.

According to the Einstein model, and provided the new Einstein frequencies are sufficiently close to the older one, the change of vibrational free energy of the imperfect cyclic cell is given by

$$\Delta F_v = \sum_{n=1}^{\infty} \frac{1}{n!} \psi^{(n)}(\omega_E^2) \, \mathrm{Sp} \, [\boldsymbol{\Lambda}]^n = \sum_{n=1}^{\infty} (\Delta F_v)_n , \tag{7}$$

where

$$\psi(z) = \beta^{-1} \ln [1 - \exp [-\beta \hbar \sqrt{z}]] + \tfrac{1}{2} \hbar \sqrt{z} ,$$

$$\beta \equiv (kT)^{-1} ,$$

and

$$[\boldsymbol{\Lambda}] = \frac{1}{M} \{ [\delta \boldsymbol{A}] + [[\boldsymbol{\xi}]^{\dagger} \cdot [\boldsymbol{B} + \delta \boldsymbol{B}]]_E \} = [\boldsymbol{\Lambda}_0] + [\boldsymbol{\Lambda}_1] . \tag{7-bis}$$

By $\psi^{(n)}(\omega_E^2)$ we mean the n th derivative of $\psi(z)$ evualuted at $z \equiv \omega_E^2$; ω_E is the Einstein frequency for the perfect lattice, M is the atomic mass. $[\ldots]_E$ means the « Einstein part » of $[\ldots]$, and Sp $[\ldots]$ is the diagonal sum of the matrix in square brackets.

i) First order contribution. To the first order in the perturbation, the vibrational free energy is given by

$$(\Delta F_v)_1 = \psi'(\omega_E^2) \, \mathrm{Sp} \, [\boldsymbol{\Lambda}] = \psi'(\omega_E^2) \sum_l \sum_{\alpha=1}^{3} \Lambda_{\alpha\alpha}(ll) .$$

The perturbation matrix $[\mathbf{\Lambda}]$ is defined by (7-*bis*); it is the sum of two terms, the first arising from the failure of the interatomic bonds around the defect while the second comes from the elastic relaxation field via the cubic tensors in the potential energy expression.

At the equilibrium relaxed configuration, the first order contribution to the vibrational free energy change of a cyclic cell is given by

$$(8) \qquad (\Delta F_v)_1 = \psi'(\omega_E^2)\ \mathrm{Sp}\,[\mathbf{\Lambda}_0] + \psi'(\omega_E^2)\ \mathrm{Sp}\,[\mathbf{\Lambda}_1] = (\Delta F_v)_1^{(\mathrm{unrelax})} + (\Delta F_v)_1^{(\mathrm{elast})} .$$

If the interatomic forces are of short range type, the first matrix $[\mathbf{\Lambda}_0]$ vanishes rapidly as we consider lattice points far from the defect. $[\mathbf{\Lambda}_0]$ is then substancially different from zero over a small set J of lattice points around the defect; we call j the members of this set (see Section 2·1). Remembering the expression for the tensors $\boldsymbol{A}(0)/M \equiv \boldsymbol{A}(ll)/M$ (Einstein part of the dynamical matrix for a cubic lattice) we can write for a vacancy

$$\mathrm{Sp}\,[\mathbf{\Lambda}_0] = \frac{1}{M} \sum_{l \neq 0}^{(N)} \sum_{\alpha=1}^{3} \delta A_{\alpha\alpha}(ll) = \frac{1}{M} \sum_{j \neq 0}^{(J)} \sum_{\alpha=1}^{3} \delta A_{\alpha\alpha}(jj) = -3 \cdot \omega_E^2 .$$

For an unrelaxed cyclic cell, the first order contribution to the change of the vibrational free energy is then given by

$$(8a) \qquad (\Delta F_v)_1^{(\mathrm{unrelax})} = -3\psi'(\omega_E^2) \cdot \omega_E^2 = -\frac{3}{2} \hbar\omega_E \left\{ \frac{1}{2} + (\exp[\beta\hbar\omega] - 1)^{-1} \right\} .$$

The elastic correction for the change of the vibrational free energy comes from the second term in the perturbation.

By help of simmetry considerations, and remembering the cyclic boundary conditions on the elastic displacements we have

$$\sum_{l=0}^{(N)} \boldsymbol{B}(ll, l+j) \cdot \boldsymbol{\xi}_{l+j} = 0 \ ;$$

hence

$$\mathrm{Sp}\,[\mathbf{\Lambda}_1] = \frac{1}{M} \sum_{l \neq 0}^{(N)} \sum_{\alpha=1}^{3} \Big\{ \sum_{l' \neq 0} [\boldsymbol{B}(ll) + \delta\boldsymbol{B}(ll')] \cdot \boldsymbol{\xi}_{l'} \Big\}_{\alpha\alpha} =$$

$$= -\frac{1}{M} \sum_{j \neq 0}^{(J)} \sum_{\alpha=1}^{3} [\boldsymbol{B}(0, j) \cdot \boldsymbol{\xi}_j]_{\alpha\alpha} + \frac{1}{M} \sum_{j \neq 0}^{(J)} \sum_{\alpha=1}^{3} \Big\{ \sum_{j' \neq 0}^{(J)} \delta\boldsymbol{B}(jjj') \cdot \boldsymbol{\xi}_{j'} \Big\}_{\alpha\alpha} ,$$

where $\boldsymbol{B}(0, j) \equiv \boldsymbol{B}(ll, l+j)$, and the summations in the last expression are limited to the reduced set J.

If the interaction energy is a two-body potential of central type, the perturbation of the cubic tensors is

$$\delta \boldsymbol{B}(j' - j) \equiv \delta \boldsymbol{B}(jjj') = - \delta_{jj'} \boldsymbol{B}(0, j) , \qquad (j \neq 0) . \tag{9}$$

The elastic contribution to the vibrational free energy change of a cyclic cell is then found to be

$$(\Delta F_v)_{\mathrm{I}}^{(\mathrm{elast.})} = 2 \frac{\psi'(\omega_E^2)}{M} \sum_{j \neq 0}^{(J)} \sum_{\alpha=1}^{3} \{\delta \boldsymbol{B}(j) \cdot \boldsymbol{\xi}_j\}_{\alpha\alpha} . \tag{8b}$$

ii) Second order contribution. The second order contribution comes from the second term in the Taylor expansion (7):

$$(\Delta F_v)_{\mathrm{II}} = \frac{1}{2} \psi''(\omega_E^2) \, \mathrm{Sp} \, [\boldsymbol{\Lambda}]^2 .$$

Neglecting terms containing second powers of the displacements, the square of the perturbation tensor is given by (*)

$$[\boldsymbol{\Lambda}]^2 \simeq \frac{1}{M^2} \{[\delta \boldsymbol{A}]^2 + 2 [\delta \boldsymbol{A}] \cdot ([\boldsymbol{B} + \delta \boldsymbol{B}] \cdot [\boldsymbol{\xi}]_E)\} , \tag{10}$$

where the second term yields the elastic contribution to the second order vibrational free energy of the imperfect cyclic cell.

3. – Influence of boundary conditions.

In the preceding sections we studied the properties of a defect using a cyclic cell and imposing the periodicity conditions on the boundary. The use of the periodicity conditions is equivalent to studying the properties of an imperfect unit cell of an infinite cyclic lattice, where the unit cells have the same original size as the actual crystal (**). The extensive properties of a defect are then evaluated including the « interaction terms » between the defect we are studying and the defects belonging to the nearest cyclic cells.

Let us consider the actual crystal with a free surface; when we create a defect in the interior of the crystal kept at constant volume, the extensive

(*) The commutator gives not contribution to the Spur of a product of two matrices.

(**) Owing to the periodicity boundary conditions, the volume of a cyclic cell does not change because of any distortion which satisfies the cyclic condition.

properties suffer a change which differs from those in a cyclic cell of the infinite lattice only for the corresponding interaction term.

Moreover, considering that the free surface conditions are satisfied when there is no stress component normal to the surface, the elastic distortion in the actual imperfect crystal will be slightly different if the normal stresses across the boundary wall between cyclic cells are not zero. If a law of superposition for the elastic displacements is valid, the distortion in the real crystal can be obtained superimposing *a*) the displacements due to a defect obtained by using the cyclic lattice condition, and *b*) the displacements in the perfect crystal due to a distribution of forces normal to the surface, opposite to those acting across the boundary wall from the neighbouring cells.

KANZAKI discussed the effects of the cyclic conditions in the static approximation. In this approximation, the thermodynamic potential of the system is the elastic energy, for which the interaction term vanishes as the square of the inverse linear dimension of the crystal. Furthermore, the « image forces» , by which we take into account the existence of the free surface, merely arise from the elastic interaction at the boundary between neighbouring cells.

For a vibrating crystal, the thermodynamic potential is the Helmholtz free energy.

The interaction between imperfect neighbouring cells of the infinite lattice gives a non-vanishing contribution to the vibrational free energy, and now the « image forces » are opposite to the thermodynamic forces acting across the boundary wall from the neighbouring cells.

3·1. *The interaction term.* – The vibrational Helmoltz free energy of the defect can be obtained from that of an imperfect cyclic cell by subtracting the interaction term:

$$\Delta F_v^{(\mathrm{free})} = \Delta F_v^{(\mathrm{cycl})} - \Delta F_v^{(\mathrm{int})} , \tag{11}$$

where $\Delta F_v^{(\mathrm{cycl})}$ is the term calculated in the preceding section.

In the Einstein approximation the interaction term, to the first order, is given by

$$(\Delta F_v)_{\mathrm{I}}^{(\mathrm{int.})} = \mathrm{Sp}\,\{[\boldsymbol{\xi}]^{\dagger}\cdot[\delta \boldsymbol{B}^{(\sigma)}]\}\,\frac{\psi'(\omega_E^2)}{M} ,$$

when we define $[\delta \boldsymbol{B}^{(\sigma)}]$ as the difference between the cubic tensors in the unit cyclic cell and those in the actual crystal with free surface,

$$[\delta \boldsymbol{B}^{(\sigma)}] \equiv [\boldsymbol{B}^{(\mathrm{cycl})}] - [\boldsymbol{B}^{(\mathrm{free})}] .$$

Remembering that for a perfect cyclic cell, we have $\mathrm{Sp}\{[\xi]^{\dagger}\cdot[\boldsymbol{B}^{(\mathrm{cycl})}]\}=0$, and the expression (9) for the perturbation on the cubic tensors due to the defect $[\delta\boldsymbol{B}]$, we have:

$$\mathrm{Sp}\{[\xi]^{\dagger}\cdot[\delta\boldsymbol{B}]^{(\sigma)}\}=\sum_{j\neq 0}^{(J)}\sum_{\alpha=1}^{3}\{\delta\boldsymbol{B}(j)\cdot\xi_{j}\}_{\alpha\alpha}-\sum_{l\neq 0}^{(N)}\sum_{\alpha=1}^{3}\Big\{\sum_{l'}^{(N)}\boldsymbol{B}^{(\mathrm{free})}(ll')\cdot\xi_{l'}\Big\}_{\alpha\alpha}. \tag{12}$$

The volume V_0 is supposed to remain unchanged.

The last summation in the second term of the right-hand side of (12), can be evaluated as follows. Consider a sphere, centered at the vacant lattice site and crossing a set of lattice points; let $(a/2)l_0$ be the radius of this sphere. The last term in (12) becomes

$$\sum_{l\neq 0}^{(N)}\sum_{\alpha=1}^{3}\Big\{\sum_{l'}^{(N)}\xi_{l'}\cdot\boldsymbol{B}^{(\mathrm{free})}(ll')\Big\}_{\alpha\alpha}=\sum_{l\neq 0}^{l\leqslant l_0}\sum_{\alpha=1}^{3}\Big\{\sum_{l'}^{(N)}\xi_{l'}\cdot\boldsymbol{B}^{(\mathrm{free})}(ll')\Big\}_{\alpha\alpha}+\sum_{l}^{l\geqslant l_0}\sum_{\alpha=1}^{3}\{\ldots\}_{\alpha\alpha}.$$

If l_0 is large enough, the true displacement vectors in the summation on the region external to the sphere can be replaced by an asymptotic expression. For large value of l, KANZAKI finds

$$\xi_{\alpha}(l)=\frac{1}{|\boldsymbol{R}_l^{(0)}|^2}I_{\alpha}(\mu_1,\mu_2,\mu_3)\,,\qquad(\alpha=1,2,3),$$

where $I_{\alpha}(\boldsymbol{\mu})$ are smooth functions of the director cosines μ_1, μ_2, μ_3 of the radius vector $\boldsymbol{R}_l^{(0)}$.

For present purposes, we assume a field of pure shear modulated on the directions of $\boldsymbol{R}_l^{(0)}$

$$\xi_l=C(\boldsymbol{\mu})\frac{\boldsymbol{R}_l^{(0)}}{|\boldsymbol{R}_l^{(0)}|^3}.$$

The summation on the outer region becomes (*)

$$\sum_{l}^{l>l_0}\sum_{\alpha=1}^{3}\Big\{\sum_{l'}^{(N)}\xi_{l'}\cdot\boldsymbol{B}^{(\mathrm{free})}(ll')\Big\}_{\alpha\alpha}\simeq\bar{C}\pi a^{-3}\int_{(a/2)l_0}^{\infty}\sum_{\alpha=1}^{3}\Big\{\sum_{l}\boldsymbol{B}(0,l)\cdot\frac{\boldsymbol{R}_l^{(0)}+\boldsymbol{R}}{|\boldsymbol{R}_l^{(0)}+\boldsymbol{R}|^3}\Big\}_{\alpha\alpha}R^2\,\mathrm{d}R\,,$$

where $\bar{C}$ means the average of $C(\boldsymbol{\mu})$ on the total solid angle.

(*) We note that for a crystal with free surface, there are not contributions coming from the surface itself, if the displacements are considered up to the first order.

3·2. *Image forces.* – Defining $\delta \boldsymbol{A}^{(\sigma)}(ll') \equiv \boldsymbol{A}^{(\mathrm{cycl})}(ll') - \boldsymbol{A}^{(\mathrm{free})}(ll')$ as the difference between the second order tensors in the $\boldsymbol{A}$-matrix of a cyclic cell and those for the actual crystal with free surface, the static contribution to the image forces on the lattice point l is

$$\boldsymbol{f}_l^{(i,\,s)} = -\sum_{l'} \delta \boldsymbol{A}^{(\sigma)}(ll') \cdot \boldsymbol{\xi}_{l'} .$$

For a f.c.c. lattice, the static contribution to the image pressure is given by

$$\Delta p^{(i,\,s)} = \frac{f_n}{a^2/2} , \tag{13a}$$

where $f_n = \boldsymbol{f}_l^{(i,\,s)} \cdot \boldsymbol{n}$ is the normal component of the images forces, averaged on the lattice points of the superficial phase: $\boldsymbol{n}$ is the inner versor normal to the surface.

If $\varepsilon(a) = \sum_{l \neq 0} \frac{1}{2} q(|\boldsymbol{R}_l^{(0)}|)$ is the rigid lattice energy per atom in a perfect crystal, to the first order in the displacement field, KANZAKI showed that

$$(\Delta p^{(i,\,s)})_1 = -\frac{2}{N} \frac{\mathrm{d}\varepsilon(a)}{\mathrm{d}\Omega} .$$

In order to calculate the vibrational contribution to the image forces, we consider the vibrational Helmholtz free energy of a crystal of volume $(1+\delta)$ times its original volume at temperature T as a function $F_v(T, \delta)$. For small δ we expand [6]

$$F_v(T, \delta) = F_0^{(v)}(T) + \delta \cdot F_1^{(v)}(T) + \dots ,$$

where the coefficient $F_1^{(v)}(T)$ of the linear term in the dilatation arises from the anharmonicity in the potential energy:

$$F_1^{(v)}(T) = N \sum_{\alpha=1}^{3} \Big\{ \sum_{j \neq 0}^{(J)} \boldsymbol{B}(0, j) \cdot \boldsymbol{R}_j^{(0)} \Big\}_{\alpha\alpha} \frac{\psi'(\omega_E^2)}{M} . \tag{14}$$

For an imperfect crystal, this linear term will exceed that for the perfect crystal by an amount $\delta \cdot \Delta F_1^{(v)}(T)$. Now $\partial F / \partial \delta$ is proportional to the pressure and therefore the vibrational contribution to the image pressure is given by

$$\Delta p^{(i,v)} = \frac{1}{V_0} \Delta F_1^{(v)}(T) . \tag{13b}$$

(6) R. E. PEIERLS: *Quantum Theory of Solids* (Oxford, 1955), p. 31.

Neglecting the fourth order tensors in the Taylor expansion of the energy, the change in the linear term of the vibrational free energy is calculated as follows:

$$\Delta F_1^{(v)}(T) = 2 \sum_{j \neq 0}^{(J)} \sum_{\alpha=1}^{3} \left\{ \sum_{j'} \delta \boldsymbol{B}(jjj') \cdot \boldsymbol{R}_{j'}^{(0)} \right\}_{\alpha\alpha} \frac{\psi'(\omega_E^2)}{M} .$$

Remembering (9) and (14), we find

$$\Delta F_1^{(v)} = -\frac{2}{N} F_1^{(v)}$$

Taking into account that the perfect crystal is supposed to be in thermodynamic equilibrium at the temperature T and external pressure p_{ext},

$$p_{ext} = -\left(\frac{\partial F}{\partial V}\right)_T = -\left\{ \frac{\mathrm{d}\varepsilon(a)}{\mathrm{d}\Omega} + \frac{F_1^{(v)}(T)}{V_0} \right\},$$

the actual image pressure is finally given by

$$\Delta p^{(i)} = \Delta p^{(i,s)} + \Delta p^{(i,v)} = \frac{2}{N} p_{ext} + (\Delta p)_{II}^{(i,s)} + \ldots$$

where $(\Delta p)_{II}^{(i,s)}$ is the second order contribution to the static image pressure. Usually we assume $p_{ext} \sim 0$; therefore, if all the employed approximations are valid, the image pressure for a vacant lattice site comes merely from the second or higher order contributions to the static image forces.

The volume change due to the distortion, $\Delta V = -V_0 K_T^{-1} \Delta p^{(i)}$ (K_T being the isothermal compressibility), is easily found through use of (13 *a*) and (6). The actual image pressure is proportional to the inverse power of the initial volume, so that the volume change due to the distortion does not depend on volume.

Owing to the uniform dilatation $\delta = \Delta V / V_0$, the rigid lattice energy of the actual crystal suffers a non-vanishing change

$$\Delta U(\delta) = \frac{\mathrm{d}\varepsilon(a)}{\mathrm{d}\Omega} \Delta V, \tag{15}$$

which is formally temperature-independent, and the vibrational free energy is affected by an amount

$$\Delta F_v(\delta, T) = F_1^{(v)}(T) V_0^{-1} \Delta V , \tag{16}$$

which is temperature-dependent. The above contributions are opposite in sign, so that they cancel each other in making up the Helmholtz free energy, provided the external equilibrium pressure is taken vanishingly small.

The explicit temperature dependence of (16) gives rise to a change of entropy

$$\Delta S(\delta, T) = -\left(\frac{\partial F_1^{(v)}(T)}{\partial T}\right)_{V=V_0} \cdot \Gamma^{-1} \Delta\Gamma . \tag{17}$$

The entropy change arising from the uniform dilatation due to the image pressure has been evaluated for a vacancy in a f.c.c. lattice by HUNTINGTON, SHIRN and WAJDA by thermodynamic considerations applied to an elastic model.

By help of (13) and (7), the entropy change due to the relaxation of the normal stresses at the boundary walls is found to be

$$\Delta S(\delta, T) = -\sum_{\lambda=1}^{3}\Big\{\sum_{j\neq 0}^{(J)} \boldsymbol{B}(0, j)\cdot \boldsymbol{R}_j^{(0)}\Big\}_{\lambda\lambda} \frac{\hbar^2}{8kMT^2}\left(\sinh\frac{\hbar\omega_E}{2kT}\right)^{-2}\frac{\Delta\Gamma}{\Omega} . \tag{18}$$

From the above considerations we can conclude that this entropic contribution should not be considered in making up the Helmholtz free energy for the formation of the defect.

4. – Numerical results.

The increase of the Helmholtz free energy upon the formation of a vacant lattice point in a monoatomic f.c.c. crystal with two-body interactions is given by the sum of four terms (exclusive of the mixing entropy):

$$\Delta F = \Delta U_L + \Delta U_{\text{elast}} + \Delta U_{\text{Z.p.E.}} + \Delta F_{\text{th}} ,$$

where $\Delta U_L = -\frac{1}{2}\sum_{l\neq 0}^{(N)} \varphi(|\boldsymbol{R}_l^{(0)}|)$ is the change in energy for a rigid lattice, $\Delta U_{\text{elast}} = -\frac{1}{2}[\xi]^{\dagger}\cdot[\boldsymbol{f}]$ is the relaxation energy, $\Delta U_{\text{Z.p.E.}}$ and ΔF_{th} are the changes in the zero point energy and in the thermal free energy for a crystal with free surface; of course, $\Delta U_{\text{Z.p.E.}} + \Delta F_{\text{th}} = \Delta F_v^{(\text{free})}$, which is given by (11).

The numerical evaluation is made for argon in the range of temperature from 0 °K to 80 °K, assuming a (12, 6) interatomic potential $q(r) = Ar^{-12} - Br^{-6}$ where $A = 1.63\cdot 10^{-7}$ erg·Å^{12}, $B = 1.05\cdot 10^{-10}$ erg·Å^6 (7). For the lattice constants $a(T)$ we use the theoretical values of ZUCKER (8); these values are in good agreement with the experimental results by DOBBS *et al.* (9).

(7) E. R. DOBBS and G. O. JONES: *Rep. Progr. Phys.*, **20**, 517 (1957).

(8) I. J. ZUCKER: *Phil. Mag.*, **3**, 987 (1958).

(9) E. R. DOBBS, B. F. FIGGINS, G. O. JONES, D. C. PIERCEY and D. P. RILEY: *Nature*, **178**, 483 (1956).

TABLE I. – *Displacements of the atoms up to the sixth neighbours, in the second approximation, in units of* 10^{-3} Å; *x, y, z are the principal crystallographic directions in a f.c.c. lattice.*

R_l $(a/2)$	(110)				(200)				(211)				(220)				(310)				(222)			
R_l^2 $(a^2/2)$	1				2				3				4				5				6			
T (°K)	ξ_x	ξ_y	ξ_z	ξ	ξ_x	ξ_y	ξ_z	ξ	ξ_x	ξ_y	ξ_z	ξ	ξ_x	ξ_y	ξ_z	ξ	ξ_x	ξ_y	ξ_z	ξ	ξ_x	ξ_y	ξ_z	ξ
0	12.1	−12.1	0	17.1	10.4	0	0	10.4	3.23	2.54	2.54	4.83	3.97	3.97	0	5.62	1.16	0.66	0	1.34	1.79	−1.79	1.79	3.10
20	11.3	−11.3	0	16.0	10.7	0	0	10.7	2.97	2.38	2.38	4.49	3.69	3.69	0	5.22	1.26	0.72	0	1.45	−1.67	−1.67	1.67	2.88
40	7.10	−7.10	0	10.0	12.0	0	0	12.0	1.62	−1.54	1.54	2.71	2.23	2.23	0	3.15	1.77	1.07	0	2.07	1.03	−1.03	−1.03	1.78
60	0.63	−0.63	0	0.89	14.0	0	0	14.0	0.46	0.24	−0.24	0.57	0.02	0.02	0	0.03	2.55	1.60	0	3.01	−0.04	−0.04	0.04	0.08
80	9.37	9.37	0	13.2	17.0	0	0	17.0	3.66	1.75	1.75	4.42	3.49	3.49	0	4.93	3.73	2.42	0	4.45	1.47	1.47	1.47	2.54
0 (Kanzaki)	8.51	−8.51	0	12.03	15.43	0	0	15.43	−1.89	−1.85	1.85	3.23	2.65	2.65	0	3.75	2.32	1.41	0	2.71	−1.23	−1.23	−1.23	2.12

TABLE II. – *Perturbation tensor (in units of* 10^{-2} eV·Å^{-2}) *for each first and second neighbour of the vacancy. In the last column the perturbation tensor for all other atoms with* $l > l_0$ *is listed.*

	First neighbour			Second neighbour			Atoms with $l > l_0$
T (°K)	$\sum_{\alpha=1}^{3} \{\delta \boldsymbol{A}(ll)\}_{\alpha\alpha}$	$\sum_{\alpha=1}^{3} \{\sum_{l'} [\boldsymbol{B}(ll') + \delta \boldsymbol{B}(ll')] \cdot \boldsymbol{\xi}_{l'}\}_{\alpha\alpha}$	$M \sum_{\alpha=1}^{3} \{\boldsymbol{\Lambda}(l)\}_{\alpha\alpha}$	$\sum_{\alpha=1}^{3} \{\delta \boldsymbol{A}(ll)\}_{\alpha\alpha}$	$\sum_{\alpha=1}^{3} \{\sum_{l'} [\boldsymbol{B}(ll') + \delta \boldsymbol{B}(ll')] \cdot \boldsymbol{\xi}_{l'}\}_{\alpha\alpha}$	$M \sum_{\alpha=1}^{3} \{\boldsymbol{\Lambda}(l)\}_{\alpha\alpha}$	$\sum_{l}^{l>l_0} \sum_{\alpha=1}^{3} \{\sum_{l'} [\boldsymbol{B}(ll') + \delta \boldsymbol{B}(ll')] \cdot \boldsymbol{\xi}_{l'}\}_{\alpha\alpha}$
0	−7.156	0.848	−6.307	0.216	−0.002	0.214	8.626
20	−6.986	0.725	6.261	0.215	−0.002	0.213	7.461
40	−6.214	0.159	−6.055	0.207	−0.003	0.205	2.120
60	−5.312	−0.516	5.828	0.198	−0.003	0.195	−4.235
80	−4.340	−1.273	−5.612	0.186	−0.004	0.182	−11.36

The displacements of the atoms in the neighborhood of the defect up to the sixth neighbours, evaluated in the second approximation, are shown in Table I at different temperatures; and the values evaluated by KANZAKI using a (10, 6) interatomic potential with $A = 2.130 \cdot 10^{-8}$ erg·Å^{10}, $B = 1.569 \cdot 10^{10}$ erg·Å^{6} and a lattice constant $a = 5.40$ Å are listed in the same table. At high temperatures the oscillating character of the elastic solution in the neighbourhood of the defect does not appear.

The traces of the perturbation matrices in the unrelaxed lattice and the correction due to the relaxation are listed in Table II. The perturbation in the unrelaxed lattice is evaluated only for the first and second neighbours of the vacancy; the effect decreases rapidly with the distance from the defect. To evaluate the correction due to the relaxation for each of this atoms, the summation is made over their first and second neighbours; for the atoms far from the defect the sum is over their first neighbours only; we assume that the coefficient $\bar{C}$ for the radial displacement (see Section 3·1) in this region is obtained by averaging over the three directions [100], [110], [111]:

T (°K)	0	20	40	60	80
$\bar{C}$ (Å^3)	0.12	0.11	— 0.03	0.08	0.027

In the middle region we assume that the displacement field can be obtained by extrapolating the elastic solution valid in the region far from the defect: the numerical values are given for $l_0 = 2$.

Table III shows the contribution of first and second order to the changes

TABLE III. – *First and second order changes in the zero point energy and in the thermal free energy from the lattice whole (in units of* 10^{-2} eV).

T (°K)	$\Delta U^{(\text{unrelax})}_{\text{Z.p.E.}}$	$\Delta U^{(\text{elast})}_{\text{Z.p.E.}}$	$\Delta F^{(\text{unrelax})}_{\text{th}}$	$\Delta F^{(\text{elast})}_{\text{th}}$	
0	— 0.412	0.092	0	0	First order contributions
20	— 0.407	0.080	— 0.039	0.008	
40	— 0.384	0.021	— 0.236	0.013	
60	— 0.355	— 0.059	— 0.495	— 0.083	
80	— 0.321	— 0.168	— 0.779	— 0.407	
0	— 0.026	$< 10^{-3}$	0	0	Second order contributions
20	— 0.026	$< 10^{-3}$	— 0.010	$< 10^{-3}$	
40	— 0.024	$< 10^{-3}$	— 0.041	$< 10^{-3}$	
60	— 0.022	$< 10^{-3}$	— 0.075	$< 10^{-3}$	
80	— 0.020	$< 10^{-3}$	— 0.110	— 0.002	

in the vibrational free energy: it appears that these changes are at least an order of magnitude larger than the relaxation energy. The second order contribution is calculated in the first nearest neighbours approximation.

The fractional changes of volume $\Delta V/\Omega$ due to the distortion are listed in Table IV. At low temperature, the present results are similar to the value previously found by KANZAKI in the static approximation. As the temperature increases, the interatomic forces between nearest neighbours, in thermodynamic equilibrium with zero external pressure, change from repulsion to attraction, owing to thermal expansion. Therefore the dilatation due to the elastic distortion becomes positive. This situation applies for the lightest van der Waals crystals only.

TABLE IV. – *Fractional changes of volume due to distortion and correspondent entropy changes, in units of k.*

T (°K)	$\Delta V/\Omega$	$\Delta S(\delta, T)/k$
0	— 0.028	0
20	— 0.026	— 0.40
40	— 0.017	— 0.49
60	— 0.002	— 0.07
80	0.020	+ 0.64

The entropy changes due to the volume dilatation are listed in the same table. The activation free energy for the formation of a point defect is not affected by the above entropic term.

In Table V the four contributions to the changes in the free energy are listed at different temperatures; ΔU_L is evaluated by means of the Jones and Ingham summations over the entire lattice, while for the evaluation of ΔU_{elast} the sum is made over the first and second neighbours of the defect.

TABLE V. – *The four contributions (in units of* 10^{-2} eV) *to the changes in the Helmoltz free energy for the formation of a vacancy in solid argon.*

T (°K)	ΔU_L	$\Delta U_{\text{Z.p.E.}}$	ΔU_{elast}	ΔF_{th}
0	9.043	— 0.050	— 0.346	0
20	9.033	— 0.044	— 0.353	— 0.041
40	8.974	— 0.022	— 0.387	— 0.264
60	8.868	— 0.011	— 0.436	— 0.653
80	8.698	— 0.026	— 0.509	— 1.298

The concentration of vacancies $n = \exp[-\Delta F/kT]$ at different temperatures is listed in Table VI; also the experimental value obtained near the melting

point by D. L. MARTIN, assuming that the « curl up » in the specific heat before the melting point is due to defect formation, is listed in the same table (*).

TABLE VI. – *Concentration of vacancies in solid argon at different temperatures. The last data is the experimental value obtained by* D. L. MARTIN.

T (°K)	20	40	60	80	exp.
n	$2.19 \cdot 10^{-22}$	$1.28 \cdot 10^{-11}$	$2.98 \cdot 10^{-7}$	$4.73 \cdot 10^{-5}$	$3.74 \cdot 10^{-3}$

The total Helmholtz free energy change ΔF as a function of temperature is shown in Fig. 1; this change is practically equivalent to the Gibbs free energy change ΔG, if the external pressure is almost equal to zero. Since, in the range of temperature considered, the external pressure may be regarded as constant, the activation entropy and the activation enthalpy for the formation of the defect are given by the slope and the ordinate intercept of the tangent to the curve $\Delta G(T)$ at the considered temperature. In the high temperature region $\Delta G(T)$ is a nearly linear function; in this region the vacancy concentration is given by $n(T) = \exp[\Delta S/k] \cdot \exp[-\Delta H/kT]$, where ΔS and ΔH are temperature-independent parameters, calculated for a particular temperature of the considered range. The above approximation is not valid in the low temperature region, where $\Delta G(T)$ does not show a linear behaviour, owing to the quantum effects.

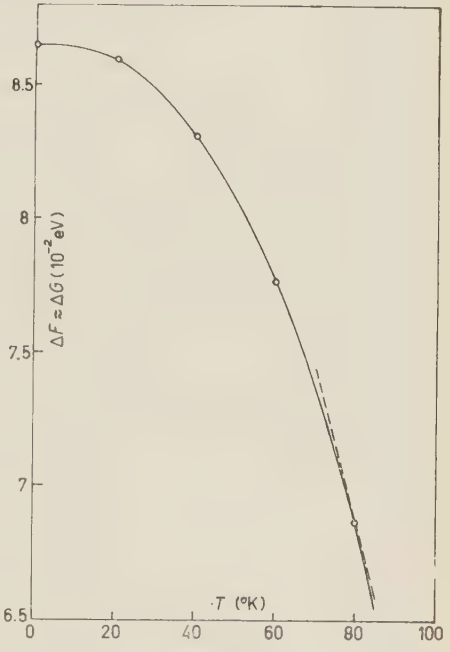

Fig. 1.

The concentrations of vacancies in the other inert gases Ne, Kr and Xe at the same reduced temperature, close to the melting point, are calculated neglecting the corrections due to the displacement field and to the anharmonicity, because of the uncertainty in the interatomic potential of these crystals. These values are listed in Table VII.

(*) The discrepancy with the values found from theoretical previsions could be due to the fact that the excess specific heat may be not entirely due to the defects.

TABLE VII. – *Concentration of vacancies in crystals of inert gases neon, krypton and xenon.*

Crystal	T (°K)	n
Ne	24	$1.6 \cdot 10^{-5}$
Kr	109	$1.4 \cdot 10^{-5}$
Xe	147	$0.44 \cdot 10^{-5}$

5. – Discussion.

In this paper, the calculations of the equilibrium thermodynamic properties of a point lattice defect are developed using the Einstein model in the harmonic approximation; anharmonicity effects are considered in evaluating the elastic corrections and the volume dilatation due to the defect. We neglected the change of anharmonicity terms of the vibrational free energy as well as the coupling between nuclear vibrations.

Previous calculations ([10]) show that, using the Einstein model, the anharmonic contribution in a perfect lattice is a small percentage of the harmonic vibrational free energy. Therefore, the harmonic approximation seems to be sufficiently accurate for the present purposes.

The use of the Einstein model could appear to be a very crude approximation in the study of the influence of defects on the vibrational properties of crystals. However, in the high temperature limit we find the following expressions for the vibrational entropy of a vacancy in a f.c.c. lattice:

$$\lim_{T\to\infty} (\Delta S_v)_{\mathrm{I}}^{(\mathrm{unre'ax})} = \tfrac{3}{2} k \qquad \text{(first order contribution)}$$

and

$$\lim_{T\to\infty} (\Delta S_v)_{\mathrm{II}}^{(\mathrm{unrelax})} = 0.187\, k \quad \text{(second order contribution)}$$

which are independent of the physical constants of the crystals.

These results are consistent with the Kirkwood classical calculation obtained with a second order perturbation technique, including contributions from the change of the coupling terms ([11]). Therefore, the Einstein model seems sufficiently accurate for evaluating extensive thermodynamic properties of a vacancy in the classical limit. We hope that the same conclusion is still valid at temperatures near to Debye temperature, for the van der Waals crystals.

([10]) J. H. HENKEL: *Journ. Chem. Phys.*, **23**, 681 (1955).
([11]) K. F. STRIPP and J. G. KIRKWOOD: *Journ. Chem. Phys.*, **22**, 1579 (1954).

Our results are obtained supposing that the interaction energy between the atomic nuclei in the crystal is a two-body potential of central type.

Strictly speaking, the validity of the present calculations is restricted to the class of simple van der Waals crystals. In a less rigorous sense, our considerations on the vibrational properties can be applied to non-polar crystals and metals, provided that a « spring and masses » model for the lattice dynamics is still valid; for these crystals the greatest uncertainty arises from the energy of the defect in the rigid lattice.

* * *

The authors wish to express their gratitude to Dr. R. Fieschi for many discussions and comments.

RIASSUNTO

Si studia l'influenza di un posto reticolare vacante sulle proprietà termodinamiche di equilibrio di un cristallo cubico, a varie temerature comprese fra lo zero ed il punto di fusione. La variazione delle proprietà vibrazionali è valutata per mezzo di un modello di Einstein. Si estende al caso di temperature diverse da zero lo studio del campo elastico di rilassamento attorno al difetto; l'energia libera vibrazionale è inoltre valutata tenendo conto del rilassamento stesso. Si discutono le « forze immagine » che corrispondono ad un posto vacante, includendo il termine vibrazionale attraverso l'anarmonicità dell'energia potenziale. Si riportano i risultati numerici per cristalli di gas rari.

Diffraction of X-Rays by Some Liquid Mixtures.

E. Tartaglione

Istituto di Fisica Sperimentale dell'Università - Napoli

(ricevuto il 18 Maggio 1960)

Summary. — In this note are reported intensity measurements of the diffraction ring of the X-rays by mixtures of polar and non-polar liquids which present some remarkable anomalies in the measure of the mechanical momentum generated in a rotating electric field. The measures being into evidence the presence of particular molecular associations in the zone in which the anomalies in the mechanical momentum are noted.

It has been noted [1] that in some polar and non-polar liquid mixtures, placed in a rotating electric field, the generated mechanical momentum which is due to the electrical conductivity of the liquid presents for certain concentrations much higher values (*i.e.* 1000 times) than those to be expected on the basis of the electrical conductivity of these mixtures. Such an anomaly is noted at rather low frequencies (50 Hz, 150 Hz) for which is to be excluded a Born type effect as it appears, as is known, at much higher frequencies (10 kHz, 100 kHz), while at lower frequencies the conductivity effect is practically zero. The results obtained show seemingly that for these mixtures some modification should take place which does not regard the electrical conductivity alone. To the purpose of exposing eventual structural modifications the behaviour of some of these liquids and their mixtures, with respect to the diffraction by X-rays, has been studied.

The liquids studied were:

1) Benzene, nitrobenzene and their mixtures.
2) Benzene, acetone and their mixtures.
3) Dioxane, ethyl alcohol and their mixtures.

[1] A. Carrelli and M. Marinaro: *Nuovo Cimento*, **11**, 262 (1959).

For each pair of liquids, mixtures of appropriate concentrations have been examined; each sample, placed in a basin having very thin mica walls half a millimeter distant from each other, has been irradiated with the Cu K_α radiation ($\lambda = 1.54$ Å) obtained by filtering through a small plate of Ni of appropriate thickness the radiation emitted from an X-ray tube with copper anticathode fed with a voltage of 30 kV and a current of 15 mA.

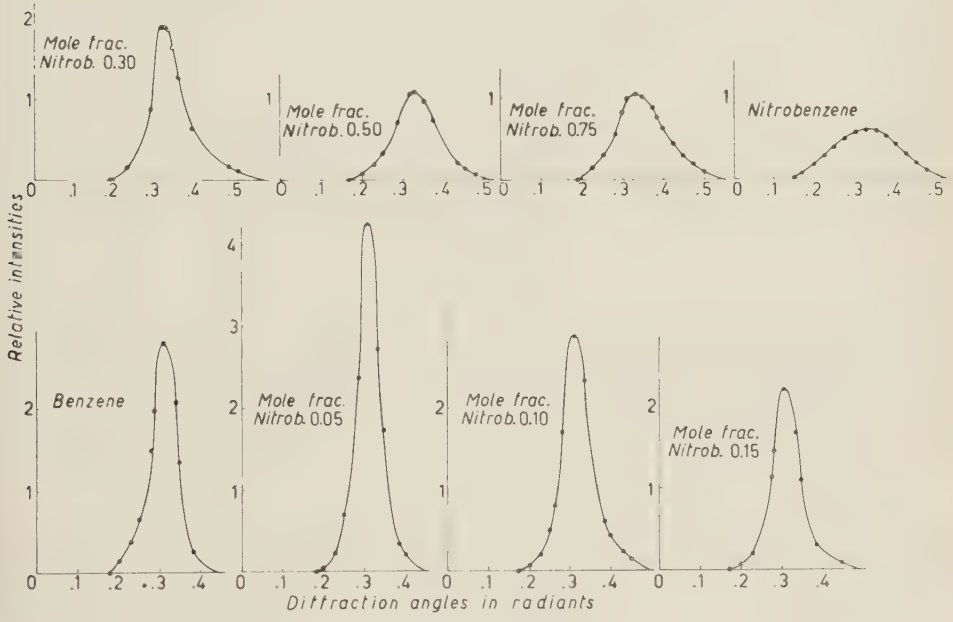

Fig. 1.

The small beam of X-rays has been fed in a Pb collimator 3 cm long and having a circular hole of 0.8 mm in diameter at the extremity of which the basin containing the sample in question has been placed. For measuring the intensity of diffracted X-rays the photographic method using Ferrania films type N has been adopted. The exposure time, for each sample has been 10 minutes and care was taken to develop simultaneously all photographs relative to one pair of liquids and their mixtures.

Each sample presents a characteristic halo of diffraction. Following a method previously described ([2]), from the microphotometry performed in relation to a diameter of the diffraction halo, angular distributions of the relative intensities of diffracted X-rays have been obtained. Fig. 1 refers to one of the studied mixtures and precisely to benzene-nitrobenzene. From the

([2]) F. Cennamo: *Nuovo Cimento*, **10**, 395 (1953).

analysis of these curves (and of those relative to the other two series of studied mixtures) it can be noted that the relative intensity, measured at the characteristic maxima of diffraction, depends on the concentration of the mixture, while the position of these maxima is more or less independent. In Fig. 2,

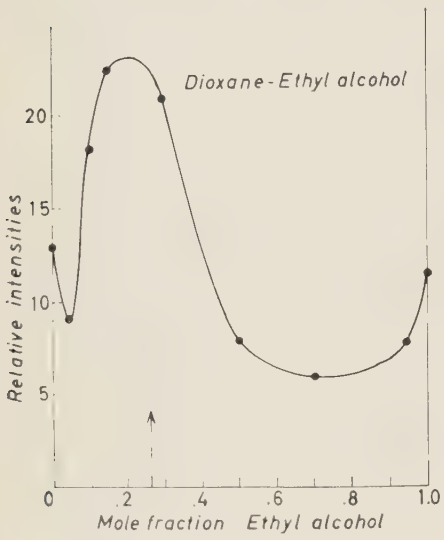

Fig. 2.

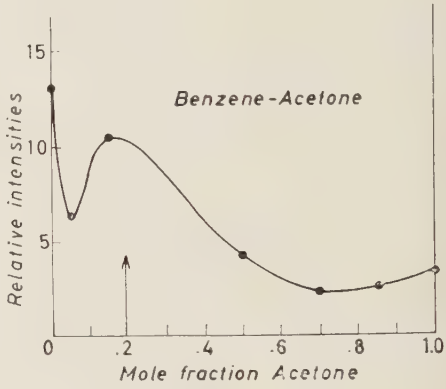

Fig. 3.

3 and 4 the distributions of relative intensities measured at their maxima are plotted against the molecular fractions of the polar component for the three series of mixtures studied. It is noted that for two series of these mixtures (benzene-acetone Fig. 2 and dioxane-ethyl alcohol Fig. 3) one obtains a similar behaviour; that is, the intensity measured at the maximum decreases by a 0.05 molecular fraction of the polar component and further increases bringing forth a maximum of about 0.17 molecular fraction of acetone in benzene and about 0.23 of ethyl alcohol in dioxane. On the other hand the series of benzene-nitrobenzene mixtures (Fig. 4) presents a maximum of the intensity in the 0.05 molar fraction of the polar component.

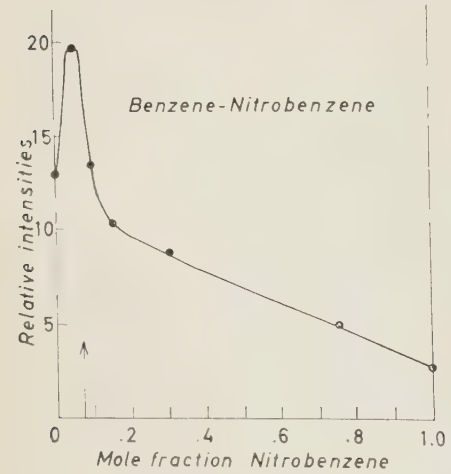

Fig. 4.

The principal cause of the diffraction ring is due to the presence of a molecular order in the liquid and therefore an increase of the intensity of the

maximum of the diffraction ring should correspond to an increase of such an order and then to the formation of molecular associations aligned in the liquid. It would seem, in such a way, that the addition of a polar liquid in a non-polar one, at least in the cases studied by us, produces certain phenomena of molecular association for particular concentrations.

It is important to point out the fact that for all three of the examined mixtures, the concentration at which one obtains a maximum in the distribution of the intensity of diffracted X-rays corresponds, with good approximation, to that at which it presents the anomaly in the rotational mechanical momentum in a rotating electric field.

In Fig. 2, 3 and 4 the concentrations at which the mechanical momentum is anomalous are indicated with an arrow on the abscissa axis.

This should lead to place this anomaly in relation with the formation of molecular associations for the studied mixtures.

* * *

Thanks are due to Prof. A. Carrelli, Director of the Institute of Experimental Physics of the University of Naples, who has suggested the subject matter of this work and has placed at the authors' disposal the necessary equipment for fulfilling the same.

RIASSUNTO

In questa nota vengono riportate misure di intensità dell'anello di diffrazione dei raggi X da parte di miscugli di liquidi polari e non polari che presentano delle anomalie notevoli nella misura del momento meccanico generato in campo elettrico ruotante. Le misure mettono in evidenza la presenza di particolari associazioni molecolari nella zona in cui si notano le anomalie nel momento meccanico.

Evaluation of Future Levels of Radioactive Fallout.

K. G. Vohra and U. C. Mishra

Atomic Energy Establishment Trombay - Bombay

(ricevuto il 20 Giugno 1960)

Summary. — The evaluations of future levels of strontium-90 deposition on the ground have been carried out for three different cases: (i) no more nuclear weapon tests are carried out after October, 1958; (ii) tests continue to be carried out at the same average rate as in the past, and (iii) tests are carried out at the highest rate observed in the past *i.e.* during the year 1958. These evaluations are done for Bombay, India, and are based on the ground deposition data on 1st October, 1958, and stratospheric inventories due to injections in the equatorial and polar regions as given by Libby. For the case (i) the maximum level of ground deposition will be 28 mC/square mile and this value will be reached in 1963. The maximum values of ground deposition for cases (ii) and (iii) are 152.7 mC/square mile and 438.7 mC/square mile respectively. The factors relating the ground deposition of strontium-90 to its concentration in the human bone have been discussed. The estimated concentrations of strontium-90 in the human bone are 4.8, 26.5 and 76 $\mu\mu$C strontium-90 per gram of bone calcium for cases (i), (ii) and (iii) respectively.

1. – Introduction.

The world-wide fallout from H-bomb tests continues to be deposited for several years after the tests, due to the stratospheric storage of fission-products debris from the tests. About 50 H-bomb tests have been carried out during the period November, 1952 to October, 1958 (1). The explosive power of these

(1) V. S. Bhatnagar, V. V. Shirvaikar and C. Rangaraja: *A Chronological List of Nuclear Explosions*, Atomic Energy Establishment Trombay Report no. AEET/AM/6 (January, 1959).

bombs has been reported to range from 1 megaton to 20 megatons equivalent of TNT. These explosions yield large quantities of fission-products because the equivalent fission-power of a H-bomb is known to be about 50 per cent of its explosive power (2).

A major fraction of the fission-products released by H-bomb tests goes to the stratosphere and is dispersed on a world-wide scale. The rate of deposition of these products in the various regions of the globe is known to depend on several factors such as the latitude of explosion (3), and the climatic conditions of the region. The fission-products from these tests that do not enter the stratosphere are dispersed widely in the troposphere due to the seasonal winds and are also deposited, the degree of deposition at any place depending on meteorological factors. These variations in the degree of deposition due to stratospheric and tropospheric components give rise to non-uniform deposition of fission-products on the earth.

The long-term hazard of bomb testing can be evaluated from the cumulative deposition of the long-lived fission products on the ground. The fission product strontium-90 has been generally considered to be of greater significance because of its high fission yield and selective deposition in the human bone. In this report an attempt has been made to calculate the future levels of ground deposition of strontium-90. The assumption made in these evaluations is that the cumulative deposition on the ground will give rise to higher concentrations of strontium-90 in the human bone due to its passage from soil to human bone via grass and milk, cereals, and other vegetable foods.

The present evaluation of cumulative deposition on the ground has been carried out for three different cases: i) no more nuclear weapon tests are carried out after October, 1958, when the last H-bomb test was reported, ii) tests continue to be carried out at the same rate as in the past, and iii) the injections into the stratosphere continue at the highest rate observed in the past *i.e.* during the year 1958.

In computing the future levels of deposition the known data on the present levels of deposition at Bombay have been used. It is also assumed that the stratospheric inventories are different for the tests carried out in the equatorial and polar regions. The future injections for equatorial and polar regions are also considered separately because the deposition of activity from the equatorial injections is considered to be uniform all over the world, and that from the polar injections shows a latitude dependence and is confined to the hemisphere of injection.

(2) *Fallout from nuclear weapons tests*, Report on Public Hearings held in May, 1959 issued by the U. S. Congressional Joint Committee on Atomic Energy.

(3) L. Machta: *Meteorological interpretation of strontium-90 fallout*, U.S.A.E.C. Report no. HASL-42 (October, 1958).

2. – Case (i): no more tests after October 1958.

The evaluations for this case have been done using the data on the cumulative deposition of strontium-90 at Bombay as on 1st October, 1958 (4), and the data on the stratospheric reservoir due to equatorial injections and that due to polar injections, as estimated by LIBBY (5).

The level of deposition of strontium-90 at any time «t» after 1st October, 1958 can be estimated from the following equation:

$$G_d(t) = G_d(0)\exp[-t/T_r] + S_e(0)\{1-\exp[-t/T_e]\}\exp[-t/T_r] + \\ + \alpha\cdot S_p(0)\{1-\exp[-t/T_p]\}\exp[-t/T_r],$$

where: $G_d(t)$ is the level of ground deposition at any time «t» after 1st October, 1958, mC/square mile;

$G_d(0)$ is the level of ground deposition at time $t=0$ *i.e.* 1st October, 1958, mC/square mile.

$S_e(0)$ is stratospheric reservoir at $t=0$ due to the equatorial injections, in equivalent units of mC/square mile.

$S_p(0)$ is stratospheric reservoir at $t=0$ due to polar injections, in equivalent units of mC/square mile.

T_r is mean radioactive life of strontium-90, in years.

T_e is mean stratospheric residence time of strontium-90 for equatorial injections, in years.

T_p is mean stratospheric residence time for polar injections, in years.

α is the factor for preferential deposition for the region under consideration over the average deposition level for the hemisphere.

The actual values that can be substituted in the equation are: $G_d(0) = 15.1$ mC/square mile as obtained from the cumulative deposition data for Bombay (4), $S_e(0) = 9$ mC/square mile and $S_p(0) = 15$ mC/square mile (3), $T_r = 40$ years, $T_e = 5$ years, and $T_p = 1$ year. The value of α for Bombay has been estimated to be 0.737 (discussed later in this paper). The values of S_e

(4) K. G. VOHRA, C. RANGARAJAN and M. C. JAIN: *Measurements on the ground deposition of fission products from nuclear test explosions*, Atomic Energy Establishment Trombay Report number AEET/AM/11 (1959).

(5) W. F. LIBBY: *Proc. of the National Academy of Sciences of U.S.A.*, **45**, no. 7, 959 (1959).

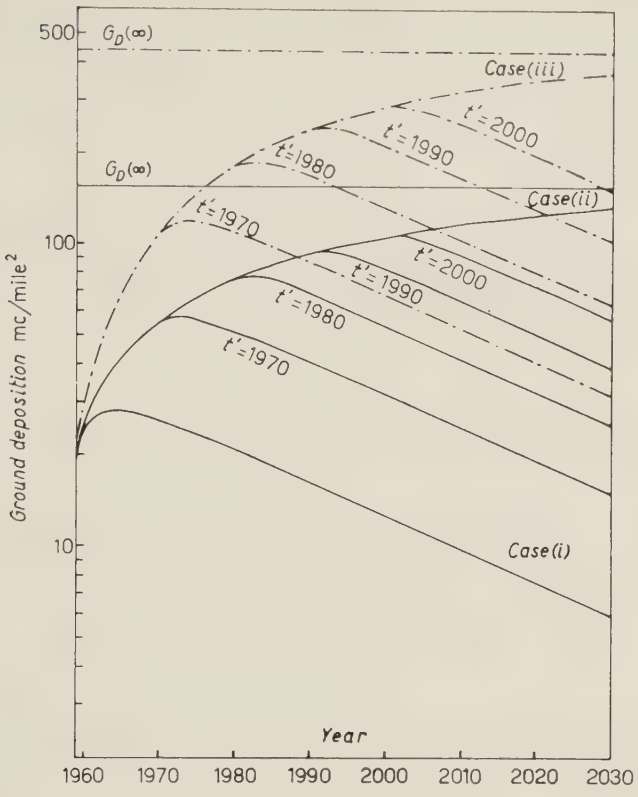

Fig. 1. – Future Levels of Strontium-90. Deposition at Bombay.

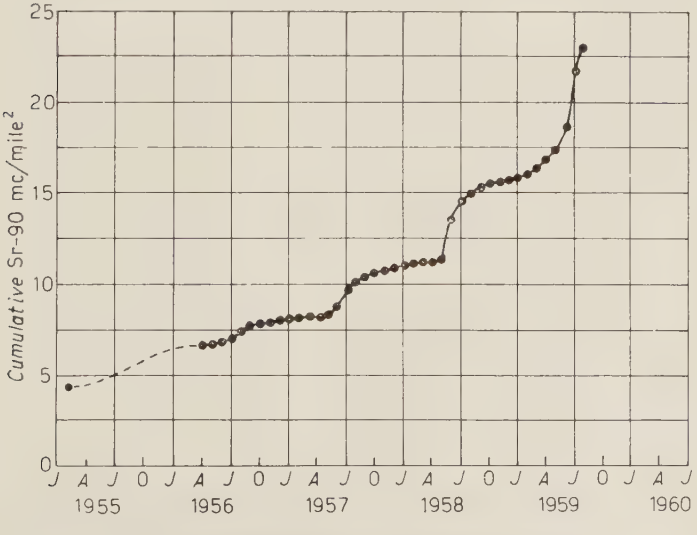

Fig. 2. - Strontium-90 in Bombay fallout.

and S_p in mC/square mile are equivalent to the corresponding values in megatons of fission-power on the assumption that 1 megaton of fission-power gives 0.5 mC/square mile of deposition on the ground if the activity is distributed uniformly over the earth's surface and 1 mC/square mile of deposition if the activity is restricted to one hemisphere only.

The computed future levels of ground deposition are plotted in Fig. 1. Fig. 2 gives the cumulative deposition data for Bombay up to September, 1959. It is interesting to note that the predicted value of $G_d(t)$ for September, 1959 closely agrees with the level shown in Fig. 2; the former value is 22.7 m³/square mile and the latter value is 22.8 m³/square mile.

3. – Case (ii): tests continue at the average rate of past testing.

In this case we assume that strontium-90 is injected into the stratosphere at a constant rate *i.e.* the same average rate as in the past. Let R_e and R_p be the rates of injection at the equatorial and polar regions respectively. We can compute the future levels of cumulative ground deposition from the future equatorial and polar injections by evaluating the following integrals.

$$G_d^e(t) = \int_0^t R_e\left(1 - \exp\left[-\overline{t - t_i}/T_e\right]\right) \exp\left[-\overline{t - t_i}/T_r\right]) \cdot \mathrm{d}t_i \,,$$

$$G_d^p(t) = \int_0^t R_p\left(1 - \exp\left[-\overline{t - t_i}/T_p\right]\right) \exp\left[-t - t_i/T_r\right) \cdot \mathrm{d}t_i \cdot \alpha \,.$$

where: $G_d^e(t)$ is the cumulative ground deposition from the equatorial injections.

$G_d^p(t)$ is the cumulative ground deposition from the polar injections.

$R_e \cdot \mathrm{d}t_i$ gives the amount of strontium-90 injected between time t_i and $(t_i + \mathrm{d}t_i)$, from equatorial tests, and

$R_p \cdot \mathrm{d}t_i$ gives the amount of strontium-90 injected between time t_i and $(t_i + \mathrm{d}t_i)$, from polar tests.

By evaluating the above integrals and substituting the values of T_r, T_e, and T_p we get the following equations.

$$G_d^e(t) = R_e \cdot (40/9)\left\{8 + \exp\left[-t \cdot (9/40)\right] - 9 \exp\left[-t/40\right]\right\},$$

$$G_d^p(t) = R_p \cdot (40/41)\left\{40 + \exp\left[-t \cdot (41/40)\right] - 41 \exp\left[-t/40\right]\right\} \cdot \alpha \,.$$

If we assume $R_e = R_p = R$ (*i.e.* equal injection rates from the equatorial and polar regions).

$$G_d^e(t) + G_d^p(t) = R\{40(\alpha\cdot(40/41) + 8/9) + \alpha\cdot(40/41)\exp[-t\cdot(41/40)] + \\ + (40/9)\exp[-t(9/40)] - 40(\alpha+1)\exp[-t/40]\}.$$

The total ground deposition for case ii) will be given by the sum of the deposition levels from the past tests, future equatorial tests and future polar tests *i.e.*

$$G_D(t) = G_d(t) + G_d^e(t) + G_d^p(t)\,,$$

R for case ii) as estimated from the past testing is 4.75 megatons per year [6] or 2.375 mC/square mile/year and $\alpha = 0.737$. The values of $G_D(t)$ have been calculated for different values of «t» and the future levels for this case are plotted in Fig. 1. The asymptotic value for this case is:

$$G_D(\infty) = 40\,R\,\{\alpha\cdot(40/41) + 8/9\} = 152.7 \text{ mC/square mile}\,.$$

This is the maximum value which will be attained if the tests are continued indefinitely at this rate.

In the above evaluations it is assumed that the activity from the equatorial injections is uniformly distributed all over the world and that from the polar injections shows a non-uniform distribution accounted for by the factor α. The factor α is the ratio of the actual deposition at any latitude less the world-wide deposition level, to the average deposition level in the hemisphere less the world-wide deposition level. The values of 7 mC/square mile and 18 mC/square mile have been used as world-wide average and northern hemisphere average respectively as on 1st October, 1958, given by W. F. Libby. This gives

$$\alpha = \frac{15.1 - 7}{18 - 7} = 0.737\,.$$

This value of α for Bombay seems to be reasonable because Bombay is located at 19° N and one may expect a smaller fraction of fallout from the polar injections to reach this latitude. The value of α may be larger than 1 for higher latitudes.

[6] N. G. Stewart, R. G. D. Osmond, R. N. Croohs and E. M. R. Fisher: *The world-wide deposition of long-lived fission products from nuclear test explosions*, A.E.R.E. Harwell Report no. HP/R/2354 (October, 1957).

4. – Case (iii): **the tests are carried out at the highest rate observed in the past, *i.e.* during 1958.**

The evaluation of future deposition for this case can be done using the formulae derived for case ii), by substituting the value of R for the year 1958, the year of highest testing rate in the past. This value of R is estimated to be 13.75 megatons or 6.825 mC/square mile. The values of $G_D(t)$ have been calculated for $R = 6.825$ mC/square mile per year and different values of «t». The computed future levels for this case are also shown in Fig. 1. The asymptotic value for this case is 438.7 mC/square mile. All the assumptions made in case ii) also apply to this case.

5. – Future levels of ground deposition if tests are stopped at any subsequent time t' after 1st October, 1958, for cases (ii) **and** (iii).

For cases ii) and iii) we have, so far, assumed that the tests will continue to be carried out indefinitely. However, it is also a likely case that the tests are carried out for some years and then stopped at a future date. The ground deposition levels for these cases can be computed as follows. If the tests are stopped at any time t' after 1st October, 1958, the ground deposition levels $G_D(t')$ at time t' are known for cases ii) and iii). Knowing the ground deposition level $G_D(t')$, and equatorial and polar stratospheric reservoirs $S_e(t')$ and $S_p(t')$ respectively, the levels of ground deposition for $t > t'$ can be computed in the same way as for case i). $S_e(t')$ and $S_p(t')$ can be computed using the following equations,

$$S_e(t') = S_e(0) \exp\left[-t' \cdot \overline{T_e + T_r}/T_e T_r\right] + R \cdot T_e T_r/(T_e + T_r) \cdot \cdot \left(1 - \exp\left[-t' \cdot \overline{T_e + T_r}/T_e T_r\right]\right),$$

$$S_p(t') = S_p(0) \exp\left[-t' \cdot \overline{T_p + T_r}/T_p T_r\right] + R \cdot T_p T_r/(T_p + T_r) \cdot \cdot \left(1 - \exp\left[-t' \cdot \overline{T_p + T_r}/T_p T_r\right]\right).$$

In these equations $S_e(0)$, $S_p(0)$ and R are known. The levels of ground deposition corresponding to $S_e(t')$ and $S_p(t')$ for values of $t > t'$ are given by

$$G_d^e(t) = S_e(t')\left(1 - \exp\left[-\overline{t - t'}/T_e\right]\right) \exp\left[-\overline{t - t'}/T_r\right],$$

$$G_d^p(t) = S_p(t')\left(1 - \exp\left[-\overline{t - t'}/T_p\right]\right) \exp\left[-\overline{t - t'}/T_r\right] \cdot \alpha .$$

Therefore $G_D(t)$ for cases ii) and iii) for $t > t'$ is given by

$$G_D(t) = G_D(t') \exp [- t - t'/T_r] + G_d^e(t) + G_d^p(t) .$$

The values of $G_D(t)$ for $t > t'$ for cases ii) and iii) are also plotted in Fig. 1, for four different values of t'.

6. – Discussion.

The prediction of future levels of fallout, whether the tests are stopped or continued, depends on the mechanism by which the fission products from the H-bomb tests are dispersed in the atmosphere and deposited on a world-wide scale. It has been extensively reported that the degree of deposition of fallout shows a sort of latitude dependence, being higher in the northern hemisphere than in the southern hemisphere, minimum at the equator and maximum in the middle latitudes of the northern hemisphere ([6-8]). This latitude dependence has been attributed to the meteorological phenomena of mixing between the stratosphere and the troposphere. Several mechanisms of mixing have been reported *e.g.*, MACHTA ([7]), STEWART ([6]), MARTELL ([9]) and LIBBY ([10]). The patterns of fallout explained by the above authors are applicable only to a general case of world-wide deposition. However, there are several regions of the world which are affected by peculiar meteorological conditions—*e.g.*, the regions influenced by the monsoon winds—which may not fit in the general pattern of world-wide fallout. Therefore the evaluation of future fallout in any region can, probably, be carried out more reliably from a knowledge of the past fallout. In the present evaluation of future fallout at Bombay the past data based on actual measurements has been used in such a way that any peculiar meteorological phenomena affecting the level of deposition is taken care of.

The results of present evaluation support Libby's estimates of stratospheric inventory considering equatorial and polar injections separately, and using different values of residence time for equatorial and polar injections. The present estimates based on these assumptions show that the predicted level

---

([7]) L. MACHTA: *Discussion of meteorological factors and fallout distribution*, U.S.A.E.C. Report no. HASL-42 (October, 1958).

([8]) L. T. ALEXANDER: *Strontium-90 distribution as determined by the analysis of soils, public hearings on fallout from nuclear weapons tests* (May 5-8, 1959), issued by the U. S. Congressional Joint Committee on Atomic Energy.

([9]) E. A. MARTELL: *Science*, **129**, 1197 (1959).

([10]) W. F. LIBBY: *Proc. of the National Academy of Science of U.S.A.*, **42**, 365 (1956).

of deposition for September, 1959 closely agrees with the experimentally estimated value for that period.

The significance of these predicted levels of strontium-90 deposition on soil may be judged by estimating the concentrations of strontium-90 in the bone as a result of soil contamination. Assuming an average of 20 g of available calcium per square foot of soil to a depth of 2.5 inches, 1 mC of strontium-90 deposited per square mile is equivalent to 1.8 μμC strontium-90 per gram of available soil calcium. Therefore multiplication of surface deposition level in mC square mile by 1.8 gives the strontium-90 activity in μμC/g of available soil calcium *i.e.* the specific activity of soil calcium. Multiplication of this by the strontium-90/calcium discrimination ratio from soil to bone should give the average specific activity of calcium deposited in the human bone at equilibrium with the surface deposition level. For case i) the maximum level of ground deposition at Bombay is 28 mC/square mile. This would give about 50 μμC of strontium-90 per gram of soil calcium. Strontium-90/calcium discrimination ratio depends upon several factors such as food habits, nutritional status and metabolic conditions of the people. Strontium-90/calcium discrimination ratio from soil to bone for India, as derived from per capita consumption of principal foodstuffs, is 0.097 ([11]). This would give an equilibrium bone concentration of 4.85 μμC strontium-90 per gram of bone calcium. For cases ii) and iii) the equilibrium bone concentrations are estimated to be 26.45 and 76 μμC strontium-90 per gram of calcium respectively. The maximum permissible concentrations of strontium-90 for large segments of population as fixed by the International Commission on Radiological Protection is 100 μμC strontium-90 per gram of bone calcium, but values as low as 10 μμC strontium-90 per gram of calcium ([12]) and even 1 μμC strontium-90 per gram of calcium have been suggested ([13]).

The above estimates of strontium-90 concentration in the human bone may not be very correct because of the following:

a) The quantities of the available calcium in the different soils may be different from the assumed value of 20 grams per square foot of soil.

b) The discrimination ratio of strontium-90/calcium from soil to human bone may vary with the food habits of different communities.

c) The discrimination ratio of strontium/calcium from soil to human bone assumes that strontium-90 is metabolically similar to calcium, but actually

([11]) W. LANGHAM and E. C. ANDERSON: *Entry of radioactive fallout into the biosphere and man*, U.S.A.E.C. Report no. HASL-42 (October, 1958), p. 293.
([12]) R. E. LAPP: *Science*, **125**, 933 (1957).
([13]) W. O. CASTOR: *Science*, **125**, 1291 (1957).

the metabolism of strontium-90 may be influenced by the abundance of calcium in the different foods [14].

d) Strontium-90 may not be intimately mixed with calcium in the soil and may not become as easily available to the plant as calcium.

There are also other factors which would affect the evaluation of bone content from the deposition data, such as, penetration of strontium-90 into the deeper layers of soil by leaching by rainwater, and direct pick up of strontium-90 by foliar action. The leaching effect will tend to reduce the ultimate deposition in the bone, whereas foliage retention will increase it. Thus, the present estimates may be valid only for a general case.

* * *

Our thanks are due to SHRI A. S. RAO for offering useful suggestions in the preparation of this paper, and to SHRI V. S. BHATNAGAR for taking keen interest in discussions.

([14]) H. A. KORNBERG: *On the passage of pairs of elements through food chains*, U.S.A.E.C. Report no. H.W-60127 (May, 1959).

RIASSUNTO (*)

La valutazione dei futuri livelli di deposizione sul terreno di stronzio 90 è stata fatta in tre differenti ipotesi: (i) dopo l'Ottobre 1958 non si eseguono più prove di armi nucleari; (ii) le prove continuano alla stessa frequenza media come per il passato, e (iii) le prove continuano alla massima frequenza osservata in passato, cioè durante il 1958. Tali calcoli sono stati fatti per Bombay e sono basati sui dati di deposizione al suolo al 1° Ottobre 1958 e a rilevazioni stratosferiche a seguito di iniezioni nelle regioni equatoriali e polari comunicate da Libby. Per il caso (i) il livello massimo di deposizione al suolo sarà di 28 mC/miglio quadrato e sarà raggiunto nel 1963. I livelli massimi di deposizione al suolo pei casi (ii) e (iii) sono rispettivamente 152.7 mC/miglio quadrato e 438 mC/miglio quadrato. Si sono discussi i fattori che mettono in relazione la deposizione al suolo dello stronzio 90 con la sua concentrazione nel tessuto osseo umano, che si è stimata in 4.8, 26.5 e 76 $\mu\mu$C di stronzio 90 per grammo di calcio osseo nei casi (i), (ii) e (iii) rispettivamente.

(*) *Traduzione a cura della Redazione.*

The Conformal Invariance in Quantum Field Theory (*) (**).

J. Wess

Institute for Theoretical Physics, University of Vienna - Vienna

(ricevuto il 18 Luglio 1960)

Summary. — The properties of a conformal invariant quantum field theory are considered. A short discussion of the conformal group in four dimensions and of the topology, introduced into the pseudo-euclidean space by this group is given. With the help of the commutation relations the spectrum of the generators in Hilbert-space is investigated. We find that the only possible discrete eigenvalue of P^2 and of the P^ν's is zero and that the generator for scale transformations S has a continuous spectrum. The eigenfunctions of S in the x-representation are calculated, they form a complete set. The conservation laws valid in an invariant theory and the commutation relations predict a certain form of the conserved quantities expressed in terms of the energy-momentum tensor and of the co-ordinates. For scalar, spinor and vector fields the generators are derived by the action principle of Schwinger.

Introduction.

It is well known that the symmetry properties of a physical system are an important tool. It reduces the mathematical complexity of the system and it also leads to physical consequences, such as conservation laws.

It was shown by E. Noether [1] that in the Lagrangian formalism a conservation law is an immediate consequence of an invariance of the action integral and, on the other hand, the knowledge of a conservation law indicates

(*) Scientific Note no. 6. Contract no. 61(052)-265.

(**) The research reported in this document has been sponsored in part by The United States Government.

(1) E. Noether: *Göttinger Nachrichten* (1918), p. 235.

a certain symmetry of the Lagrangian. But it is not sufficient for the existence of a conservation law that the equations of motion are invariant. *E.g.* in elementary mechanics the equations of motion with a friction force are invariant under time displacement but the Lagrangian is not and no conserved energy exists. Hence we consider the invariance of the action integral to be more important, and therefore we shall use the Lagrangian formalism. The invariance of the equations of motion are an immediate consequence of the invariance of the action integral.

In a quantized theory the conserved quantities are the generators of the symmetry transformation in Hilbert-space. Therefore they have to satisfy the commutation relations valid for the generators. This yields some new information concerning the conserved quantities.

Recently, there was some interest in the conformal group in four dimensions ([2]). It has been known since the work of H. BATEMAN ([3]) that this group is the largest group of space-time transformations which leaves the Maxwell equations invariant. The investigation of the conformal invariance of various systems has been the subject of numerous papers ([4]), and it turned out, that the action integrals in field theory for massless free field are always conform-invariant.

In this paper we shall give a short review of these investigations and the methods used and extend these investigations to quantized systems. Especially we are interested in the spectrums of the generators as there was made some attempt to characterize elementary particles by the eigenvalues of the generator of scale transformations S. It follows directly from the commutation relations that the only possible discrete eigenvalue of $-P^2$ and of the P_ν's is zero. Therefore, we cannot expect that conformal symmetry is realized in nature. For the operator S we find a continuous spectrum in the x-representation and in the one particle subspace of quantum field theory.

Using the Lagrangian formalism of quantum field theory introduced by SCHWINGER it is straightforward to derive the generators in terms of the fields. This will be done for massless scalar, spinor, and vector fields.

In a physical Lagrangian there will be terms such as the mass term, which are not conformal invariant. Nevertheless it may be possible to separate a conformal invariant part which may under certain conditions be the important

([2]) H. P. DÜRR, W. HEISENBERG, H. MITTER, S. SCHLIEDER and K. YAMAZAKI: *Zeits. Naturfor.*, **14a**, 441 (1959).

([3]) H. BATEMAN: *Proc. London Math. Soc.*, **8**, 223 (1910); E. CUNNINGHAM: *Proc. London Math. Soc.*, **8**, 77 (1910).

([4]) E. BESSEL-HAGEN: *Math. Ann.*, **84**, 258 (1921); J. A. MCLENNAN: *Nuovo Cimento*, **3**, 1360 (1956); **5**, 640 (1957); F. GÜRSEY: *Nuovo Cimento*, **3**, 988 (1956); F. BOPP: *Ann. Phys.*, **4**, 96 (1959); P. A. M. DIRAC: *Ann. Math.*, **37**, 429 (1936); W. A. HEPNER: *The group of γ-matrices and the conformal group*, preprint.

part, *e.g.* at high energy the mass term becomes unimportant. In such a case, the knowledge of the conformal symmetry and its consequences may be of some help.

From the point of view of general relativity it may be of some interest to have an example of a quantized field theory which has a larger symmetry group than the Lorentz-group.

1. – The conformal group.

In the four-dimensional, pseudoeuclidean space the conformal group is the group of co-ordinate transformations which leave the relation

$$\mathrm{d}s^2 = (\mathrm{d}x^0)^2 - (\mathrm{d}x^1)^2 - (\mathrm{d}x^2)^2 - (\mathrm{d}x^3)^2 = 0 \tag{1.1}$$

invariant. The group is composed of the full inhomogeneous Lorentz-group, the scale transformations

$$S: \qquad x'^\mu = \lambda x^\mu, \qquad (\lambda \neq 0), \tag{1.2}$$

$$\mathrm{d}s'^2 = \lambda^2 \mathrm{d}s^2 \tag{1.2a}$$

and the inversion [5]

$$I: \qquad x'^\mu = \frac{x^\mu}{x^2}, \qquad x^2 = x_0^2 - \boldsymbol{x}^2, \tag{1.3}$$

$$\mathrm{d}s'^2 = \frac{1}{x^4}\mathrm{d}s^2 . \tag{1.3a}$$

The transformations which consist of an inversion, a translation and an inversion form an Abelian subgroup:

$$A: \qquad x'^\mu = \frac{x^\mu + a^\mu x^2}{1 + 2ax + a^2x^2}, \tag{1.4}$$

$$\mathrm{d}s'^2 = (1 + 2ax + a^2x^2)^{-2}\mathrm{d}s^2 . \tag{1.4a}$$

This subgroup depends on four parameters and is continuously connected with the unit ($a = 0$). It is not hard to prove that all transformations, continuously connected with the unit, can be written as a proper Lorentz-trans-

[5] S. Lie and F. Engel: *Theorie der Transformationsgruppen* (Leipzig, 1893), p. 351.

formation, a scale transformation and a transformation of the Abelian subgroud (1.4). Thus the conformal group is a 15-parameter group. It follows from (4) that the translations are no longer an invariant subgroup.

Space-time reflections and inversion lead to disconnected parts, but it should be noted that time reflection and inversion are continuously connected. This can be shown directly by a continuous path which connects the inversion with the time reflection. But it follows immediately from the isomorphism of the conformal group to a Lorent-group in six dimensions ([6]) and the fact that each such generalized Lorentz-group consists of four parts ([7]). Thus, the whole conformal group has four disconnected parts.

Through the inversion, the light cone is mapped into infinity. As the transformations (1.4) consist of inversion, translation and inversion, again a light cone is mapped onto infinity, of course, the center is displaced from the origin. It follows from (1.4) that

$$1 + 2ax + a^2x^2 = a^2\left(x + \frac{a}{a^2}\right)^2 = 0\,. \tag{1.5}$$

is the equation for this light cone and therefore, the center is at $-a/a^2$.

From the transformation property of x^2,

$$x'^2 = \frac{x^2}{1 + 2ax + a^2x^2}\,, \tag{1.6}$$

follows that the sign of x'^2 is different from the sign of x^2 when $a^2(x+(a/a^2))^2$ is negative. Therefore, a timelike vector can become spacelike and vice versa through these transformations. As $a^2(x+(a/a^2))^2$ changes sign when the point x passes through the above mentioned light cone which is mapped onto infinity, x'^2 can only change its sign by passing through infinity as long as x^2 does not change the sign.

From (1.6) it also follows that points at the light cone transform into points at the light cone, as long as they are finite points in both co-ordinate systems. This is not necessarily true for points which are mapped onto infinity, as can be seen from an example. For all points of the plane $1+2ax = 0$ we have $x'^2 = 1/a^2$, also for the points on the cut with the light cone $x^2 = 0$. Therefore we can speak from an invariant light cone as long as we admit finite points only.

According to (1.4*a*) the sign of ds^2 is invariant. For an infinitesimal distance therefore, spacelike and timelike have an invariant meaning.

([6]) F. Klein: *Gesammelte Mathem. Abhandlungen* (Berlin, 1921).

([7]) H. Boerner: *Darstellungen von Gruppen* (Berlin, 1955), p. 264 ff.

This short discussion of the topology, introduced into the pseudo-euclidean space through the conformal group becomes very clear in two dimensions. In Fig. 1 we plot the x plane and the x' plane. The light cones $x^2 = 0$, $(x - (a/a^2))^2 = 0$ and $x'^2 = 0$, $(x' - (a/a^2))^2 = 0$ cut the planes in 9 parts. Through the numbers I to IX we indicate onto which part of the x' plane each part of the x plane is mapped through the transformation (1.4).

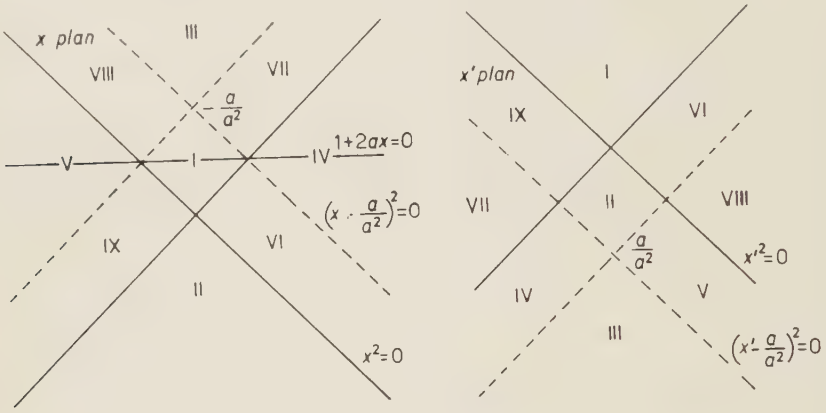

Fig. 1.

In general, a line in the x-plane transforms into a hyperbola, but it follows from

$$(x'-y')^2 = \frac{(x-y)^2}{(1+2ax+a^2x^2)(1+2ay+a^2y^2)}, \tag{1.7}$$

that light paths transform into light paths. The volume element $\mathrm{d}x = \mathrm{d}x^0\,\mathrm{d}x^1\,\mathrm{d}x^2\,\mathrm{d}x^3$ is not invariant ($\sqrt{-g}\,\mathrm{d}x$ is invariant), but

$$S: \qquad \mathrm{d}x = \frac{1}{\lambda^4}\,\mathrm{d}x', \tag{1.3b}$$

$$A: \qquad \mathrm{d}x = (1-2ax'+a^2x'^2)^{-4}\,\mathrm{d}x'. \tag{1.4b}$$

Many interesting questions of a continuous group can be treated already with the help of the infinitesimal transformations, which in our case are

$$\begin{cases} c_\nu P^\nu & : x'^\mu = x^\mu + c^\mu, \\ a_{\mu\nu}M^{\mu\nu} & : x'^\mu = x^\mu + a^\mu_\nu x^\nu, \qquad a_{\mu\nu} = -a_{\nu\mu}, \\ \varepsilon S & : x'^\mu = x^\mu + \varepsilon x^\mu, \\ \alpha_\mu A^\mu & : x'^\mu = x^\mu + \alpha^\mu x^2 - 2x^\mu \alpha x. \end{cases} \tag{1.8}$$

The infinitesimal transformations form a ring, the so called Lie-ring. We shortly indicate the way, how to find the structure constants c^i_{nm} of this ring. The group is parametrized through 15 parameters α^l in a way that the unit element I has the parameters $\alpha^l = 0$ and there is a one to one correspondence between the group elements in the neighbourhood of the unit element and the 15 numbers α^l in the neighbourhood of $\alpha^l = 0$. We simply denote group elements by $\{\alpha^1 \dots \alpha^{15}\}$ $\{\alpha\}$. The parameters γ of the product $\{\alpha\}\{\beta\}$ $\{\gamma\}$ are differentiable functions of the parameters α and β.

We develop these functions and using $I = \{0\}$ we find

$$\gamma^i = \alpha^i + \beta^i + \alpha^i_{nm}\alpha^n\beta^m + \dots . \tag{1.9}$$

The structure constants are defined by

$$c^i_{nm} = a^i_{nm} - a^i_{mn} . \tag{1.10}$$

Now we make use of the fact that our group is a group of transformations of variables x

$$y = \{\alpha\}[x] \tag{1.11}$$

and again we develope in α:

$$y = x + A_i[x]\alpha^i + A_{ik}[x]\alpha^i\alpha^k + \dots . \tag{1.11a}$$

The transformation

$$z = \{\alpha\}\{\beta\}[x] = \{\gamma\}[x] \tag{1.12}$$

gives rise to the identity

$$A_i[x]a^i_{mn}\alpha^n\beta^m = A_i\left[x + A_j[x]\alpha^j\right]\beta^i - A_i[x]\beta^i - A_{ij}[x](\alpha^i\beta^j + \alpha^j\beta^i) . \tag{1.13}$$

Here we used (1.9) and (1.11a).

Eq. (1.13) leads to the formula we need:

$$c^l_{ij}A_l\alpha^j\beta^i = A_i\left[x + A_j[x]\alpha^j\right]\beta^i - A_i[x]\beta^i - \\ - A_j\left[x + A_i[x]\beta^i\right]\alpha^j - A_j[x]\alpha^j . \tag{1.14}$$

For linear transformations (1.14) becomes the well known commutation relation

$$[A_i, A_j]_- = A_iA_j - A_jA_i = c^l_{ij}A_l . \tag{1.15}$$

Now we only to insert the infinitesimal transformations (1.8) into (1.14) to calculate the structure constants. For linear representations, the commutation relations between the generators of the transformations are

$$
\left\{
\begin{aligned}
&[P^\nu, P^\mu]_- &&= 0\,,\\
&[M^{\mu\nu}, M^{\lambda\sigma}]_- &&= f^{\mu\sigma}M^{\nu\lambda} + g^{\nu\lambda}M^{\mu\sigma} - g^{\mu\lambda}M^{\nu\sigma} - g^{\nu\sigma}M^{\mu\lambda}\,,\\
&[M^{\mu\nu}, P^\lambda]_- &&= g^{\nu\lambda}P^\mu - g^{\mu\lambda}P^\nu\,,\\
&[S, P^s]_- &&= P^s\,,\\
&[S, M^{\mu\nu}]_- &&= 0\,,\\
&[A^\mu, A^\nu]_- &&= 0\,,\\
&[A^\mu, P^\nu]_- &&= 2\{M^{\mu\nu} - g^{\mu\nu}S\}\,,\\
&[A^\lambda, M^{\mu\nu}]_- &&= g^{\lambda\mu}A^\nu - g^{\lambda\nu}A^\mu\,,\\
&[A^\lambda, S]_- &&= A^\lambda\,.
\end{aligned}
\right. \tag{1.16}
$$

2. – Representation of the generators in Hilbert-space.

In quantum theory the generators are operators in Hilbert-space. The P^ν's are the energy-momentum operators and the $M^{\mu\nu}$'s the operators of angular momentum. Recently, there was made some attempt to identify the generator S with a leptonic number operator ([2]).

We shall draw some conclusions from the commutation relations (16) for these operators. We assume that in a reasonable theory the P_ν's are hermitian operators and therefore can be brought into diagonal form. We further assume that $P^2 = P^\nu P_\nu$ has discrete eigenvalues μ_i and a continuos range of eigenvalues λ. The corresponding eigenvectors $|\ \rangle$ should be normalized in the sense that

$$
\langle \mu_i \mu_k \rangle = \delta_{ik}\,, \qquad \langle \lambda\lambda' \rangle = \delta(\lambda - \lambda')\,, \qquad \langle \mu_i\, \lambda \rangle = 0\,. \tag{2.1}
$$

From

$$
[S, P^2]_- = 2P^2 \tag{2.2}
$$

follows that S and P cannot be both diagonal. Therefore the vector $S|\mu_i\rangle$ is a linear combination of other eigenvectors:

$$
S|\mu_i\rangle = \sum_e c_{ie}|\mu_e\rangle + \int \mathrm{d}\lambda\, c_{i\lambda}|\lambda\rangle\,. \tag{2.3}
$$

With the help of (1.2) and (2.3) eq. (2.2) becomes for matrix elements between two eigenvectors of the discrete spectrum

$$c_{rs}(\mu_r - \mu_s) = 2\mu_s \delta_{rs} . \tag{2.2a}$$

We find that $c_{rs} = 0$ for $r \neq s$ and that $\mu_s \neq 0$. The only possible discrete eigenvalue of P^2 is zero. The rest of the spectrum has a continuous range only. For matrix elements in the continuous range eq. (2.2) becomes

$$(\lambda - \lambda')c_{\lambda\lambda'} = 2\lambda\,\delta(\lambda - \lambda') \tag{2.2b}$$

and has the solution $c_{\lambda\lambda'} = -2\lambda(\mathrm{d}/\mathrm{d}\lambda)\,\delta(\lambda - \lambda')$.

The same applies to the commutator $[SP^\nu] = P^\nu$.

In the next sections where we discuss scalar, spinor, and vector fields, we shall derive the generators by the action principle of Schwinger. We expect that they are of the form

$$T = \int_\sigma \mathrm{d}\sigma_\nu T^\nu(x) , \tag{2.4}$$

and the conservation law

$$\frac{\partial}{\partial x_\nu} T^\nu(x) = 0 , \tag{2.4a}$$

to be satisfied if the theory is invariant against the transformation generated by T. Hence T is independent of the surface σ and for practical purposes we can take a surface $t = \text{const.}$

$$T = \int_{t=\text{const.}} \mathrm{d}^3x\, T^0(x) . \tag{2.4b}$$

In the Heisenberg picture the time dependence of an operator is given by

$$\frac{\mathrm{d}T}{\mathrm{d}t} = i[H, T]_- + \frac{\partial T}{\partial t} , \tag{2.5}$$

where $H = P^0 = \int \mathrm{d}^3x\, \theta^{00}(x)$, ($\theta^{\mu\nu}$ is the energy-momentum tensor) and $\partial T/\partial t = 0$ only if T does not depend on the time explicitly. For the generators of the conformal group we know the commutators $[H, T]_-$, (see eq. (1.16)), and the conservation law $\mathrm{d}T/\mathrm{d}t = 0$ is a consequence of (2.4a). Thus, in the case of $T = S$ eq. (2.5) becomes

$$iH + \frac{\partial S}{\partial t} = i\int \mathrm{d}^3x\, \theta^{00}(x) + \frac{\partial}{\partial t}\int \mathrm{d}^3x\, S^0(x) = 0 . \tag{2.5a}$$

Therefore, the part of S which depends explicitly on the time has to be of the form

$$-i\int \mathrm{d}^3x\ \theta^{00}(x)t\,.$$

From reasons of Lorentz invariance we conclude that, apart from terms which do not contribute to the surface integral

$$S^\nu(x) = -i\left[\theta^{\nu\varrho}(x)x_\varrho + \tilde{S}^\nu(x)\right], \tag{2.6}$$

where $\tilde{S}^\nu(x)$ depends on the x^ν's only via the fields.

With the same method we find that for the generators A^μ we have to expect:

$$A^{\mu\varrho}(x) = (g^{\mu\nu}x^2 - 2x^\mu x^\nu)\theta^\varrho_\nu(x) - 2x^\mu\,\tilde{S}^\varrho(x) + \tilde{A}^{\mu\varrho}(x)\,. \tag{2.7}$$

We shall see that the form of the generators derived by the action principle actually agrees with (2.6) and (2.7).

For a point particle with velocity of light ($c = 1$) we write the classical energy momentum tensor:

$$\theta^{\mu\nu}(x) = mn^\mu n^\nu\int \mathrm{d}t\,\delta(x - a - nt)\,, \tag{2.8}$$

where $n^2 = 0$, $\delta(x - a - nt)$ is a four dimensional δ-function and m is the mass of the particle. With this tensor it is easy to verify that the conservation law (2.4a) holds for the quantities

$$\begin{cases} S^\nu &= x_\nu\theta^{\mu\nu}\,, \\ A^{\mu s} &= (g^{\mu\nu}x^2 - 2x^\mu x^\nu)\theta^s_\nu\,. \end{cases} \tag{2.9}$$

In this case $\tilde{S} = \tilde{A} = 0$.

We can evaluate the quantities S and A^μ and we get

$$\begin{cases} S &= a_\nu P^\nu\,, \\ A^\mu &= P^\mu a^2 - 2a^\mu a_\nu P^\nu\,, \end{cases} \tag{2.9a}$$

a^μ is the space time co-ordinate of the particle in any co-ordinate system. If we choose a system with the x^1 axis in the direction of motion, the S and A^μ's allow a simple interpretation. As $P^2 = 0$ they have the form $S = E(a^0 - a^1)$ and $A^0 = -E(a^0 - a^1)^2$, $A^1 = E(a^0 - a^1)^2$ and they are obviously conserved for a light path where $a^1 = a^0 + \text{const}$.

2'1. *Spectrum of the operator S.* – In quantum mechanics the classical quantities (2.9) become operators. In the x-representation at the time $t = 0$ the scale transformation operator is represented by

$$\boldsymbol{xp} = -i\boldsymbol{x}\nabla = -ir\frac{\partial}{\partial r}. \tag{2.10}$$

This operator is not hermitean but we find by partial integration

$$-i\int \mathrm{d}\Omega \int_0^\infty \mathrm{d}r r^2 \psi^* r \frac{\partial}{\partial r}\psi = i\int \mathrm{d}\Omega \int_0^\infty \mathrm{d}r\, r^2 \psi \left\{ r\frac{\partial}{\partial r} + 3 \right\} \psi^* . \tag{2.11}$$

Therefore the operator

$$S = -i\left\{ r\frac{\partial}{\partial r} + \frac{3}{2} \right\}, \tag{2.12}$$

is hermitean and satisfies the correct commutation relations. The eigenfunctions of S to the eigenvalue s are

$$u_s(r) = \frac{1}{\sqrt{2\pi}}\frac{1}{\sqrt{r^3}} \exp\left[is \ln r\right]. \tag{2.13}$$

They are orthonormal and complete in the sense that

$$\begin{cases} \displaystyle\int_0^\infty u_{s'}^*(r)\, u_s(r)\, r^2\, \mathrm{d}r = \delta(s - s'), \\ \displaystyle\int_{-\infty}^{\infty} u_s^*(r')\, u_s(r)\, \mathrm{d}s = \frac{1}{r^2}\delta(r - r'). \end{cases} \tag{2.14}$$

The range of s is the range of all real numbers.

The unitary operator corresponding to a finite scale transformation is obtained from S by integration:

$$U = \exp\left[\lambda \left\{ \frac{3}{2} + r\frac{\partial}{\partial r} \right\} \right]. \tag{2.15}$$

It is readily shown that

$$\exp\left[\lambda \left\{ \frac{3}{2} + r\frac{\partial}{\partial r} \right\} \right] f(r) = \exp\left[\frac{3}{2}\lambda \right] f(r e^{\lambda}), \tag{2.16}$$

and that U is a unitary operator.

In quantum field theory certain commutation relations exist between the field operator and the generator S. In the next section we will find this commutators for scalar, spinor, and vector fields. For a spinor field they are (*)

$$-i[S, \psi] = \frac{3}{2}\psi + x_\nu \frac{\partial}{\partial x_\nu}\psi \,. \tag{2.17}$$

In the one-particle subspace there are states of the form

$$\int_{t=0} \mathrm{d}^3x\, u_s(\boldsymbol{x})\psi^*|0\rangle = |s\rangle \,, \tag{2.18}$$

where $u_s(\boldsymbol{x})$ are eigenfunctions of the operator (2.12) and $|0\rangle$ is the vacuum state. By the use of the invariance of the vacuum state against scale transformations from (2.17) and (2.18) follows

$$S|s\rangle = \int_{t=0} \mathrm{d}^3x\, u_s(\boldsymbol{x})[S\psi^*]_-|0\rangle = i\int_{x=0} \mathrm{d}^3x\, u_s(\boldsymbol{x})\left\{\frac{3}{2} + \frac{r}{\partial r}\right\}\psi^*(x)|0\rangle \,. \tag{2.19}$$

By partial integration we find

$$S|s\rangle = s|s) \,. \tag{2.20}$$

Thus we see that already in the one particle subspace the spectrum of the operator S is continuous and has the range of all real numbers.

2·2. *Transformation property of the D function.* – To prove the invariance of field commutators we shall need the transformation properties of the function

$$D(x) = \frac{1}{2\pi}\varepsilon(x^0)\,\delta(x^2) \,. \tag{2.21}$$

We have ween that the light cone is invariant as long as x and x' are finite points. If we consider only such points we find

$$\delta(x'^2) = \delta\left(\frac{x^2}{1 + 2ax + a^2x^2}\right) = |1 + 2ax + a^2x^2|\,\delta(x^2) \,. \tag{2.22}$$

For points on the light cone the sign of x'^0 is

$$\varepsilon(x'^0) = \frac{|x'^0|}{x'^0} = \frac{|x^0|(1 + 2ax + a^2x^2)}{x^0|1 + 2ax + a^2x^2|} \,. \tag{2.23}$$

(*) These are the commutation relations used by W. HEISENBERG (2).

Finally we get

$$D(x') = (1 + 2ax + a^2x^2)\, D(x)\,. \tag{2.24}$$

In the same way, using (1.7) we find

$$D(x'-y') = (1 + 2ax + a^2x^2)(1 + 2ay + a^2y^2)\, D(x-y)\,. \tag{2.24a}$$

That we can restrict ourselves to finite points becomes clear when we understand $D(x)$ as a distribution in the sense of L. SCHWARZ, *i.e.* we have to consider the functional

$$D(f) = \int D(x) f(x)\, \mathrm{d}x\,, \tag{2.25}$$

where the testing function $f(x)$ goes to zero, when x goes to infinity.

We transform (2.15) into the new co-ordinate system

$$D(f) = \int D(x') \frac{f'(x')}{(1 - 2ax' + a^2x'^2)^3}\, \mathrm{d}x'\,. \tag{2.25a}$$

We made use of (1.4*b*) and (2.24). As $f'(x') \equiv f(x)$ it has a finite value when x' goes to infinity, therefore $f'(x')(1 - 2ax' + a^2x'^2)^{-3}$, the new testing function goes to zero for $x' \to \infty$.

For scale transformations we had

$$D(x'-y') = \frac{1}{\lambda^2}\, D(x-y)\,. \tag{2.24b}$$

Under the infinitesimal transformations $\mathrm{d}x^\mu$ and $\partial/\partial x^\mu$ transforms like

$$\mathrm{d}x'^\mu = (1 + \varepsilon - 2\alpha x)\, \mathrm{d}x^\mu + 2(x_s d^\mu - x^\mu \alpha_s)\, \mathrm{d}x^s\,, \tag{2.26a}$$

$$\frac{\partial}{\partial x'_\mu} = (1 - \varepsilon + 2\alpha x) \frac{\partial}{\partial x_\mu} + 2(x^s\alpha^\mu - x^\mu\alpha^s) \frac{\partial}{\partial x^s}\,. \tag{2.26b}$$

Taking into account the fact, that $D(x-y)$ is a function of $(x^\nu - y^\nu)$ we find with (2.26*b*)

$$\frac{\partial}{\partial y'_\mu} D(x'-y') = (1 + 3\alpha x + 3\alpha y) \frac{\partial}{\partial y_\mu} D(x-y) + \\ - [x''(x_s + y_s) - \alpha_s(x'' + y'')] \frac{\partial}{\partial y_s} D(x-y)\,. \tag{2.27}$$

To discuss the invariance properties of the Lagrangian formalism, we have to define the transformation properties of the fields involved. When we deal with scalar, spinor, or vector fields, the transformation properties are defined for the Lorentz-group. We shall see that they can be defined also for the transformations (2) and (4) in such a way, that the usual action integral is invariant. As a consequence, the field equations are invariant and we can write down the conservation laws.

If, in the quantized theory, the commutation relations are invariant too. we can expect, that the representation of the fields and the transformed fields are equivalent; *i.e.*, the fields are correlated by an unitary transformation and the action principle of Schwinger furnishes us with the generators of these transformations in terms of the fields. For these generators the commutation relations (6) must be satisfied, using the commutation relations for the fields. However, the question as to whether or not these generators can be integrated to the unitary transformations in Hilbert-space is still open.

3. – For a scalar field we define

$$\text{(3.1)} \qquad \begin{cases} S: & \varphi'(x') = \frac{1}{\lambda}\varphi(x)\,, \\ I: & \varphi'(x') = x^2\varphi(x)\,. \end{cases}$$

From the scalar character of the field follows:

$$\text{(3.2)} \qquad A: \quad \varphi'(x') = (1 + 2ax + a^2x^2)\,\varphi(x)\,,$$

of course, this transformation has the group properties. With (1.3*b*), (1.4*b*) and (2.26*b*) it is easy to verify, that the action integral

$$\text{(3.3)} \qquad W = \frac{1}{2}\int \mathrm{d}x\,\varphi_{,\mu}\varphi'^{\mu}\,,$$

is invariant up to a divergence under the infinitesimal transformations

$$\text{(3.4)} \qquad \delta W = \frac{1}{2}\int \mathrm{d}x'\,\varphi'_{,\mu}\,\varphi'^{,\mu} - \frac{1}{2}\int \mathrm{d}x\,\varphi_{,\mu}\varphi^{\mu} = \int \mathrm{d}x\,\frac{\partial}{\partial x_\mu}\,(\alpha_\mu\varphi^2)\,.$$

This is sufficient for the invariance of the field-equations and for the existence of conservation laws, which we derive now [1].

In general, the variation of the action integral $W = \int \mathscr{L}\,\mathrm{d}x$ under an infinitesimal variation

$$\text{(3.5)} \qquad \begin{cases} x' = x + \Delta x\,, \\ \varphi'(x') = \varphi(x) + \Delta\varphi\,, \end{cases}$$

turns out to be

$$\text{(3.6)} \qquad \delta\int \mathscr{L}\,\mathrm{d}x = \int \mathrm{d}x \left(\frac{\partial \mathscr{L}}{\partial \varphi} - \frac{\partial}{\partial x_s}\frac{\partial \mathscr{L}}{\partial \varphi_{,s}}\right)\delta\varphi + \\ + \int \frac{\partial}{\partial x_s}\left[\frac{\partial \mathscr{L}}{\partial \varphi_{,s}}\Delta\varphi + \left(g_{sv}\mathscr{L} - \frac{\partial \mathscr{L}}{\partial \varphi_{,s}}\varphi_v\right)\Delta x_v\right]\mathrm{d}x\,,$$

if $\mathscr{L}$ contains only the first derivations of φ. Thus, if the fields satisfy the field equations, the variation is expressible through a divergence. If now W is invariant under (3.5), then the variation (3.6) has to vanish; if W is invariant up to a divergence, such as (3.4), then the variation (3.6) is equal to this divergence; in both cases we obtain an identity, expressible as a divergence, this is a continuity equation.

For a scalar field, the divergence of (3.6) becomes (*)

$$\text{(3.7)} \qquad \frac{\partial}{\partial x_s}\left(\varphi_{,s}\Delta\varphi - \theta^v_s \Delta x_v\right).$$

With the help of the field equations it is readily verified, that eq. (2.4) holds for the quantities

$$\text{(3.8)} \qquad S_s = -\varphi\varphi_{,s} - x^v\theta_{vs}\,,$$

$$\text{(3.8)} \qquad A_{sv} = 2x_v\varphi\varphi_{,s} - g_{sv}\varphi^2 + (2x^\mu x_v - g^\mu_v x^2)T_{s\mu}\,.$$

The field commutator

$$\text{(3.9)} \qquad [\varphi(x), \varphi(y)]_- = -\,i\,D(x-y)$$

turns out to be invariant. From (2.3) and (2.24*a*) follows

$$\text{(3.9}a\text{)} \qquad [\varphi'(x), \varphi'(y')]_- = \\ = (1 + 2ax + a^2x^2)(1 + 2ay + a^2y^2)\,[\varphi(x), \varphi(y)]_- = -\,i\,D(x'-y')\,.$$

For scale transformations it is obvious.

(*) $\theta^{\mu v} = \varphi^{,\mu}\varphi^{,v} - \frac{1}{2}g^{\mu v}\varphi^{,\lambda}\varphi_{,\lambda}\,.$

From the action principle we learn that the generators of the transformations in Hilbert-space are

$$\left\{\begin{array}{l} S = \int \mathrm{d}\sigma^s S_s \,, \\ A_v = \int \mathrm{d}\sigma^s A_{sv} \,. \end{array}\right. \tag{3.10}$$

The integrals are independent of the surface. This was the reason why we added te term φ^2 in A_v. This term does not occur in (3.6) but it commutes with φ on space-like surfaces and makes A_v independent of the surface. For space-like surfaces it is easy to verify that

$$\left\{\begin{array}{l} i\,[S,\, \varphi(x)] \;\; = \delta\varphi = \Delta\varphi - x^v \varphi_{,v} \,, \\ i\,[A_v,\, \varphi(x)] = \delta\varphi \,. \end{array}\right. \tag{3.11}$$

As a consequence of (3.11) the generators satisfy the commutation relations (1.16).

4. – For a Weyl-field we define

$$\psi'(x') = \mathrm{Det}\,(F^{-1})\, F^{-1}\, \psi(x) \,, \tag{4.1}$$

where F is the matrix defined by

$$F^{+}\sigma^v F\, \mathrm{d}x_v = \sigma^v\, \mathrm{d}x'_v \,, \tag{4.2}$$

σ^0 is the unit matrix, σ^1, σ^2, σ^3 are the Pauli matrices in the usual representation and $\mathrm{d}x'$ is related to $\mathrm{d}x$ through (2.26a). In case of the scale transformation F is obviously $\lambda^{\frac{1}{2}}$ and we have

$$S\colon \qquad \psi'(x') = \lambda^{-\frac{3}{2}} \psi(x) \,. \tag{4.3}$$

To find the matrix F for the transformation (1.4) we make use of the relation

$$(x_v \sigma^v)(x_\mu \overline{\sigma}^\mu) = x^2 = \mathrm{Det}\,(x_v \sigma^v) \,, \tag{4.4}$$

where $\overline{\sigma}^v$ are the conjugates of σ^v: $\overline{\sigma}^0 = \sigma^0$, $\overline{\sigma}^i = -\sigma^i$.

Eq. (4.4) can also be written in the form

$$(4.4a) \qquad (x_\nu \bar{\sigma}^\nu)^{-1} = \frac{1}{x^2} x_\nu \sigma^\nu ,$$

and leads to the identity

$$(4.5) \qquad \begin{cases} I: & (x'_\nu \sigma^\nu) = \dfrac{x_\nu}{x^2} \sigma^\nu = (x_\nu \bar{\sigma}^\nu)^{-1} , \\ P: & (x'_\nu \sigma^\nu) = (x_\nu + e_\nu) \sigma^\nu = x_\nu \sigma^\nu + e_\nu \sigma^\nu . \end{cases}$$

For the transformation $A = IPI$ it follows

$$(4.6) \qquad \begin{cases} A: & (x'_\nu \sigma^\nu) = \dfrac{(x_\nu + a_\nu x^2)\, \sigma^\nu}{1 + 2ax + a^2 x^2} = \overline{\left[(x_\nu \bar{\sigma}^\nu)^{-1} + (a_\nu \sigma^\nu)\right]^{-1}} . \\ & x'_\nu \sigma^\nu \ = \left[(x_\nu \sigma^\nu)^{-1} + a_\nu \bar{\sigma}^\nu\right]^{-1} . \end{cases}$$

Now we use $\mathrm{d}M^{-1} = -M^{-1}\mathrm{d}M\, M^{-1}$ and calculate $\mathrm{d}x'_\nu \sigma^\nu$:

$$(4.7) \qquad \mathrm{d}x'_\nu \sigma^\nu = \left[(x_\nu \sigma^\nu)^{-1} + (a_\nu \bar{\sigma}^\nu)\right]^{-1} [x_\nu \sigma^\nu]^{-1} (\sigma^\mu \mathrm{d}x_\mu) [x_\nu \sigma^\nu]^{-1} \left[(x_\nu \sigma^\nu)^{-1} + (a_\nu \bar{\sigma}^\nu)\right]^{-1} .$$

Comparing this with (4.2) shows that

$$(4.8) \qquad F = [x_\nu \sigma^\nu]^{-1} \left[(x_\nu \sigma^\nu)^{-1} + (a_\nu \bar{\sigma}^\nu)\right]^{-1} = \frac{1 + x_\nu a_\mu \bar{\sigma}^\nu \sigma^\mu}{1 + 2ax + a^2 x^2} .$$

According to (4.1) we have to define

$$(3.9) \qquad A: \quad \psi'(x') = (1 + 2ax + a^2 x^2)(1 + a_\nu x_\mu \bar{\sigma}^\nu \sigma^\mu)\, \psi(x) ,$$

that becomes for the infinitesimal transformations

$$(4.9a) \qquad A: \quad \psi'(x') = (1 + 2\alpha x + \alpha_\nu x_\mu \bar{\sigma}^\nu \sigma^\mu)\, \psi(x) .$$

The action integral

$$(4.10) \qquad W = \frac{1}{i} \int \psi^+(x) \sigma^\nu \frac{\partial}{\partial x^\nu} \psi(x)\, \mathrm{d}x$$

is invariant against scale transformations. For the transformations (1.4) it need some calculation to prove it.

We note that

$$(4.11) \qquad \sigma^\varrho \frac{\partial}{\partial x^\varrho} (1 - 2\alpha x - \alpha_\nu x_\mu \bar{\sigma}^\nu \sigma^\mu) = 0 ,$$

and therefore we get

$$\psi^{+}(x)\sigma^{v}\frac{\partial}{\partial x^{v}}\psi(x) = (\mathrm{Det}\ F)^{2}\psi^{+\prime}(x')F^{+}\sigma^{v}F\frac{\partial}{\partial x^{v}}\psi'(x')\,. \tag{4.12}$$

From (2.26a), (2.26b) and (4.2) follows

$$F^{+}\sigma^{v}F\frac{\partial}{\partial x^{v}} = (1-4\alpha x)\,\sigma^{v}\frac{\partial}{\partial x'^{v}}\,, \tag{4.13}$$

and from (1.4b) and $(\mathrm{Det}\ F)^{2} = (1-4\alpha x)$ follows the invariance of the action integral and consequently the invariance of the field equations.

For the Lagrangian (4.10) the divergence of (3.6) becomes

$$\frac{\partial}{\partial x_{\varrho}}\left\{\frac{1}{i}\psi^{+}\sigma^{\varrho}\Delta\psi + T^{\varrho}_{v}\Delta x^{v}\right\}, \tag{4.14}$$

where

$$T_{\mu v} = -\frac{1}{i}\psi^{+}\sigma^{\mu}\psi_{,v} \qquad \text{and} \qquad J^{\varrho} = \psi^{+}\sigma^{\varrho}\psi\,.$$

From the invariance of W follows a continuity equation for the quantities

$$\begin{cases} S^{s} = \dfrac{3}{2}iJ^{s} + T^{s}_{v}x^{v}, \\ A^{s}_{v} = \dfrac{2}{i}J^{s}x_{v} + T^{s}_{\mu}(g^{\mu}_{v}x^{2} - 2x^{\mu}x_{v}) + \dfrac{1}{i}\psi^{+}\sigma^{s}\bar{\sigma}^{v}\sigma^{\mu}\psi x_{\mu}\,. \end{cases} \tag{4.15}$$

With the help of the symmetric energy momentum tensor $\theta_{\mu v}$

$$\theta_{\mu v} = -\frac{1}{4i}\{\psi^{+}\sigma_{\mu}\psi_{,v} + \psi^{+}\sigma_{v}\psi_{,\mu} - \psi^{+}_{,v}\sigma_{\mu}\psi - \psi^{+}_{,\mu}\sigma_{v}\psi\} \tag{4.16}$$

the conserved quantities can be brought into a much simpler form. It is well known that the tensor $\theta_{\mu v}$ is obtained from the tensor $T_{\mu v}$ by adding a divergence

$$\theta_{\mu v} = T_{\mu v} + \frac{\partial}{\partial x_{s}}G_{s\mu v}\,, \tag{4.17}$$

where

$$G^{s\mu v} = \tfrac{1}{2}(H^{s\mu v} + H^{\mu v s} + H^{v\mu s})$$

and

$$H^{s\mu\nu} = \frac{i}{4}\psi^{+}\sigma^{s}(\bar{\sigma}^{\mu}\sigma^{\nu} - \bar{\sigma}^{\nu}\sigma^{\mu})\psi = -H^{s\nu\mu}.$$

For a function $f_{\nu}(x)$ which vanishes sufficiently at infinity the integral

$$\int \mathrm{d}\sigma_{\mu} \frac{\partial}{\partial x^{s}} (G^{s\mu\nu} f_{\nu}(x)) = 0 , \tag{4.18}$$

vanishes as a consequence of $G^{\varrho\mu\nu} = -G^{\mu\varrho\nu}$. Therefore

$$\int \mathrm{d}\sigma_{\mu}\theta^{\mu\nu} = \int \mathrm{d}\sigma_{\mu} T^{\mu\nu} . \tag{4.19}$$

If we add $(\partial/\partial x_{\varrho})(G_{\varrho\mu\nu}\Delta x^{\nu})$ to the quantities (4.15) we get in both cases $\theta^{\mu\nu}\Delta x_{\nu}$ and from (4.18) follows

$$S = \int \mathrm{d}\sigma_{s} S^{s} = \int \mathrm{d}\sigma_{s}\theta^{s\nu}x_{\nu} ,$$

$$A^{\mu} = \int \mathrm{d}\sigma_{s} A^{\varrho\mu} = \int \mathrm{d}\sigma_{\varrho}\theta^{\varrho\nu}(g^{\mu}_{\nu}x^{2} - 2x_{\nu}x^{\mu}) . \tag{4.20}$$

This form agrees with (2.6) and (2.7) and remembering that $\theta^{s\mu}$ is symmetric and has a vanishing trace it is easy to verify that eq. (2.4) is valid.

The field commutators

$$\begin{cases} [\psi(x), \psi(y)]_{+} = 0 , \\ [\psi(x), \psi^{+}(y)]_{+} = \bar{\sigma}^{\mu} \dfrac{\partial}{\partial y^{\mu}} D(x - y) , \end{cases} \tag{4.21}$$

are invariant. The action principle leads to the generators in Hilbert-space and it is readily shown that

$$i\left[\int \mathrm{d}\sigma_{s}\theta^{s\nu}\Delta y_{\nu}, \psi(x)\right]_{-} = \delta\psi . \tag{4.22}$$

The current $J^{s}(x)$ transforms under (1.4) like

$$J^{s'}(x') = (1 + 6\alpha x)J^{s}(x) + 2(x_{\mu}\alpha^{s} - x^{s}\alpha_{\mu})J^{\mu}(x) \tag{4.23}$$

and therefore $\int \mathrm{d}\sigma_{s} J^{s}(x)$ is invariant. It is also easily seen for scale transformations.

5. – The Maxwell equations are invariant, when the *vector field* $a^{\nu}(x)$ transform contravariantly. From (2.26*b*) follows for the infinitesimal transformations

$$\begin{cases} a^{\nu'}(x') = (1 + 2\alpha x)\, a^{\nu}(x) + 2(x_{\varrho}\alpha^{\nu} - x^{\nu}\alpha_{\varrho})\, a^{\varrho}(x)\,, \\ a^{\nu'}(x') = (1 - \varepsilon)\, a^{\nu}(x)\,. \end{cases} \tag{5.1a}$$

With this definition, the action integral

$$L = -\frac{1}{4}\int \mathrm{d}x (a_{\nu,\mu} - a_{\mu,\nu})^2\,, \tag{5.2}$$

is invariant, and therefore the Maxwell equations are invariant. However the Lorentz condition

$$\frac{\partial}{\partial x_{\nu}}\, a_{\nu}(x) = 0\,, \tag{5.3}$$

is not invariant under (5.1) for we find

$$\frac{\partial}{\partial x'_{\nu}}\, a'_{\nu}(x') = -\,4\alpha_{s} a^{s}(x)\,. \tag{5.4}$$

Therefore, the transformation (5.1) has to be completed by a gauge transformation: it should be noted that this gauge transformation depends on the field $a_{\nu}(x)$.

As a consequence, the variation of the action integral

$$L = -\frac{1}{2}\int a_{\nu,\mu} a^{\nu,\mu}\, \mathrm{d}x \tag{5.5}$$

can not be zero under the variation (5.1), but turns out to be

$$-\frac{1}{2}\delta\int a_{\nu,\mu} a^{\nu,\mu}\, \mathrm{d}x = -\int \mathrm{d}x \left\{ \frac{\partial}{\partial x_{\mu}} (a_{\nu} a^{\nu} \alpha_{\mu} + 2\alpha_{\nu} a^{\nu} a_{\mu}) - 4 a^{\nu}_{,\nu}\, a^{\sigma}\alpha_{\sigma} \right\}. \tag{5.6}$$

We find that the expectation value of the variation, taken for states which obey the Lorentz-condition, is invariant up to a divergence. This is not sufficient to prove the invariance of the equations of motion, but it is sufficient to derive a conservation law which is satisfied for the expectation values.

By a direct procedure we get from (3.6), (5.1), (5.1a), (5.6) (*)

$$A_{\varrho\mu}\alpha^{\mu} = T_{\varrho v}\Delta x^{v} - 2\alpha x a_{\lambda,\varrho}a^{\lambda} + \alpha_{\varrho}a_{v}a^{v} + 2a_{\varrho}a^{v}\alpha_{v} - 2(x^{\lambda}\alpha^{\sigma} - x^{\sigma}\alpha^{\lambda})a_{\sigma,\varrho}a_{\lambda}\,, \tag{5.7}$$

$$S_{\varrho} = a_{v,\varrho}a^{v} + T_{\varrho v}x^{v}\,.$$

It is easy to verify that $(\partial/\partial x_s)S_s$ is zero and that the expectation value of $(\partial/\partial x_s)A_s(x)$ is also zero.

We can write the conserved quantities in a different and more convenient form

$$\begin{cases} \widetilde{A}_{\varrho}(x) = \theta_{\varrho v}\Delta x^{v}\,, \\ \widetilde{S}_{\varrho}(x) = \theta_{\varrho v}x^{v}\,. \end{cases} \tag{5.7a}$$

Again, the expectation values of $(\partial/\partial x_s)\widetilde{A}_s(x)$ is zero.

Therefore, the integrals: $\int S_{\varrho}\,\mathrm{d}\sigma^{\varrho}$, $\int \widetilde{S}_s\,\mathrm{d}\sigma^{s}$ and the expectation values of the integrals $\int A_s\,\mathrm{d}\sigma^{s}$, $\int \widetilde{A}_s\,\mathrm{d}\sigma^{s}$ are independent of the surface and we can evaluate them for a plane $x^0 = \text{const}$. Disregarding terms, which are space divergences one finds for the expectation values,

$$\begin{cases} \left\langle \int S_s\,\mathrm{d}\sigma^{s} \right\rangle = \left\langle \int \widetilde{S}_s\,\mathrm{d}\sigma^{s} \right\rangle, \\ \left\langle \int A_s\,\mathrm{d}\sigma^{s} \right\rangle = \left\langle \int \widetilde{A}_s\,\mathrm{d}\sigma^{s} \right\rangle. \end{cases} \tag{5.8}$$

As the equations of motion derived from (5.15) are not invariant under (5.1) we cannot expect that the commutators

$$\begin{cases} [a_v(x),\, a_\mu(y)] = ig_{v\mu}D(x-y)\,, \\ [a_{v,\lambda}(x),\, a_\mu(y)] = ig_{v\mu}\dfrac{\partial}{\partial x^{\lambda}}D(x-y)\,, \end{cases} \tag{5.9}$$

are invariant. But using (2.24a), (2.27) and (5.1) one verifies that they are invariant for x, y space-like. Therefore, if the transformation (5.1) is completed by a gauge transformation, the commutators are invariant for all x and y.

For the scale transformations the field commutators are invariant. The operator $\int_{\sigma}\mathrm{d}\sigma^{s}\,S_s$ is the generator of the transformation (5.1a), and is inde-

(*) $T_{\varrho v} = -\tfrac{1}{2}g_{\varrho v}a^{\lambda,\sigma}a_{\lambda,\sigma} + a^{\lambda}{}_{,\varrho}a_{\lambda,v}\,,$

$\theta_{\varrho v} = -\tfrac{1}{2}g_{\varrho v}a^{\lambda,\sigma}(a_{\lambda,\sigma} - a_{\sigma,\lambda}) + (a_{\varrho,\lambda} - a_{\lambda,\varrho})(a_{v}{}^{,\lambda} - a^{\lambda}{}_{,v})\,.$

pendent of the surface σ. The operator $\int_\sigma \mathrm{d}\sigma^s A_s$ is the generator of the transformation (4.1) on the surface σ. However, this operator is not independent of the surface. As the commutators of the fields are invariant only for space-like points, we cannot expect to find a constant operator, which generates the transformation (5.1).

It is easy to verify explicitly that

$$i\left[\int_\sigma \mathrm{d}\sigma^s S_s,\, a_\mu(x)\right] = \delta a_\mu(x)\,, \tag{5.10}$$

for any surface and that

$$i\left[\int_{x\in\sigma} \mathrm{d}\sigma^s A_s,\, a_\mu(x)\right] = \delta a_\mu(x)\,, \tag{5.10a}$$

for any space-like surface through x.

From (4.23) and (5.1) follows that $\int \mathrm{d}x\, a_\varrho J^\varrho$ is invariant.

6. – In the case of a non-vanishing mass the action integral is not invariant. *E.g.* for a scalar field we have a term of the form $\int m^2 q^2\,\mathrm{d}x$ which transforms like

$$\begin{cases} S: & \int m^2\varphi^2\,\mathrm{d}x = \int \dfrac{m^2}{\lambda^2}\,\varphi'^2\,\mathrm{d}x'\,, \\ A: & \int m^2\varphi^2\,\mathrm{d}x = \int \dfrac{m^2}{(1-2ax'+a^2x'^2)}\,\varphi'^2\,\mathrm{d}x'\,. \end{cases} \tag{6.1}$$

If we demand that the mass has to be transformed like

$$\begin{cases} S: & m' = \dfrac{m}{\lambda}\,, \\ A: & m' = (1+2ax+a^2x^2)m\,, \end{cases} \tag{6.2}$$

we find that the Lagrangian remains invariant in the sense that

$$\int m^2\varphi^2\,\mathrm{d}x = \int m'^2\varphi'^2\,\mathrm{d}x'\,. \tag{6.3}$$

This is not sufficient to derive a conservation law. Nevertheless the unitary transformations may exist [8]:

$$U\varphi(xm)U^{-1} = \varphi'(xm)\,. \tag{6.4}$$

[8] J. E. WESS: *Nuovo Cimento*, **14**, 527 (1959).

The generators of this transformation correspond to the ones used by W. HEISENBERG. They have to obey the same commutation relations (16). Therefore all the properties of the generators which we derived in Section 1 and 2 using only the commutation relations are still valid. This makes it hard to believe that the eigenvalues of the operators S are suitable to characterize elementary particles.

* * *

The author would like to express his thanks to Professor W. THIRRING for suggestions and helpful comments and for useful discussions with Prof. B. ZUMINO and Dr. K. BAUMANN.

RIASSUNTO (*)

Si considerano le proprietà di una teoria conforme invariante del campo quantizzato. Si fa una breve discussione sul gruppo conforme nelle quattro dimensioni e sulla topologia, introdotta da questo gruppo nello spazio pseudo-euclideo. Con l'aiuto delle relazioni di commutazione si esamina lo spettro dei generatori nello spazio Hilbertiano. Si trova che il solo possibile autovalore discreto di P^2 e dei P^ν è zero e che il generatore per trasformazioni di scala ha uno spettro continuo. Si calcolano le autofunzioni di S nella rappresentazione x, che formano un gruppo completo. Le leggi di conservazione valide in una teoria invariante e le relazioni di commutazione predicono una certa forma delle quantità conservate espresse in termini del tensore energia-momento e delle coordinate. Per i campi scalari, spinoriali e vettoriali si derivano i generatori col principio di azione di Schwinger.

(*) *Traduzione a cura della Redazione.*

On the Decay of ^{129}Cs.

S. Jha, H. G. Devare and R. M. Singru

Tata Institute of Fundamental Research - Bombay

(ricevuto il 26 Luglio 1960)

Summary. — The radiations from the decay of ^{129}Cs have been investigated by β-ray spectrometer and coincidence scintillation spetrometer. New γ-rays of 790 and 920 keV have been detected. The conversion coefficients of the γ-rays and percentages of the electron captures to different excited states of ^{129}Xe have been estimated. A level scheme of ^{129}Xe and the possible spin and parity assignments to different levels have been suggested.

1. – Introduction.

It is fairly well established from the work of several workers ([1-5]) that the 31-hour $^{129}_{55}$Cs decays by electron captures to the excited states of ^{129}X at 320 keV, 411 keV and 585 keV with the emission of the γ-rays of energy 40 keV (mostly converted), 92 keV, 174 keV, 279 keV, 319 keV, 371 keV, 411 keV, 545 keV and 585 keV. The existing data seem to be consistent with the assumption ([6]) that the excited states of ^{129}Xe occur at 40 keV, 235 keV (isomeric state with a half life of 8.0 days), 320 keV, 410 keV and 585 keV. In Coulomb excitation, only the state at 320 keV presumably is excited, because only a γ-ray of energy 290 keV is reported to have been observed ([7-8]).

([1]) R. W. Fink, F. L. Reynolds and D. H. Templeton: *Phys. Rev.*, **77**, 614 (1950).
([2]) A. H. Wapstra, N. F. Verster and M. Boelhouwer: *Physica*, **19**, 138 (1953).
([3]) W. E. Nervik and G. T. Seaborg: *Phys. Rev.*, **97**, 1092 (1955).
([4]) G. J. Nijgh: *Thesis* (Amsterdam, 1955).
([5]) B. L. Robinson and R. W. Fink: *Phys. Rev.*, **98**, 221 (1955).
([6]) *Nuclear data sheets*, NRC 58-8-22; National Research Council, Washington, D.C.
([7]) G. F. Pieper, C. E. Anderson and N. P. Heydenberg: *Bull. Am. Phys. Soc.*, **3**, 38 (1958).
([8]) G. M. Temmer and N. P. Heydenberg: *Phys. Rev.*, **104**, 967 (1956).

It is reported that no positrons are emitted in the decays of ^{129}Cs ([1]). The electron capture decay energy of this isotope is estimated, by the method of Way and Wood ([9]), to be about 1200 keV.

This work was undertaken to see if there are any higher energy γ-rays emitted in the decay of this isotope, if one could get some data on the conversion coefficient of the γ-rays and if one could estimate the branching ratios to various levels of ^{129}Xe. It was surprising that no electron capture decay to the ground state and the 40 keV state of ^{129}Xe was suggested by earlier workers. Estimates of these branching ratios have been made in this work.

2. – Experimental procedure.

The source of ^{129}Cs was prepared by $^{127}_{53}$I(α, 2n) reaction with the α beam of about 50 MeV in the cyclotron of the Birmingham University, England. The target material was sodium iodide, from which caesium was chemically extracted. Any iodide other than alkali iodide would have been preferable because separating sodium from caesium was found tedious. The source was rather thick for the measurement of the internal conversion lines in the β-ray spectrometer.

The internal conversion electron spectrum was studied in a thin lens magnetic spectrometer ([10]) provided with a thin window GM counter detector. The peaks corresponding to the K and L conversion of 319 keV, 370 keV and 410 keV γ-rays were observed. The conversion coefficients of the 370 keV and 410 keV γ-rays were estimated by the comparison technique, by comparing in the same geometry the K and L conversion lines of the 411 keV γ-ray from ^{198}Au.

3. – Scintillation spectrometer studies.

The γ-rays from ^{129}Cs were studied in a scintillation spectrometer with 2 in. $\times$ 1½ in. NaI(Tl) crystal mounted on a 6292 DuMont photomultiplier. The spectrum, taken with a single channel analyser with the source at a distance of 5 cm, is reproduced in Fig. 1. In order to detect the higher energy γ-rays, the source was brought closer and a lead plate (3 mm) was used to absorb the lower energy γ-rays. The spectrum is reproduced in Fig. 2 and shows the presence of 790 keV and 920 keV γ-rays.

([9]) K. Way and M. Wood: *Phys. Rev.*, **94**, 119 (1954).

([10]) T. D. Nainan, H. G. Devare and A. Mukerji: *Proc. Ind. Acad.*, **44**, 111 (1956).

The γ-ray spectrum was analysed with the help of standard sources (^{88}Y, ^{137}Cs, ^{85}Sr, ^{198}Au, ^{51}Cr and ^{203}Hg) by successively peeling off the contribution of each γ-ray from the composite spectrum. The energies and relative

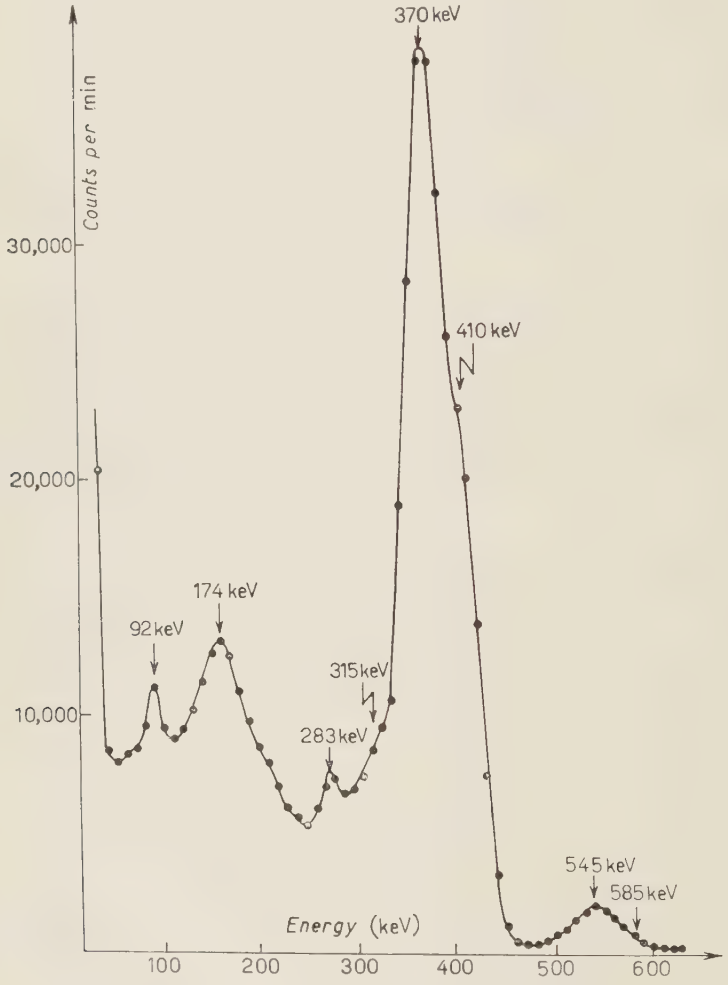

Fig. 1. – Spectrum of γ-rays emitted in the decay of ^{129}Cs taken with the source at 5 cm from a $1\frac{1}{2}$ in. diam. $\times$ 2 in. high NaI(Tl) crystal.

intensities of the γ-rays are given in Table I, where the first column gives the energy of the γ-ray in keV, the second column gives the intensity of the conversion electron lines as found by NIJGH (4), the third column gives the relative intensities of the γ-rays as observed by us, and the fourth column gives our estimate of the K conversion coefficient. The half-lives of all these γ-rays

(except the one at 790 keV) were followed for about five half-lives. They all seemed to decay with a half-life of about 30 hours. The ratio of the inten-

TABLE I.

Transition energy in keV	K conversion electron intensity (*)	γ-ray intensity (**)	K conversion coefficient (**)
40 keV	460	not observed	22 $\pm$ 4 (***)
92	11.4	1.5	2.7 $\pm$ 0 8
174	0 35	1.5	0.083 $\pm$ 0.025
280	1.36	8	0.06 $\pm$ 0.018
320	1.2	13	0.033 $\pm$ 0.01
370	13.2	100	0.047 $\pm$ 0.01
410	10	100	0.021 $\pm$ 0.004
545	0.52	14	0.013 $\pm$ 0.004
585	0.22	3	0.026 $\pm$ 0.008
790	—	0.15	
920	—	0.3	—

(*) Data by C. J. NIJGH: *Nuclear Data Sheets.*
(**) Our experimental results.
(***) Calculated in terms of our experimental determination of α_K for 370 keV γ-ray.
(****) Measured in the decay of ^{129}I ([11]).

sities of the 920 keV and 790 keV γ-rays were found to remain constant over one half life; this comparison could not be continued longer because of the low

TABLE II.

Energy of the ray in gate	Energy of the γ-ray found in coincidence
92 keV	100 keV, 170 keV, 280 keV, 315 keV
174 keV	92 keV, 140 keV (composite), 174 keV (?), 200 keV
280 keV	92 keV, 174 keV, 290 keV (composite), 440 keV
545 keV + 585 keV	225 keV

intensity of the 790 keV γ-ray. A γ-ray of energy around 1 100 keV was observed when the spectrum was studied with a 4 in. $\times$ 4 in. NaI(Tl) crystal but

([11]) E. DER MATEOSIAN and C. S. WU: *Phys. Rev.*, **95**, 458 (1954).

it seemed to decay with a half-life much longer than 30 hours. It is difficult to see which impurity could have given rise to a γ-ray of this energy. Repeated purifications were made to remove the trace of alkalis other than caesium and all the alkaline earth impurities.

The γ-rays from ^{129}Cs were studied also in a scintillation coincidence spectrometer with a resolving time of 0.1 μs. The results of the coincidence studies are given in tabular form in Table II.

It may be remarked in this connection that the coincidence studies as made here only indicate the correctness of the decay scheme given by the Nuclear Delta Group ([6]) and also the existence of higher levels. Because of the poor statistics of the coincidence measurements, not much weight is being attached to them in drawing conclusions about the decay scheme. The existence of γ-rays arising from transitions from 920 keV and 790 keV levels to the intermediate levels cannot be ruled out from the results of present studies.

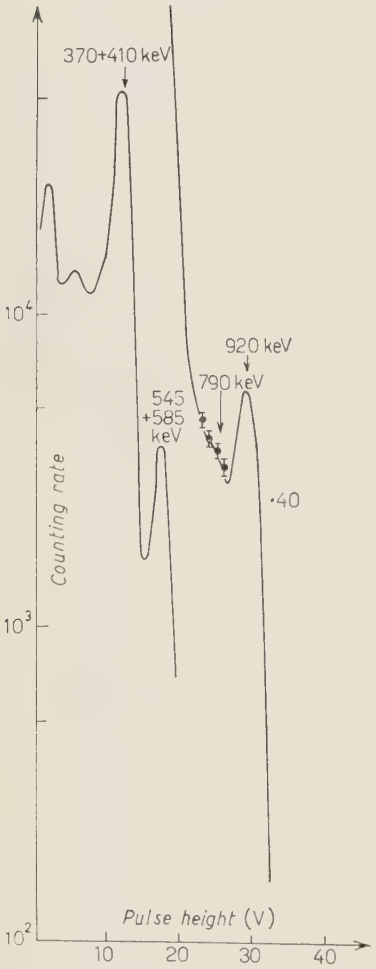

Fig. 2. – Spectrum of γ-rays in the high energy region.

4. – Estimates of the conversion coefficients and branching ratios.

The internal conversion coefficients of the 370 keV and 410 keV γ-rays were estimated in the following way. The internal conversion electron spectrum of ^{129}Cs and ^{198}Au were taken in the lens spectrometer in the same geometry. The intensity of the 412 keV γ-ray of the ^{198}Au source was compared with that of the 370 keV and 410 keV γ-rays from ^{129}Cs in the scintillation spectrometer. Then from the known conversion coefficient of the 412 keV γ-ray of ^{198}Au (α_K = 0.028) the K conversion coefficients of the 370 keV and the 410 keV γ-rays were calculated to be α_K for (370 keV) = 0.047 $\pm$ 0.01 and α_K for

(410 keV) = 0.021 ± 0.004. The large error in the values of the conversion coefficients is due to the considerable error in the estimate of the ratio of the areas under the conversion lines in the 370 keV and the 410 keV γ-rays because of the large low energy tail caused by the thickness of the source.

The K conversion coefficient for 585 keV, 545 keV, 320 keV, 280 keV, 174 keV and 92 keV γ-rays were calculated by combining Nijgh's values ([4]) for the relative intensities of the K conversion electrons with our values of the relative intensities of the unconverted γ-rays and by making use of our value of the K conversion coefficient of the 370 keV γ-ray ($\alpha_K = 0.047 \pm 0.01$). These results are given in Table I column 3.

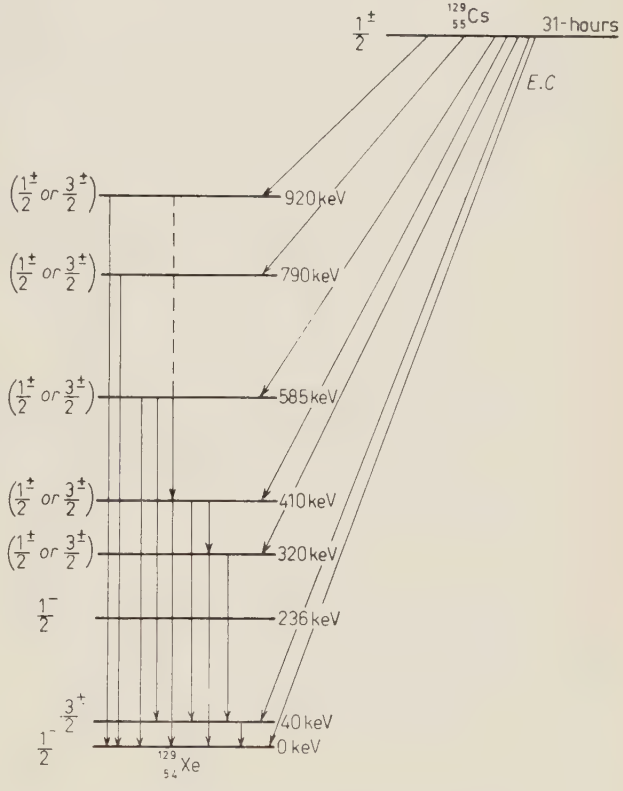

Fig. 3. – A tentative decay scheme.

If one assumes the decay scheme given in Fig. 3, one can calculate the electron capture branchings to the excited levels of ^{129}Xe. In order to calculate the branching to the 40 keV state, the value of $\alpha_K = 22 \pm 4$ and $K/L \sim 10$ for the 40 keV transition as given by DER MATEOSIAN and WU ([11]) in their study of the decay $^{129}\mathrm{I} \rightarrow {}^{129}\mathrm{Xe}$ were used along with Nijgh's values of the conversion electron intensities and our values of the relative γ-ray intensities.

In order to find the percentage of electron captures leading directly to the ground state, the total K X-ray intensity was measured with a NaI(Tl) crystal with a thin aluminium cover and also the number of K X-rays in coincidence with 370 keV and 410 keV γ-rays. The value of the ratio of the probability of the captures of the L electrons and K electrons in the electron capture decay of ^{129}Cs was taken to be 0.12 ([12]). This corresponds to a decay energy of about

([12]) H. BRYSK and M. E. ROSE: *Rev. Mod. Phys.*, **30**, 1169 (1958).

1200 keV. The result of this measurement gave the ratio (Total number of K X-rays emitted in the decay ^{129}Cs)/(Number of K X-rays in coincidence with 370 keV and 410 keV γ-rays). This ratio was found to be 1.94 ± 0.2. A certain percentage of electron capture transitions had to be assumed leading to the ground state of ^{129}Xe in order to match the value of this ratio calculated from the data of the Table I, which was found to be 1.25 ± 0.12.

The relative branching ratios for the electron capture decay of ^{129}Cs, as calculated by us, are given in Table III. Due to the uncertainties in the data used to estimate the branching ratios, the figures quoted for these ratios have a rather large error, about 30%.

TABLE III.

Level in the daughter nucleus	Percentage branching	log ft
920 keV	0.07%	7.6
790 keV	0.04%	8.2
585 keV	4.7 %	6.5
410 keV	52.8 %	5.8
320 keV	4.0 %	6.9
40 keV	15.1 %	6.6
ground state	22.7 %	6.4

Because of the incomplete coincidence studies, it has been found difficult to estimate the contribution to the low energy γ intensities from possible transitions between higher levels. For this reason also, there should be some error in the branching ratios.

5. – Discussion.

From the present work, combined with the results of the earlier workers, a tentative decay scheme has been presented. Because of the uncertainties in the value of the conversion coefficients and that of the log ft to the various levels, the spin and parity assignments cannot be made with any degree of confidence for the levels of ^{129}Xe. Some general conclusions can however be drawn. Since all the levels of ^{129}Xe except the $h_{11/2}$ level at 235 keV are fed by electron capture from the $\frac{1}{2}^+$ ground state of ^{129}Cs with a log $ft \sim 6$, the spins and parities of these levels cannot be very different from $\frac{1}{2}\pm$ or $\frac{3}{2}\pm$. The same conclusion seems to follow from the relative intensities of the γ-rays starting from the higher levels and landing at the ground state ($\frac{1}{2}^+$) and the 40 keV state ($\frac{3}{2}^+$) of ^{129}Xe. It may be remarked in this connection that it seems very unusual that the 55-th proton in ^{129}Cs and ^{127}Cs should occupy

a level with an angular momentum of $\frac{1}{2}$, when all the isotopes, of $_{51}$Sb, $_{53}$I, $_{55}$Cs and $_{57}$La, whose spins are known, have spins either $\frac{5}{2}^+$ or $\frac{7}{2}^+$.

The fact that all the five levels in ^{129}Xe between 320 keV and 920 keV have spins and parities $\frac{1}{2}\pm$ and/or $\frac{3}{2}\pm$ is extremely difficult to understand on shell model. But these levels and a few more of higher spins, not fed in the electron capture decay of ^{129}Cs, could arise from the interaction of the last odd proton with the surface vibrations of the spherical core (GLENDENNING [13]).

* * *

Our grateful thanks are due to Mr. K. P. GOPINATHAN for all the care he took for the chemical separation. We are very much obliged to Dr. R. K. GUPTA for his assistance in the preparation of this paper.

Note added in the prof.

GLENDENNING (*Phys. Rev.*, **119**, 213 (1960) has calculated the energies of low-lying even-parity states of ^{129}Xe. Some of the levels reported in this work seem to agree with the calculations. No special attention was given in our work to the possibilities of γ-rays between 600 keV and 700 keV. GLENDENNING suggests $\frac{7}{2}^-$ for the 320 keV level. In our view, it is very unlikely that this level has a high spin.

([13]) N. K. GLENDENNING: *Phys. Rev.* (to be published).

RIASSUNTO (*)

Le radiazioni di decadimento del ^{129}Cs sono state analizzate con uno spettrometro a raggi β e con uno spettrometro a coincidenza a scintillazione. Si sono trovati nuovi raggi γ di 790 e 920 keV. Si sono valutati i coefficienti di conversioni dei raggi γ e le percentuali delle catture di elettroni in differenti stati eccitati del ^{129}Xe. Si suggeriscono uno schema dei livelli del ^{129}Xe e le possibili attribuzioni di spin e parità ai differenti livelli.

(*) *Traduzione a cura della Redazione.*

Wavelength Dependence of the Refractive Index of a Plasma in the Optical Region.

U. Ascoli-Bartoli (*), A. De Angelis and S. Martellucci

Laboratorio Gas Ionizzati del C.N.E.N. - Roma

(ricevuto il 30 Luglio 1960)

Summary. — The experiment described in this paper is designed to put in evidence the part played by free electrons in the refractivity of noble gas plasmas. The variations in density of the neutral gas and their relation to the degree of ionization are studied. The method of analysis employed is that of optical interferometry. The limits of the sensitivity of this method are also discussed. The plasma was excited by a radio-frequency field.

1. – Introduction.

It is generally accepted that with optical methods of research on ionized gases it is possible to carry out measurements of certain parameters while leaving them in a virtually undisturbed state. On the other hand, it is equally true that measurements of this kind frequently present considerable difficulty of interpretation and sometimes give rise to uncertainty. We come up against a typical example of this when we consider the problem of determining the electron density in a plasma by measuring the broadening of a line by the Stark effect. It is common knowledge that the interpretation of this phenomenon gives rise to difficulties both in the theory and in its application (1).

Of more recent introduction are microwave techniques; but even these, at least up to the present, have had a somewhat restricted field of application due to the strong dependence of the refractivities on the magnetic field, the

(*) Istituto Sperimentale delle Ferrovie dello Stato, Roma.

(1) H. Fischer and L. Mansur: *Proc. of the Conference on Extremely High Temperatures* (New York, 1958).

poor spatial resolution, and the difficulty of applying them to dense plasmas, as in the case, for example, of shock waves [2].

More promising, however, is the optical interferometry method which R. A. ALPHER and D. R. WHITE [3] have used with shock waves. The method proved particularly useful in the spatial determination of the plasma density in a shock wave inside a tube.

The purpose of this paper is thus to provide a practical demonstration of the fact that this method, which has been successfully experimented with in the case of higher plasma densities, can also be employed for lower densities such as are found, for instance, in radiofrequency discharges. This further constitutes a test of the technique employed in such a way that it can be applied to specific problems of plasma physics.

When one of us started the present work, with the collaboration of Professor F. RASETTI [1], we were not aware of the paper which had by then been published by R. A. ALPHER and D. R. WHITE, but even when this came to our notice we considered it worth-while to carry on the experiment. Shortly after the letter [1] was published we discovered that the refractivity of the atom gas also contributed to the phenomenon observed. For that reason it was essential to examine the phenomenon as a function of the wavelength of the incident light as, indeed, was foreseen in the communication itself.

2. – Theoretical section.

The following considerations concern an argon plasma, but they will, naturally, apply *mutatis mutandis* to any type of noble gas. In fact, we ourselves reproduced the experiment with xenon.

In this experiment, the argon gas was enclosed in a cylindrical glass or quartz tube. By means of a Jamin interferometer a system of fringes can be produced as a result of interference taking place between a light beam traversing the tube along its length and a beam following the same geometrical path in the atmosphere (Fig. 1). Any variation in the refractivity of the gas caused by the ionizing discharge will produce a shift in the fringe system in one or the other direction depending on whether the refractivity increases or decreases. The fringe shift expressed in number of fringes is proportional to the variation in the optical path

$$s = L\Delta(n-1)/\lambda\,, \tag{2.1}$$

[2] K. B. PERSSON: *Phys. Rev.*, **106**, 191 (1957).
[3] R. A. ALPHER and D. R. WHITE: *Physics Fluids*, **2**, 2 (1959).
[4] U. ASCOLI-BARTOLI and F. RASETTI: *Nuovo Cimento*, **10**, 13 (1959).

where L is the thickness of the plasma traversed by the light and $\Delta(n-1)$ the variation in the refractivity given by

$$\Delta(n-1) = (n-1)_{\text{plasma}} - (n-1)_{\text{argon}} . \tag{2.2}$$

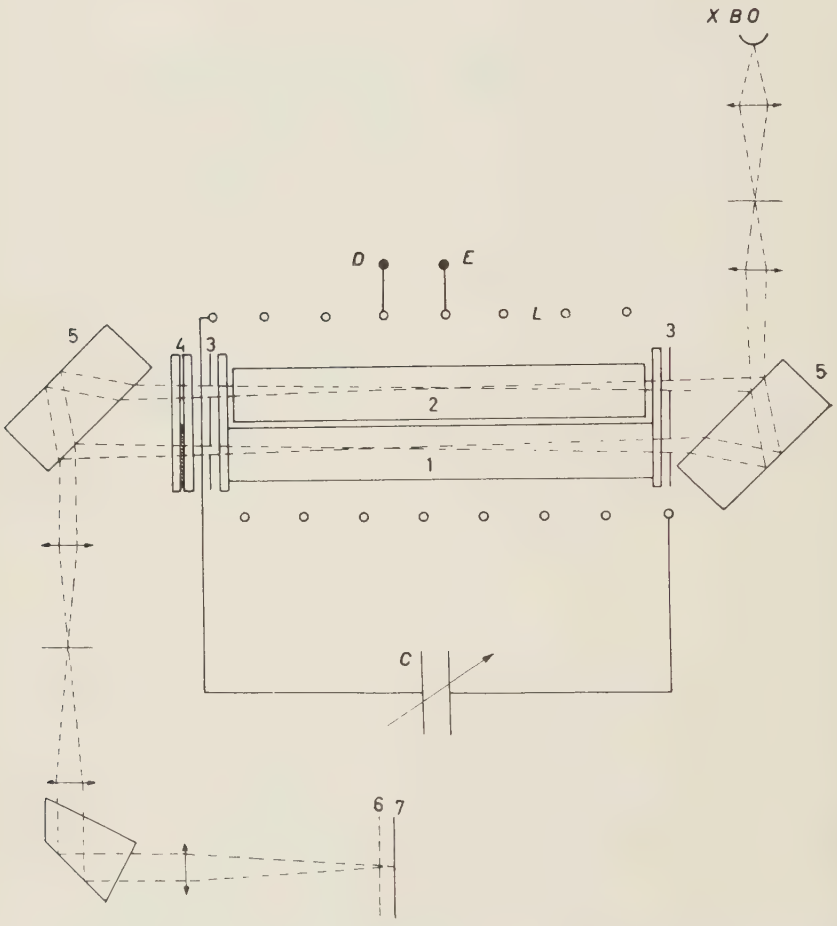

Fig. 1. – Schematic representation of experimental equipment: 1) discharge tube with optical windows; 2) open air-filled tube; 3) diaphragms; 4) water-filled compensator; 5) interferometer plates; 6) screen with 18 windows; 7) photographic plates.

2·1. *Refractive index of neutral gas.* – For the refractivity of non-excited argon both classical and quantum theory yield the well-known formula which holds for gases up to a reasonable degree of compression

$$n-1 = \frac{2\pi e^2}{m} \sum_k N_k/(\omega_k^2 - \omega^2) , \tag{2.3}$$

or, assuming $N_k = f_k N$

$$n - 1 = \frac{2\pi e^2 N}{m} \sum_k f_k/(\omega_k^2 - \omega^2) \,, \tag{2.3'}$$

where the symbols have their well-known significance. Tables of the numerical values of the oscillator strengths for certain gases can be found in other works [5].

If we confine our considerations to wavelengths in the visible region we need only be concerned with one or two resonance frequencies, namely those with the highest values of the oscillator strengths. In the case of argon the resonance wavelengths occur in the far ultraviolet

$$\lambda[(3p^6)\ {}^1S_0 \to (3p^5)\, 4s\, (\tfrac{3}{2})1] = 1\,066.7 \text{ Å} \,,$$

$$\lambda[(3p^6)\ {}^1S_0 \to (3p^5)\, 4s'(\tfrac{1}{2})1] = 1\,048.3 \text{ Å} \,.$$

Here (2.3) can be developed in a series of powers which, if stopped at the first term in λ^{-2} reduces to Cauchy's formula

$$n - 1 = A + B/\lambda^2 \,. \tag{2.4}$$

This formula will hold good throughout the visible region and in the near ultraviolet, since the resonance lines have extremely short wavelengths, a fact which eliminates the possibility of any anomalous dispersion in the visible region. This is of great importance in our considerations.

In the table below is given [5] a list of constants A and B for certain atomic gases and the values for the respective polarizability at low frequency. These values of the constants, valid at standard conditions of temperature and pressure, represent very well the variation of the refractivities of the considered gases versus wavelength.

Atoms	α (cm^3)	A	B (cm^2)
He	$2.07 \cdot 10^{-25}$	$3.48 \cdot 10^{-5}$	$0.08 \cdot 10^{-14}$
Ne	$3.96 \cdot 10^{-25}$	$6.66 \cdot 10^{-5}$	$0.16 \cdot 10^{-14}$
A	$16.54 \cdot 10^{-25}$	$27.92 \cdot 10^{-5}$	$1.56 \cdot 10^{-14}$
Kr	$24.80 \cdot 10^{-25}$	$41.89 \cdot 10^{-5}$	$9.92 \cdot 10^{-14}$
Xe	$40.40 \cdot 10^{-25}$	$68.23 \cdot 10^{-5}$	$6.92 \cdot 10^{-14}$

[5] C. W. Allen: *Astrophysical Quantities* (London, 1955).

In order to have a clear idea of the functional relationship between the refractivity of the argon and the density of the atoms, we should recall that such dependence is linear at reasonably low gas pressures. If we combine the Gladstone-Dale formula, viz.

$$n - 1 = kN_a , \tag{2.5}$$

(where N_a is the density of the atoms) with Cauchy's dispersion formula, we obtain the refractivity of the argon as a function of the density

$$n - 1 = (1.03 \cdot 10^{-23} + 0.58 \cdot 10^{-33}/\lambda^2) N_a , \tag{2.6}$$

where λ is in cm and N_a in cm^{-3}.

2·2. *Plasma refractive index.* – If we consider the plasma as a mixture of A I gas, A II gas and electron gas, bearing in mind that the refractivity of gaseous mixtures can be expressed by

$$n - 1 = \sum_i k_i N_i , \tag{2.7}$$

(where N_i is the density of the i-th component of the mixture, and k_i is the specific refractivity) we may extend the additivity of refractivities to include plasma. In our case we may write

$$(n-1)_{\text{plasma}} = (n-1)_{\text{AI}} + (n-1)_{\text{AII}} + (n-1)_{\text{electrons}} . \tag{2.8}$$

We should, strictly, have included terms referring to multiple ionizations, but the formula holds good in spite of this omission, in view of the extreme unlikelihood of a multiple ionization (6).

Let us consider the contribution of each component in turn.

We should note first that the refractivity of the neutral argon is slightly lower than that of the initial argon owing to the fact that the density of neutral atoms has been reduced from N_a, prior to ionization, to $N_a - \varepsilon N_a$, where ε is the percentage of ionized atoms.

There have been no measurements made of the refractivity of A II gas, but an attempt may be made to work out its value from that of neutral gas, which is known, by using Slater's screening constants method (7) and the

(6) F. DE LA RIPELLE: *Journ. Phys. Rad.*, **10**, 319 (1949).

(7) J. D. HIRSCHFELDER, C. F. CURTISS and R. B. BIRD: *Molecular Theory of Gases and Liquids* (New York, 1954).

polarizability formula (since polarizability is directly proportional to refractivity). The formula

$$\alpha = (4/9\,a_0) \sum_i (\overline{r_i^2})^2 \tag{2.9}$$

is elaborated from quantum mechanics by means of the variational method in which a_0 is the Bohr radius, and $\overline{r_i^2}$ is the mean value of the square of the distance of the i-th electron from the nucleus. This method is highly questionable, however, even if it remains one of the most recommendable for determining the polarizability of a gas (*). Values obtained by means of this method should therefore be considered to hold only as regards the order of magnitude. We thus have

$$\alpha_{\mathrm{A\,II}}/\alpha_{\mathrm{A\,I}} = 0.72\,.$$

In another method, the polarizability is derived from the magnetic susceptibility

$$\chi = -e^2 L(N_e a_0 \alpha)^{\frac{1}{2}}/4m_e c^2\,, \tag{2.10}$$

where L is the number of atoms per gram, and N_e the number of atomic electrons. The remaining symbols have their customary meaning. L. H. Thomas and K. Umeda (8) have calculated as a function of the atomic number the values of the magnetic susceptibility of all the neutral atoms and ionized atoms up to four times. With their method one has

$$\alpha_{\mathrm{A\,II}}/\alpha_{\mathrm{A\,I}} = 0.34\,.$$

From these two values, which are valid only as regards the order of magnitude, it was found that the refractivity of the A II gas is of the same order of magnitude as that of the A I gas.

Concluding these remarks on the contribution made by ions and neutral atoms to the refractive index of an ionized gas, we may say that, given the dependence of the polarizability on the fourth power of the mean radii of the outermost electrons, we should expect a higher polarizability when the atom or ion is in an excited state. Nevertheless we think this higher value may be disregarded since the population of the excited levels is considerably lower than that of the ground state. In fact, assuming a Boltzmann energy distri-

(*) For a fuller treatment see R. A. Alpher and D. R. White (3).

(8) L. H. Thomas and K. Umeda: *Journ. Chem. Phys.*, **24**, 1113 (1956).

bution at a temperature of 10000 °K, the Klein-Rosseland relation shows that for the resonance levels,

$$n_r/n_0 \simeq 10^{-4} .$$

A further remark common to atom and ion gases is that, strictly speaking, since we are dealing with a plasma, an accurate calculation of their polarizability would require one to take into account local microscopic fields within the plasma, which would account for a slight increase in polarizability. This has been observed experimentally by R. A. ALPHER and D. R. WHITE ([3]).

On these grounds the refractivity of the neutral gas plus the ion gas approximately equalizes the refractivity of the initial N_a atoms, unless there is a different density distribution within the tube.

At this point it will be appropriate to examine the contribution made by the electron gas. Since all resonance frequencies are zero for a gas of free electrons, the formula (2.3′) becomes

$$n - 1 = -2\pi e^2 N_e/m\omega^2 , \tag{2.11}$$

which holds good for frequencies at which the free electrons can be considered independent. In (2.11) N_e is the number of electrons per cm³.

A more general formula may be derived from other considerations, by taking into account the collisions of the electrons with heavier particles ([9,10]). This formula, for frequencies in the visible region, becomes

$$n^2 = 1/(1 - \omega_p^2/\omega^2) , \tag{2.12}$$

where

$$\omega_p^2 = 4\pi N_e e^2 (m_i + m_e)/m_i m_e \simeq 4\pi N_e e^2/m_e ,$$

since $m_e \ll m_i$. For frequencies in the visible region $\omega_p^2/\omega^2 \ll 1$; furthermore, since for not too high densities $(n - 1) \ll 1$, the formula (2.12) coincides with (2.11).

2·3. *Influence of magnetic fields.* – Let us assume a uniform magnetic field $\boldsymbol{B}$, and that this field is normal to the mean velocity of the electrons and ions; the plasma refractive index will differ from the case of $\boldsymbol{B} = 0$. An exhaustive treatment of this has been made by V. FERRARO ([11]), and his results are given here.

([9]) L. SPITZER jr.: *Physics of Fully Ionized Gases* (New York, 1956).
([10]) S. K. MITRA: *Upper Atmosphere* (Calcutta, 1952).
([11]) V. FERRARO: *Suppl. Nuovo Cimento*, **13**, 9 (1959).

If then $\boldsymbol{B} \neq 0$ the formula (2.12), considering the more general case, becomes

$$n^2 = [1 - \omega_p^2/\omega^2(1 - \omega_e/\omega)(1 + \omega_i/\omega)]^{-1}\,, \tag{2.13}$$

where

$$\omega_e = eB/m_e \qquad \text{and} \qquad \omega_i = ZeB/m_i$$

represent respectively the cyclotron frequency of electrons and ions. If we disregard the motion of the ions (*i.e.* if $\omega_i = 0$) we obtain

$$n^2 = [1 - \omega_p^2/\omega^2(1 \pm \omega_e/\omega)]^{-1}\,. \tag{2.14}$$

We thus have a polarization of the incident electromagnetic wave. The plus/minus sign in (2.14) refers respectively to a clockwise or counterclockwise rotating polarized wave.

With the same formula (2.14) we can then observe that the presence of the magnetic field introduces a corrective term, which, however, may be disregarded in the visible region for practically obtainable intensities of the magnetic field. It will thus be seen that a magnetic field of about 10^8 gauss is required for a radiation of $\lambda = 5\,000$ Å to make $\omega = \omega_e$. For magnetic fields which are obtainable in practice and, in particular, for those which we are able to produce with our radiofrequency field, $\omega_e/\omega \ll 1$; then (2.14) coincides with (2.12). Our assumption, therefore, that the influence of magnetic fields may be completely disregarded, is justified.

2·4. *The effect of atoms.* – From the foregoing, the variation in refractivity is given by

$$\begin{aligned}\Delta(n-1) &= (n-1)_{\text{plasma}} - (n-1)_{\text{argon}} = \\ &= (n-1)_{\text{AI}} + (n-1)_{\text{AII}} + (n-1)_{\text{electrons}} - (n-1)_{\text{argon}} \simeq (n-1)_{\text{electrons}}\,,\end{aligned} \tag{2.15}$$

which, when expressed as a function of the wavelength, becomes

$$\Delta(n-1) = -e^2 N_e \lambda^2/2\pi m c^2\,. \tag{2.16}$$

This will hold true on the assumption that there are no variations in the density of the gas contained in the discharge tube. Nevertheless, this does not correspond to the facts. In cases where the gas is not subjected to any excitation, we may say that there is uniform density distribution in the tube. We must equally admit that, when, on the other hand, the discharge tube is placed in a radiofrequency field, there will inevitably be variations in density, which contribute to a variation in the refractivity. Naturally we are

interested in densities which vary in a radial direction, because, with our experimental arrangement it is possible to examine the behaviour of the phenomena only radially. In order to calculate how much these variations in the density of the argon gas contribute to variations in refractivity we employ formula (2.6) so that the variation in refractivity is

$$\Delta(n-1) = (1.03\cdot10^{-23} + 0.58\cdot10^{-33}/\lambda^2)\,\Delta N_a - e^2 N_e \lambda^2/2mc^2 . \tag{2.17}$$

For the shift of the fringe system expressed in number of fringes the following type of formula is used

$$s(\lambda) = (c_1 \Delta N_a/\lambda + c_2 \Delta N_a/\lambda^3 - c_3 N_e \lambda) L , \tag{2.18}$$

where

$$\begin{cases} c_1 = 1.03\cdot10^{-23}\ \mathrm{cm}^3 , \\ c_2 = 0.58\cdot10^{-33}\ \mathrm{cm}^5 , \\ c_3 = 4.46\cdot10^{-14}\ \mathrm{cm} . \end{cases} \tag{2.19}$$

Examining the behaviour of $s(\lambda)$ we may, for the sake of convenience, refer to the shift produced by a plasma column of unit length. For $\Delta N_a > 0$ the function shows a zero for the wavelength

$$\lambda_0 = \sqrt{[c_1 \Delta N_a + (c_1^2 \Delta N_a^2 + 4c_2 c_3 N_e \Delta N_a)^{\frac{1}{2}}]/2c_3 N_e} .$$

For greater wavelength values the shift is negative, for smaller it is positive.

For $\Delta N_a < 0$, on the other hand, the function shows a maximum for the wavelength

$$\lambda_{max} = \sqrt{[-c_1 \Delta N_a + (c_1^2 \Delta N_a^2 - 12 c_2 c_3 N_e \Delta N_a)^{\frac{1}{2}}]/2c_3 N_e} .$$

Nevertheless, we may disregard the term in λ^{-3} in the expression (2.18); since, in the wavelength range with which we are concerned here, it is small compared with the other two. We may therefore write

$$s(\lambda) = (c_1 \Delta N_a/\lambda - c_3 N_e \lambda) L . \tag{2.20}$$

From this, putting $L = 1$, it will be seen that, for $\Delta N_a > 0$, the function shows a zero for

$$\lambda_0 = (c_1 \Delta N_a/c_3 N_e)^{\frac{1}{2}} = 1.52\cdot10^{-5}\,(\Delta N_a/N_e)^{\frac{1}{2}} \qquad (\lambda \text{ in cm})$$

and a maximum for $\Delta N_a < 0$, for

$$\lambda_{max} = (-c_1 \Delta N_a / c_3 N_e)^{\frac{1}{2}} = 1.52 \cdot 10^{-5} (-\Delta N_a / N_e)^{\frac{1}{2}} \qquad (\lambda \text{ in cm}).$$

From these formulae we can see that the effect of the variations in the atom density (we shall refer to this more briefly as the effect of the atoms) prevails for the short wavelengths and will be negligible only at very long wavelengths or, in the visible region, for ionizations in excess of 10%. In the visible region therefore, the effect of the atoms will be observable with a variation in sign for the fringe shift for $\Delta N_a > 0$, or with a minimum of the magnitude of the fringe shift for $\Delta N_a < 0$, only if we have, as may be seen in the expression for λ_0 and λ_{max}, $10 \leqslant |\Delta N_a| / N_e \leqslant 30$ (*i.e.* either for low ionizations of a few per cent, or for wide variations in atom density of about 10% or more). If at a given radius we observe an increase in the density of neutral atoms, we inevitably observe at another radius a rarefaction of these atoms, since the tube is closed during the discharge.

We may now examine individual cases for values of ΔN_a and N_e which have some interest for our working conditions. With the contents of the tube at a pressure of a few mm Hg, the density of the argom atoms, at least by order of magnitude, will be $N_a = 10^{17}$ cm^{-3}. We now calculate $s(\lambda)$, for $L = 1$, for negative and positive variations in atom density, of 10% and 50%, *i.e.* for $\Delta N_a = (\pm 10^{16}, \pm 5 \cdot 10^{16})$ cm^{-3} and for ionizations of 5‰, 1%, 5%, 10%, 50%, *i.e.* for $N_e = (5 \cdot 10^{14}, 10^{15}, 5 \cdot 10^{15}, 10^{16}, 5 \cdot 10^{16})$ cm^{-3}. In Fig. 2 are plotted the functions (2.20) calculated in these cases; the full lines refer to $\Delta N_a > 0$ and the dashed lines to $\Delta N_a < 0$, while the straight lines represent the contributions of the free electron gas alone. It is clear that wide variations in the atom density will mask the effects of low electron densities. For heavy ionizations, however, these variations, even those of 50%, no longer exert any practical influence in the visible region, and $s(\lambda)$ coincides fairly completely with the straight line representing the free electrons.

The contribution made by the latter, however, is quite evident, even at low ionizations. In fact, if we consider the refractivity of a gas of free electrons and the refractivity of a gas of neutral atoms A I, at a given wavelength, *e.g.* $\lambda = 5\,460$ Å

$$(n-1)_{\text{A I}} = +1.06 \cdot 10^{-23} N_a ,$$

$$(n-1)_{\text{electrons}} = -13.33 \cdot 10^{-23} N_e ,$$

we can see that the contribution per electron is at least ten times as great as that for a neutral atom, as well as being opposite in sign. Furthermore, the refractivities of free electrons and neutral atoms are different functions of the

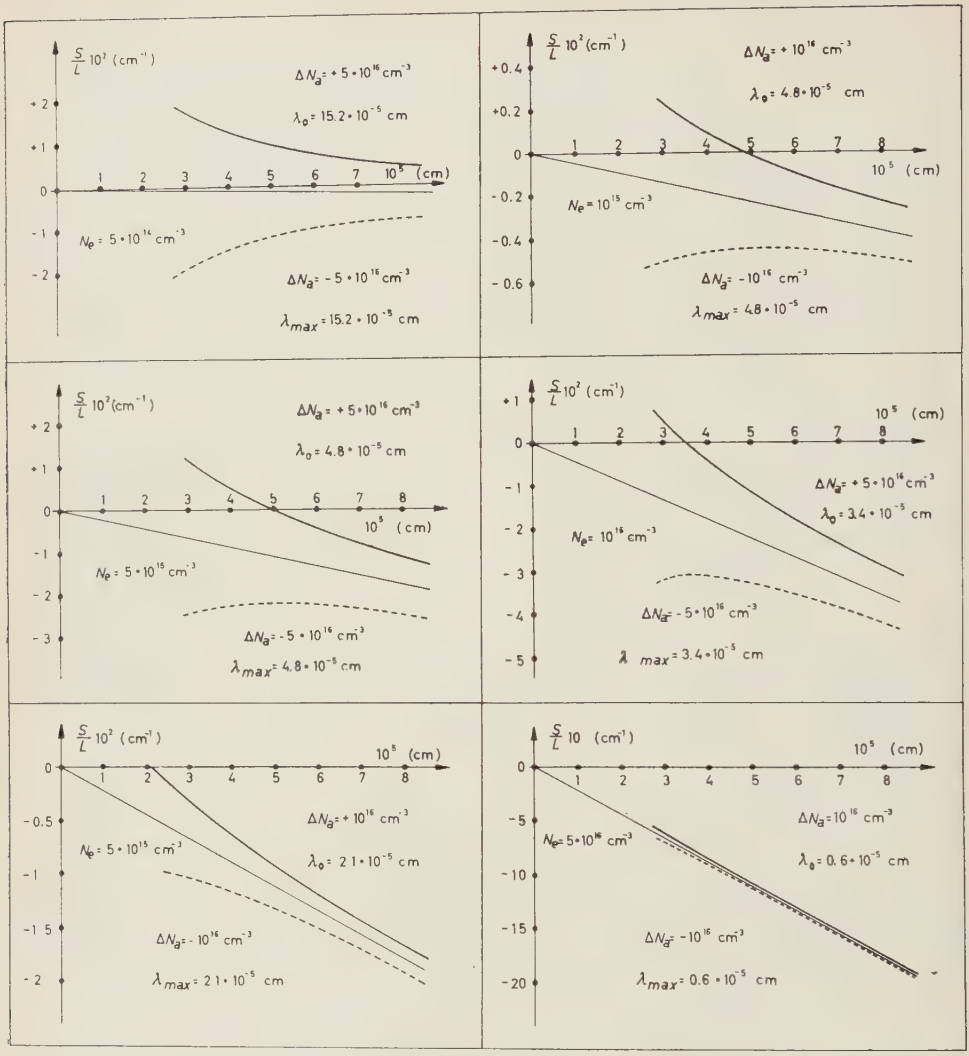

Fig. 2. – Theoretical behaviour of fringe system shift *versus* wavelength. Full lines represent shift due to electrons and an increase of atom density. Dashed lines represent fringe shift due to electrons and a decrease in atom density. The straight line through the origin represents the electron contribution.

wavelength, the former being proportional to the square of the wavelength, while that of the neutral atoms varies little throughout the visible spectrum. For all these reasons, and owing to the sensitivity of the interferometric method employed, it is possible to separate the contribution of the electron component from that of the atom component, even in cases of low percentage ionizations.

3. – Experimental section.

3·1. *Instrumentation and techniques.* – The measurements we carried out consist chiefly in the determination of the variation of the optical path for radiations of wavelengths comprised between approximately 4200 and 6500 Å, in a column of a gas before and after ionization. For this purpose we used the apparatus shown schematically in Fig. 1.

The light source used is a high pressure xenon-filled Osram arc lamp X B O 162, giving an essentially continuous spectrum with a maximum of intensity towards the red. The light is focused by means of an achromatic lens on a one-millimetre circular aperture. A 75 mm focal-length lens forms an image of the aperture at a point midway between the two glass plates of the interferometer. It was impossible to use parallel light beams since in this case, owing to the poor conditions of the interferometer used (an instrument built in the middle of the last century) we did not succeed in obtaining a satisfactory system of interference fringes. Following reflections on the first plate of the interferometer the two beams thus obtained pass through a diaphragm having two 3 mm circular apertures, spaced 18 mm apart. One of the beams, the strong one, passes through the discharge tube, the other through an open, air-filled tube whose function is to prevent strong thermal convection currents being formed in the vicinity of the heated discharge tube. In order to obtain a better definition of the light pencils a diaphragm similar to the first is placed in front of the second interferometer plate. With these diaphragms one can obtain sufficiently narrow light beams to allow a fairly accurate examination of the radial behaviour of the discharge. The resulting fringe pattern is then focused by means of an achromatic lens on the slit in a Hilger constant deviation spectrograph.

The better to interpret the variation of refractivity in the gas during ionization one should photograph the fringe systems side by side before and after discharge. This was done by placing a screen containing eighteen small windows in front of the photographic plate, to isolate as many narrow portions of the continuous spectrum. Before the discharge a photograph is taken of the fringe system, the plate being exposed only through the windows mentioned above. Then the plate holder is horizontally moved to bring the windows in correspondence of the unexposed plate areas and a new photograph is taken with the discharge on. In this way one obtains a photograph of the fringe system not as a continuous function of the wavelength but corresponding to determined wavelength intervals only.

For an evaluation of the shift of the fringe system photographed with the discharge on as compared with the discharge off, we used reference lines consisting of 0.01 mm tungsten wires placed parallel to one another horizontally

across the slit of the spectrograph. For a quantitative evaluation of the fringe shift care has been taken that the fringes are parallel to the images of the wires, which are of course straight lines, as the shift is measured by the variation of the distance of the reference line from a determined minimum of intensity. This cannot be obtained without special expedients, since the air traversed by the second ray gives rise to different refractivities for the various wavelengths with the result of bending the fringes across the spectrum. We were able to avoid this difficulty by constructing a water filled compensator (*). *i.e.* placing across the path of the ray traversing the discharge tube a given thickness of water to render the optical path equal to that through the air-filled tube. Water was chosen because its dispersion curve in the visible region is almost exactly proportional to that of air. In our case a thickness of water of about 0.15 mm had to be used. The compensator actually consists of two plates of optically finished glass held 0.15 mm apart by a piece of celluloid of that thickness. Distilled water is then introduced between the plates. The compensator is then placed across the path of the rays before the second plate of the interferometer. Fig. 3 shows two photographs of the fringe system, one taken with the compensator in use, the other without. The efficiency of the compensator can be seen quite clearly.

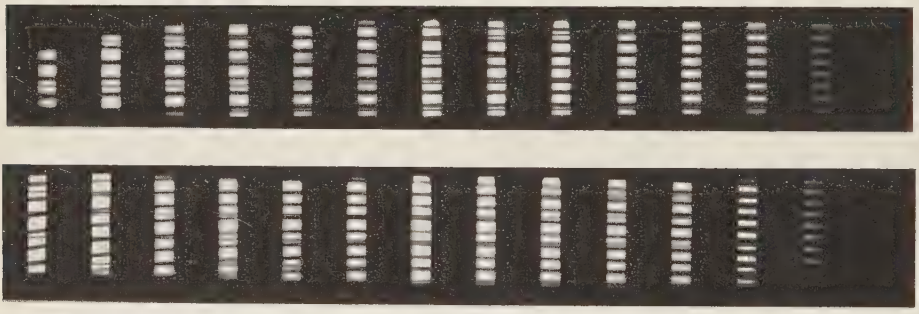

Fig. 3. – Photograph of fringe system: *a*) with compensator; *b*) without compensator.

Another trouble is the superposition of the intense light emitted by the plasma on the interference pattern. This has been minimized by reducing the aperture of the spectrograph collimator lens. The numerical aperture of the entire optical system has a very low value. Therefore it is necessary to use highly sensitive photographic plates in spite of the very intense light source employed. The following were tried: Gevaert Scientia 52 A 86 and 73 A 64, Gevaert Gevapan 36 and Ilford HPS. The last mentioned was in fact chosen

(*) We owe this important expedient to a suggestion by Professor F. RASETTI.

as it has the advantage of a high and fairly uniform sensitivity even if its range does not extend into the longer wavelengths and it is somewhat coarse-grained.

We used for this experiment quartz tubes 30 cm long and of 1.6 cm internal diameter. At each end are attached windows of optical glass which project from one side of the tube for about (15÷20) mm in order to intersect both light rays. The windows are sealed to the tube with silver chloride.

Discharge excitation is produced by a radiofrequency field. The radiofrequency source consists of a self-exciting oscillator using two 6 C 21 tubes in a push-pull circuit connected to an H.V. supply varying from 1500 to 7500 V. Power is supplied to the discharge tube through the circuit shown in Fig. 4. T is the discharge tube; L is a coil of 8 cm diameter and 30 cm

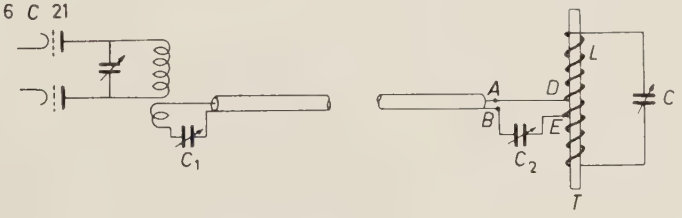

Fig. 4. – Schematic view of R.F. coupling.

length consisting of 8 turns of silver tubing. C_1 and C_2 are 100 $\mu\mu$F variable condensers. The capacitance of C_1 is fixed simply by introducing between A and B a suitable dummy load (incandescent lamp) in place of C_2, L and C. The other parameters (capacitance of C_2 and C and the number of turns of the coil between D and E) were varied in order to produce a discharge as intense as possible in the tube. This was obtained generally when the power delivered by the R.F. supply was approaching a maximum. The aspect of the discharge varied greatly as the capacitance of C varied. It goes without saying that we tried to operate in the same position each time. The LC circuit has its own frequency around 20 MHz. The power transferred to the discharge tube in our experimental conditions has been measured by means of a calorimetric method ([12]) to be about $\frac{1}{2}$ kW against a power delivered by the H.V. supply of about 4.5 kW.

3·2. *Measurements and analysis of the results.* – The purpose of our experiment is essentially to test the validity of formula (2.20) for argon and xenon. With the R.F. power available, satisfactory results were obtained for pressures of a few mm Hg. Only in this case was the fringe shift of sufficient mag-

([12]) F. CABANNES: *Ann. Phys.*, **10**, 1026 (1955).

nitude to be measurable within a reasonably small error throughout the spectrum.

In order to examine the refractivity of the plasma at different distances from the tube axis, the two-tube system was fixed on a carriage which could be displaced by means of a screw, transversally to the direction of the beams. The carriage was moved in one-millimetre steps, so as to take a photograph at each millimetre of the tube radius. The spatial resolution of the apparatus was of the same order of magnitude. To estimate this resolution we used the following simplifying hypothesis. Let us suppose that the beam is a cone with apex placed at the middle of the tube and of sectional radius $\varrho_0 = 1.5$ mm at the ends of the tube and neglect the fact that the beam converges to an image of finite magnitude. Under these conditions the density of luminous energy versus the distance from the cone axis is given by the following formula

$$dW/d\varrho = 2(1 - \varrho/\varrho_0)/\varrho_0 ,$$

from which one can obtain $\overline{\varrho} = \varrho_0/3$. Therefore the radial dependence of the refractivity is examined with a resolution function having the shape of a triangle of 3 mm basis.

Photographs of fringes taken under these conditions show shifts up to about a fringe, which are strongly dependent upon the wavelength and upon the distance from the tube axis. These fringe shifts may be positive or negative. Fig. 5 illustrates two typical interferograms, one *a*) showing a shift of the fringe system negative throughout, and the other *b*) positive throughout.

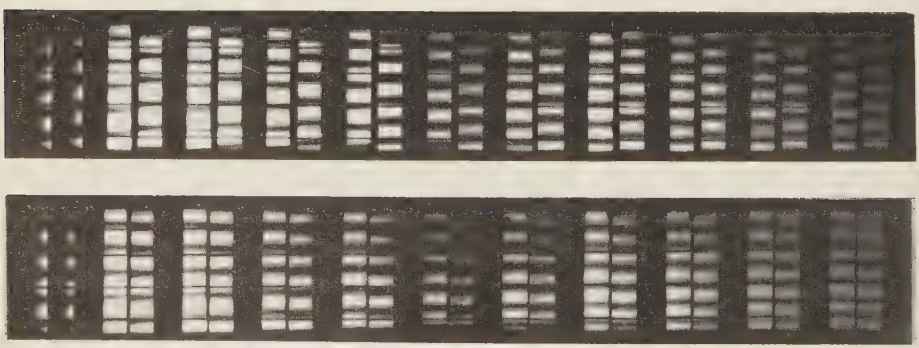

Fig. 5. – Typical interferograms showing fringe shift: *a*) downwards; *b*) upwards.

A Hilger and Watts recording microphotometer was employed to measure the shift of the fringe system following ionization of the gas. Error in the measurement of the fringe shift was about 3% to 5%. The values of ΔN_a, N_e and errors on these measurements were determined by the least squares

method. Let us call a and b the two coefficients appearing in the formula (2.20) and whose values are

$$a = \quad c_1 L \Delta N_a ,$$

$$b = - c_3 L N_e .$$

These are determined by the least squares method. By knowing c_1 and c_3 and assuming that the length of the plasma column coincides with that of the discharge tube, the values of ΔN_a and N_e are also obtained. The error on c_1 and c_3 is negligible with respect to δL, δa and δb and therefore it can be omitted. The error on a and b, neglecting the indetermination of wavelength due to the small width of the windows used, becomes

$$\delta a/a = \frac{\sum_i^{1,n} \lambda_i^2 \sum_i^{1,n} \delta s_i/\lambda_i + n \sum_i^{1,n} \lambda_i \delta s_i}{\sum_i^{1,n} \lambda_i^2 \sum_i^{1,n} s_i/\lambda_i + n \sum_i^{1,n} s_i \lambda_i} ,$$

$$\delta b/b = \frac{\sum_i^{1,n} 1/\lambda_i^2 \sum_i^{1,n} \lambda_i \delta s_i + n \sum_i^{1,n} \delta s_i/\lambda_i}{\sum_i^{1,n} 1/\lambda_i^2 \sum_i^{1,n} \lambda_i s_i + n \sum_i^{1,n} s_i/\lambda_i} ,$$

where δs_i are the differences between the experimental values of the fringe shift and the values given by the least squares functions, s_i and λ_i the experimental values of fringe shifts and wavelengths. The error on L is about 3 % assuming that the length of the plasma column coincides with that of the discharge tube with an indetermination of one centimetre for a tube about 30 cm long. This error is mainly due to the indefinition of the plasma contour. In conclusion the errors on the variation of atomic and electronic density are given by

$$\delta(\Delta N_a)/\Delta N_a = [(\delta a/a)^2 + (\delta L/L)^2]^{\frac{1}{2}} ,$$

$$\delta N_e/N_e = [(\delta b/b)^2 + (\delta L/L)^2]^{\frac{1}{2}} .$$

These errors are of the same order of magnitude. They rise from about 3 % for a mean shift of one fringe, to about 10 % for a mean shift of a few hundredths of a fringe.

In the previous considerations the lack of reproducibility of the discharges has been neglected. This effect is mainly due to the difficulty of obtaining always the same R.F. coupling to the discharge tube, and to the fact that the quartz tube is subject to strong heating, and in case of frequent discharges, its conditions may vary ([12]). However for a given discharge tube the repro-

ducibility appears rather good if the coupling remains fixed, and the discharges are separated by at least 30 minutes. This is confirmed by the analysis of some interferograms made using the above-mentioned measurements and keeping, of course, fixed the radial position of the discharge tube.

4. – Results.

We give here the results of three series of measurements carried out on argon at pressures of 5 mm Hg and 10 mm Hg, and on xenon at a pressure of 2.2 mm Hg. These three groups are here indicated by (α), (β) and (γ) re-

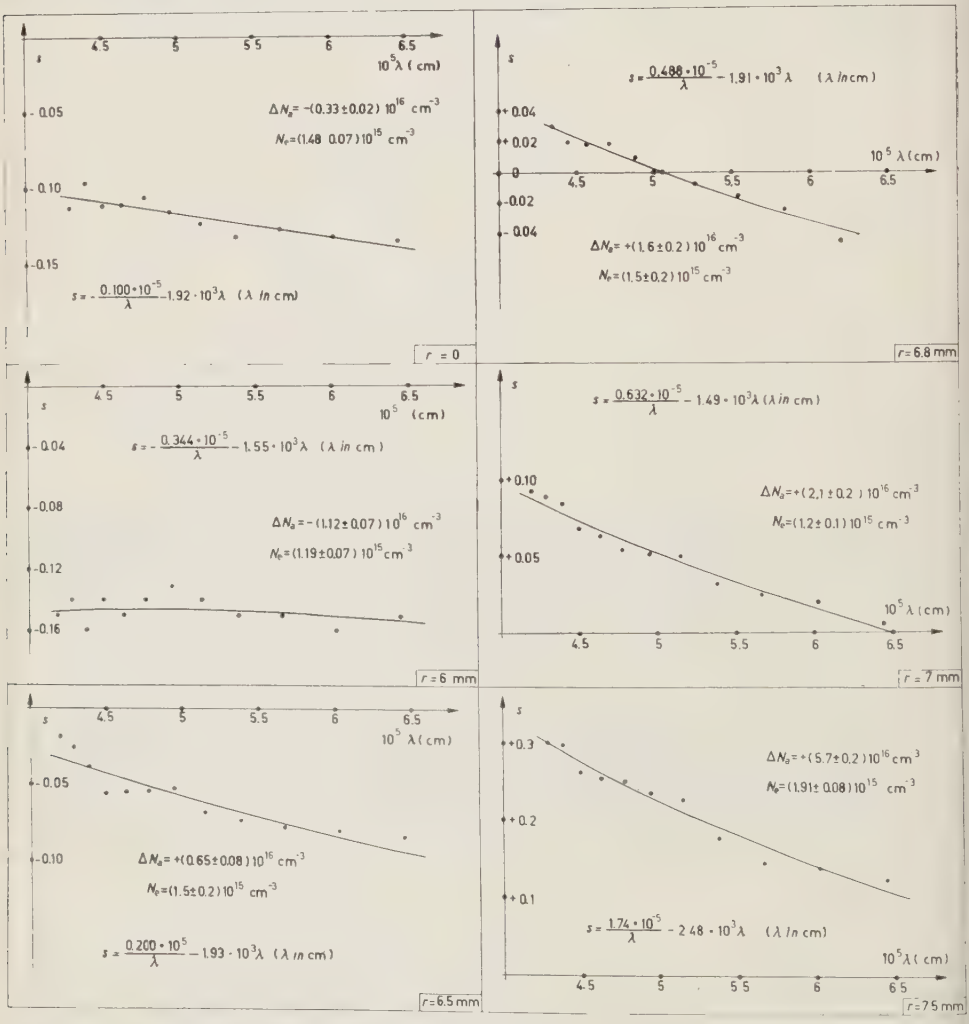

Fig. 6. – Fringe shift *versus* wavelength for different values of radius r and for discharge in argon at a pressure of 5 mm Hg (α).

spectively. Figs. 6-8 show the shift in fractions of a fringe versus the wavelength for the three sets of measurements. The curves plotted in these figures are obtained from the formula (2.20) by means of the least squares method.

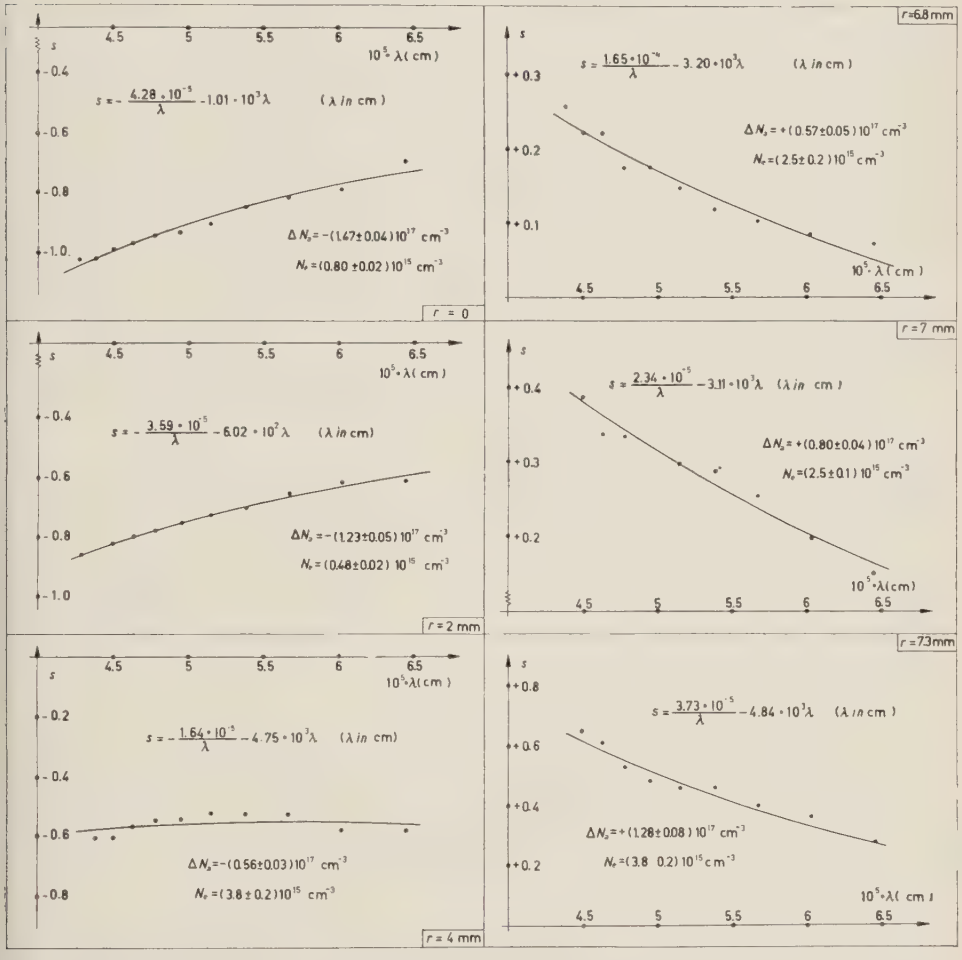

Fig. 7. – Fringe shift *versus* wavelength for different values of radius r for discharge in argon at a pressure of 10 mm Hg (β).

It is shown that the fringe shifts can be interpreted as due to the combined effects of density changes of the neutral atoms and of the presence of the electron gas. Of course the atom and electron densities reported represent only the average values along the tube length which can considerably differ from the local values.

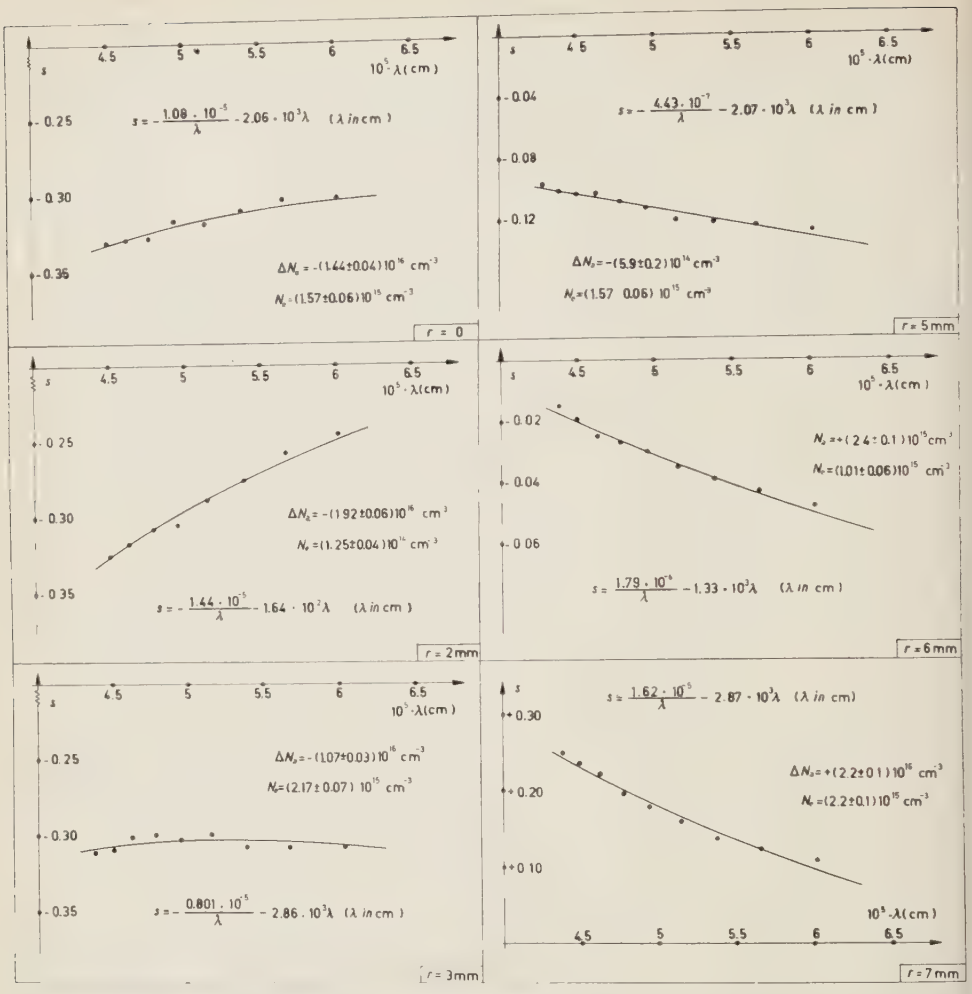

Fig. 8. – Fringe shift *versus* wavelength for different values of radius r for discharge in xenon at a pressure of 2.2 mm Hg (γ).

From the above-described diagrams one can deduce the behaviour of the atom and electron densities versus the distance from the tube axis assuming that the discharge is reproducible. The results are reported in Figs. 9-11. The curves of the atom density show the expected behaviour, that is a rarefaction on the tube axis and a correspondent increase near the wall. Argon at 10 mm Hg (β) and xenon at 2.2 mm Hg (γ) show a stronger rarefaction on the axis than argon at 5 mm Hg. If we allow that there is equal pressure throughout the discharge tube, since in all cases $N_a \gg N_e$, it will be seen from the formula $p = (N_a + 2N_e)KT$ that the gas temperature is inversely proportional to N_a. The curves of the electronic density show, on the con-

trary, a strange behaviour with several minima and maxima which change their position in the three sets of measurements. These curves contain experi-

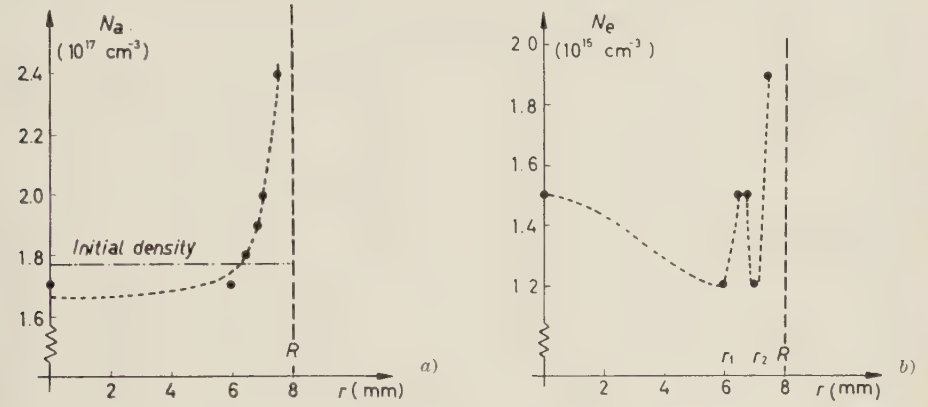

Fig. 9. – Radial behaviour of atom density (a) and electron density (b) in a discharge in argon at a pressure of 5 mm Hg (α).

imental errors difficult to evaluate due to the imperfect reproducibility of the discharge. A reason leading us to doubt the correctness of the results

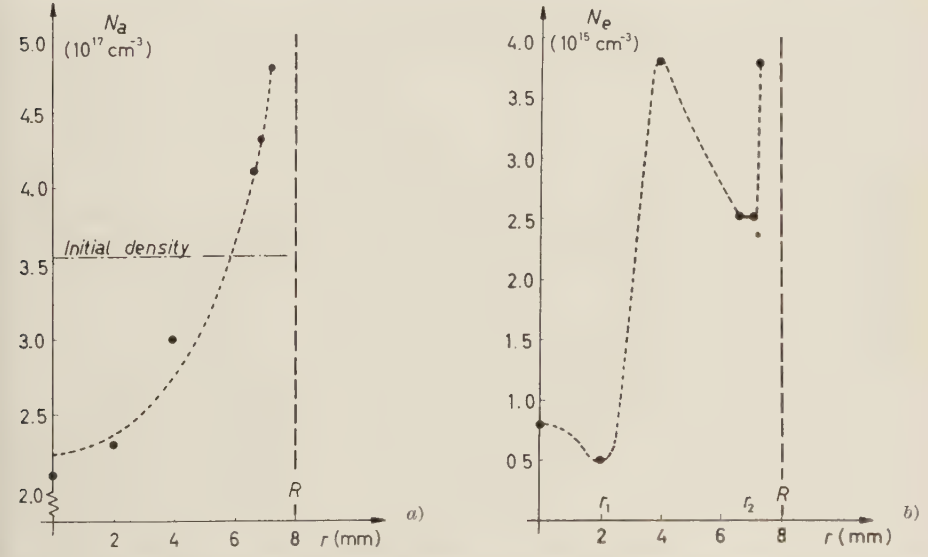

Fig. 10. – Radial behaviour of atom density (a) and electron density (b) in a discharge in argon at a pressure of 10 mm Hg (β).

is the fact that with the available resolution it is impossible to obtain maxima and minima so sharp as the above-mentioned ones, especially for argon at

5 mm Hg. From the N_e curves one sees that the discharge area could be divided roughly into three zones separated by the points r_1 and r_2 in Figs. 9*b*, 10*b* and 11*b*. The heavy concentration of electrons seen in the r_2-R zone is

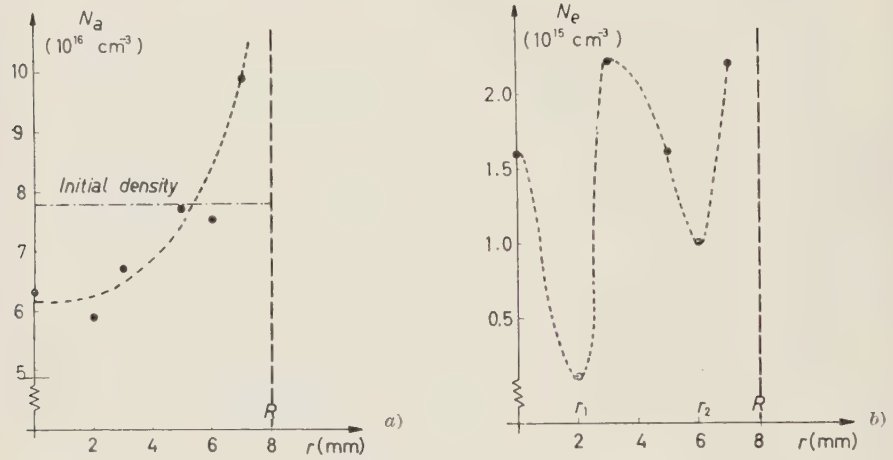

Fig. 11. – Radial behaviour of atom density (*a*) and electron density (*b*) in a discharge in xenon at a pressure of 2.2 mm Hg (γ).

probably due to a spurious effect from secondary emission of electrons from the walls of the very hot quartz tube ([13]). Furthermore the silver chloride used as a cementing agent evaporated during the discharges, as was confirmed by the appearance in the r_2-R zone of silver spectrum lines. In the r_1-r_2 zone an annular type discharge has occurred. In the discharge (α) where the power transferred to the tube was greater than in discharges (β) and (γ), the r_1-r_2 zone is considerably closer to the tube wall. The discharge did not fill the tube throughout its length but was contracted at its extremities towards the axis; this probably gave rise to the other maximum for $N_e(r)$ in the 0-r_1 zone.

The three curves discussed show that the R.F. coupling used was not suitable for the study of the radial distribution of electron densities, since it sets up non-uniform fields. It was noted that, besides depending greatly on the manner in which the R.F. power was coupled to the gas, the type of discharge depends to a considerable degree on the initial temperature of the tube wall. On the other hand, the entire question of dependence of N_a and N_e on the radius of the discharge tube and on the R.F. coupling is not the purpose of our experiment. We mention it here merely because the data at our disposal supplied some indication on that dependence. However, the experimental device used was not suitable for this research.

([13]) S. C. Brown: *Basic Data of Plasma Physics* (New York, 1959).

5. – Conclusions.

As was to be expected, this method of determining electron densities, even if very precise, is rather poor in sensitivity. Assuming that the minimum observable fraction of fringe is of the order of one hundredth, it will be seen that with a tube L cm long the minimum perceivable electronic density in the violet (around 4000 Å) is about $5.6 \cdot 10^{15}/L$ electrons $\times$ cm^{-3}. Measurements must be performed on at least two wavelengths in order to have information on the effect of the atoms. The above number refers to the shortest wavelength used since this gives us the minimum sensitivity for measuring electron densities. The method cannot be employed for weak discharges or discharges on short optical paths except where an interferometric method can be used in the far infra-red region. On the other hand, as R. A. Alpher and D. R. White have shown, the method can be very useful in discharges where high electron densities are obtained, *e.g.* with shock waves and in other experiments for thermonuclear researches.

* * *

We are very indebted to Professor F. Rasetti for many fruitful discussions and suggestions given us during this experiment.

RIASSUNTO

L'esperienza descritta in questo articolo tende a mettere in evidenza il contributo degli elettroni liberi alla refrattività di plasma di gas nobili. Sono inoltre prese in esame le variazioni di densità del gas neutro e la loro dipendenza dal grado di ionizzazione. Il metodo di analisi impiegato è quello dell'interferometria ottica. Di questo metodo si discutono i limiti di sensibilità. Il plasma è stato prodotto con un campo di radiofrequenza.

The Plasma-Sheath Transition in a Magnetic Field.

J. E. Allen and F. Magistrelli

Laboratorio Gas Ionizzati EURATOM - C.N.E.N.
c/o Laboratori Nazionali di Frascati - Roma

(ricevuto il 1° Agosto 1960)

Summary. — A criterion for sheath formation is presented which allows for the effect of a weak magnetic field. Relevant measurements have been made using a low pressure mercury arc in which an azimuthal or « pinch-type » magnetic field could be applied.

1. – Introduction.

It is known, from the work of Tonks and Langmuir [1] and others [2-9], that the positive ions in an ordinary low pressure plasma are accelerated towards the plasma boundary by electrostatic fields. These fields are weak, since the plasma is almost electrostatically neutral, but they extend over considerable distances. The positive ions, therefore, gain considerable energy as they move towards the plasma boundary. In fact the ions leave the plasma and enter the surrounding space-charge sheath with an energy which is com-

(1) L. Tonks and I. Langmuir: *Phys. Rev.*, **33**, 1070 (1929); **34**, 876 (1929).

(2) D. Bohm, E. H. S. Burhop and H. S. W. Massey: *The Characteristics of Electrical Discharges in Magnetic Fields*, eds. A. Guthrie and R. K. Wakerling (New York, 1949), chap. 2.

(3) D. Bohm: *The Characteristics of Electrical Discharges in Magnetic Fields*, eds. A. Guthrie and R. K. Wakerling (New York, 1949), chap. 3.

(4) R. L. F. Boyd: *Proc. Roy. Soc.*, A **201**, 329 (1950).

(5) J. E. Allen and P. C. Thonemann: *Proc. Phys. Soc.*, B **67**, 768 (1954).

(6) J. E. Allen, R. L. F. Boyd and P. Reynolds: *Proc. Phys. Soc.*, B **70**, 297 (1957).

(7) E. R. Harrison: *Journ Electronics and Control*, **5**, 319 (1958).

(8) I. B. Bernstein and I. N. Rabinowitz: *Physics of Fluids*, **2**, 112 (1959).

(9) E. R. Harrison and W. B. Thompson: *Proc. Phys. Soc.*, **74**, 145 (1959).

parable with the thermal energy of the electrons, *i.e.* $\frac{1}{2} m_2 v_2^2 \simeq \frac{1}{2} k T_1$, where the suffixes 1 and 2 refer to the electrons and positive ions respectively. This relation is sometimes referred to as the Bohm criterion for sheath formation ([3]).

The work cited above, however, deals with a plasma in the absence of a magnetic field. It is of interest, therefore, to enquire into the effects produced by the latter, especially since the self-magnetic field of the discharge itself ([10]) may appreciably affect the above criterion for sheath formation ([5]). The object of the present paper is to present a modified sheath criterion, which allows for the effect of a weak magnetic field, together with measurements made using a low pressure mercury arc.

The measurements were made using an azimuthal or « pinch-type » magnetic field produced by a current-carrying wire situated at the axis of a discharge tube. Measurements were made, using Langmuir probes, both with and without the applied magnetic field, the direction of the latter being reversible.

A preliminary report on this work was given at the Fourth International Conference on Ionization Phenomena in Gases ([11]).

2. – Theory.

Fig. 1. illustrates the co-ordinate system which will be used in a simple calculation referring to conditions just inside the sheath, the curvature of the

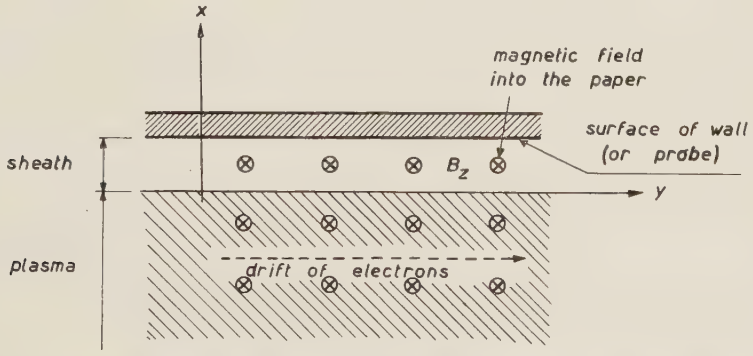

Fig. 1. The co-ordinate system used in the analysis of a plane plasma-sheath transition.

latter being neglected. The magnetic field is in the z-direction but can assume positive or negative values. It will be assumed that the electrons have

([10]) P. C. Thonemann and W. T. Cowhig: *Proc. Phys. Soc.*, B **64**, 345 (1951).

([11]) J. E. Allen and F. Magistrelli: *Proc. of the Fourth Intern. Conf. on Ionization Phenomena in Gases* vol. **2** (1959), p. 599.

a Maxwellian distribution superposed upon a constant drift velocity $\bar{v}$ in the y-direction, *i.e.* it is assumed that the distribution function has the form

$$f(u, v, w) = n_1 \left\{\frac{m_1}{2\pi k T_1}\right\}^{\frac{3}{2}} \exp\left[-\frac{m_1}{2kT_1}\left[u^2 + (v - \bar{v})^2 + w^2\right]\right],$$

where $\bar{v}$ does not vary with x. This assumption cannot be exactly true since there is an electron current to the wall (or probe); this current is very small, however, because most of the electrons are reflected by the strong electrostatic field which exists in the sheath.

An ordinary Maxwellian distribution exists in a co-ordinate system moving with a velocity $\bar{v}$ and the electric field measured in this system is given by

$$E' = E + \frac{\bar{v}H}{c},$$

if $(\bar{v}/c)^2 \ll 1$. Boltzmann's relation in this new co-ordinate system can be written

$$\left\{\begin{array}{l} n_1 = n_{1s} \exp\left[e_1 \int_0^x E' \,\mathrm{d}x / kT_1\right], \\ \textit{i.e.} \\ n_1 = n_{1s} \exp\left[\dfrac{e_1 \int_0^x (E + (\bar{v}H/c))\,\mathrm{d}x}{kT_1}\right], \end{array}\right. \tag{1}$$

where the potential is measured relative to the plasma-sheath boundary, *i.e.* $V = 0$ at $x = 0$; the electron density is, of course, the same in both reference systems since the transformation from one system to the other is non-relativistic.

If it is assumed that all the positive ions enter the sheath with an energy $e_2 V_0$ then their density in the sheath can be written

$$n_2 = n_{2s}(1 - (V/V_0))^{-\frac{1}{2}}, \tag{2}$$

where n_{2s} is the ion density at the sheath edge.

At the sheath edge $n_{1s} = n_{2s} = n_s$, and $\mathrm{d}n_1/\mathrm{d}x = \mathrm{d}n_2/\mathrm{d}x$ to a high degree of approximation (5), so that

$$\frac{kT_1}{2e_2 V_0} = 1 + \frac{\bar{v}H}{cE_s}, \tag{3}$$

assuming that the ions are singly charged and using equations (1) and (2); E_s is the electric field at the plasma-sheath boundary. This formula, which reduces to the Bohm sheath criterion [3] when $H = 0$, shows that the ratio $kT_1/2e_2V_0$ is increased by a « pinch » field ($H > 0$) and decreased by an « anti-pinch » field ($H < 0$).

In practice the ions will not all have the same energy when they enter the sheath so that equation (3) is not expected to hold exactly. For this reason it can be replaced by

$$\frac{kT_1}{2e_2V_0} = \frac{1}{\alpha^2}\left(1 + \frac{\bar{v}H}{cE_s}\right), \tag{4}$$

where α is a quantity of the order of unity [5].

3. – Apparatus.

The mercury vapour discharge tube, which is of Pyrex glass about 80 cm long, and 80 mm in diameter, is shown in Fig. 2. C is the cathode, A_1 is the main anode, A_2 an auxiliary anode, i the igniter and U is an umbrella which

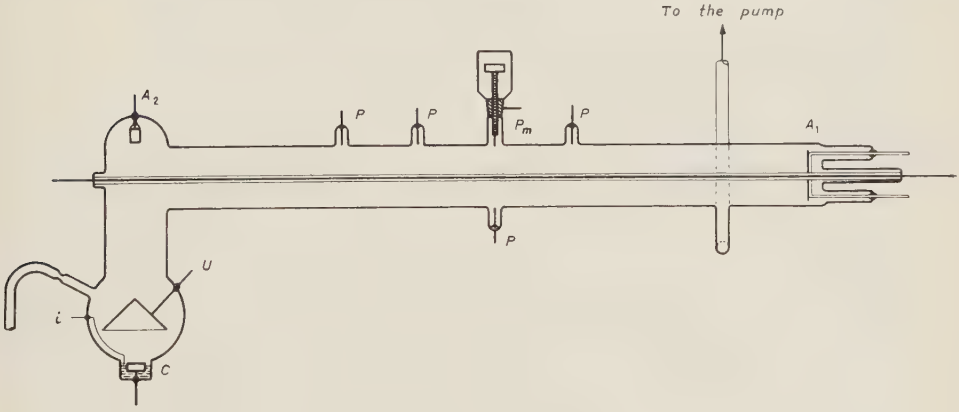

Fig. 2. – The discharge tube.

prevents direct jets of mercury from the cathode spot from entering the horizontal tube. The main anode (which is water-cooled) is nickel-plated copper, the auxiliary anode is molybdenum, the igniter is tungsten and the umbrella is nickel. A nickel spiral protrudes through the surface of the cathode pool and serves to anchor the cathode spot.

The electrodes marked P are Langmuir probes consisting of tungsten rods of 2 mm diameter; they are sleeved with glass tubing such that the collecting

area of each probe is equal to the cross-sectional area of the tungsten rod. The probe marked P_m is radially movable by means of a stainless steel screw which has a pitch of 1 mm. The screw, which has a head containing two pieces of soft iron, is inside the vacuum system and is rotated by means of a magnet.

A glass capillary tube containing a wire is situated at the axis of the discharge tube and is sealed to the latter so that the wire is not within the vacuum system. The discharge tube is continuously evacuated by a two-stage mercury diffusion pump. The use of vacuum grease and rubber gaskets has been avoided and the residual pressure is about 10^{-7} mm Hg. The pumping tube has a U-bend, as shown in Fig. 2, which is submerged in the same thermostatically controlled bath as the cathode bulb. This is in order to have a good control of the mercury vapour pressure within the tube. It is also possible to raise the level of the liquid in order to cover the whole tube; the experiments reported in this paper were carried out under the latter condition.

The bath temperature T_b can be varied from -5 °C up to 10 °C corresponding to a variation of the mercury vapour pressure from $1.2 \cdot 10^{-4}$ to $5.4 \cdot 10^{-4}$ mm Hg. The electron mean free path in this pressure range is greater than the tube diameter.

4. – Experimental results.

Using the movable probe P_m placed at the wall (as shown in Fig. 2) measurements were made both with and without an applied magnetic field. The latter was produced by passing a direct current I_f through the central wire and was applied both in the « pinch » direction and the « anti-pinch » direction. With the currents used in these experiments the applied magnetic field strength at the wall was of the order of one gauss. The discharge tube was placed with its axis parallel to the horizontal component of the earth's

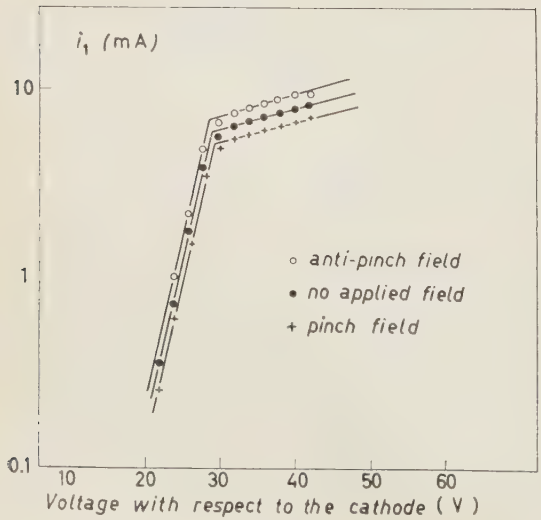

Fig. 3. – Typical probe characteristics (electron currents).

magnetic field so that effects due to the latter could be ignored. Fig. 3 and Fig. 4 show typical probe characteristics obtained.

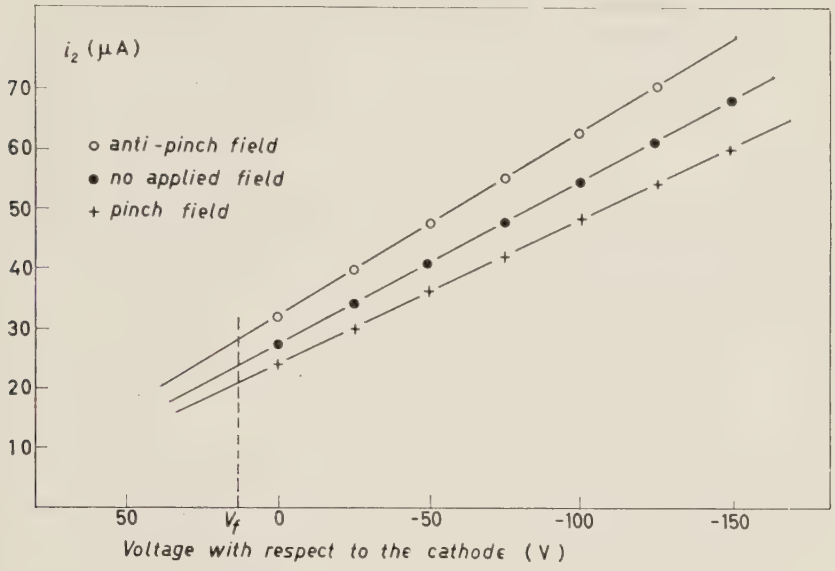

Fig. 4. – Typical probe characteristics (ion currents).

The electron saturation current was determined in the usual way and the ion current was determined by extrapolating the ion current characteristic to the floating potential V_f. The corresponding current densities are given respectively by

$$j_i = n_s e_1 \sqrt{\frac{kT_1}{2\pi m_1}}, \tag{5}$$

and

$$j_2 = n_s e_2 \sqrt{\frac{2e_2 V_0}{m_2}}. \tag{6}$$

Using (5) and (6) one can write

$$\frac{kT_1}{2e_2 V_0} = 2\pi \frac{m_1}{m_2}\left(\frac{j_1}{j_2}\right)^2,$$

so that the quantity $kT_1/2e_2V_0$ can be determined from the probe characteristics.

Equation (4) can be written in the form

$$\frac{kT_1}{2e_2V_0} = \frac{1}{\alpha^2}\left(1 + \frac{E^*}{E_s}\right),$$

where $E^* = \bar{v}H/c$.

If it is supposed that α and E_s remain constant (or approximately constant) as the magnetic field is varied, the plot of $kT_1/2e_2V_0$ as a function of E^* should be a straight line which intercepts the ordinate axis at the point α^{-2} and whose slope is $(\alpha^2 E_s)^{-1}$.

Fig. 5*a* and Fig. 5*b* show results obtained for different values of the arc current I_a and the bath temperature T_b. Each experimental point was obtained by averaging over ten measurements and the straight line through these points was determined by apply-

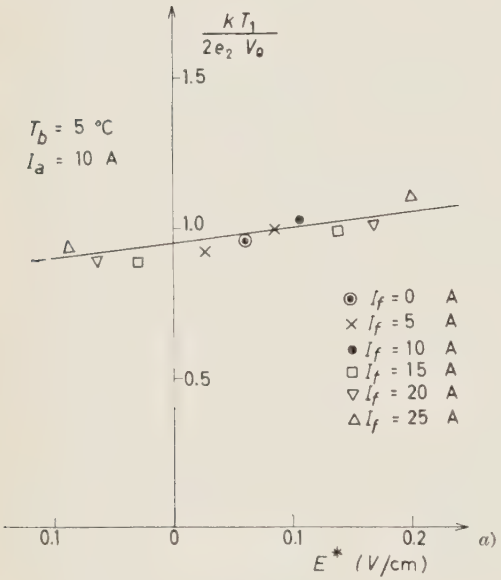

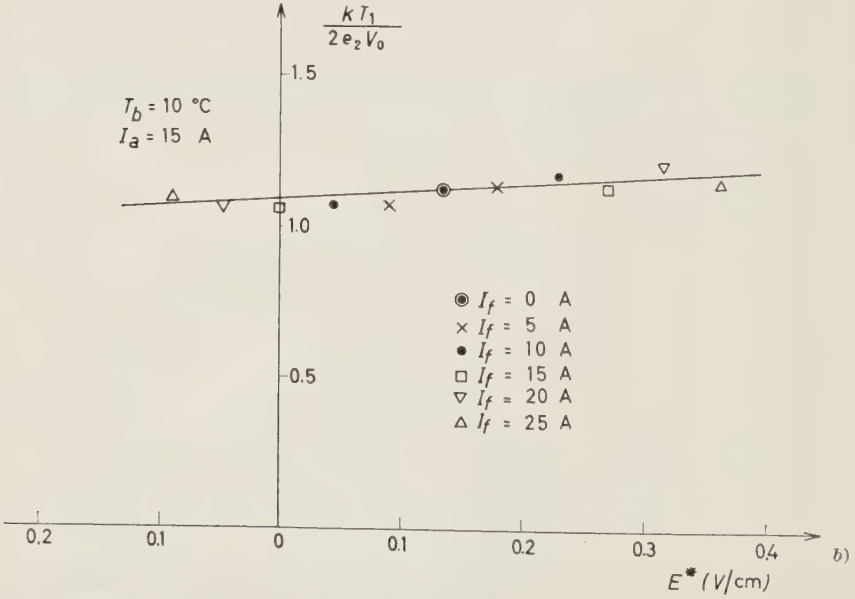

Fig 5. – Typical experimental curves giving the variation of $kT_1/2e_2V_0$ as a function of E^*: (*a*) bath temperature 5 °C, arc current 10 A; (*b*) bath temperature 10 °C, arc current 15 A.

ing the method of least squares. Measurements have been made also in other experimental conditions and Fig. 6 summarizes the results obtained.

In plotting Fig. 5 and 6 it has been assumed that the drift velocity is not affected by the magnetic field. The drift velocity $\bar{v}$ was determined experimentally. Assuming that the drift velocity is constant over the cross-section of the tube the arc current can be written as

$$I_a = \bar{v} e_1 \int_{r_c}^{r_0} 2\pi n(r)\, \mathrm{d}r ,$$

where r_c is the outer radius of the central capillary tube and r_0 is the discharge tube radius. Using the movable probe the plot of n as a function of r was obtained and the integral graphically calculated. Table I gives the results obtained for $\bar{v}$ in different experimental conditions together with the values of the electron temperature T_1 and of the plasma density n_s at the sheath edge.

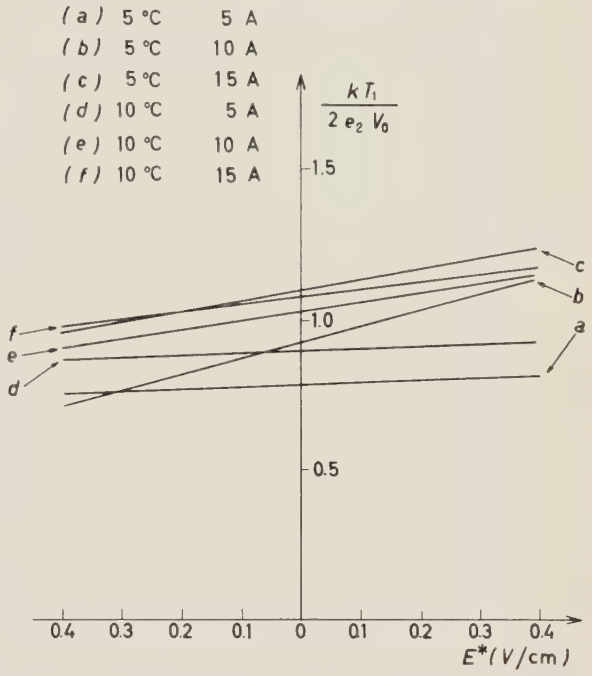

Fig. 6. – Graphical summary of the experimental results.

Table I.

T_b (°C)	I_a (A)	$\bar{v} \cdot 10^{-7}$ (cm/s)	$T_1 \cdot 10^{-3}$ (°K)	$n_s \cdot 10^{-10}$ (cm^{-3})
5	5	3.0	31	1.3
	10	1.7	22	4.5
	15	2.3	27	5.8
10	5	2.7	25	1.6
	10	1.5	21	5.1
	15	1.9	22	7.4

The numerical values of α and E_s, which have been derived from the straight lines plotted in Fig. 6, are given in Table II. The corresponding values of $kT_1/e_2 r_0$ are given for comparison.

TABLE II.

T_b (°C)	I_a (A)	α	E_s (V/cm)	kT_1/e_2r_0 (V/cm)
5	5	1.1	10	0.63
	10	1.0	2.4	0.45
	15	0.95	3.5	0.55
10	5	1.1	11	0.51
	10	0.98	3.5	0.43
	15	0.96	4.7	0.45

5. – Discussion.

The observed variation of the ratio $kT_1/2e_2V_0$ with magnetic field strength, for a given discharge, is qualitatively that predicted by the elementary theory; *i.e.* $kT_1/2e_2V_0$ varies linearly with $\bar{r}H/c$, as can be seen in Fig. 5. The values of α (see Table II) are all near unity, as they should be. Furthermore the derived values of the electric field E_s given in Table II seem to be of a reasonable order of magnitude when compared with the corresponding values of kT_1/e_2r_0, the latter quantity being a rough measure of the mean electrostatic field in the plasma (1). The variation of E_s with arc current, however, is not expected since one would expect $E_s(kT_1/e_2r_0)^{-1}$ to increase with increasing current according to the theory of Tonks and Langmuir (1).

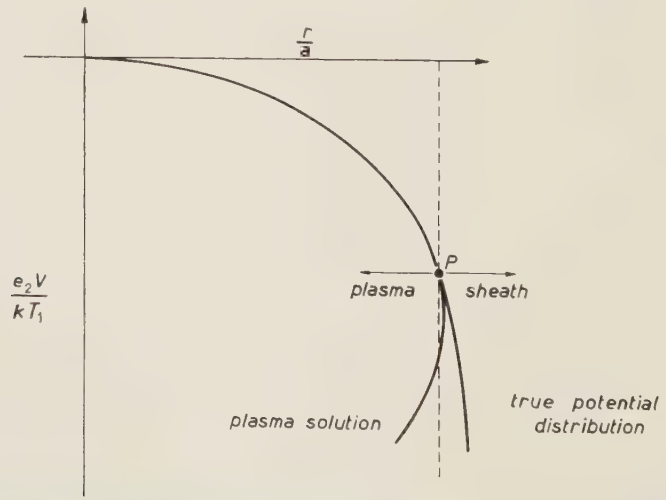

Fig. 7. Diagram illustrating the radial distribution of potential and the « plasma solution » of Tonks and Langmuir (1); a is an adjustable constant.

The theory of Tonks and Langmuir deals mainly with the potential distribution within the plasma; their potential distribution, which is known as the « plasma solution », is illustrated schematically in Fig. 7. This solution was obtained by making the assumption that $|n_1 - n_2| \ll n_1$ and at a certain point P (see Fig. 7) this assumption breaks down and the space-charge sheath commences. The definition of the sheath edge is somewhat arbitrary but it can be assumed that the plasma merges into the sheath when $|n_1 - n_2|/n_1 \sim 1\%$. The position of the point P depends on the ratio between the Debye distance (λ) and the tube radius (r_0), the range of validity of the « plasma solution » being greater when the ratio λ/r_0 is small. Thus the point P moves to the right as the Debye distance is decreased (for a given tube radius); *i.e.* the electric field increases at the sheath edge, since this is represented by the slope at the point P.

In the present experiments, however, the variation of the electric field does not show this monotonic increase. It is conceivable that the observed results are due to oscillations in the sheath; very high frequency oscillations have been detected by Gabor, Ash and Dracott ([12]) but it is not known whether such oscillations are usually present or whether they are excited only in particular circumstances.

* * *

The authors wish to thank Mr. A. Mola for his assistance in the experimental work. They also wish to thank Prof. B. Brunelli for his interest and support.

([12]) D. Gabor, E. A. Ash and D. Dracott: *Nature*, **176**, 916 (1955).

RIASSUNTO

È dato un criterio riguardante la formazione della guaina al contorno di un plasma in presenza di un campo magnetico. Sono state fatte misure in proposito usando un arco a vapori di mercurio a bassa pressione. Lungo l'asse del tubo di scarica vi è un filo percorso da una corrente che produce un campo magnetico azimutale; il valore di questo campo può essere positivo o negativo. Le misure sono state fatte usando sonde di Langmuir con e senza il campo magnetico applicato. I risultati mostrano che vi è un effetto del campo magnetico nel senso previsto dalla teoria. Si possono ottenere dalle misure i valori del campo elettrico al contorno del plasma. Non è ben chiaro, però, il comportamento di questo campo al variare della corrente dell'arco.

Studies on Extensive Air Showers.

Part I. – Sea Level Observations on the Variation with Shower Size of the Total Number of Nuclear-Interacting Particles in Showers of $(10^4 \div 2.5 \cdot 10^6)$ Particles.

B. K. Chatterjee, G. T. Murthy, S. Naranan, B. V. Sreekantan and M. V. Srinivasa Rao

Tata Institute of Fundamental Research - Bombay

(ricevuto il 1° Agosto 1960)

Summary. — An experiment carried out at sea level on the lateral distribution of nuclear-interacting particles in air showers and the variation of their number with the size of the showers, is described; the showers recorded ranged in size from 10^4 to $2.5 \cdot 10^6$ particles. The results indicate that the number of nuclear-interacting particles is proportional to $N_e^{0.45 \pm 0.05}$ for showers of size N_e less than about $6 \cdot 10^5$ particles, and the number is proportional to $\sim N_e^{1.2}$ for larger sizes. What has been obtained in this experiment and in similar experiments conducted by other groups (Nicol'sky *et al.* and Lehane *et al.*), is the *average* number of nuclear-interacting particles in a large number of showers of a given size. The possibility that such an average may not be meaningful if large intrinsic fluctuations (other than normal statistical variations) exist, is pointed out.

1. – Introduction.

Nicol'sky *et al.* [1] have, in an experiment carried out at a mountain altitude of 650 g cm^{-2}, determined the variation with shower size of the total number of nuclear-interacting particles, (N-particles), in extensive air showers which ranged in size from $4 \cdot 10^3$ to 10^6 particles. A similar study has been carried out by Lehane *et al.* [2], at sea level, for showers whose sizes ranged from $5 \cdot 10^4$ and $2 \cdot 10^6$ particles. The experiment of Nicol'sky *et al.* showed

[1] S. I. Nikol'sky: *Proc. of the Oxford Conf. on Extensive Air Showers* (1956), p. 19.
[2] J. A. Lehane, D. D. Millar and M. H. Rathgeber: *Nature*, **182**, 1699 (1958).

that the number of N-particles varied with shower size, N_e, as $N_e^{0.2}$ for showers of size less than $4 \cdot 10^5$ particles, while the variation was given by $N_e^{1.0}$ for larger shower sizes; the change of the exponent was sudden and occurred at a shower size of $\sim 4 \cdot 10^5$ particles (at an altitude of 650 g cm^{-2}). This sudden change of slope, in the curve representing the variation of the total number of N-particles with shower size, has been interpreted by NIKOL'SKY *et al.* as indicating that nuclear collisions of particles of energy greater than $6 \cdot 10^{14}$ eV are radically different in their characteristics from those due to particles of lower energy.

In this paper we report an experiment carried out at sea level at Bombay, on the variation of the number of N-particles with shower size. The shower size recorded ranged from 10^4 to $2.5 \cdot 10^6$ particles. The results indicate that the number of N-particles is proportional to $N_e^{0.15 \pm 0.05}$ for showers of size less than about $6 \cdot 10^5$ particles, and the exponent becomes ~ 1.2 for larger sizes.

2. – Experimental arrangement.

The extensive air shower array was set up on the terrace of the building of the Tata Institute of Fundamental Research, in Colaba, Bombay. The lay-out of the detectors (Fig. 1), was therefore determined to some extent

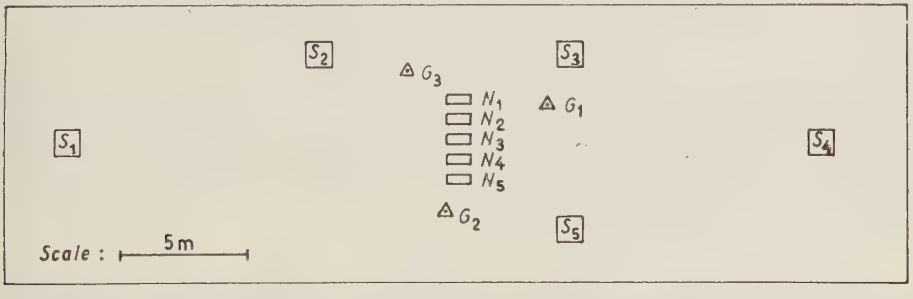

Fig. 1. – Extensive air shower array. S_1-S_5 are liquid scintillators, each of area 1 m^2; N_1-N_5 are N-detectors, each of area 0.4 m^2; G_1, G_2, G_3 are Geiger counter trays, each of area 500 cm^2.

by the dimensions of the terrace. S_1, S_2, S_3, S_4, S_5 are five liquid scintillation counters each of area 1 m^2; they were spread over an area of 30 m $\times$ 6 m. N_1, N_2, N_3, N_4, N_5 are five N-detectors placed close to each other at the centre of the array of scintillation counters. Each N-detector had an effective area of 0.4 m^2 and consisted of enriched BF_3 neutron counters embedded in paraffin and lead (Fig. 2); the BF_3 counters were 75 cm long, 2.5 cm in dia-

meter. Cadmium sheets were inserted between the various N-detectors to prevent slow neutrons produced in one detector from reaching an adjacent detector. The N-particles produce nuclear interactions in the lead and paraffin, and evaporation neutrons from these interactions are slowed down in the paraffin layer and detected as thermal neutrons by the BF_3 counters. A detector of this type has several advantages over the « Jánossy-type » of penetrating-shower detector, in which the N-particle is detected through the shower of penetrating particles it produces. The penetrating-shower detector has a relatively high energy threshold—about 5 to 10 GeV—for detecting nuclear interactions. On the other hand, the neutron detector responds to interactions of much lower energy, down to about 100 MeV, though with decreasing efficiency. In addition to penetrating showers, the penetrating-shower detector also responds to electron-photon cascades produced by high energy electrons and photons resulting particularly from the electromangetic interactions of μ-mesons. The neutron detectors respond exclusively to nuclear interactions. Another great advantage is that with a few neutron counters large effective areas can be built up.

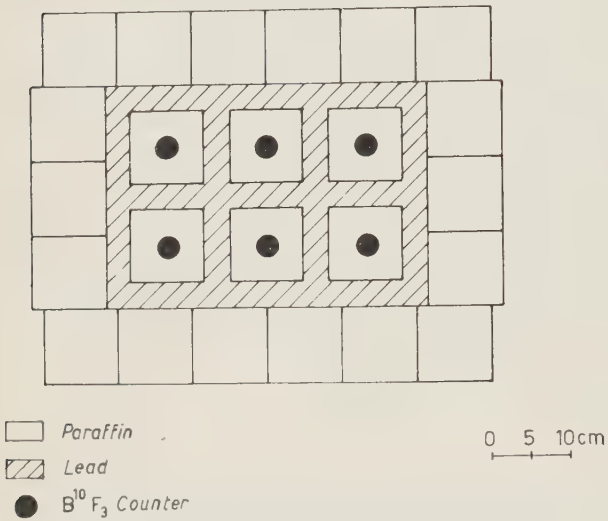

Fig. 2. – Cross-section of N-detector.

Selection and display. – The air showers were selected by a triple coincidence of three Geiger counter trays G_1, G_2 and G_3 (Fig. 1) each of area 500 cm². Pulses from the photomultipliers looking at the scintillators, and pulses from the neutron counters were displayed on four oscilloscopes. The triple coincidence master-pulse triggered first a 30 μs sweep in each oscilloscope, and then a second sweep 500 μs long, displaced vertically with respect to the first. The photomultiplier pulses, after suitable amplification, delay and attenuation, were displayed on the 30 μs sweeps and the N-detector pulses on the 500 μs sweeps. The non-overloading amplifiers and the display system were designed so that electron densities could be measured over the range of 1 to 1000 particles per m². It was possible to identify the particular N-detectors that were

activated, and also to determine the total number of pulses from the BF_3 counters in each of the N-detectors.

3. – Experimental results.

The experiment was in operation for three months at Bombay (sea level) during which period about 5 000 showers were recorded.

The shower sizes and the core positions were determined assuming a lateral distribution function of the Nishimura-Kamata type [3] for an age parameter $s = 1.25$. The computation was done with the aid of two mechanical analogue computers built for the purpose. The shower sizes recorded ranged from 10^4 to $2.5 \cdot 10^6$ particles, and the core-distances extended up to 25 m from the centre of the array. The error in size was 20 to 30 percent and the error in core position 1 to 2 m up to 10 m from the centre and about 3 to 5 m for cores beyond 10 m. In about 600 out of the 5 000 showers recorded, associated pulses from at least one of the five N-detectors were observed.

Showers were classified according to their size N_e, and the distance, r, of the core from the centre of the N-detectors. For this puspose, the following six intervals of shower sizes were chosen:

$$1.0 \cdot 10^4 \div 2.5 \cdot 10^4 \qquad 1.6 \cdot 10^5 \div 4.0 \cdot 10^5$$

$$2.5 \cdot 10^4 \div 6.3 \cdot 10^4 \qquad 4.0 \cdot 10^5 \div 1.0 \cdot 10^6$$

$$6.3 \cdot 10^4 \div 1.6 \cdot 10^5 \qquad 1.0 \cdot 10^6 \div 2.5 \cdot 10^6$$

For each group of showers a further classification was carried out using the following intervals for r,

$$0 \div 2.5 \text{ m} \qquad 6.3 \div 16 \text{ m}$$

$$2.5 \div 6.3 \text{ m} \qquad 16 \div 25 \text{ m}$$

a) *Density of* N*-particles.* If the assumption is made that there are no large intrinsic fluctuations in the densities of N-particles in showers of same N_e and r, then the density $\Delta(N_e, r)$ will be the same for all such showers within normal statistical variations, and is given by:

$$\Delta(N_e, r) = \frac{1}{s\varepsilon m} \ln \frac{T}{T - Q}, \tag{1}$$

---

[3] K. Greisen: *The Extensive Air Showers.* Chap. I: *Progress in Cosmic Ray Physics*, vol. **3**, ed. by J. G. Wilson (Amsterdam, 1956).

where s = area of each N-detector, m = total number of N-detectors, ε = efficiency of the N-detector for the detection of N-particles, T = total number of showers of size N_e with cores at a distance r from the N-detectors, Q = number of showers in which one or more N-detectors were activated. For our set-up, $s = 0.4$ m^2, $m = 5$ and $\varepsilon = 0.25$.

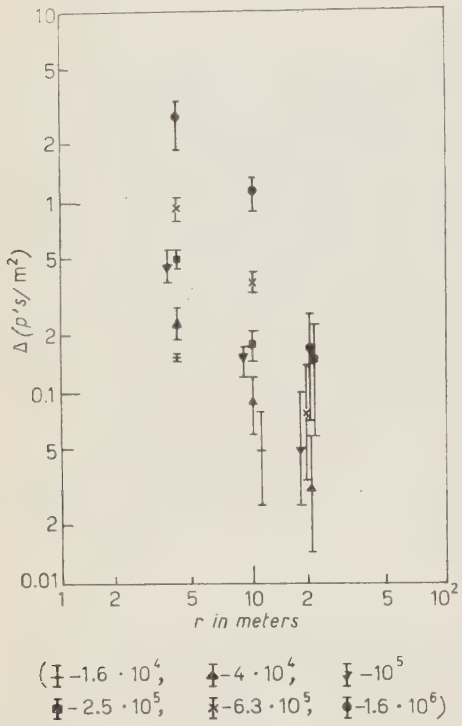

Fig. 3. – Lateral distribution of density of N-particles.

b) Lateral distribution of N-particles. The lateral distribution of N-particles has been calculated using equation (1). The results are plotted for different shower sizes in Fig. 3.

If we assume that the lateral distribution function is independent of shower size, then we can combine the lateral distributions obtained for the various groups to arrive at a statistically more significant function. This combined distribution may be expressed by a power-law of the form:

$$f(r) \propto r^{-1.2 \pm 0.05} \quad \text{for } 2.5 \text{ m} \leqslant r \leqslant 25 \text{ m} .$$

c) Total number of N-particles as a function of shower size. By integrating the observed lateral density distribution curves, we have estimated the total number of N-particles, up to a distance of 16 m from the core, in various groups of showers (of different sizes). Up to this distance, we consider that the data are statistically significant for the individual groups of showers. The variation of the total number of N-particles, N_N, thus obtained, (within 16 m from the core), is plotted in Fig. 4 as a function of the shower size N_e. It is seen that

$$N_N \propto N_e^{0.45 \pm 0.05}$$

for

$$1.6 \cdot 10^4 \leqslant N_e \leqslant 6.3 \cdot 10^5 .$$

The density of N-particles as a function of shower size N_e and core-distance r, may therefore be expressed as

$$\Delta(N_e, r) \propto N_e^{\alpha} r^{-\beta} , \tag{2}$$

where

$$\alpha = 0.45 \pm 0.05$$

and

$$\beta = 1.2 \pm 0.05$$

for

$$1.6 \cdot 10^4 \leqslant N_e \leqslant 6.3 \cdot 10^5$$

and

$$2.5 \leqslant r \leqslant 16 \text{ m}.$$

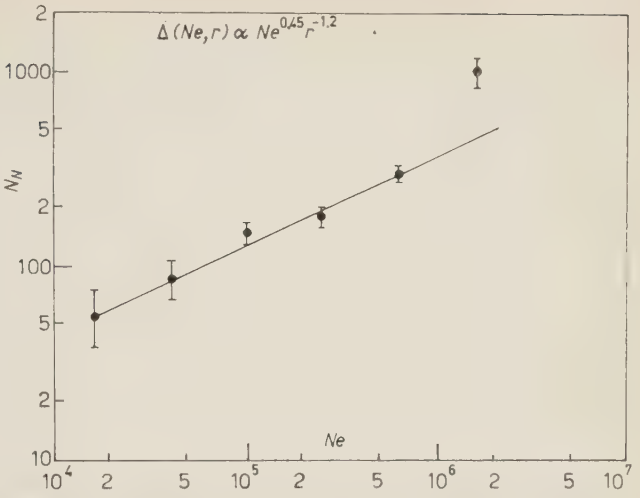

Fig. 4. – Variation of number of N-particles with shower size. (The straight line corresponds to a least-square fit of the experimental points in the interval $1.6 \cdot 10^4 \div 6.3 \cdot 10^5$).

The errors indicated above are purely statistical errors (standard deviations). The absolute values of density may, however, be subject to systematic errors owing to uncertainty in the value of ε, the efficiency of the N-detectors for detection of N-particles. The absolute values are not likely to be in error by more than 30 per cent.

It may be seen from Fig. 4 that the point corresponding to a shower size of $1.6 \cdot 10^6$ particles lies at a value considerably higher than that expected from the extrapolation of the straight line passing through the other points. The pure chance probability that this last point lies not on this straight line is about 1 per cent.

4. – Discussion.

The lateral distribution function and the dependence of the total number of N-particles on shower size determined in this experiment are in very good agreement with the results of WALLACE *et al.* [1], obtained at sea level, using a standard IGY neutron monitor in association with the Australian air shower set-up [2]. WALLACE *et al.* have given the relation

$$\Delta(N_e, r) \propto N_e^{0.47 \pm 0.1} r^{-0.92 \pm 0.1}$$

for

$$10^5 \leqslant N_e \leqslant 2 \cdot 10^6 \qquad \text{and} \qquad 5 \leqslant r \leqslant 50 \text{ m}.$$

[4] G. S. WALLACE, M. M. WINN and K. W. OGILVIE: *Nature*, **182**, 1653 (1958).

Our lateral distribution also agrees with that of DMITRIEV *et al.* [5] who find a value of 1.1 for β (see eq. (2)) for showers of size $8 \cdot 10^4$ at sea level.

LEHANE *et al.* have determined the lateral distribution function and the variation with shower size of the total number of N-particles, using a penetrating shower detector in association with an extensive air shower set-up. The lateral distribution function has been given by them as

$$f(r) \propto \exp\,[-r/20]\, r^{-0.5}\,.$$

This function agrees with our lateral distribution function up to 16 m, within the experimental errors. The total number of N-particles has been determined by LEHANE *et al.* by integrating the above function up to 50 m from the core. On the basis of the distribution given by them, about 20 per cent of the particles lie within a distance of 16 m from the core. To compare the results on the variation of the total number of N-particles with shower size, we have normalized the Australian data with ours at a shower size of $3 \cdot 10^5$ particles, where the statistical errors of observation are minimum in both experiments. The combined results are plotted in Fig. 5. Their data are represented by the five points marked with crosses. LEHANE *et al.* state that

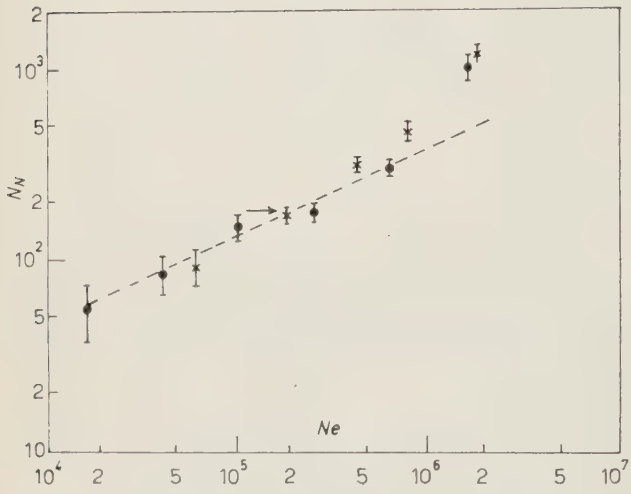

Fig. 5. – Combined plot of variation of N_N with N_e (×— LEGANE *et al.*; ·— present experiment; → indicates the normalization point. The straight line corresponds to the least square fit of the present data.

$$N_N \propto N_e^{0.6 \pm 0.1}$$

for

$$6 \cdot 10^4 \leqslant N_e \leqslant 8 \cdot 10^5\,.$$

The data of LEHANE *et al.*, however, extend beyond $N_e = 8 \cdot 10^5$ particles. The point corresponding to the largest shower size investigated by them, viz. $2 \cdot 10^6$, lies at a higher value of N_N than would be expected on the basis of a

(5) V. A. DMITRIEV, G. V. KULIKOV and G. B. KRISTIANSEN: as quoted by G. COCCONI: *Hand. d. Phys.*, **45** (1958).

straight line passing through the other points, with a slope of 0.6 ± 0.1. In this respect, their observations are in agreement with ours. A strict comparison of the two sets of results should not, however, be made since the experimental arrays are different, particularly in the type of N-detectors used, and their energy response; also, the lateral distributions have been integrated up to different distances from the core, viz. 16 m and 50 m in the two experiments. Therefore, the slope of 0.6 ± 0.1 obtained by LEHANE *et al.* for showers of size $< 10^6$ need not be considered to be in disagreement with the slope obtained in the present experiment, viz. 0.45 ± 0.05.

A point of interest that emerges from the two sets of data is the following: *In both the experiments*, the number of N-particles observed at the largest shower size investigated, (at $N_e > 10^6$), is much larger than that to be expected on the basis of the extrapolation of the straight line fitted to the observations on shower sizes $N_e < 10^6$ particles. There is therefore an indication that a change of slope occurs even at sea level. The data do not permit us to state whether the change of slope is sudden or gradual.

According to the observations of NICOL'SKY *et al.*, at mountain altitude, ($650\ \mathrm{g\,cm^{-2}}$), the exponent, (α), changes from a value of 0.2 to 1.0 rather suddenly at a shower size of about $4 \cdot 10^5$ particles. If this change of slope is connected with the primary particles, then the change should occur both at mountain altitude and at sea level at shower sizes which correspond to the same primary energy; *i.e.* the change observed at a shower size of $4 \cdot 10^5$ particles at $650\ \mathrm{g\,cm^{-2}}$ should be seen at a shower size of about 10^5 particles at sea level. This is definitely not indicated in Fig. 5. The indication is that it occurs at a shower size larger than 10^5 particles. The fact that it occurs not at the same primary energy but perhaps at about the same shower size, at mountain altitude and at sea level, may be connected with the development of the nucleonic cascade.

However, it should be pointed out that in none of the experiments has it been possible to determine the lateral distribution and the number of N-particles in individual showers. A statistical method has been employed, in which showers lying in the same size interval, with cores striking at the same distance (interval) from the N-detectors are grouped together; assumptions are then made that: *a*) the numbers of N-particles in showers of same size N_e, *b*) the lateral distributions of N-particles in showers of the same or different sizes and *c*) the ages of the showers, are constant (except for normal statistical variations). Figs. 4 and 5 may therefore be said to correspond to the variation of the *average* number of N-particles with shower size: this average is at present rather *ill*-defined. Intrinsic fluctuations can exist in the various characteristics mentioned above, and selection biases may thus be introduced in the detection and analysis of air showers as a consequence of these fluctuations. Our experimental set-up was designed specifically to check whether the density of N-par-

ticles remains constant in showers of the same size whose cores strike at a given distance from the N-detectors. Preliminary results of this experiment (which will be reported in Part II of this series), indicate the existence of fairly wide fluctuations outside normally acceptable statistical variations. Further experiments are being carried out to determine the exact magnitude and frequency of the fluctuations, and their dependence on the size, zenith angle and age of the showers. This might make it possible to isolate the various causes of these fluctuations and to evaluate their relative contributions. The real meaning that may be attached to the variation of the «*average*» number of N-particles with shower size, when it is obtained after ignoring these fluctuations will be known only when all of the data on fluctuations are available.

* * *

It gives us great pleasure to thank Prof. M. G. K. MENON for his interest in this investigation and for helpful discussions. We are indebted to Prof. S. MIYAKE for his valuable comments. We wish to express our thanks to Dr. M. YASIN of the Atomic Energy Establishment, Trombay, for the large number of neutron counters used in these experiments which have given trouble-free service. We are thankful to Mr. V. S. NARASIMHAM who analysed a considerable part of the shower-data. Our thanks are also due to Mr. S. G. KHAIRATKAR for the analysis of the showers using the analogue computer, and to Mess.rs F. GONSALVES, A. R. APTE, K. F. DINSHAW and V. S. PRABHU for their help in the construction and setting up of the air shower array and the associated electronic equipment.

RIASSUNTO (*)

Si descrive un esperimento effettuato al livello del mare sulla distribuzione laterale delle particelle che interagiscono coi nuclei negli sciami dell'aria e sulla variazione del loro numero con la dimensione dello sciame; gli sciami registrati variavano in dimensione da 10^4 a $2.5 \cdot 10^6$ particelle. I risultati indicano che il numero di particelle che interagiscono coi nuclei è proporzionale a $N_e^{0.45 \pm 0.05}$, per sciami di dimensione N_e inferiore a circa $6 \cdot 10^5$ particelle, e proporzionale a $\sim N_e^{1.2}$ per dimensioni maggiori. Ciò che si è ottenuto con questo esperimento ed altri simili eseguiti da altri gruppi (NIKOL'SKY *et al.* e LEHAN *et al.*), è il numero *medio* di particelle che interagiscono coi nuclei in un gran numero di sciami di una data dimensione. Si mette in rilievo la possibilità che una tale media sia priva di significato se esistono ampie fluttuazioni intrinseche (diverse dalle normali variazioni statistiche).

(*) *Traduzione a cura della Redazione.*

IL NUOVO CIMENTO Vol. XVIII, N. 6 16 Dicembre 1960

Magnetic Confinement of Charged Particles.

J. W. Gardner

Atomic Power Division, English Electric Co., Ltd. - Whetstone, Leicester

(ricevuto il 10 Agosto 1960)

Summary. — The motion of charged particles in a cylindrical magnetic field is analysed by a perturbation-theoretic method in which the cylindrical field is treated as a perturbation of a uniform field, and is found to contain axial drift terms. These terms are evaluated to second order and used to formulate the conditions for a self-confining effect, such as would be required for plasma-containment in a thermonuclear reactor.

1. – Introduction.

The confinement of a plasma of charged particles is of considerable current interest for thermonuclear research, since the useful production and application of thermonuclear power depends *inter alia* on the containment of the reacting gas at a temperature of some 10^8 or 10^9 degrees absolute. The self-constricted (pinched) discharge has been widely discussed as a possible means of achieving this end: see for example the reviews by Post [1] and by Thompson [2]. However, it is well known that an ionized gas confined by a magnetic field is subject to many instabilities and as Thompson has pointed out [2] further progress must depend on a thorough mathematical analysis of these instabilities, including the search for stable configurations.

In a previous communication [3] the present author has adumbrated a possible analytical approach to the study of one of these instabilities, namely the « kinking » of the pinched discharge. The method proposed was based on

(1) R. F. Post: *Rev. Mod. Phys.*, **28**, 338 (1956).
(2) W. B. Thompson: *Nature*, **179**, 886 (1957).
(3) J. W. Gardner: *Nuovo Cimento*, **6**, 1228 (1957)

a perturbation-theoretic treatment of the motion of charged particles in a cylindrical magnetic field. It was pointed out that the general question of confinement in a fixed external field can be investigated without regard to the detailed motions of the particles: results for the cases of cylindrical and toroidal external fields have already been published elsewhere ([4,5]). However, in self-confining effects such as the pinched discharge one must clearly consider, in addition to any external fields which may be present, the magnetic field due to the motions of the particles themselves. If these motions include a systematic drift in such a direction as to reinforce the current producing the external confining field then a self-confining effect appears *prima facie* possible, although whether this effect will in fact occur must obviously depend also on the particle density and temperature. A complete analysis should moreover include investigation of any random or periodic components of the particle motions whose characteristic time is not short compared with the instability growth time.

As was announced in reference ([3]) the perturbation-theoretic method there proposed is capable, within the limits of its validity, of giving quantitative results for the particle motions. The purpose of the present paper is to describe the details of such a perturbation theory for the case of a cylindrical magnetic field. In particular it is shown that a systematic drift of particles will occur in such a direction as to reinforce the external magnetic field, and the magnitude of this drift is computed. These results are then used to formulate the conditions for self-confinement and obtain a relation between the total current and thermal energy in the pinched discharge, which is shown to be in reasonable agreement with that obtained by the conventional (statistical) method. The paper closes by briefly considering the possible extension of the present method to the investigation of particle motions in a toroidal field: the detailed treatment of this case is however deferred to a subsequent publication.

2. – Statement of the problem: basic equations.

The main part of the present paper is addressed to the investigation of the motion of a single charged particle in a cylindrical magnetic field: the consideration of extensions to many particles and to toroidal fields in postponed to Section 6.

We may suppose the cylindrical field to be produced by a filament current I(e.m.u.) flowing in the positive diretion along the z-axis, so that in

([4]) J. W. GARDNER: *Proc. Phys. Soc.*, B **62**, 300 (1949).
([5]) J. W. GARDNER: *Can. Journ. Phys.*, **31**, 459 (1953).

cylindrical co-ordinates r, θ, z, the magnetic field $\boldsymbol{H}$ has components

$$H_r = H_z = 0 \,, \tag{2.1}$$

$$H_\theta = 2I/r \,. \tag{2.2}$$

Our problem is, then, to formulate and solve for appropriate boundary conditions the equations for $\boldsymbol{q}(r, \theta, z, t)$, the vector position at any time t of a particle having charge e (e.s.u.) and mass m (grammes) moving under the influence of the magnetic field $\boldsymbol{H}$.

The present treatment will be completely relativistic if m be interpreted as the relativistic mass, related to the rest mass m_0 by the Lorentz transformation

$$m = m_0(1 - \beta^2)^{-\frac{1}{2}} \tag{2.3}$$

with

$$\beta \equiv \dot{q}/c \,; \tag{2.4}$$

c being the light velocity.

Using the notation of HEITLER ([6]) the classical equations of motion of a massive point-charge, in their most general form, may be written

$$\frac{1}{c}(\dot{\boldsymbol{u}}) = \boldsymbol{K}_s + \boldsymbol{K}_e \,, \tag{2.5}$$

where $\boldsymbol{u}$ is the kinetic momentum and the dot signifies differentiation with respect to time; $\boldsymbol{K}_s$ is the radiation damping force and $\boldsymbol{K}_e$ is the force from external fields; and e is here interpreted as the ratio of the electromagnetic to the electrostatic unit of charge rather than the light velocity. In the present notation $(1/c)(\dot{\boldsymbol{u}})$ becomes $m\ddot{\boldsymbol{q}}$ and the non-relativistic form of $\boldsymbol{K}_s$ is given by

$$\boldsymbol{K}_s = \frac{2}{3}\frac{e^2}{c^3}\dddot{\boldsymbol{q}} \,. \tag{2.6}$$

A relativistic form for $\boldsymbol{K}_s$ has also been given by HEITLER ([6]) but, as he remarks, at particle speeds for which this differs significantly from (2.6) the classical description implied by (2.5) is in any case no longer valid, and quantum effects must be taken into account.

Anticipating the approximations to be introduced by the perturbation treatment in the next section we shall in fact neglect $\boldsymbol{K}_s$ in comparison with

([6]) W. HEITLER: *Quantum Theory of Radiation* (Oxford, 1954), chap. I.

$\boldsymbol{K}_e$ and equate the right-hand side of (2.5) to the Lorentz force $(e/c)(\dot{\boldsymbol{q}} \times \boldsymbol{H})$ so that (2.5) becomes

$$m\ddot{\boldsymbol{q}} = \frac{e}{c}(\dot{\boldsymbol{q}} \times \boldsymbol{H}) . \tag{2.7}$$

The three components of the vector equation (2.7) can be readily obtained by using equations (2.1) and (2.2) for the r-, z- and θ-components of $\boldsymbol{H}$ and recalling the familiar expressions [7] of the corresponding components of $\dot{\boldsymbol{q}}$, $\ddot{\boldsymbol{q}}$, viz.:

$$\dot{q}_r = \dot{r} , \tag{2.8a}$$

$$\dot{q}_\theta = r\dot{\theta} , \tag{2.8b}$$

$$\dot{q}_z = \dot{z} , \tag{2.8c}$$

$$\ddot{q}_r = \ddot{r} - r\dot{\theta}^2 , \tag{2.9a}$$

$$\ddot{q}_\theta = r\ddot{\theta} + 2\dot{r}\dot{\theta} , \tag{2.9b}$$

$$\ddot{q}_z = \ddot{z} . \tag{2.9c}$$

It will also be convenient to introduce a quantity γ defined by

$$\gamma \equiv \frac{e}{mc} H_\theta = \frac{2eI}{mcr} . \tag{2.10}$$

Making the above substitutions in (2.7) we have then, after some re-arrangement,

$$\ddot{r} - r\dot{\theta}^2 = -\gamma \cdot \dot{z} , \tag{2.11}$$

$$r\ddot{\theta} + 2\dot{r}\dot{\theta} = 0 , \tag{2.12}$$

$$\ddot{z} = \gamma \cdot \dot{r} . \tag{2.13}$$

These equations of motion are exact except for the neglect of radiation damping.

Using (2.11)–(2.13), or rather their Cartesian form, it was shown in reference [1] that, under suitable conditions of initial projection, the radial component of motion would be oscillatory with small amplitude about the time average of r, say a; and that the axial component of motion would in general contain a unidirectional drift. By the method of reference [4], however, a more detailed examination of the motion, including specifically an evaluation of the axial drift term, would not have been possible without extensive nu-

[7] See for example: E. T. Whittaker: *Analytical Dynamics* (Cambridge, 1959).

merical computation. The perturbation theory developed in the following sections gives, within the limits of its validity (*), a more detailed picture of the motion.

3. – Perturbation theory: zero order solutions.

It will be convenient to introduce new co-ordinates ξ, η, ζ defined as follows:

(3.1a) $$\xi = r - a \,,$$

(3.1b) $$\eta = z \,,$$

(3.1c) $$\zeta = a\theta \,.$$

Recalling that a has already been defined as the time average of r it is evident that $\langle\xi\rangle$, the time average of ξ, must vanish (**).

It will further be assumed that a suitable initial projection of the particle secures that ξ is always much smaller than a (***): this is consonant with the conventional treatment of the pinched discharge which assumes the current to be confined to a cylindrical shell whose thickness is small compared with its radius (see for example Post, reference (1)). In these circumstances it is clearly sensible to attempt a perturbation theory in terms of ξ/a using the following expansions for γ, ξ, η, ζ:

(3.2) $$\gamma = \omega \sum_{j=0}^{\infty} \left(-\frac{\xi}{a}\right)^j ,$$

with

(3.2a) $$\omega \equiv 2eI/mca \,;$$

(3.3a) $$\xi = \xi_0 + \sum_{j=1}^{\infty} \xi_j \,;$$

(3.3b) $$\eta = \eta_0 + \sum_{j=1}^{\infty} \eta_j \,;$$

(3.3c) $$\zeta = \zeta_0 + \sum_{j=1}^{\infty} \zeta_j \,.$$

(*) The conditions for this validity are, as we shall see, those normally assumed in the analysis of the pinched discharge.

(**) It will be convenent later to modify this statement to allow $\langle\xi\rangle$ to contain first and higher order terms; the validity of expansions (3.2) and (3.3) will be unaffected.

(***) It is shown in reference (4) that this condition is fulfilled if $mc\dot{q}/e \ll A$, where $\boldsymbol{A}$ is the vector potential defined by $\boldsymbol{H} = \operatorname{curl} \boldsymbol{A}$. In the present notation the condition becomes $\dot{q} \ll r\gamma$. Incidentally the formula (14) for A_θ in reference (1) contains a misprint. It should read

$$A_\theta = 4aI \int_0^{\pi/2} \frac{(2\sin^2\theta - 1)\,\mathrm{d}\theta}{\{(a^2 + r^2) + z^2 - 4ar\sin^2\theta\}^{\frac{1}{2}}} \,,$$

In equations (3.3) the quantities ξ_j, η_j, and ζ_j are all of the order of $\xi_0(\xi/a)^j$; the negative sign occurs in (3.2) because, in view of (2.10) and (3.1a), $|\gamma|$ decreases with increasing r and increasing ξ. Up to now we have left the sign of e, and hence of γ, undefined; to fix our ideas we shall hereinafter suppose the particles in question to be electrons so that e is negative and so therefore is γ, because all the other quantities occurring in (2.10) are by definition positive. In what follows we denote $|\gamma|$ by Γ.

Translated into the new co-ordinates defined by equations (3.1), equations (2.11)–(2.13) become

$$\ddot{\xi} = (\xi + a)\left(\frac{\dot{\zeta}}{a}\right)^2 + \Gamma\dot{\eta}\,, \tag{3.4}$$

$$\ddot{\eta} = -\Gamma\dot{\xi}\,, \tag{3.5}$$

$$\ddot{\zeta} = -\frac{2\dot{\xi}\dot{\eta}}{(\xi + a)}\,. \tag{3.6}$$

Using the expansions (3.2) and (3.3) in the equations (3.4) to (3.6) each of these exact equations can, by equating terms of the same order appearing on its left-hand and right-hand sides, be resolved into an infinite family of equations of which any given member contains only terms of order $\xi_0(\xi/a)^j$, for $j = 0, 1, 2, \ldots$. The first and second order perturbation equations, and their solutions, are discussed in the Sections **4**-**6** below; we conclude the present section with a brief comment on the zero order equations.

These last equations are obtained by substituting $\xi = \xi_0$, $\eta = \eta_0$, $\zeta = \zeta_0$ $\Gamma - \omega$ into (3.4)–(3.6) and neglecting terms of order ξ_0^2/a or smaller, which procedure readily yields the following:

$$\ddot{\xi}_0 = \omega\dot{\eta}_0\,, \tag{3.7}$$

$$\ddot{\eta}_0 = -\omega\dot{\xi}_0\,, \tag{3.8}$$

$$\ddot{\zeta}_0 = 0\,. \tag{3.9}$$

Equations (3.7)–(3.9) represent the well known helical motion of an electron in a uniform magnetic field H_0, say, in the ζ-direction: ξ_0 and η_0 vary periodically with angular frequency $\omega = eH_0/mc$, whilst ζ_0 increases at a uniform rate W_0, say, the initial velocity of projection of the electron in the positive ζ-direction. From the definition of ω in (3.2a) we see that H_0 must be identified with $2I/a$; any valid theory which treats a cylindrical field as a perturbation of a uniform field must of course give this as a zero order result.

The explicit form of the solutions of (3.7)–(3.9) naturally depends on the initial conditions of projection. As we shall see in the next section, the higher

order solutions involve ξ_0, η_0, ζ_0 and their time derivatives, and it will be convenient in this connection to postulate the following initial conditions:

$$\left.\begin{aligned} &(3.10a) && \xi_0 = \alpha \ll a\ ; && \dot{\xi}_0 = 0 \\ &(3.10b) && \eta_0 = 0\ ; && \dot{\eta}_0 = -\alpha\omega \\ &(3.10c) && \xi_0 = 0\ ; && \dot{\zeta}_0 = W_0 \end{aligned}\right\} \text{ at time } t\ .$$

The conditions (3.10), in conjunction with (3.7)–(3.9), then lead to the following explicit zero order solutions:

$$\xi_0 = \alpha \cos \omega t\ ; \tag{3.11}$$

$$\eta_0 = -\alpha \sin \omega t\ ; \tag{3.12}$$

$$\xi_0 = W_0 t\ . \tag{3.13}$$

4. – First order solutions.

The first order equations, obtained by making the substitutions (3.2), (3.3) in equations (3.1)–(3.6) and retaining only terms of order (ξ_0^2/a) are readily found to be

$$\ddot{\xi}_1 = \frac{(\dot{\zeta}_0)^2}{a} + \omega \left\{\dot{\eta}_1 - \frac{\xi_0 \dot{\eta}_0}{a}\right\}, \tag{4.1}$$

$$\ddot{\eta}_1 = \omega \left\{\frac{\xi_0 \dot{\xi}_0}{a} - \dot{\xi}_1\right\}, \tag{4.2}$$

$$\ddot{\zeta}_1 = 2\,\frac{\dot{\xi}_0 \zeta_0}{a}\ . \tag{4.3}$$

Using the zero order solutions (3.11)–(3.13) above to substitute explicit expressions for ξ_0, and for the time derivatives $\dot{\xi}_0$, $\dot{\eta}_0$, $\dot{\zeta}_0$ in equations (4.1)–(4.3) we obtain

$$\ddot{\xi}_1 = \frac{W_0^2}{a} + \omega \left\{\dot{\eta}_1 + \frac{\alpha^2 \omega}{a} \cos^2 \omega t\right\}, \tag{4.4}$$

$$\ddot{\eta}_1 = -\omega \left\{\dot{\xi}_1 + \frac{\alpha^2 \omega}{a} \cos \omega t \sin \omega t\right\}, \tag{4.5}$$

$$\ddot{\zeta}_1 = \frac{2\alpha}{a} W_0 \omega \sin \omega t\ . \tag{4.6}$$

The last of these integrates immediately to give (with initial conditions (*) $\zeta_1 = \dot{\zeta}_1 = 0$ at $t = 0$)

$$\zeta_1 = \frac{2\alpha}{a} W_0 \left\{ t - \frac{1}{\omega} \sin \omega t \right\} . \tag{4.7}$$

Equations (4.4) and (4.5) are most readily solved by forming from them a single differential equation in the complex variable μ_1 defined by

$$\mu_1 \equiv \xi_1 + i\eta_1 . \tag{4.8}$$

To do this we multiply (4.5) by i and add it to (4.4); the resulting equation, after some algebraic manipulation and substituting from (4.8) may be written

$$\ddot{\mu}_1 + i\omega\dot{\mu}_1 = \frac{W_0^2}{a} + \frac{(\alpha\omega)^2}{2a} \{1 + \exp[-2i\omega t]\} . \tag{4.9}$$

We may note immediately that the presence of a constant term, in addition to the periodic term, on the right-hand side of (4.9) means that μ_1 must contain a term linear in t, corresponding to a systematic drift in at least one of the components ξ_1, η_1. Essaying a solution of the form

$$\mu_1 \equiv A + Bt + C \exp[-2i\omega t] , \tag{4.10}$$

together with initial conditions

$$\left.\begin{aligned} \mu_1 &= 0 \quad (4.11a) \\ \dot{\mu}_1 &= 0 \quad (4.11b) \end{aligned}\right\} \text{ at } t = 0 ,$$

one finds

$$A = \alpha^2/4a , \tag{4.12a}$$

$$B = -i \left\{ \frac{W_0^2}{a\omega} + \frac{\alpha^2\omega}{2a} \right\} , \tag{4.12b}$$

$$C = -\alpha^2/4a . \tag{4.12c}$$

Substituting from equations (4.12) back into (4.10), recalling (4.8) and

(*) We shall adopt the convention that all perturbations vanish at $t = 0$, so that the zero order solutions are uniquely exact at this time; this means, that $\langle \xi \rangle$ in general contains terms of order α^2/a and less, when a is now interpreted as some arbitrary value of r close, but not equal, to $\langle r \rangle$.

equating real and imaginary parts we have after some re-arrangement

$$\xi_1 = \frac{\alpha^2}{4a}(1 - \cos 2\omega t) = \frac{1}{2a}(\alpha \sin \omega t)^2, \tag{4.13}$$

$$\eta_1 = \frac{\alpha^2}{4a}\sin 2\omega t - \left(\frac{W_0^2}{a\omega} + \frac{\alpha^2\omega}{2a}\right)t\,. \tag{4.14}$$

Equations (4.13) and (4.14), together with (4.7) above, complete the first order solutions. These results together with the zero order solutions (*) (3.11)–(3.13) are used in the next section to obtain the second order solutions. The physical significance of the first and second order solutions is discussed in Section 6.

5. – Second order solutions.

By substituting the expansions (3.2), (3.3) in equations (3.4)–(3.6) and retaining only terms of order (ξ_0^3/a^2) the second order equations are found to be

$$\ddot{\xi}_2 = \xi_0\left(\frac{\dot{\zeta}_0}{a}\right)^2 + \frac{2\dot{\zeta}_0\dot{\zeta}_1}{a} + \omega\left[\dot{\eta}_2 - \frac{\dot{\eta}_1\xi_0}{a} + \dot{\eta}_0\left\{\left(\frac{\xi_0}{a}\right)^2 - \frac{\xi_1}{a}\right\}\right], \tag{5.1}$$

$$\ddot{\eta}_2 = \omega\left[\frac{\xi_0\dot{\xi}_1}{a} - \dot{\xi}_2 - \dot{\xi}_0\left\{\left(\frac{\xi_0}{a}\right)^2 - \frac{\xi_1}{a}\right\}\right], \tag{5.2}$$

$$\ddot{\zeta}_2 = \frac{2}{a}\left(\frac{\xi_0\dot{\xi}_0\dot{\zeta}_0}{a} - \dot{\xi}_0\dot{\zeta}_1 - \dot{\xi}_1\dot{\zeta}_0\right). \tag{5.3}$$

Considering (5.3) first, and substituting for ξ_0, $\dot{\xi}_0$, $\dot{\zeta}_0$, $\dot{\zeta}_1$, and $\dot{\xi}_1$ the expressions given by the appropriate zero order and first order solutions above (equations (3.11), (3.13), (4.7) and (4.13)), one obtains after some cancellation

$$\ddot{\zeta}_2 = \frac{4\alpha^2\omega W_0}{a^2}(1 - 2\cos\omega t)\sin\omega t\,. \tag{5.4}$$

With the boundary conditions:

$$\left.\begin{aligned} \xi_2 &= 0 \quad (5.5a)\\ \dot{\xi}_2 &= 0 \quad (5.5b)\end{aligned}\right\} \text{ at } t = 0\,,$$

(*) For convenient reference the zero, first and second order solutions, with appropriate initial conditions, are all collected in the Appendix.

equation (5.4) integrates to give

$$\dot{\zeta}_2 = \frac{4\alpha^2 W_0}{a^2}(\cos^2\omega t - \cos\omega t)\,, \tag{5.6}$$

and

$$\zeta_2 = \frac{2\alpha^2 W_0}{a^2}\left\{t - \frac{\sin\omega t}{\omega}(2 - \cos\omega t)\right\}. \tag{5.7}$$

Turning now to the solution of equations (5.1) and (5.2) it is evident from inspection that the recipe adopted in Section **4** above of forming a single differential equation in a complex variable will apply equally well here. Accordingly we define

$$\mu_2 \equiv \xi_2 + i\eta_2\,, \tag{5.8}$$

multiply (5.2) by i and add it to (5.1) to obtain, after rearrangement,

$$\ddot{\mu}_2 + i\omega\dot{\mu}_2 = \omega(\dot{\eta}_0 - i\dot{\xi}_0)\left\{\left(\frac{\xi_0}{a}\right)^2 - \frac{\xi_1}{a}\right\} - \frac{\omega\xi_0}{a}(\dot{\eta}_1 - i\dot{\xi}_1) + \xi_0\left(\frac{\dot{\zeta}_0}{a}\right)^2 + 2\,\frac{\dot{\zeta}_0\dot{\zeta}_1}{a}\,. \tag{5.9}$$

By inserting the appropriate first order and zero order solutions into the right-hand side and using exponential forms for trigonometric functions, (5.9) may be transformed to

$$\ddot{\mu}_2 + i\omega\dot{\mu}_2 = \frac{4W_0^2\alpha}{a^2} + \left(\frac{5\alpha^3\omega^2}{8a^2} - \frac{\alpha W_0^2}{a^2}\right)\exp[i\omega t] + \frac{\alpha^3\omega^2}{8a^2}\exp[-3i\omega t]\,. \tag{5.10}$$

Essaying a solution of the form (*)

$$\mu_2 = D + Et + F\exp[i\omega t] + G\exp[-i\omega t] + H\exp[-3i\omega t]\,, \tag{5.11}$$

together with the boundary conditions

$$\left.\begin{aligned} \mu_2 &= 0 \quad (5.12a)\\ \mu_2 &= 0 \quad (5.12b)\end{aligned}\right\} \text{ at } t = 0\,,$$

(*) It is interesting to note that the solution includes an $\exp[-i\omega t]$ term even though no such term appears in (5.10). The absence of such a term from (5.10) is an essential concomitant of the initial physical requirement that the particle's radial distance from the filament current producing the field should never differ much from a: for it may be readily verified that an $\exp[-i\omega t]$ term in (5.10) requires a $t\cdot\exp[-i\omega t]$ term in the solution, implying radial oscillations of indefinitely increasing amplitude about a.

we find

$$D = \frac{3}{2}\alpha\left(\frac{W_0}{a\omega}\right)^2 + \frac{7}{12}\frac{\alpha^3}{a^2}, \tag{5.13a}$$

$$E = -4i\cdot\frac{\alpha W_0^2}{a^2\omega}, \tag{5.13b}$$

$$F = \frac{\alpha}{2}\left(\frac{W_0}{a\omega}\right)^2 - \frac{5\alpha^3}{16a^2}, \tag{5.13c}$$

$$G = -\frac{7}{2}\alpha\left(\frac{W_0}{a\omega}\right)^2 - \frac{\alpha^3}{4a}, \tag{5.13d}$$

$$H = -\frac{\alpha^3}{48a}. \tag{5.13e}$$

Substituting from equations (5.13) back into equation (5.11), recalling (5.8) and equating real and imaginary parts we have, after some algebra,

$$\xi_2 = \left(\frac{3}{2}g + \frac{7}{12}h\right) - \left(3g + \frac{9}{16}h\right)\cos\omega t - \frac{h}{48}\cos 3\omega t, \tag{5.14}$$

$$\eta_2 = -4g\omega t + \left(4g - \frac{h}{16}\right)\sin\omega t + \frac{h}{48}\sin 3\omega t, \tag{5.15}$$

with

$$g \equiv \alpha\left(\frac{W_0}{a\omega}\right)^2, \tag{5.16a}$$

$$h \equiv \alpha^3/a^2. \tag{5.16b}$$

These equations, together with (5.7) above complete the second order solutions.

6. – Discussion and conclusion.

In order to have confidence in the above perturbation theory it is necessary to confirm that it gives results which are self-consistent and physically sensible. To be consistent with the basic assumptions of Section 3 the zero, first and second order solutions for any co-ordinate (ξ, η or ζ) must be in the approximate ratio $1 : \alpha/a : (\alpha/a)^2$. It is immediately apparent from an inspection of the results listed in the Appendix that all the periodic solutions have amplitudes satisfying this criterion. Moreover the ξ-component of velocity contains only terms periodic about a mean value zero, showing that there is no sys-

tematic drift away from the initial position $\xi_0 = \alpha$, so that the condition $\xi \ll a$ for the validity of expansion (3.2) and (3.3a) is satisfied for all times t.

The η- and ζ-components of velocity contain terms representing a steady drift away from the initial position. To second order these drifts are

$$\langle \dot{\eta} \rangle = \langle \dot{\eta}_0 \rangle + \langle \dot{\eta}_1 \rangle + \langle \dot{\eta}_2 \rangle \,, \tag{6.1}$$

with

$$\langle \dot{\eta}_0 \rangle = 0 \,, \tag{6.1a}$$

$$\langle \dot{\eta}_1 \rangle = -\frac{\alpha^2 \omega}{2a} - \frac{W_0^2}{a\omega} \,, \tag{6.1b}$$

$$\langle \dot{\eta}_2 \rangle = -\frac{4\alpha W_0^2}{a^2 \omega} \,; \tag{6.1c}$$

and

$$\langle \dot{\zeta} \rangle = \langle \dot{\zeta}_0 \rangle + \langle \dot{\zeta}_1 \rangle + \langle \dot{\zeta}_2 \rangle \,, \tag{6.2}$$

with

$$\langle \dot{\zeta}_0 \rangle = W_0 \,, \tag{6.2a}$$

$$\langle \dot{\zeta}_1 \rangle = \frac{2\alpha W_0}{a} \,, \tag{6.2b}$$

$$\langle \dot{\zeta}_2 \rangle = \frac{2\alpha^2 W_0}{a^2} \,. \tag{6.2c}$$

Evidently if the drifts (6.1) and (6.2) continue indefinitely a time will eventually be reached when η and ζ are no longer small compared with a and expansions of the form (3.3) would appear *prima facie* inadmissible. Upon consideration, however, it is seen that one can if necessary define new co-ordinates η^*, ζ^* after time t according to:

$$\eta^* = \eta - \langle \dot{\eta} \rangle t \,, \tag{6.3}$$

$$\zeta^* = \zeta - \langle \dot{\zeta} \rangle t \,, \tag{6.4}$$

such that η^*, $\zeta^* \ll a$; and define expansions in η^*, ζ^* to replace (3.3b) and (3.3c). The legitimacy of transformations (6.3) and (6.4) is clear if we recollect the original definitions (3.1b) and (3.1c) which show that the η- and ζ-drifts represent respectively motion parallel to, and around, the filament current I, but that neither implies any departure from the basic condition that the electron's radial distance from I remains always close to a. In fact, under the

conditions of a pinched discharge to be considered below the co-ordinates η, ζ never approach a in a time comparable with the instability growth time.

It is also of interest to enquire under what conditions $\langle\dot{\eta}_2\rangle$ represents a small correction to $\langle\dot{\eta}_1\rangle$. It is clear form (6.2) that

$$\langle\dot{\zeta}_2\rangle = \frac{a}{\alpha}\langle\dot{\zeta}_1\rangle\,, \tag{6.5}$$

and one might reasonably expect a similar relation to hold between $\dot{\eta}_2$ and $\langle\eta_1\rangle$, although this is not automatically required by the conditions for the validity of the expansions (3.3). If we define a number φ such that

$$\langle\dot{\eta}_2\rangle = \frac{\varphi\alpha}{a}\langle\dot{\eta}_1\rangle\,, \tag{6.6}$$

then substitution from (6.1) into (6.6) readily yields

$$\left(\frac{W_0}{\alpha\omega}\right)^2 = \frac{\varphi}{2(4-\varphi)}\,. \tag{6.7}$$

Now for $\langle\dot{\eta}_2\rangle$ to be a small correction to $\langle\dot{\eta}_1\rangle$ the factor $\varphi\alpha/a$ in (6.6) must be of the order of a/α, since this is our definition of « smallness » in the present context. Thus, whatever α/a, φ should clearly not be much greater than unity; if we postulate $\varphi \gtrsim 1.5$, equation (6.7) then implies the relation

$$W_0^2 \leqslant (\alpha\omega)^2. \tag{6.8}$$

Recalling the initial conditions (3.10) for $\dot{\xi}_0$, $\dot{\eta}_0$, $\dot{\zeta}_0$, together with our convention that all higher order velocity components are defined to vanish at $t=0$ it is evident that W_0, $\alpha\omega$ represent *exactly* the initial velocity components in the ξ-direction and in the $\eta\zeta$-plane respectively. Thus the magnitude of the electron velocity $\dot{q}$ (a constant of the motion) is given exactly by

$$\dot{q}^2 = W_0^2 + (\alpha\omega)^2\,. \tag{6.9}$$

Moreover, if the initial direction of this velocity obeys an isotropic distribution law, then

$$E\{W_0^2\} = \tfrac{1}{2}E\{(\alpha\omega)^2\} = \tfrac{1}{3}\dot{q}^2\,, \tag{6.10}$$

where $E\{x\}$ means the expectation value of x. Equation (6.10) suggests that the condition (6.8) is not unduly restrictive: for a large number of electrons

having their initial velocities isotropically distributed it is as often satisfied as not.

A useful check on the physical reasonableness of the above results is afforded by their application to formulate the conditions for a self-confining current. For this purpose we imagine a large number of electrons moving simultaneously in a cylindrical magnetic field, and suppose their mutual electrostatic repulsions to be neutralized by an appropriate positive space charge. In these circumstances each electron moves according to the above equations for an isolated electron, although the initial conditions will vary from to electron. (One may assume, for example, that their initial velocities obey a Maxwellian distribution law.)

Equations (6.1) show that all the electrons confined by the magnetic field of a filament current I flowing in the positive z-direction acquire a systematic drift in the negative z-direction, which constitutes an additional current in the *positive* z-direction. Thus the drift current induced by the magnetic field of I reinforces I itself and the first condition for a self-confining effect is satisfied. Our model also conforms to the conventional picture of the pinched discharge (1) in which the pinched current is assumed confined to a cylindrical shell whose thickness ($\approx 2\alpha$) is small compared with its mean radius ($\approx a$).

Now for a known initial distribution of electron velocities and positions one can clearly obtain a characteristic drift velocity V by averaging (6.1) over all electrons. Further, if the electrons are distributed with a uniform density n per cm length, parallel to V, the total drift current—apart from sign—is evidently neV/c, and for a self-confining discharge this must be identified with the effective axial current I, leading to (*)

$$I = neV/c\,. \tag{6.11}$$

In view of (6.1) and (3.2a) the expression for V must clearly contain I in the denominator, and a rough calculation based on the (admittedly crude) assumption that all electrons have the same kinetic energy $\frac{3}{2}kT$—where k is Boltzmann's constant and T absolute temperature—gives the following result:

$$V = \frac{3ckT}{eI}\,. \tag{6.12}$$

The pinched current is conventionally expressed in terms of the *total* number of particles per cm length, N say, and in view of our previous assumption

(1) It should be noted, however, that because in the pinched discharge the electrons oscillate back and forth between the cylindrical surfaces of the shell containing the current the effective current to be used in computing V is (approximately) $I/2$.

about the distribution of positive space charge we must clearly have

$$N = 2n \,. \tag{6.13}$$

Substitution of (6.12) and (6.13) into (6.11) then gives

$$I^2 = \tfrac{3}{2} N k T \,. \tag{6.14}$$

Equation (6.14) compares reasonably with the result

$$I^2 = 2 N k T \,, \tag{6.15}$$

obtained by the usual derivation, equating the kinetic and magnetic pressures. (See for example reference [1].) It should be recalled of course that the primary object of the present analysis was not the obtaining of a relation such as (6.14) but a detailed description of the individual particle motions which is not given by the conventional derivation of (6.15), treating the discharge as a statistical assembly. In view of this the agreement between (6.14) and (6.15) appears satisfactory; it could clearly be improved, if desired, by using a more realistic assumption about the electron energy distribution and a proper time-averaged value of the effective current in the computation of V (instead of taking it as $I/2$).

We conclude with a remark on the possible extension of the present analysis to the motion of charged particles in a toroidal field. The cylindrical field, as we have seen, provides no effective means of longitudinal confinement of the particles; a toroidal field provides in principle a way to reduce these losses, by closing the end of the discharge on itself [4,8]. Moreover, even a « cylindrical » discharge in the region of kinking is locally toroidal, so that an analysis of particle motions in a toroidal field is required for the study of these instabilities.

A possible approach to this problem would appear to be afforded by a logical extension of the present treatment: just as we have treated a cylindrical field as a local perturbation of a uniform field so it should be possible to treat a toroidal field as a local perturbation of a cylindrical field, and analyse the motion in terms of this perturbation. It is proposed to develop this idea in detail in a subsequent paper.

* * *

The author is indebted to the English Electric Company for permission to publish.

[8] S. W. Cousins and A. A. Ware: *Proc. Phys. Soc.*, A **64**, 159 (1951).

Appendix

In this appendix are assembled for convenient reference the solutions, with the boundary conditions indicated, of the zero, first and second order equations for ξ, η, ζ. (Eq. (3.7)–(3.9), (4.1)–(4.3) and (5.1)–(5.3) of the text.)

Zero order. – For boundary conditions:

$$\left.\begin{aligned} \xi_0 &= \alpha; & \dot{\xi}_0 &= 0 \\ \eta_0 &= 0; & \dot{\eta}_0 &= -\alpha\omega \\ \zeta_0 &= 0; & \dot{\zeta}_0 &= W_0 \end{aligned}\right\} \text{ at } t = 0\,,$$

eq. (3.7)–(3.9) give

$$\begin{aligned} &\xi_0 = \alpha\cos\omega t; && \dot{\xi}_0 = -\alpha\omega\sin\omega t; && \ddot{\xi}_0 = -\alpha\omega^2\cos\omega t\,, \\ &\eta_0 = -\alpha\sin\omega t; && \dot{\eta}_0 = -\alpha\omega\cos\omega t; && \ddot{\eta}_0 = \alpha\omega^2\sin\omega t\,, \\ &\zeta_0 = W_0 t; && \dot{\zeta}_0 = W_0; && \ddot{\zeta}_0 = 0\,. \end{aligned}$$

First order. – For boundary conditions:

$$\left.\begin{aligned} \xi_1 &= \dot{\xi}_1 = 0 \\ \eta_1 &= \dot{\eta}_1 = 0 \\ \zeta_1 &= \dot{\zeta}_1 = 0 \end{aligned}\right\} \text{ at } t = 0\,,$$

eq. (4.1)–(4.3) give

$$\xi_1 = \frac{1}{2a}(\alpha\sin\omega t)^2 = \frac{\alpha^2}{4a}(1-\cos 2\omega t)\,;$$

$$\dot{\xi}_1 = \frac{\alpha^2\omega}{2a}\sin 2\omega t; \qquad \ddot{\xi}_1 = \frac{\alpha^2\omega^2}{a}\cos 2\omega t;$$

$$\eta_1 = \frac{\alpha^2}{4a}\sin 2\omega t - \left(\frac{W_0^2}{a\omega} + \frac{\alpha^2\omega}{2a}\right)t;$$

$$\dot{\eta}_1 = \frac{\alpha^2\omega}{2a}\cos 2\omega t - \left(\frac{W_0^2}{a\omega} + \frac{\alpha^2\omega}{2a}\right); \qquad \ddot{\eta}_1 = -\frac{\alpha^2\omega^2}{a}\sin 2\omega t;$$

$$\zeta_1 = \frac{2\alpha W_0}{a}\left(t - \frac{1}{\omega}\sin\omega t\right);$$

$$\dot{\zeta}_1 = \frac{2\alpha W_0}{a}(1-\cos\omega t); \qquad \ddot{\zeta}_1 = \frac{2\alpha W_0}{a}\omega\sin\omega t\,.$$

Second order. – For the boundary conditions:

$$\left.\begin{aligned} \xi_2 &= \dot{\xi}_2 = 0 \\ \eta_2 &= \dot{\eta}_2 = 0 \\ \zeta_2 &= \dot{\zeta}_2 = 0 \end{aligned}\right\} \text{ at } t = 0 ,$$

eq. (5.1)–(5.3) give

$$\xi_2 = \left\{\frac{3}{2}\,\alpha\left(\frac{W_0}{a\omega}\right)^2 + \frac{7}{12}\,\frac{\alpha^3}{a^2}\right\} - \left\{3\alpha\left(\frac{W_0}{a\omega}\right)^2 + \frac{9}{16}\,\frac{\alpha^3}{a^2}\right\}\cos\omega t - \frac{\alpha^3}{48a^2}\cos 3\omega t ,$$

$$\dot{\xi}_2 = \left\{\frac{3\alpha W_0^2}{a^2\omega} + \frac{9}{16}\,\frac{\alpha^3\omega}{a^2}\right\}\sin\omega t + \frac{\alpha^3\omega}{16a^2}\sin 3\omega t ,$$

$$\ddot{\xi}_2 = \left(\frac{3\alpha W_0^2}{a^2} + \frac{9}{16}\,\frac{\alpha^3\omega^2}{a^2}\right)\cos\omega t + \frac{3}{16}\,\frac{\alpha^3\omega^2}{a^2}\cos 3\omega t ,$$

$$\eta_2 = -\frac{4\alpha W_0^2 t}{a^2\omega} + \left\{4\alpha\left(\frac{W_0}{a\omega}\right)^2 - \frac{\alpha^3}{16a^2}\right\}\sin\omega t + \frac{\alpha^3}{48a^2}\sin 3\omega t ,$$

$$\dot{\eta}_2 = -\frac{4\alpha W_0^2}{a^2\omega} + \left\{\frac{4\alpha W_0^2}{a^2\omega} - \frac{\alpha^2\omega}{16a^2}\right\}\cos\omega t + \frac{\alpha^3\omega}{16a^2}\cos 3\omega t ,$$

$$\ddot{\eta}_2 = \left(\frac{\alpha^3\omega^2}{16a^2} - \frac{4\alpha W_0^2}{a^2}\right)\sin\omega t - \frac{3\alpha^3\omega^2}{16a^2}\sin 3\omega t ,$$

$$\zeta_2 = \frac{2\alpha^2 W_0}{a^2}\left\{t - \frac{\sin\omega t}{\omega}(2 - \cos\omega t)\right\} ,$$

$$\dot{\zeta}_2 = \frac{4\alpha^2 W_0}{a^2}(\cos^2\omega t - \cos\omega t) = \frac{2\alpha^2 W}{a^2}(1 - 2\cos\omega t + \cos 2\omega t) ,$$

$$\ddot{\zeta}_2 = \frac{4\alpha^2\omega W_0}{a^2}(1 - 2\cos\omega t)\sin\omega t .$$

RIASSUNTO (*)

Si esamina il movimento delle particelle cariche in un campo magnetico cilindrico con un metodo perturbativo teorico in cui il campo cilindrico è trattato come una perturbazione di un campo uniforme, e si trova che contiene termini di trascinamento assiale. Questi termini sono valutati sino al secondo ordine e vengono usati per formulare le condizioni per un effetto di auto-confinamento, quale sarebbe richiesto per il contenimento del plasma in un reattore termonucleare.

(*) *Traduzione a cura della Redazione.*

IL NUOVO CIMENTO Vol. XVIII, N. 6 16 Dicembre 1960

On the Parity Conservation in the Reaction $K^- + p \to \Sigma^+ + \pi^-$ (*).

A. Caforio, A. Ferilli, D. Ferraro and M. Merlin

Istituto di Fisica dell'Università - Bari

L. Guerriero (**), I. Laboragine, G. A. Salandin and F. Waldner

Istituto di Fisica dell'Università - Padova
Istituto Nazionale di Fisica Nucleare - Sezione di Padova

G. Poiani and M. de Pretis Cagnodo (***)

Istituto di Fisica dell'Università - Trieste
Istituto Nazionale di Fisica Nucleare - Sottosezione di Trieste

(ricevuto il 16 Agosto 1960)

Summary. — We have analyzed 143 protonic decays of Σ^+, emerging from K^- capture stars in nuclear emulsion, in order to detect the possible parity non conservation in the strong capture reaction. The forward-backward asymmetry A of the decay has been determined, obtaining the value $A = (4.4 \pm 7.8)\%$. This result is in accordance with the hypothesis of strict parity conservation.

1. – Introduction.

The parity conservation in strong interactions is known to be well established by a number of facts in nuclear physics. Various experiments have been devised recently to check once more such an invariance property ([1,2]),

(*) Preliminary results of the present experiment have been given at the Kiev Conference (July 1959, Glaser report).

(**) Now at the M.I.T. Cambridge, Mass.

(***) Now at the Laboratorio del Sincrotrone Nazionale, Frascati.

([1]) L. Rosen and J. E. Brolley jr.: *Phys. Rev. Lett.*, **2**, 98 (1959).

([2]) D. Bodanski, S. F. Eccles, G. W. Farwell, M. E. Rickey and P. C. Robison: *Phys. Rev. Lett.*, **2**, 101 (1959).

by observing the validity of the reciprocity theorem, as applied to cross-sections of strong inverse processes. A more direct approach, suggested and applied in other experiments ([3,4]), depends on the determination of the longitudinal polarization of the reaction products, which is expected to be zero if parity conservation is fullfilled by the reaction. Such measurement is particularly suited, if the reaction products happen to be unstable, since it is related to some features of the angular distribution of these decay products. This is the case, for example, for some reactions involving strange particles. The possibility of a lack of parity conservation for such reactions has been discussed by various authors ([5-7]).

One reaction well suited for such measurement is

$$K^- + p = \Sigma^+ + \pi^- \tag{1}$$

for which some experimental results already exist ([8]).

In order to determine the possible polarization of the Σ^+ hyperons, one is forced to confine oneself to the $\pi^0 + p$ decay mode, since it is the only one for which the asymmetry parameter is expected to be substantially different from zero ([9]).

In our case, the experiment has been performed using the emulsion technique; we have measured the forward-backward asymmetry in the angular distribution of the proton from the decay of Σ^- produced in nuclear capture of K^- via reaction (1). The asymmetry should give a good index of the polarization of the Σ^+, since the depolarization, even in a condensed medium like nuclear emulsion, is certainly small (due to the short lifetime of the hyperons) if only Coulomb interaction occurs.

Nuclear interactions of the Σ^+ before escaping the parent nucleus may modify the polarization possibly produced in reaction (1). However the available experimental data ([10]) as well as the results of the present work seem to indicate that the probability of a nuclear interaction of the Σ^+ without its absorption, is small.

([3]) R. A. Salmeron and A. Zichichi: *Nuovo Cimento*, **11**, 461 (1959).

([4]) F. S. Crawford jr., M. Cresti, M. L. Good, F. T. Solmitz and M. L. Stevenson: *Phys. Rev. Lett.*, **2**, 11 (1959).

([5]) H. Blumenfeld, W. Chinowski and L. M. Lederman: *Nuovo Cimento*, **8**, 296 (1958).

([6]) D. H. Wilkinson: *Phys. Rev.*, **109**, 1603 (1958).

([7]) B. d'Espagnat and J. Prentki: *Nuovo Cimento*, **12**, 164 (1959).

([8]) J. Leitner, P. Nordin jr., A. H. Rosenfeld, F. T. Solmitz and R. D. Tripp: *Phys. Rev. Lett.*, **3**, 238 (1959).

([9]) R. L. Cool, B. Cork, J. W. Cronin and W. A. Wenzel: *Phys. Rev.*, **114**, 912 (1959).

([10]) K^--Collaboration: *Nuovo Cimento*, **15**, 873 (1960).

2. – Experimetal criteria.

We have used a stack of 50 Ilford G-5 emulsion sheets and 50 Ilford K-5, dimensions 3 in. × 4 in. × 400 μm, exposed to the K^- beam of the Berkeley Bevatron. The stars due to capture of the K^- at rest have been found by area scanning in the central part of the stack (*).

Each of the two sections of the stack showed a rather low value for the grain density corresponding to minimum ionization (~ 6 grains/50 μm) so that it was possible to obtain rather accurate calibration curves of ionization *vs.* velocity, even for rather slow particles. The search for Σ^+'s undergoing protonic decay has been pursued according to the following criteria, with the aim of obtaining grain counts of high statistical accuracy, and eliminating a noticeable number of small-angle Coulomb scatters:

i) only prongs with $g^* \geqslant 3$ times the minimum, dip angle $\leqslant 30°$ and a path length $\geqslant 100$ μm have been followed;

ii) all apparent scatters (sudden changes in direction) with projected angle $\geqslant 3°$ have been recorded;

iii) only events with secondary proton range $\geqslant 10$ μm and space angle $> 10°$ have been considered.

450 apparent scatterings have been observed among a total of about 10 000 K^- capture stars (K_e not included).

For each event the ionization was measured, in order to know the residual range of the primary track; 347 of them turned out to be events in flight with a residual range $\geqslant 100$ μm, which was the lower limit imposed by our present experimental technique.

From the analysis of the remaining 103 events with residual range < 100 μm, we have concluded that 79 of them are consistent with a decay at rest of a Σ^+, as the range of the secondary proton agreed with the expected value (1680 ± 30) μm within the spread arising from straggling and errors in measurements (**). (See Fig. 1). For each one of these events we have determined the angle between the direction of emission of the Σ^+ and of the proton.

(*) This part of the scanning has been carried out at the Tufts University under the guidance of Prof. J. Schneps.

(**) The range of the secondary proton does not provide a safe criterion if the decay angle is about 90°; for this reason such events have been desregarded, as will be described later.

The remaining 24 events, with residual range < 100 μm, have been assumed to be events in flight and added to the 347 events with estimated residual

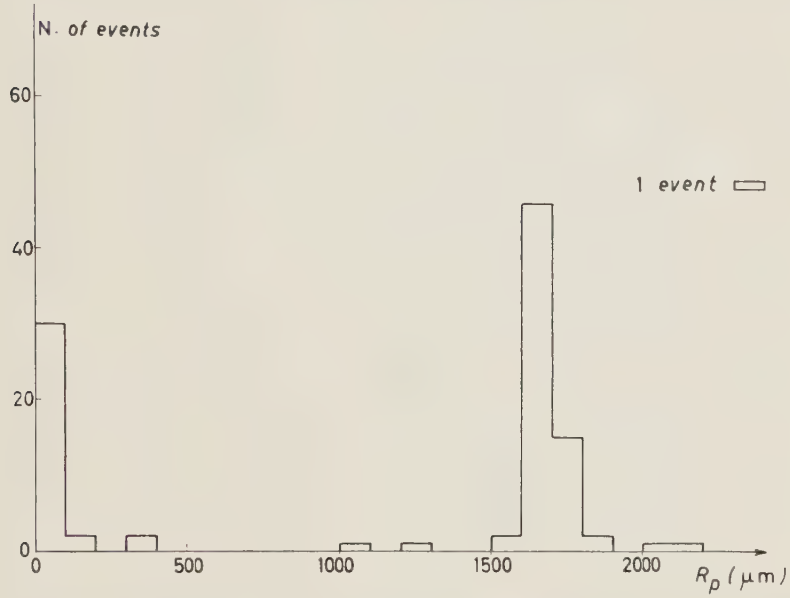

Fig. 1. Ranges distribution of the secondary tracks of the events with estimated residual range of the primary $\leqslant 100$ μm.

range $\geqslant 100$ μm. For the total of these 371 events in flight, the angle between primary and secondary track at the point of deflection was also measured.

Such events may be originated by:

a) decay in flight of a Σ^+;

b) elastic or inelastic scattering of a proton, a deuteron or a triton;

c) capture in flight of a Σ, giving an one-prong star;

d) scattering of a Σ^- giving a zero-prong capture star when at rest;

e) scattering of a Σ^+ decaying at rest into a pion escaping detection.

The most likely occurrences are those indicated in *a*) and *b*), as can be foreseen from the general features of the K^- capture in complex nuclei [11]; this assumption will be proved to be satisfactory from what follows. Therefore, the following method has been applied in order to get a discrimination of events of type *a*).

[11] K^--Collaboration: *Nuovo Cimento*, **14**, 315 (1959).

Each event has been analyzed according to the two hypotheses that it was due to an elastic scattering of a proton or to a decay in flight of a Σ^- into a proton; in both cases the relevant « reduced deviation » has been calculated:

$$S_p = \frac{g - g'}{\sigma(g')}, \qquad S_\Sigma = \frac{g - g''}{\sigma(g'')},$$

where: g = measured ionization of the primary;

g' = expected ionization of the primary if the event is due to an elastic scattering of a proton;

g'' = expected ionization of the primary if the event is due to a decay in flight of a Σ^+;

$\sigma(g')$ = standard error of g' (from the spread of the calibration points);

$\sigma(g'')$ = standard error of g'' (from the spread of the calibration points and the errors on θ_{lab} and R_p).

The kinematics of the decay has been calculated by a graphical method, which has also allowed the calculation of the propagated errors on the quantity β_Σ (velocity of the Σ^+ at the point of decay) from the experimental errors (*).

The results of such an analysis are summarized in Fig. 2. The dashed lines correspond to a limit of error of 2 times the standard deviation; the true Σ^- decays have a probability of 97% of falling inside the vertical strip; the same probability applies to the elastic scatterings of protons with reference to the horizontal strip; the same is true for elastic scattering of Σ's, due to the small mass difference $(m_\Sigma - m_p)$. The inelastic scatterings of protons fall mainly on the lower half-plane, elastic scatterings of deuterons and tritons on the upper half-plane. Inelastic scatterings of deuterons and tritons as well as captures in flight of Σ's could result in a point anywhere across the diagram:

(*) From the experimental data θ_{lab} and R_p it is possible to calculate the velocity β_Σ of the Σ^+ at decay. The Lorentz transformation

$$p_L = \gamma_\Sigma p'_L + \beta_\Sigma \gamma_\Sigma E'_p .$$

being linear in p_L and p'_L (longitudinal momenta of the proton in the lab. and c.m. system) it can be suitably represented by a nomogram ([12]). The value θ'_{CM} is found by direct reading. There are generally two solutions, yielding different values for θ'_{CM}: as a rule, one of them was ruled out being clearly in disagreement with the measured grain density.

([12]) M. D'OCAGNE: *Traité de Nomographie* (Paris, 1921).

however the occurence of events of this kind is reckoned to be negligibly small due to the low frequency of such particles among the prongs of the K^- capture stars.

Fig. 2. – Plotting of all events in flight according to the values S_p and S_Σ (see Sect. 2).

It turns out that events compatible with Σ^+ decay in flight amount to 77. However 13 of these are also compatible with elastic scatterings of a proton. This class of events will be discussed in the following section.

3. – Doubtful events.

It appears from the intersection of the two strips of Fig. 2 that there are some doubtful events, which are both consistent with a Σ^+ decay and with an elastic scattering of a proton. We define as doubtful events those, for which the measured velocity of the primary (β_{prim}) lies between the limits of two standard deviations both by considering them as proton scatterings and as Σ^+ decays.

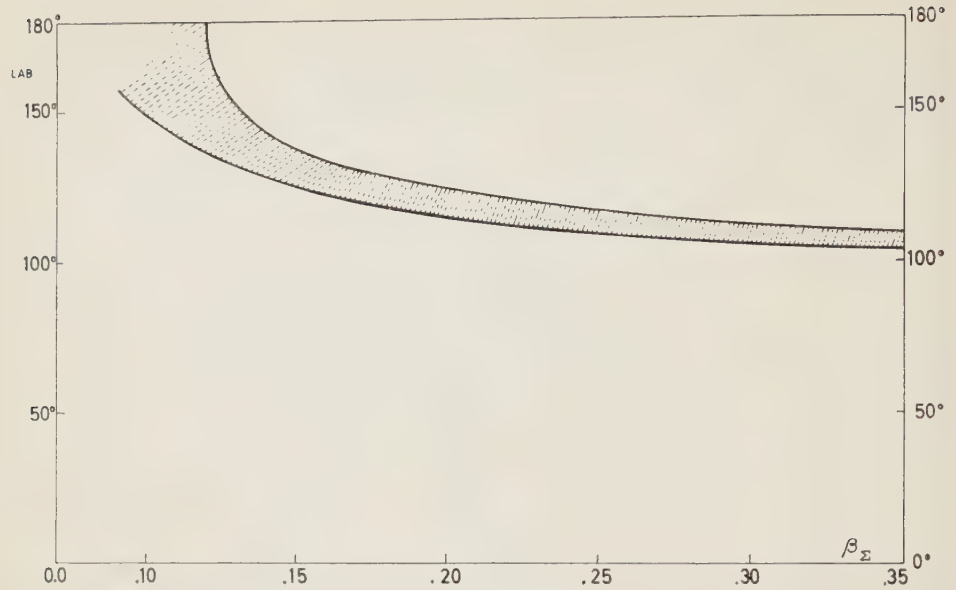

Fig. 3. - The hatched area shows the geometrical conditions of the decay in which the velocities of Σ^+ and of the decay proton are equal within 2 standard deviations

Decays of Σ's which can originate doubtful events are those within the limits of the hatched area in Fig. 3. The percentage of such events as a function of β_{prim}, deduced from a simple geometrical argument and assuming isotropic distribution in the c.m. system is reported in Fig. 4. Taking into

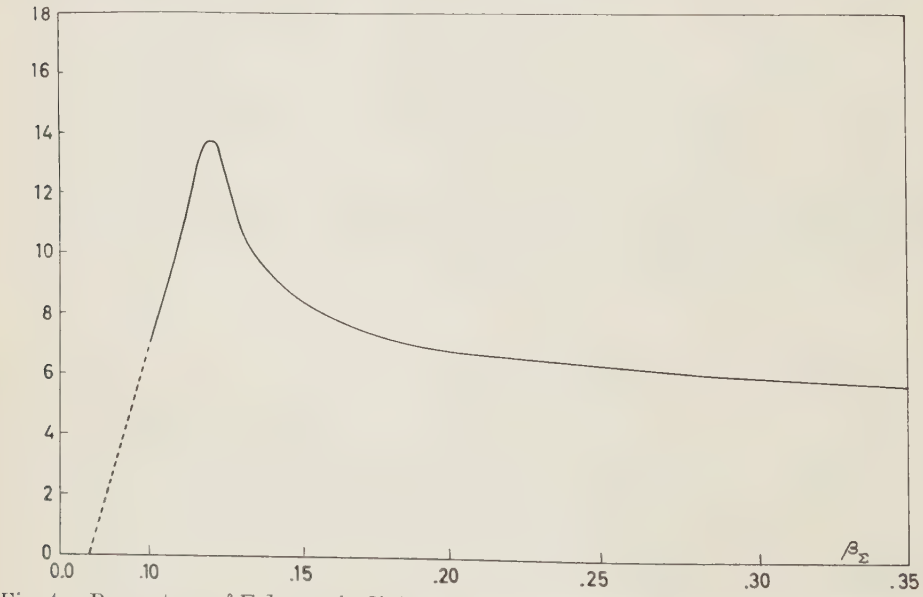

Fig. 4. – Percentage of Σ decays in flight giving rise to doubtful events, as a function of β_Σ.

account the energy spectrum of the Σ's in our sample, it turns out that the fraction of these events is nearly 0.06 of the total number of Σ^+ decays in flight, *i.e.* 4 events in our case.

It appears from Fig. 3 that these events must have all a decay angle in the c.m. system, $\theta'_{CM} > 100°$.

On the other hand, we have tried to evaluate the order of magnitude of the number of proton scatterings giving rise to doubtful events. The calculation of the scattering cross-section of protons on nuclei in photographic emulsion, for a given set of energies ([13-15]) yielded a number of 7 events. The experimental number of doubtful events is 13, in agreement with the above estimates, therefore we may consider as due to true decays in flight nearly $\frac{1}{3}$ of the doubtful events; of course they contribute to the backward tail of the angular distribution.

4. – Angular distribution.

Fig. 5 shows the c.m. angular distribution obtained. For events near 90° their classification turns out to be too sensitive even to minor experimental uncertainties. Therefore we have disregarded all events lying within the limits $90° \pm \gamma$, in order to calculate the asymmetry parameter. Such a cut-off eliminates also the uncertainty arising from the low energy events, as stated in Section 2. The best choice for the angle γ, arising as a compromise between kinematic considerations and the need not to loose information, turned out to be about 11° ($\sin\gamma = 0.2$). The asymmetry parameter for an angular distribution of the type $(1 + \alpha^\circ \bar{p} \cos\theta'_{CM})$ is given by

$$A = \frac{1}{1 + \sin\gamma} \cdot \frac{F - B}{F + B},$$

Fig. 5. – Angular distribution of the Σ^+ decay in the c.m. system. The dashed lines correspond to the limits $90° \pm \gamma$.

([13]) I. E. Dayton and G. Schrank: *Phys. Rev.*, **101**, 1358 (1956).
([14]) B. B. Kinsey and T. Stone: *Phys. Rev.*, **103**, 975 (1956).
([15]) G. W. Gleenless, L. G. Kuo and M. Petrovic': *Proc. Roy. Soc.*, **243**, 206 (1957).

where F is the number of events in the forward interval ($\theta'_{CM} < 90° - \gamma$), and B is the number of events in the backward interval ($\theta'_{CM} > 90° + \gamma$). Thus we get, from $F = 60$ and $B = 54$ (*),

$$A = (4.4 \pm 7.8)\ \% .$$

5. – Conclusions.

The value thus found for the asymmetry parameter A enables us to conclude that the product of $\alpha^\circ \bar{p}$, if not zero, is certainly small; in particular, our data is in agreement with the value $\alpha^\circ \bar{p} = 0$, that implies absence of longitudinal polarization of the Σ^+.

In fact, we know (8), from the study of the reaction

$$\pi^+ + p = \Sigma^+ + K^+$$

that for the protonic decay of the Σ^+, $\alpha^0 \bar{p} = 0.7 \pm 0.3$, whence: $\alpha^0 \geqslant 0.7 \pm 0.3$. The above condition may be restated in a more conclusive form if the selection rule $\Delta I = \pm \frac{1}{2}$ is assumed to hold at decay (9). From this assumption it follows: $\alpha^0 > 0.97 \pm 0.03$. As $\alpha^0 \sim 1$ the protonic decay of Σ^+ can be regarded as a good analyzer of polarization, and we are allowed to infer from our data that:

$$p \sim 2A = (8.8 \pm 16)\ \%$$

which implies a percentage of the same order of parity violating terms in the interaction (1).

* * *

It is a pleasant duty to thank Prof. J. SCHNEPS for the loan of the plates and Prof. LOFGREN and the Berkeley Bevatron Staff for the exposure of the stack. Profs. N. DALLAPORTA, C. FRANZINETTI, M. BALDO-CEOLIN and Dr. P. CAZZOLA are gratefully acknowledged for many useful discussions. Thanks are due to Profs. P. BUDINI and A. ROSTAGNI for the kind interest in our work.

(*) The quoted Figures F and B are already corrected for the following effects: for the geometrical loss due to the selection criteria iii) of Section 2, which has led to an increase by two units in the value of F; and for the estimated percentage of Σ^-s among the doubtful events, which has led to the addition of 4 events to the value B, as stated in Section 3.

We thank the observers of the plate groups of Bari, Padova and Trieste for their helpful co-operation.

Finally the Bari group wish to thank the Italian C.N.R. for financial support.

RIASSUNTO

Abbiamo analizzato 143 decadimenti protonici di Σ^+ provenienti da stelle di cattura di K^- in emulsione nucleare, allo scopo di rivelare l'eventuale non conservazione della parità nella reazione di produzione. Si è determinato il coefficiente di asimmetria avanti-indietro, che è risultato: $A = (4.4 \pm 7.8)\%$. Il risultato è ben compatibile con l'ipotesi che la parità sia totalmente conservata.

IL NUOVO CIMENTO Vol. XVIII, N. 6 16 Dicembre 1960

A Method for Faster Analysis of Bubble Chamber Photographs.

P. V. C. Hough (*) and B. W. Powell

CERN - Geneva

(ricevuto il 18 Agosto 1960)

Summary. — A measuring system is described which will enable photographs of bubble chambers to be measured in a time ~ 30 s per event. The design is such that the system can be developed in the direction of automatic pattern recognition without needing an on-line computer. Current difficulties and specific lines of future development are also discussed.

1. – Introduction.

The high rate at which interesting photographs can now be obtained by using a bubble chamber in conjunction with a particle accelerator has led to the construction in a number of laboratories of semi-automatic machines for the measurement of these photographs. Although these lead to a considerable improvement in the speed and reliability of measurements, there remain experiments, where the scanning time is short, for which a substantially faster but equally accurate measuring machine would significantly reduce the time needed for analysis.

During the past year we have been studying the possibility of constructing such a machine and, in view of the consideration now being given to this problem and that of automatic pattern recognition in various laboratories, we think it worth-while to present our ideas before an operational machine is completed. We have chosen to abandon mechanical track following systems in favour of one in which a spot of light a little smaller than the mean bubble diameter (*i.e.* ~ 15 μm) is made to carry out a rectangular scan over the film itself.

(*) On leave from the University of Michigan, Ann Arbor, Mich.

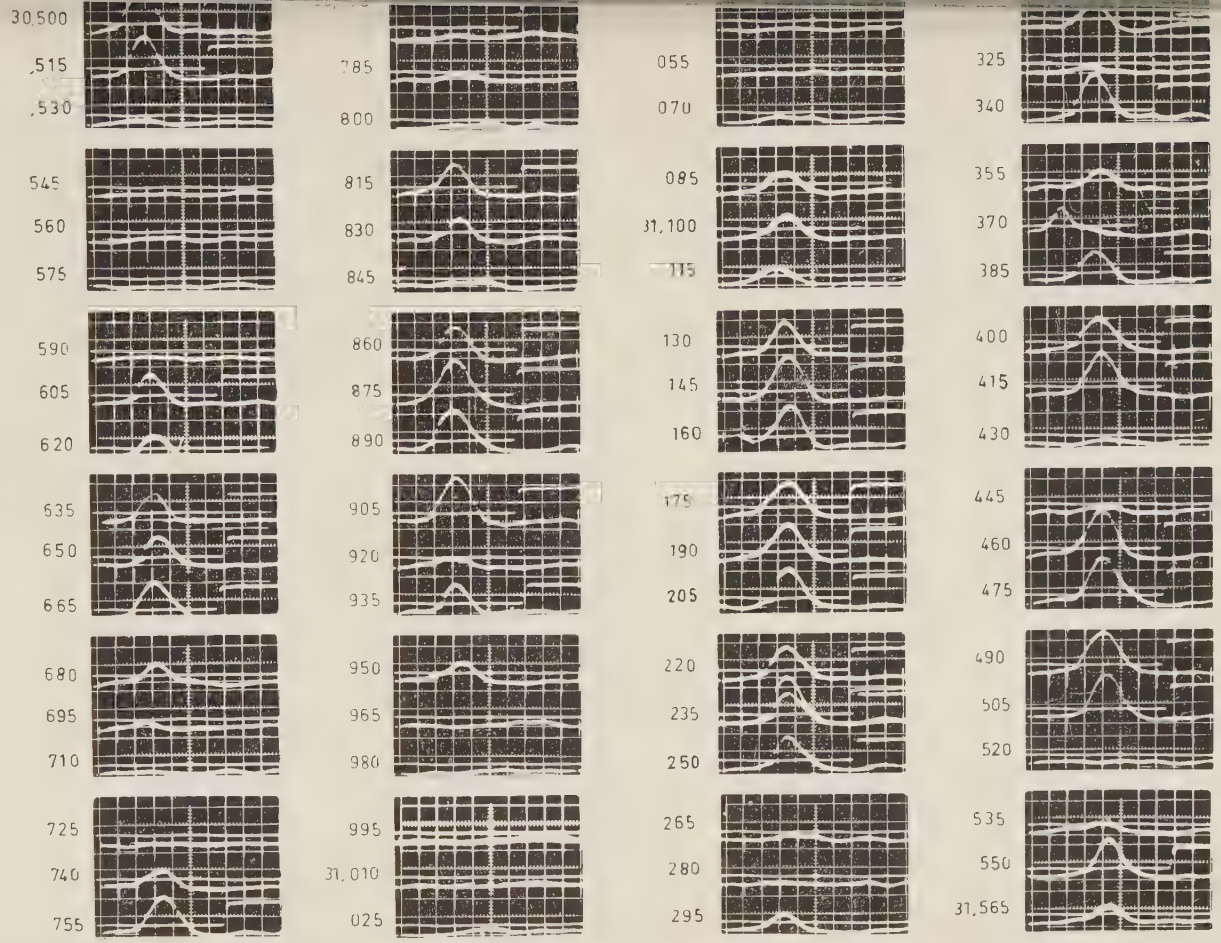

Fig. 1. – The pulses shown represent the signals obtained from a minimum track sampled at 15 μm intervals along its length and the numbers shown on the diagram correspond to the displacement along the track. The time base was such that each square corresponds to 1 μs and this is equivalent to 10 μm on the film. It will be seen that a certain minimum pulse height is required before a satisfactory track centre pulse can be generated.

One then uses the partial extinction of the light when the spot traverses a bubble image to locate the tracks registered on the film. A measuring system of this kind has the advantage that it can be developed into one capable of varying degrees of pattern recognition.

2. – The principle of the measuring system.

We have built a mechanical system to generate a flying spot (*). With this we can scan a 35 mm film with a series of lines 15 μm apart at a rate of 200 lines/s. This corresponds, therefore, to scanning a complete photograph

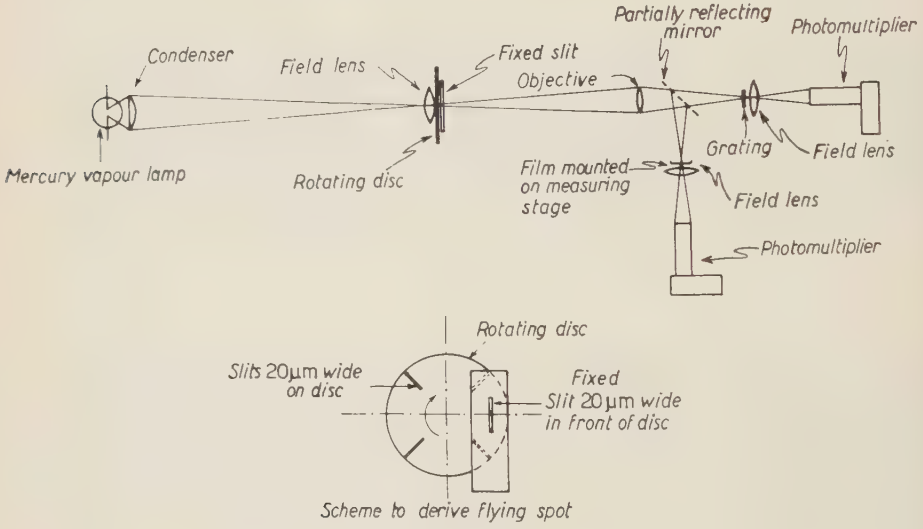

Fig. 2.

in ~ 10 s. In spite of the various sources of noise in the system we have been able to recognize unambiguously the passage of the spot across a large proportion of the bubble images of a typical minimum ionizing track. The linear density of such recognizable bubbles was found to be ~ 25 per cm track length in the chamber and could be increased by a suitable choice of chamber operating conditions. In Fig. 1 some examples are shown of pulses generated by the spot in traversing a minimum track. The step pulses also visible in Fig. 1 are generated at a constant time delay after the spot has traversed the centre of

(*) The laboratory has purchased a Ferranti type 5/71 high definition oscilloscope and it is planned to investigate the alternative of generating a satisfactory spot electronically.

the track, the centre being defined by the vertical line which would divide the area under the pulse into two equal parts.

The optical system is shown schematically in Fig. 2. The spot is generated by the intersection of a fixed straight slit with a radial slit which is mounted on a rotating disc. The whole of the fixed slit is illuminated by a 500 W mercury vapour lamp. The fixed slit is then imaged onto the film by means of the objective so that the rotation of the disc leads to a spot of light which repeatedly traverses the same straight line on the film. The film is supported on a microscope stage so that it can be moved at constant speed in the di-

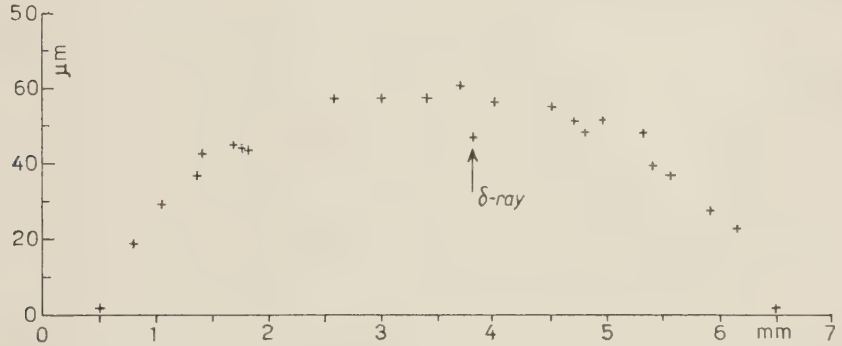

Fig. 3. – The figure shows the deviations from a straight line of the points obtained when measuring a minimum ionizing track 6 mm in length and of 80 mm radius on the film. The vertical scale is greatly expanded to demonstrate the scatter among the points.

rection perpendicular to the line of scan. In this way the spot is able to sweep over the whole surface of the film. The light which traverses the film at any point is collected by a field lens onto the cathode of the photomultiplier and the oscillograms shown in Fig. 1 represent the collector voltage as the spot traverses a bubble image.

By means of a partially reflecting mirror (Fig. 2) a second spot of light is imaged onto an accurate grating (*). This consists of alternate opaque and transparent lines of equal width with a pitch of 1000 lines/inch. The light transmitted by the grating is collected onto a photomultiplier which gives an approximately sinusoidal output as the spot traverses the grating. By counting these pulses, and by interpolation we are able to digitize the motion of the spot across the film. To digitize the second motion (*i.e.* the displacement of the film by the microscope) we plan to use the well tested Ferranti Moiré fringe system.

(*) Generously provided by the National Physical Laboratory, England.

Using the instrument in its present form we have measured some examples of minimum ionizing bubble chamber tracks. This has enabled us to test the efficiency with which we can digitize the co-ordinates of individual bubbles when using the grating system described above. An example of a track measured in this way is shown in Fig. 3 (*). As a result of our tests we believe that we should be able to achieve an accuracy of ± 2 μm when the machine is in its final form.

3. – The selection of the tracks.

The system described above enables us automatically to recognize, and to determine the co-ordinates of, a large proportion of the bubble images on a picture. This, however, is not enough to form the basis of a working instrument.

It is possible to transfer the co-ordinates of all the bubbles on a relatively complex picture from the measuring machine onto magnetic tape and then to read these into the store of a large computer such as the IBM 7090 (**). We do not, however, at present known how to sort out this information within the computer so as to reject tracks and other sources of background while retaining those tracks which represent interesting events. To overcome this difficulty we propose for the present machine to select the tracks to be measured when the photographs are first examined for interesting events.

At the moment, the most promising method for doing this is by preparing photographically, at the scanning table, a mask. This could then be used to obscure the unwanted tracks by the direct superposition of two films on the measuring machine. The mask would be prepared in the following way. The bubble chamber photograph is projected onto an opaque screen such as a sheet of paper. On this screen the observer marks over the event and the fiducial marks with lines about 2 mm wide. The projector is then switched

(*) Each point in Fig. 3 represents an average over several successive sweeps of the spot along the same path. We have used this technique to overcome the temporary limitation of a least count of 5 μm. The stability of the individual readings and the spread among the points in the figure have convinced us that the machine is capable of 2 μm accuracy and we intend therefore to provide for a least count of 2 μm

(**) With an IBM 729 IV tape unit, for instance one can write $\sim 100\,000$ words in 10 s. Since one requires not more than half a word (18 bits) to store each co ordinate to the required accuracy and since for a photograph 30×30 mm there are only 2000 scan lines along which digitizing can occur, one is able to record the co ordinates of every bubble for up to 100 tracks in the time available. By storing the information in co ordinate form the total amount of storage required is less then $2 \cdot 10^6$ bits, whereas it has sometimes been suggested that a capacity of 10^9 bits was needed for the complete storage of a bubble chamber picture.

off and the drawing directly illuminated and photographed. On development these « roads » appear as transparent lines about 200 μm wide on an otherwise opaque film. Thus by accurate superposition of two films, the second negative « gates » the first and only the bubbles which belong to the interesting tracks will be measured (*).

A system providing an automatic film advance is already under development at CERN for another application and it is thought that this can be developed into a sufficiently accurate system for both films to be moved on automatically in the final machine.

4. – Mode of operation.

We envisage that the analysis of the photographs will proceed as follows. The photographs will be examined at the scanning table for interesting events. For each event the operator will draw and photograph the roads which indicate which tracks are to be measured on all the stereoscopic views. At the same time a punched card (or « identity card ») is prepared for the event which records the number of the photograph and the possible interpretations of the event. When the roll of film has been scanned the films and cards are taken to the measuring machine where they are measured one roll at a time (*i.e.* all the photographs on one roll are measured before the other stereoscopic views are measured). The identity cards here serve only to tell the machine which photographs need measuring.

The co-ordinates of the bubbles which make up the interesting tracks are transferred via an intermediate store onto IBM magnetic tape. It is necessary that the tape run continuously while the scanning is in progress and only stop while the film is being advanced from one picture to the next. In this way the co-ordinates from 40 pictures may be stored on one reel of magnetic tape in about 6 minutes of continuous operation.

When tapes for all the stereoscopic views have been prepared, they are taken, together with the identity cards, to a large general purpose computer, such as the IBM 704. The computer reads in the co-ordinates for each photograph and is programmed to reconstruct the tracks from the succession of points, rejecting those which are spurious in origin (due for instance to a background track crossing the interesting track). When this has been done the

(*) Roads were originally conceived as coloured markings on the bubble chamber negative. In the development of ideas for a convenient and workable system, L. Kowarski first introduced the idea of a separate carrier for the roads. Alternatives to our present choice exist in which the road carrier is scanned by an auxiliary spot. While these enable the road carrier to be different in size from the original photograph the present system seems easier to construct and to use.

analysis can proceed in the normal manner, the identity cards being used to determine how the event should be interpreted. Some preliminary investigations have been made by D. LAKE and R. VAN DE WALLE into the problems of sorting the points into the corresponding tracks and it seems that the complexity of the problem and the amount of computer time needed to solve it for each photograph is not unreasonable (*).

5. – Discussion.

On the basis of our experiments to date we believe that a working machine of this type is feasible and an engineered version will be constructed at CERN. However, there are some characteristics which require further consideration.

Firstly, the accuracy with which the co-ordinates of a point on a track can be determined depends upon the orientation of the track, being particularly poor for a track lying almost parallel to the direction of scan. While such tracks are relatively rare at very high energies it is none the less important to be able to measure them. This can be achieved by remeasurement after a rotation of the film relative to the direction of scan.

The second difficulty is that of the roads. The need to provide these not only adds to the expense of the experiment since, as presented here, it substantially increases the amount of film used, but also one has the additional complication of preparing these masks when the photographs are being examined. However, this is to some extent offset by the fact that the system provides an unambiguous record for the future of what has been measured, similar in many ways to the sketches made at Berkeley or the photographic prints made at CERN.

6. – Future developments.

While the main purpose of our work is to construct a working measuring machine of the type described here, it will be noted that the manner in which the information is transferred from the film to the computer makes the machine suitable for experiments on the much more difficult problem of pattern recognition for bubble chamber photographs—*i.e.* dispensing with both the preliminary examination and the roads.

(*) The possibility of transmitting additional « ordering » information from the measuring machine to the computer to simplify programming for track recognition has been emphasized by Y. GOLDSCHMIDT-CLERMONT and his particular suggestions are incorporated in our present design.

A step in this direction would be to replace the making of actual roads by taking rough co-ordinates at the scanning table and then *computing* the positions of the roads inside the computer. Our magnetic tapes would then carry the co-ordinates of every recognisable bubble on the film but only those corresponding to bubbles within the roads would be accepted by the computer.

A preliminary study of this proposal has shown, as mentioned earlier, that with the standard equipment commercially available it is possible to store in the required time on magnetic tape all the co-ordinates required for the accurate analysis of photographs containing up to 100 tracks. The computer could then be used to determine whether or not a particular point is associated with a road whose rough co-ordinates were taken at the scanning table. With such a system, one would be able to study the possibility of decreasing the amount of information supplied to the computer for the computation of the roads and of perhaps, eventually, dispensing with it entirely.

* * *

We would like to acknowledge the support which we have received from L. Kowarski and Y. Goldschmidt-Clermont.

We wish to thank T. Lingjaerde and D. Wiskott for their advice and help. Much of our progress is due to the skill and imagination of G. Pacteau who has both designed and constructed a large part of our apparatus. We would also like to express our gratitude to P. A. Bobillier of IBM for his valuable co-operation. One of us (P. Hough) wishes to thank the Guggenheim Foundation for a Travel Fellowship.

RIASSUNTO (*)

Si descrive un sistema di misura che permetterà di misurare le fotografie delle camere a bolle nel tempo di ~ 30 s per evento. Lo schema è fatto in modo che il sistema può essere sviluppato verso il riconoscimento automatico della disposizione senza necessità dell'inserzione di una calcolatrice. Si discutono anche le difficoltà comuni e le linee specifiche degli sviluppi futuri.

(*) *Traduzione a cura della Redazione.*

IL NUOVO CIMENTO Vol. XVIII, N. 6 16 Dicembre 1960

The Electromagnetic Structure and Alternative Decay Modes of the π^0.

S. M. Berman (*) (**) and D. A. Geffen (*) (**)

Institute for Theoretical Physics, University of Copenhagen - Copenhagen

(ricevito il 22 Agosto 1960)

Summary. — In this note we point out that present experiments on the production of single Dalitz pairs in the decay of the neutral pion may yield some information about its electromagnetic structure. We show, by means of a dispersion relation, that the distribution of single Dalitz pairs in terms of the virtual photon mass is modified by a simple linear function containing only one unknown parameter, a, which would be of observable magnitude if pion intermediate states give large contributions to the dispersion relation. We also find that, independent of any assumptions about the π^0 structure, the branching ratio for the channel $\pi^0 \to e^+ + e^-$ must be greater than $4.7 \cdot 10^{-8}$ and estimate that the rate of this decay mode is surprisingly independent of the high energy behavior of the π^0 electromagnetic structure.

1. – Single Dalitz pairs.

Among the possible alternative decay channels of the neutral pion, two of which we think are of special interest are

$$\pi^0 \to \gamma + e^+ + e^- , \tag{1.1}$$

$$\pi^0 \to e^+ + e^- . \tag{1.2}$$

Figs. 1 *A* and 1 *B* show the Feynman graphs for these processes. While there

(*) National Science Foundation Postdoctoral Fellow.
(**) Present address: CERN, Geneva.
(***) Present address: Physics Dept., University of Minnesota, Minneapolis, Minn.

is fair agreement between experiment (1) and theory (2) for the branching ratio of (1.1), the possibility of more accurate experiments makes worthwhile the search for a deviation from the distribution predicted by DALITZ (2) due to the electromagnetic structure of the π^0. This deviation would occur in the region where the virtual photon mass is of the order of the pion mass. Present conjectures that contributions from pion intermediate states are enhanced by a resonant pion-pion interaction in the state of angular momentum 1, would also imply that such a deviation could be measurable. We shall consider this

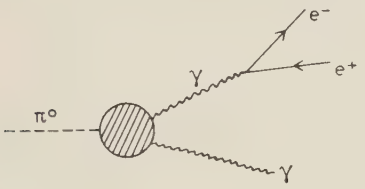

Fig. 1-*A*. – Feynman graph for process (1.1).

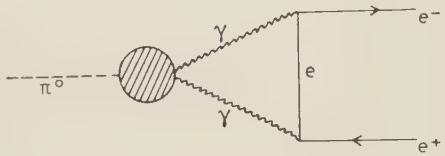

Fig. 1-*B*. – Feynman graph for process (1.2).

point in detail in this section and discuss the unobserved process (1.2) in Section 2. The latter decay mode is of special interest since the assumption of a point interaction between the pion and two photons leads to a divergent result for this decay.

The matrix element for a pseudo-scalar π^0 decaying into two photons of momenta K_1, K_2 and polarizations e_1, e_2, respectively, can be written in completely general form as (3)

$$(1.3)\qquad e_1^\mu e_2^\nu K_1^\sigma K_2^\tau \varepsilon_{\mu\tau\sigma\tau} G\Gamma(K_1^2, K_2^2, (K_1+K_2)^2) =$$

$$= e_1^\mu e_2^\nu i \int \mathrm{d}^4x \exp\left[i(K_1 - K_2)\cdot x/2\right] \langle 0 | T\left[J_\mu\left(\frac{x}{2}\right), J_\nu\left(\frac{x}{2}\right)\right] | \pi^0 \rangle ,$$

where J_μ, J_ν are the electromagnetic current operators involving strongly interacting particles, $T[\ ]$ is the time ordered product and $|0\rangle$, $|\pi^0\rangle$ represent the physical vacuum and π^0 states. In general, the right hand side of (1.3) defines the form factor Γ for arbitrary values of K_1^2 and K_2^2. G is a real con-

(1) C. P. SARGENT, R. CORNELIUS, M. RINEHART, L. M. LEDERMAN and K. ROGERS: *Phys. Rev.*, **98**, 1349 (1955); IU. A. BUDAGOV, S. VIKTOR, V. P. DZHELEPOV, P. F. ERMOSLOV and V. I. MOSKOLEV: *Žurn. Eksp. Teor. Fiz.*, **35**, 1575 (1958); N. P. SAMIOS: *Phys. Rev. Lett.*, **4**, 470 (1960).

(2) R. H. DALITZ: *Proc. Phys. Soc.*, A **64**, 667 (1951); N. M. KROLL and W. WADA: *Phys. Rev.*, **98**, 1355 (1955).

(3) We use units where $\hbar = c = 1$ and a metric with

$$A\cdot B = A_0 B_0 - \boldsymbol{A}\cdot\boldsymbol{B} .$$

stant chosen so that $\Gamma(0, 0, \mu^2) = 1$, where μ is the π^0 mass. In discussing the decay modes of a real π^0 we have the restriction that $(K + K_2)^2 = \mu^2$.

The lowest order graph in the electromagnetic coupling for channel (1.1) is shown in Fig. 1 A. The matrix element for this process can be obtained from equation (1.3) by replacing one of the polarization vectors, say e_1, by the factor

$$(4\pi\alpha)^{\frac{1}{2}} \bar{u}\gamma_\mu v K_1^{-2} ,$$

where α is the fine structure constant, and setting

$$K_2^2 = 0 .$$

The quantity of interest in process (1.1) is the distribution function in the variable representing the virtual photon mass and, including the form factor Γ, takes the form,

$$F(x) = \left[\left(\frac{x - 4m^2/\mu^2}{x}\right)^{\frac{1}{2}}\left(\frac{x + 2m^2/\mu^2}{x^2}\right)(1 - x)^3\right]\Gamma^2(x) , \tag{1.4}$$

where we have called $x = K_1^2/\mu^2$, the square of the virtual photon mass in units of the pion mass, and where we define, for simplicity,

$$\Gamma(K_1^2, 0, \mu^2) \equiv \Gamma(x) ,$$

m is the mass of the electron.

In previous treatments of this decay mode, $\Gamma(x)$ has been set equal to unity in (1.4), this approximation being justified by lowest order perturbation theory in the strong coupling. Since this argument is not conclusive, it is worth-while to consider the possibility that $\Gamma(x)$ can differ measurably from unity in the kinematically allowed range,

$$4m^2/\mu^2 \leqslant x \leqslant 1 .$$

It is easy to prove, using equation (1.3), that $\Gamma(x)$ is an analytic function of x except for a branch cut on the real axis extending from 4 to ∞. We can therefore expect a good approximation to $\Gamma(x)$ in the region of physical interest to be given by

$$\Gamma(x) = 1 + ax , \qquad |x| \leqslant 1 , \tag{1.5}$$

where a is a real constant either positive or negative. In order to understand the physical significance of a let us examine the dispersion relation for $\Gamma(x)$, assuming that no subtractions are necessary. This assumption is made extremely plausible by the fact that process (1.2) is divergent unless $\Gamma(K^2, K^2, \mu^2)$ van-

ishes as K^2 approaches infinity [4] (see also equation (2.1) in Section Q)) [5]. We have, with M the nuclear mass,

$$\Gamma(x) = \frac{1}{\pi}\int_{4}^{(2M/\mu)^2} \frac{\mathrm{d}x' \,\mathrm{Im}\,\Gamma(x')}{x'-x-i\varepsilon} + \frac{1}{\pi}\int_{(2M/\mu)^2}^{\infty} \mathrm{d}x' \,\frac{\mathrm{Im}\,\Gamma(x')}{x'-x-i\varepsilon}, \tag{1.6}$$

where the $\mathrm{Im}\,\Gamma$ is defined by

$$\varepsilon_{\mu\nu\sigma\tau}K_1^\sigma K_2^\tau G\,\mathrm{Im}\,\Gamma(K_1^2, 0, \mu^2) = \tfrac{1}{2}(2\pi)^4 \sum_n \langle 0\,|J_\nu(0)\,|n\rangle\langle n\,|J_\mu(0)\,|\pi^0\rangle\,\delta(K_1 - P_n)\,. \tag{1.7}$$

We have written the integral for Γ as the sum of two parts to emphasize the fact that, if the intermediate states containing baryon pairs give the dominant contribution to the sum in (1.7), the first integral in (1.6) can be neglected. This would justify setting $\Gamma(x)$ equal to unity in equation (1.4).

Let us consider now the contribution to Γ coming from the branch beginning at $x = 4$. Unlike the procedure of GOLDBERGER and TREIMAN [6], we consider the form factor for virtual photons and a real pion, so that the intermediate state with the lowest mass is the two-pion state with mass 2μ. From (1.7) we see that the contribution to $\mathrm{Im}\,\Gamma$ from the two pion state is proportional to $\langle 0\,|J_\nu|2\pi\rangle\langle 2\pi\,|J_\mu|\pi^0\rangle$. The first factor is the function $F_\pi(K_1^2)$ defined by FRAZER and FULCO [7] and proposed by them to be strongly resonant at a value of K_1^2 roughly in the range $10\mu^2 \leqslant K_1^2 \leqslant 20\mu^2$, in order to account for the electromagnetic structure of the nucleon. The second factor is the amplitude for the process $\gamma+\pi \to 2\pi$ where the final two pions are in the state $J=1$, $T=1$, assumed to be resonant. This matrix element has been calculated recently [8] assuming that this two pion state is dominant and it is found to be proportional to $F_\pi^*(K_1^2)$ so that the contribution to $\mathrm{Im}\,\Gamma(K_1^2)$ from the two-pion intermediate state is enhanced by the resonant

---

[4] S. D. DRELL: *Nuovo Cimento*, **11**, 693 (1959).

[5] While it is easy to think of examples where a function $F(x, y)$ vanishes for $x = y \to \infty$ but where $F(x, 0)$ does not vanish as $x \to \infty$, we think it unlikely for the case of the form factor Γ. For example Γ as calculated from lowest order perturbation theory (pion decay through a virtual nucleon-antinucleon loop) approaches zero independently as x or y goes to infinity.

[6] M. A. GOLDBERGER and S. B. TREIMAN: *Nuovo Cimento*, **9**, 451 (1958).

[7] W. R. FRAZER and J. R. FULCO: *Phys. Rev.*, **117**, 1609 (1960).

[8] M. GOURDIN and A. MARTIN: *Nuovo Cimento*, **16**, 78 (1960); HOW-SEN WONG: *Phys. Rev. Lett.*, **5**, 70 (1960). WONG also introduces the dispersion relation (1.6) and uses it to relate the π^0 lifetime to the process $\gamma+\pi \to 2\pi$.

factor $|F_\pi(K_1^2)|^2$. Unfortunately the matrix element $\langle 2\pi|J_\mu|\pi^0\rangle$, when determined from dispersion relations, involves an unknown multiplicative constant to be determined from experiment. It is clear, however, that the K_1^2 dependence of this term, for small K_1^2, can be approximated by replacing the expression obtained by an effective pole with the singularity at a mass very close to the resonant energy of the two-pion system. This can be easily verified by inserting the results of references ([7]) and ([8]) in (1.7) and (1.6).

Since the three-pion intermediate state which enters into (1.7) is the same state which gives the lowest mass contribution to the isotopic scalar part of the electromagnetic form factor of the nucleon, it is quite probable that this state also gives an important contribution to $\Gamma(x)$ and might also be resonant ([9]). Until a reliable way to treat the three-pion state is found as well as states containing nucleon or hyperon pairs we prefer to treat equation (1.6) phenomenologically by replacing the contributions from pion intermediate states by an effective pole and the high energy contribution coming from states containing baryon pairs by a constant. The effective pole approximation is a good one if the pion-pion interaction is resonant with the position of the pole at the resonant energy. If the three-pion state contribution is also important then the effective pole represents an average of the two contributions. The latter approximation of replacing the second integral on the right hand side of (1.6) by a constant for $x \sim 1$ is valid since $(2M/\mu)^2 \gg 1$. We write, therefore,

$$\Gamma(x) = \frac{\Lambda_\pi^2 \underline{b}}{\Lambda_\pi^2 - x} + (1 - \underline{b}) , \tag{1.8}$$

with, $4 < \Lambda_\pi^2 \ll (2M/\mu)^2$, and where $\underline{b}$ is a real constant, either positive or negative, which is a measure of the relative strengths of the two contributions. Strictly speaking, (1.8) is valid only provided the two-pion and three-pion resonant energies do not differ greatly from one another. If this is not the case, (1.8) must be generalized to include the three-pion pole explicitly ([10]).

In the range $|x| \leqslant 1$ we can expand (1.8) and obtain

$$\Gamma(x) = 1 + (\underline{b}/\Lambda_\pi^2)x$$

([9]) G. F. CHEW: *Phys. Rev. Lett.*, **4**, 142 (1960).

([10]) In this case we write

$$\Gamma(x) = \frac{\Lambda_{2\pi}^2 \underline{b}}{\Lambda_{2\pi}^2 - x} + \frac{\Lambda_{3\pi}^2 c}{\Lambda_{3\pi}^2 - x} + 1 - b - c ,$$

and, therefore, $\underline{a} = b/\Lambda_{2\pi}^2 + c/\Lambda_{3\pi}^2$ If $1 - b - c \approx 0$, then the distinction between this form for $\Gamma(x)$ and eq. (1.8) becomes more important.

and, hence,

$$\underline{a} = \underline{b}\,|A_\pi^2|\,.$$

To give an idea of the magnitude of $\underline{a}$ consider the case when the pion-two contribution dominates, *i.e.*, $\underline{b} = 1$ and use the results of Frazer and Fulco that $A_\pi^2 \geqslant 10$. Therefore, for this case we have $0 \leqslant \underline{a} \leqslant 0.1$. This is not the largest possible value for $\underline{a}$ (or $\underline{b}$) since, if baryon pair states are important and contribute with the opposite sign, $|\underline{b}|$ could be larger than one.

Because $f(x)$, given by (1.4), is very strongly peaked near the small value $x = 8m^2/\mu^2$, only and abnormally large value of $\underline{a}$ can disturb the overall rate. For example a value of $\underline{a}$ as large as one changes the total branching ratio for process (1.1) by only 7 %. We propose instead that $\underline{a}$ be measured by an experimental determination of the quantity,

$$H(x, y) = \int_x^1 f(x')\,\mathrm{d}x' \Big/ \int_y^x f(x')\,\mathrm{d}x', \quad 1 \geqslant x \gg 4m^2/\mu^2, \quad y < x. \tag{1.9}$$

The best choice of x and y depends on the particular conditions of the experiment. We give the expressions for H for $y = 4m^2/\mu^2$ and $y \gg 4m^2/\mu^2$, assuming $|\underline{a}|^2 \ll |\underline{a}|$.

$$\left\{\begin{aligned} H(x, 4m^2/\mu^2) &= \alpha(x, \underline{a})[2\ln \mu/m - \tfrac{7}{2} + (\tfrac{1}{2}\underline{a} - \alpha(x, \underline{a})]^{-1}\,, \\ H(x, y) &= \alpha(x, \underline{a})[\alpha(y, \underline{a}) - \alpha(x, \underline{a})]^{-1}\,, \\ \alpha(x, \underline{a}) &= -\ln x - (1-x)[1 + \tfrac{1}{2}(1-x) + \tfrac{1}{3}(1-x)^2] + \\ &\quad + (\tfrac{1}{2})\underline{a}(1-x)^4 + \underline{a}^2/5(1-x)^4[\tfrac{1}{4} + x]\,, \\ &\quad 1 \geqslant x > y \gg 4m^2/\mu^2\,. \end{aligned}\right. \tag{1.10}$$

As pointed out by DRELL [4], very wide angle single Dalitz pairs can be confused with pairs coming from the decay process (1.2). However, our estimate of the rate of this decay mode indicates it to be entirely negligible in relation to the proposed experiment.

To give an idea of the number of events required to measure $\underline{a}$ we take as an example $\underline{a} = -0.1$. This value corresponds, in our model, to $-\underline{b} \geqslant 1$ or a contribution from baryon pairs which is about twice the pion contribution but of opposite sign. Fixing y at $4m^2/\mu^2$ and taking $x = 0.1$,

$$H(0,\ 1,\ 4m^2/\mu^2) = 0.103\,5\,, \qquad \underline{a} = -0.1$$

while assuming $F(x) = 1$ or $\underline{a} = 0$ leads to

$$H(0.1, 4m^2/\mu^2) = 0.108\,0\,, \qquad \underline{a} = 0\,.$$

This would mean a decrease in the expected number of single Dalitz pairs with $x > 0.1$ of 4.2%. For a statistical error of less than 2.5%, over 1600 events with $x > 0.1$ would be required and therefore a total number of single Dalitz pairs to be counted of 16000. A large fraction of Dalitz pairs occur with $x < 0.1$ and most of these have a relatively small angle between the electron and positron momenta, making them readily distinguishable from large x events which all occur with large angles between the pair. This reduces greatly the number of events to be carefully analyzed and makes the experiment much less formidable ([11]).

2. – The branching ratio for $\pi^0 \to e^+ + e^-$.

This process is of special interest since the assumption $F = 1$ leads to a logarithmically divergente result. DRELL ([4]) has estimated the branching ratio for this process, using a dispersion relation, and he finds the amplitude proportional to $[\ln \Lambda/\mu][\ln \Lambda/m]$, where Λ is the cut-off he assumes for the function F. This result, therefore is very sensitive to the high energy behavior of F. We present here another estimate fo this process, using a different approach, and find the amplitude to depend only on $\ln \Lambda/\mu$ and in such a way as to make the result surprisingly insensitive to Λ. We also observe that the imaginary part of the decay amplitude is given exactly by quantum electrodynamics independent of any assumptions about the electromagnetic structure of the π^0. This enables us to give an exact lower bound to the decay rate.

Fig. 1 *B* shows the only graph which contributes to process (1.2) to lowest possible order in the electromagnetic coupling constant α. The effect of strong interactions with the π^0 is completely contained in the function F defined by equation (1.3) with both photons virtual. We see that the matrix element, T, for a π^0 of four-momentum q decaying into an electron and positron of four-momental s and r respectively, can be written to all orders in the strong coup-

([11]) Dr. N. SAMIOS has examined his recent ([1]) data on $\pi^0 \to \gamma + e^+ + e^-$ using eq. (1.5) and finds $\underline{a} = -0.24 \pm 0.16$. We wish to thank Dr. SAMIOS for making these results available to us. This large negative value of $\underline{a}$ corresponds to a $\underline{b} < -2.4$ and implies a surprising amount of cancellation between the two terms in (1.8). It is also conceivable that a negative value of a can occur as a result of cancellations between the contributions from the two pion and three pion intermediate states. This is possible only if the resonant energies of the two and three pion systems are considerably different and requires an even greater degree of cancellation.

ling and to lowest order in α as

$$T = 4\pi\alpha G i \int \frac{d^4K}{(2\pi)^4} \frac{\varepsilon_{\mu\nu\sigma\tau} K_\sigma q_\tau \Gamma(K^2, (q-K)^2, \mu^2)}{[K^2 + i\varepsilon][(K-s)^2 - m^2 + i\varepsilon][(q-K)^2 + i\varepsilon]} \cdot \cdot \bar{u}(s)\gamma_\nu \gamma \cdot K \gamma_\mu v(r) . \tag{2.1}$$

In considering what guess to put in for Γ, we do not at present see how to make full use of equation (1.3). Since K_1^2 and K_2^2 are both non-vanishing, it is not possible to replace the time ordered product, appearing in (1.3), by a retarded or advanced commutator over the entire range of values of K required in (2.1). If we treat $\Gamma(K^2, (q-K)^2, \mu^2)$ as a function of K_0 and $\boldsymbol{K}$, we can, however, prove that Γ is an analytic function in the region of the K_0 complex plane defined by the inequalities

$$\begin{aligned} &\operatorname{Im} K_0 > 0 , \qquad \operatorname{Re} K_0 > -(\boldsymbol{K}^2 + 4\mu^2)^{\frac{1}{2}} + \mu , \\ &\operatorname{Im} K_0 < 0 , \qquad \operatorname{Re} K_0 < \ \ (\boldsymbol{K}^2 + 4\mu^2)^{\frac{1}{2}} . \end{aligned}$$

where $\boldsymbol{K}$ is considered fixed and real and the π^0 has been taken, for convenience, at rest, *i.e.* $q = (\boldsymbol{O}, \mu)$. This follows immediately from (1.3) which can be rewritten in these two regions as,

$$\begin{aligned} &\varepsilon_{\mu\nu\sigma\tau} K_\sigma q_\tau G \Gamma(K^2, (q-K)^2, \mu^2) = \\ &= i \int \exp[iK\cdot x]\theta(\ \ x_0)\langle 0|[J_\mu(x), J_\nu(0)]|\pi^0\rangle , \quad K_0 > -(\boldsymbol{K}^2 + 4\mu^2)^{\frac{1}{2}} + \mu \\ &= -i \int \exp[iK\cdot x]\theta(-x_0)\langle 0|[J_\mu(x), J_\nu(0)]|\pi^0\rangle , \qquad K_0 < (\boldsymbol{K}^2 + 4\mu^2)^{\frac{1}{2}} . \end{aligned} \tag{2.2}$$

The analytic properties of Γ in the variable K_0 are similar to the properties of a particle propagator and suggest the choice of Γ to have a similar form.

To estimate T we take for Γ one of the simplest possible functions symmetric in the two photon variables which vanishes as $K^2 \to \infty$ and does not contradict (2.2),

$$\Gamma(K^2, (q-K)^2, \mu^2) = \Lambda^2/(\Lambda^2 - K^2 - (q-K)^2 - i\varepsilon) , \tag{2.3}$$

where we take $\Lambda^2 \gg \mu^2$. Since the two main contributions to T from the integral in (2.2) come from the regions where $K^2, (q-K)^2 \approx 0$, where Γ is essentially unity and the region $K^2 \to \infty$, we feel that (2.3) will give a reasonable estimate for T. The calculation of T, putting (2.3) in (2.1), is straightforward, provided care is taken not to drop the $i\varepsilon$ until the very end of the

calculation. This is because T has an important imaginary part corresponding to the possibility of the virtual photons both becoming real at one point in the integration. We find for the branching ratio for process (1.2)

$$\frac{R(\pi^0 \to e^+ + e^-)}{R_0(\pi^0 \to 2\gamma)} = 2\left(\frac{\alpha m}{\pi\mu}\right)^2 |N|^2 , \tag{2.4}$$

$$N = [(\ln \mu/m)^2 - 3 \ln \mu/m - \tfrac{3}{2} \ln \Lambda^2/2\mu^2 + \pi^2/12 - \tfrac{9}{8} + \\ + O(\mu^2/\Lambda^2)] - i[\pi \ln \mu/m + O(m^2/\mu^2)] .$$

The factor m/μ in the amplitude T comes from the factor $\bar{u}(s)\gamma_\nu\gamma \cdot K \gamma_\mu r(r)$ in (2.1) and will arise for a scalar π^0 as well. Although we agree with Drell on $\operatorname{Im} T$ we disagree on $\operatorname{Re} T$ where Drell finds a $[\ln \Lambda/\mu][\ln \Lambda/m]$ dependence [12]. Agreement on the imaginary part of T is essential, since an examination of equation (5) of reference [4], reproduced here

$$\operatorname{Im} T(q^2) \sim (2\pi)^4 \sum_n \delta^4(q - P_n) < \nu |\bar{u}(s) j_e(0)| n\rangle\langle n | j_\pi(0) | 0\rangle , \quad q = \nu + s$$

and which is the expression for $\operatorname{Im} T$ given by unitarity, shows that the value for it obtained by Drell is independent of Γ and is exact to all orders in the strong coupling and to order α. This is because, for $q^2 = \mu^2$ only the 2γ intermediate state contributes.

Table I. – *The branching ratio* $R(\pi^0 \to e^- + e^-)/R_0(\pi^0 \to 2\gamma)$ *for a few values of the cut-off* Λ.

Λ^2	$10\mu^2$	$2M^2$	$3 \cdot 10^4 \mu^2$
R/R_0	$6.7 \cdot 10^{-8}$	$5.7 \cdot 10^{-8}$	$4.7 \cdot 10^{-8}$

In equation (2.4) it is the real part of N which contains the dependence on the cut-off Λ but in a way which is surprisingly insensitive to Λ. Table I shows R/R_0 for a few values of Λ. The weak dependence of $\operatorname{Re} N$ on Λ is not a consequence of our assumption for the high energy behavior of Γ. For example, if instead of (2.3), one takes a form factor which behaves, for large K^2, as $(\ln K^2)/K^2$ (which is predicted by lowest order perturbation theory) or as $(K^2)^{-\frac{1}{2}}$ then the $\operatorname{Re} N$ has the same logarithmic dependence on the

[12] In applying a dispersion relation to T, Drell makes the approximation of neglecting all intermediate states except the 2γ state. The states neglected, *i.e.* ... 2π, $\gamma\gamma$, etc. all contribute to the same order in α but have total masses greater than or equal to 2μ. Since the high mass contributions to T are important there is no justification for neglecting these states.

cut-off Λ. We can see this by generalizing the form of Γ given by (2.3) to

$$\Gamma(K_1^2, K_2^2) = \int_{\Lambda^2}^{\infty} \mathrm{d}\sigma^2 \, \varrho(\sigma^2) \left[\frac{\sigma^2}{\sigma^2 - K_1^2 - K_2^2 - i\varepsilon} \right], \tag{2.5}$$

where

$$\int_{\Lambda^2}^{\infty} \varrho(\sigma^2) \, \mathrm{d}\sigma^2 = 1 .$$

For $\Lambda^2 \geqslant 10\mu^2$, N in (2.4) is modified by replacing $-\frac{3}{2} \ln \Lambda^2/2\mu^2$ in $\mathrm{Re}\, N$ by $-\frac{3}{2} \int_{\Lambda^2}^{\infty} \varrho(\sigma^2) \ln (\sigma^2/2\mu^2) \, \mathrm{d}\sigma^2$. For $\varrho(\sigma^2) = \Lambda^2/\sigma^4$, $\Gamma \sim k^{-2} \ln K^2$ for large $K_1^2 = K_2^2 = K^2$ leading to the same result as in (2.4). For a $\Gamma \sim (K^2)^{-\frac{1}{2}}$ take $\varrho(\sigma^2) = \sigma^{-2}(\Lambda^2/\sigma^2)^{\frac{1}{2}}$ which again leaves (4.2) unchanged ([13]).

Since $\mathrm{Im}\, N$ gives the dominant contribution to R/R_0 we take as a good estimate of this branching ratio the value given with $\Lambda^2 = 2M^2$ and take as an estimate of the error the contribution due to $\mathrm{Re}\, N$ alone.

$$R/R_0 = (5.7 \pm 1) \cdot 10^{-8} .$$

Furthermore, since $\mathrm{Im}\, N$ is given exactly, a rigurous lower bound on R/R_0 is obtained with $\mathrm{Re}\, N = 0$,

$$R/R_0 \geqslant 4.7 \cdot 10^{-8} .$$

Finally, it is interesting to note that the decay of a π^0 into a pair of charged heavy leptons, whose existence or non-existence is still undetermined, provides a sensitive detector for such particles. The decay rate for this mode is still given by (2.4) with m the electron mass being replaced by the mass of the unknown lepton, call it m_s (assuming of course that the charged lepton has no anomalous interactions with the electromagnetic field). The quadratic mass factor in (2.4) would make this decay mode readily visible for masses m_s in the range $10\, m < m_s < \mu/2$. For example

$$R_s/R_0 \geqslant 6.0 \cdot 10^{-6} \qquad m_s = 20\, m$$

$$R_s/R_0 \geqslant 1.1 \cdot 10^{-5} \qquad m_s = 50\, m$$

$$R_s/R_0 \geqslant 1.5 \cdot 10^{-5} \qquad m_s = 100\, m$$

([13]) Deviations from (2.4) can occur if $\varrho(\sigma^2)$ attains both large negative and positive values. It should be pointed out that (2.5) can not be taken as a valid representation of Γ (with $\Lambda^2 = (2\mu)^2$ to be consistent with (1.6)) since this would be in contradiction with the analytic properties in the variable K_0 given by (2.2). Eq. (2.5) for Γ serves only as a useful means of generating more general functional forms for Γ.

If there existed such a charged lepton S of mass m_s less than $\mu/2$, then the branching ratio for the decay mode $\pi^0 \to \gamma + S^+ + S^-$ decreases only logarithmically with the mass ratio m_S/μ. Furthermore the distribution function $f(x)$ is given exactly by (1.4), replacing m by m_S. Hence, if in the experimental analysis of single Dalitz pairs the lepton S were mistakenly identified as an electron, the observed distribution function, $f(x)$, would deviate considerably in the region of large x from (1.4). For lepton masses approximately in the range $10\,m < m_S < 50\,m$ the ratio between the number of events with large values of x and the number of events with small x would be observed to be more than 50% greater than predicted by theory. Since no such anomaly has been observed [1] we can essentially rule out the existence of such a lepton in this mass range. A more precise statement will be possible when recent data [11] are analyzed for this effect.

* * *

We would like to thank Professor NIELS BOHR and Professor AAGE BOHR for the hospitality extended to us at the Institute for the Theoretical Physics in Copenhagen.

RIASSUNTO (*)

In questa nota si mette in evidenza che gli attuali esperimenti sulla produzione di singole coppie di Dalitz nel decadimento del pione neutro possono dare alcune informazioni sulla loro struttura elettromagnetica. Si mostra, a mezzo di una relazione di dispersione, che la distribuzione di singole coppie di Dalitz in termini della massa virtuale del fotone è modificata da una semplice funzione lineare contenente solo un parametro ignoto, a, che sarebbe di grandezza osservabile se gli stati pionici intermedi dessero grandi contributi alla relazione di dispersione. Noi troviamo anche che, indipendentemente da ogni supposizione sulla struttura del π^0, il rapporto di branching per il canale $\pi^0 \to e^- + e^+$ deve essere maggiore di $4.7 \cdot 10^{-8}$ e stimiamo che l'andamento di questo modo di decadimento è sorprendentemente indipendente dal comportamento alle alte energie della struttura elettromagnetica del π^0.

(*) *Traduzione a cura della Redazione.*

IL NUOVO CIMENTO Vol. XVIII, N. 6 16 Dicembre 1960

Proton Compton Effect.

G. Bernardini (*), A. O. Hanson, A. C. Odian (**),
T. Yamagata (*) and L. B. Auerbach (***)
University of Illinois - Urbana, Ill. and CERN - Geneva

I. Filosofo (***)
Istituto di Fisica dell'Università - Padova

(ricevuto il 22 Agosto 1960)

Summary. — The elastic scattering of photons by protons has been measured for 100 MeV to 290 MeV photons at 90° c.m.s. and 139° c.m.s. scattering angles. The expected large increase in cross-section is observed at energies approaching that of $(\frac{3}{2}, \frac{3}{2})$ pion-nucleon resonance. The scattering can be qualitatively explained by the ordinary Thomson amplitude combined with that of the $(\frac{3}{2}, \frac{3}{2})$ resonance. A more detailed examination of the cross-section in the region just above the photo-meson threshold has shown that it is sensitive to the π^0 photon coupling. From the experimental data, one may conclude that the π^0 mean life should be between 10^{-16} and 10^{-18} s.

The experiment reported and discussed in the following paper was initiated a few years ago at the University of Illinois. The high-energy photon source used was the 300 MeV betatron constructed by Kerst and collaborators. The experiment was initially stimulated by the well-known paper of Gell-Mann, Goldberger and Thirring [1] on the extension of the dispersion relations of Kronig and Kramers to quantum field theory.

One of the typical examples discussed in this paper was the elastic scat-

(*) Now at CERN, Geneva.
(**) Now at Istituto Superiore di Sanità, Roma.
(***) Now at University of California, Berkeley, Cal.
(***) At the University of Illinois with an OEEC Grant awarded by the Foreign Operations Administration, Washington D.C. Now at the Armour Research Foundation, Chicago, Ill.

(1) M. Gell-Mann, M. L. Goldberger and W. E. Thirring: *Phys. Rev.*, **95**, 1612 (1954).

tering (Compton scattering) of photons by protons. This process is particularly suited to treatment by dispersion relation techniques especially since that part of the scattering amplitude which arises from the pion-nucleon interaction cannot be treated by normal perturbation methods. Apart from dispersion relations, the elastic scattering of photons by nucleons has been the subject of a few papers in which the process was treated via more or less phenomenological models. In all of them, and up to ~ 300 MeV, the two leading terms were the Thomson amplitude and the resonant amplitude arising from the pion-nucleon state $T = \frac{3}{2}$, $J = \frac{3}{2}^+$. Thus it was expected that the cross-section would increase with increasing incident photon energy ω, so that for $\omega \simeq 340$ MeV the cross-section would be about ten times the Thomson ($\omega \to 0$) limit. Hence since the beginning, it was rather clear that the experiment could be of some interest providing that an attempt was made to surpass the level of qualitative information and that enough precision would be reached on the final results. It was also clear that the interval of photon energy of main interest was that near or below photo-pion threshold, *i.e.* an interval of energy where the resonant state amplitude would not yet be overwhelming the other possible matrix terms.

As a consequence, the experiment was mainly planned for photon energies in the interval 100 MeV $\lesssim \omega \lesssim$ 250 MeV. Of course, the interval $0 < \omega \lesssim 100$ MeV would also have been of great interest. Fortunately, this region was simultaneously carefully investigated by other people ([4-7]). Measurements in the region around resonance have been reported by LITTAUER, DEWIRE and FELDMAN ([8]). The first set of data obtained at Illinois was already published in a preliminary form ([9,10]). However, an attempt to fit these results with the

([2]) C. L. OXLEY and V. L. TELEGDI: *Phys. Rev.*, **100**, 435 (1955); C. L. OXLEY: *Phys. Rev.*, **110**, 733 (1958).

([3]) G. E. PUGH, R. GOMEZ, D. H. FRISCH and G. S. JANES: *Phys. Rev.*, **105**, 982 (1957).

([4]) L. G. HYMAN, R. ELY, D. H. FRISCH and M. A. WAHLIG: *Phys. Rev. Lett.*, **3**, 93 (1959).

([5]) B. B. GOVORKOV, V. I. GOL'DANSKII, O. A. KARPUKHIN, A. V. KUTSENKO and V. V. PAVLOVSKAIA: *Dokl. Akad. Nauk*, **111**, 988 (1956); B. B. GOL'DANSKII, O. A. KARPUKHIN, A. V. KUTSENKO and V. V. PAVLOVSKAIA: *Žurn. Eksp. Theor. Fiz.*, **38**. 1695 (1960).

([6]) L. L. HIGGINS: *Scattering of gamma rays by protons below the neutral meson threshold*, UCRL-3688 (February 1957).

([7]) H. R. KRATZ, J. ROUVINA and W. B. JONES: *Bull. Am. Phys. Soc.*, **4**, 253 (1959).

([8]) R. M. LITTAUER, J. W. DE WIRE and M. FELDMAN: *Bull. Am. Phys. Soc.*, **4**. 253 (1959).

([9]) T. YAMAGATA, L. B. AUERBACH, G. BERNARDINI, I. FILOSOFO, A. O. HANSON and A. C. ODIAN: *Bull. Am. Phys. Soc.*, **1**, 383 (1956); *Proc. CERN Symposium*, **2**, 291 (1956).

([10]) T. YAMAGATA: *Ph. D. Thesis*: *Proton Compton Effect for* 190 to 280 MeV *Photons*, (University of Illinois, 1956).

theoretical predictions was considered rather unsatisfactory. In spite of the confidence given to those results, it was felt that a check and an extension of them would have been very desirable. The new results were found to be very consistent with the previous ones and, apparently, the disagreement with the available theoretical calculations was still there.

Quite recently, however, in the interpretation of the experimental results, it was possible to remove that discrepancy that one could have hardly attributed to some experimental error. This rather satisfactory stage was mainly reached via the inclusion in the over-all matrix element of the graph indicated in Fig. 17. This term was first considered by Low ([11]) and its importance was recently emphasized by Hyman *et al.* ([4]) and by Jacob and Mathews ([12]). Actually, the influence of the graph of Fig. 17 on the proton Compton scattering near the photo-meson threshold seems to be so definite that the following results can, at present, be ranked among the best in the determination of the lower limit for the mean life of the neutral pion.

1. – Experimental method.

Below the photo-pion threshold, photons are scattered almost entirely by the proton Compton effect and it is sufficient to detect only the γ-rays.

Above the photo-pion threshold, the photoproduction of neutral pions furnishes a source of high-energy photons which is about a hundred times that expected from the Compton scattering. It is necessary to discriminate between the two processes

$$\mathrm{p} + \gamma \to \mathrm{p} + \gamma \,,$$

$$\mathrm{p} + \gamma \to \mathrm{p} + \pi^0 \to \mathrm{p} + 2\gamma \,.$$

Since both reactions involve photons and recoiling protons in the final state, it is necessary to devise a quantitatively accurate method for discriminating between the protons or photons from the two reactions.

Actually, with the resolution in energy attainable by the most efficient photon counter in the energy region dealt with in the present experiment, it is not possible to separate the two processes by measurement of the photon energies. This is because, due to Doppler shifting, the photons from the decay of the neutral pions which propagate in the same direction as the pion have energies close to those of Compton photons.

([11]) F. E. Low: *Phys. Rev.*, **96**, 1428 (1954); private communication. See *Report CERN Conference* (1958), p. 98.

([12]) M. Jacob and J. Mathews: *Phys. Rev.*, **117**, 854 (1960).

On the other hand, the difference in the recoil proton energy between the two processes is appreciable. In the case of neutral pion production, in the energy range of the present experiment most of the incident photon energy is spent in the creation of the meson mass. So, for the same incident photon energy, the neutral pion recoil protons at a given angle have less energy than

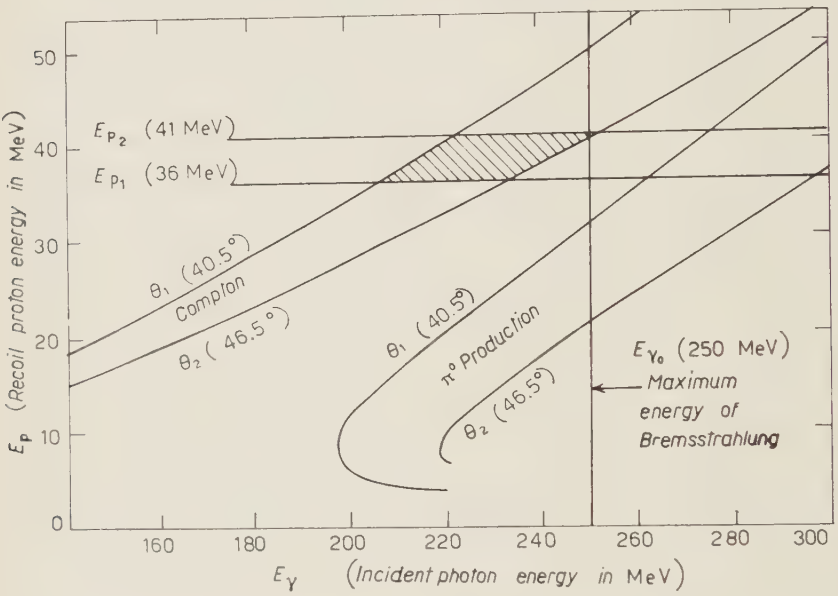

Fig. 1. Recoil proton kinematics of Compton scattering and neutral pion photoproduction.

do the Compton recoils. The proton energy can be selected quite accurately by an analysing magnet.

The background due to the neutral pion production may be eliminated completely by properly combining the maximum energy of the incident photon spectrum and the proton energy band selected by the magnet.

The separation is illustrated in Fig. 1 in which E_p (recoil proton energy) is plotted against E_γ (incident photon energy) for a constant Θ (proton angle measured from the direction of the incident photon beam), both for Compton scattering and for neutral pion production. When the measurement is limited for example, to between Θ_1 (40.5°) and Θ_2 (46.5°), all recoil protons from Compton scattering lie inside the upper strip in the figure. Neutral pion recoil protons, on the other hand, lie inside the lower strip. Now if the maximum energy of the incident photon spectrum is E_0 (250 MeV), and if one selects, by the magnet, protons with energies between E_{p1} and E_{p2} (36 and 41 MeV),

it is evident that the neutral pion events are completely excluded from the measurement.

Measurements at other energies can be made similarly by choosing proper combinations of the bremsstrahlung spectra and the magnet settings.

2. – Experimental arrangement.

A bremsstrahlung beam from a 0.040 cm diameter tungsten target in the Illinois 300 MeV betatron was collimated and passed through an evacuated tube with a sweeping magnet to remove all secondary electrons from the beam.

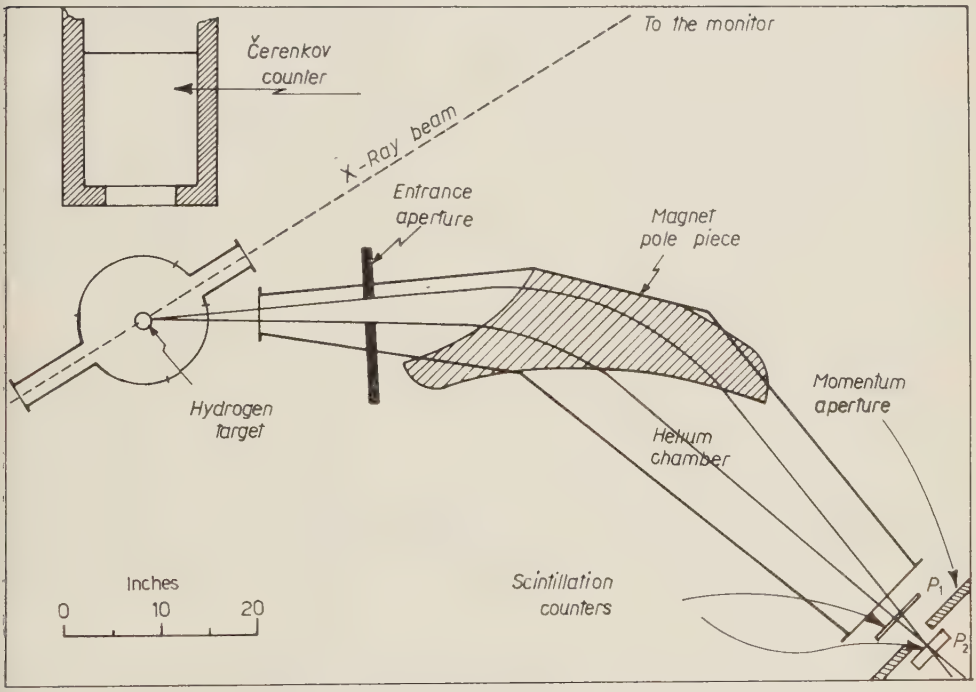

Fig. 2. – Layout of equipment.

The photon beam is incident upon a thin-walled liquid hydrogen target, as shown in Fig. 2, with the associated detector.

The recoil protons were selected in angle and momentum by the analysing magnet which was provided with an aperture which defined at all proton angles the solid angle for the protons accepted by the magnet. This aperture, made of brass, was placed on the side of the magnet facing the target and in a region where the magnetic field was still quite small. Thus the solid angle was prac-

tically independent of the value of the selected proton momentum. *This was the solid angle to be considered in evaluating the cross-section*, since the aperture of the photon counter was made rather large in order to overlap the magnet solid angle.

For a definite magnet current, the desired interval of selected momenta was obtained by a proper width of the momentum aperture, which was located at the image point of the target. This aperture consisted of two pieces of lead, 1 inch thick, arranged as a sliding screen.

To reduce the ionization energy loss and the scattering of the protons during the flight, the proton path from the exit of the target jacket to the entrance of the counter assembly was filled with a helium atmosphere. For that purpose a brass chamber, equipped with an entrance and an exit window of 0,003 inch mylar polyester sheet, was fitted inside the magnet gap.

The proton counter system consisted of two plastic scintillators. One was placed in front of, and the other behind the momentum aperture. The pulse heights in these counters were actually able to give complete and independent identification of the traversing charged particles.

The scattered photons were detected by a large, non-directional heavy lead glass Čerenkov counter. It was mounted on a sturdy iron support with four swivel castors, and was connected to a pivot by an iron bar of adjustable length the pivot being fixed on the floor at the position of the target so that it could be easily rotated around the target.

Concrete and lead shielding was used around the yoke of the proton analysing magnet in order to eliminate incorrect particle trajectories from passing through the proton counters.

The proton counter assembly itself was left free from shielding. Surrounding it with lead bricks was not effective in a further reduction of the background.

The Čerenkov counter was encased in a $\frac{1}{2}$ inch thick iron cylinder which was covered with $\frac{1}{4}$ inch of lead outside, in order to eliminate low-energy electrons and photons.

2·1. *Target system.* – The liquid hydrogen target used has been described by WHALIN and REITZ [13]. Two «appendices» or liquid hydrogen containers were used in the experiments. The first had a cylindrical shape $1\frac{1}{8}$ in. in diameter with 0,0015 inch mylar walls and had its axis perpendicular to the direction of the X-ray beam [14]. This appendix was used in the first set of runs covering X-ray energies between 190 and 280 MeV.

The second appendix had the shape of a thin convex lens 4 in. in diameter.

[13] E. A. WHALIN and R. A. REITZ: *Rev. Sci. Instr.*, **26**, 59 (1955).
[14] V. O. NICOLAI: *Rev. Sci. Instr.*, **26**, 1203 (1955).

$1\frac{1}{2}$ cm thick at the centre and about 3 mm at the edge. The axis of the lens made an angle of 30° to the beam. The walls were made of 0.0015 inch mylar.

2·2. *Proton analysing magnet.* – The proton analysing magnet had a uniform field and had the entrance edge designed to converge the beam in the vertical direction so that all protons which entered the front aperture would go through the gap without hitting the pole pieces. The exit boundary was curved to obtain good momentum resolution. In the vertical direction the protons suffered a rather strong defocusing at the exit boundary. This was compensated for by using tall counters, usually 9 inches in height.

Measurements using the hot wire technique showed that the resolution was better than 1 mm for rays coming from the source at angles of $-3°$ to $+3°$, the momentum resolution was 60 mm for a 10 per cent momentum change. A 6 mm lateral displacement of the source corresponded to a momentum shift of 1 per cent. The absolute calibration of the magnet obtained by absolute field measurements and by the hot wire method was checked against the betatron calibration by measuring the maximum energy of pair electrons from a small lead target at the source position.

2·3. *Proton counters.* – The proton counter system consisted of two plastic scintillators ($P1$ and $P2$ as shown in Fig. 2). The thinner one was placed in front of the momentum aperture and the pulse height in it is a measure of the rate of energy loss ($\mathrm{d}E/\mathrm{d}x$). The second crystal, placed behind the momentum aperture, was made thick enough to stop all protons below 70 MeV. The pulse height in this crystal indicated the energy of the proton. Although the energy of the proton was defined by the magnet, the additional information from the pulse heights was useful in rejecting background events.

The development of a satisfactory arrangement for collecting the light from a thin scintillator having a large area ($\frac{1}{8}$ in. × $6\frac{1}{2}$ in. ×9 in.) such as that in $P1$, presented some difficulty. If the collection is poor, the statistical fluctuation in the number of photo-electrons emitted from the

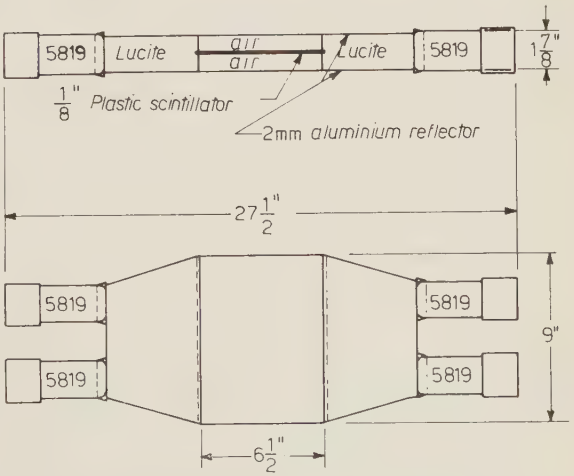

Fig. 3. - The first proton counter.

cathodes of phototubes could completely obscure information from the pulse heights. One would further desire that the light collection efficiency be made reasonably uniform all over the crystal.

The design of this counter is shown in Fig. 3. It was equipped with two lucite light pipes of trapezoidal shape, and viewed by four RCA-5819 phototubes. Polished aluminium foil of 0.002 inch thickness was used as the reflector. It was found that one could double the light collection by providing a large air space between the reflector and the scintillator surface. The pulse height was practically independent from the location of the scintillation.

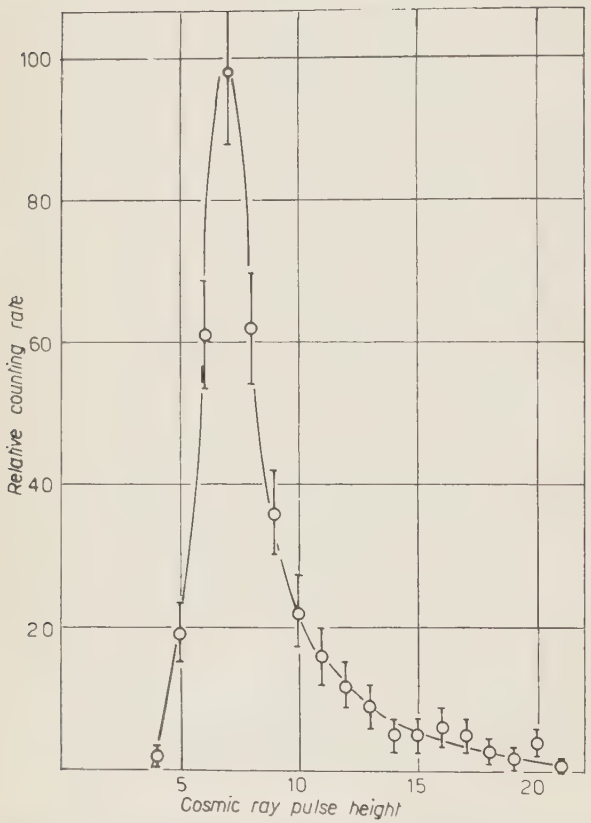

Fig. 4. - Pulse height distribution of cosmic ray pulses observed by the first proton counter.

The gain of each phototube was checked by counting radiation from a radium source placed in a standard position, and was equalized by adjustment of the individual high voltage. This check was done several times over the period of experiment, and no serious drift in the relative gain was observed. The total gain was checked every day during the run.

A preliminary test on this counter was made using cosmic rays. The counter was placed horizontally, sandwiched between two scintillators (2.75 in. $\times$ 5.75 in. and 3.4 in. $\times$ 6.6 in.) which triggered an oscilloscope. The pulse height distribution as obtained from photographs of the pulses is shown in Fig. 4. The distribution can be accounted for by the fluctuations in the ionization loss (Landau effect), slightly broadened due to the path length variation, the statistical fluctuation of photoelectrons, and the local variation of the collection efficiency.

The stopping scintillator was 5 in. wide, 9 in. high and $1\frac{1}{8}$ in. thick, and was viewed from the back through a lucite light pipe 6 in. long which was covered on the side with a layer of high reflectance white paint. The variation of the light collection efficiency of this arrangement was less than 10 per cent so that this pulse height served as a rough measure of the energy.

2·4. *The photon detector.* – The photon counters were based upon the observation of the Čerenkov light emitted by the high energy electrons produced in large lead glass cylinders by the incident photons. Various arrangements for similar counters have been described ([15-18]).

Two different lead glass Čerenkov counters were used in the experiment. The one used in the first run consisted of two cylindrical pieces of Corning lead glass 8392, each 12 in. in diameter and 7 in. thick, and joined together with Canada Balsam. The glass was viewed by twelve RCA-5819's with summed outputs. This counter was described in the CERN Symposium of 1956 ([19]).

The response of the Čerenkov counter was checked by observing its response to mono-energetic electrons selected by the magnet and it was found to be reasonably linear. It had a half width at half height of 25 per cent which was about twice that predicted by detailed Monte-Carlo evaluations ([10]). The side spread in the pulse height was consistent with the poor light collection efficiency.

In the second run, the counter consisted of a piece of cylindrical Chance Bros. lead lass, 9 in. in diameter and 8 in. thick, immersed in a water filled container having the shape of a frustum cone with reflecting walls. The cone opened out from 9 in. in diameter at the front to 12 in. at the back, which was viewed by four RCA-7046 (5 in., 14 stage) photomultipliers.

This second counter was used in the second set of runs on the Compton effect, during which the cross-sections for scattering at about 139° were measured.

The second counter was found to have somewhat better resolution than the first one for 150 MeV photons and had the further advantage of a larger output, and a better signal to noise ratio.

([15]) M. H. L. Jester: UCRL-2990 (1955).

([16]) W. B. Jones, H. R. Kratz and J. Rouvina: *Rev. Sci. Instr.*, **28**, 167 (1957).

([17]) C. E. Swartz: *Proc. of the Fifth Scintillation Counter Symposium*, IRE Transactions on Nuclear Science NS-3, no. 4 (Nov. 1956), p. 65.

([18]) A. W. Knudsen and R. Hofstadter: *Proc. of the Sixth Scintillation Counter Symposium*, IRE Transactions on Nuclear Science NS-5, no. 3 (Dec. 1958). p. 152.

([19]) I. Filosofo and T. Yamagata: *Proc. CERN Symposium*, **2**, 85 (1956).

2·5. *Electronics.* – The arrangement of the electronics was such that a fast coincidence between the two proton signals generated a trigger pulse. This was placed in slow coincidence with a similar trigger pulse initiated by the photon counter. This slow coincidence triggered a sweep on a fast oscilloscope, which was photographed and provided a permanent record of the height as well as the time between the proton and photon signals. The final selection was based on the measurement of these records.

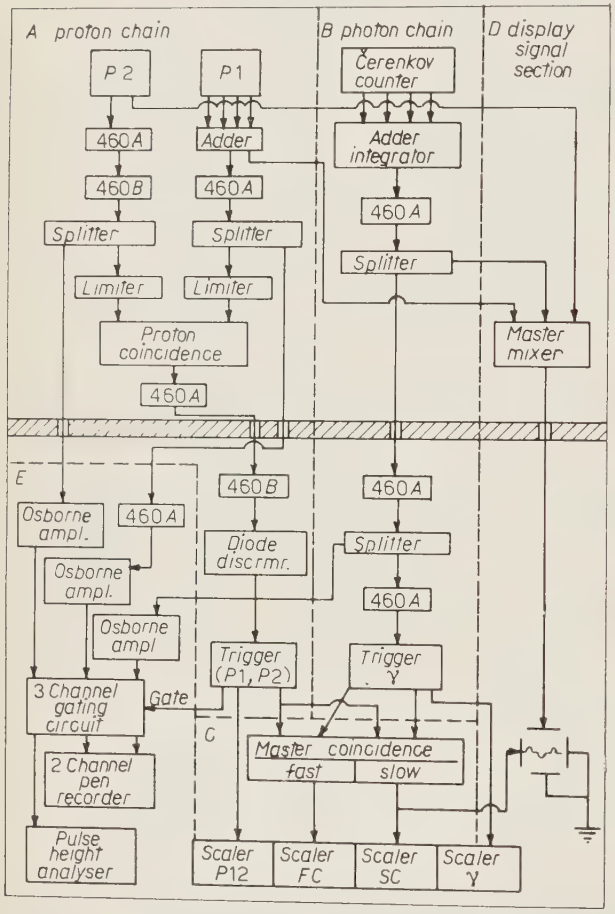

Fig. 5. – Block diagram of electronics. In the diagram, 460A and 460B refer to Hewlett Paclard wide-band amplifiers of Type 460A and 460B respectively.

A block diagram of the electronic system is shown in Fig. 5. The parts (*A*, *B* and *C*) generate a coincidence signal for triggering the oscilloscope. The part (*D*) is a mixing circuit, through which pulses are displayed on the oscilloscope screen. The part (*E*) was a pen recorder system for rough monitoring purposes.

In the proton chain (*A*), the outputs of the four phototubes on the first proton counter (*P*1) were added together in a mixer circuit. One of the two outputs of this mixer was amplified and shaped to a standard 10 ns pulse by a limiter circuit. Similarly, one of the outputs of the second proton counter (*P*2) was amplified and fed to a second limiter circuit. These limiter outputs were sent into a fast coincidence circuit, whose resolving time was about 16 ns. The coincidence circuit output went through two stages of amplifiers and a simple diode discriminating circuit. The signal was then led to a fast trigger circuit, which put out four standard pulses.

In the photon chain (B), one of the outputs was amplified and fed into another fast trigger circuit.

The master coincidence circuit (C) consisted of two sections. In one section, the ($P1$, $P2$, γ) coincidence was made with a 50 ns resolving time. In the other, the same coincidences were measured but with a 200 ns resolving time. The counts in the former consisted of true counts and a few accidental counts which fell within its resolving time. In the latter, the number of accidental counts was four times as large as in the former case. In this fashion the true and background counts could be obtained during the run, although final information was obtained later after the analysis of the films.

$P2$, γ and $P1$ pulses were fed to the master mixing circuit (D), with the γ and $P1$ pulses delayed by 150 ns and 300 ns respectively with respect to the $P2$ pulse.

The three pulses were displayed on a Tektronix Model 517 A oscilloscope. A sweep with a speed of 50 ns/cm was used. It was triggered by the master coincidence output with the longer resolving time. The purpose of this was to obtain information on background as well as true events.

The oscilloscope traces were photographed with a DuMont Type 314 Oscillograph Record Camera. Eastman Kodak Linagraph Ortho Film ran at a constant speed in the camera, so that the film length indicated the time elapsed between the events.

The processed films were projected on a screen from which the pulse heights and the timing of the three pulses were measured.

The pen recorder system (E) displayed the same information as was photographed but it had the advantage that it could be observed during the runs. Usually, the $P2$ and γ pulses were displayed on the pen oscillograph and $P1$ on the 5-channel pulse-height analyser.

3. – Experimental data.

3·1. *Main runs.* – In the first run in 1956, Compton scattering was measured at two betatron energies, 210 MeV and 250 MeV, with the proton analyser magnet set at 25°. The magnet was then rotated to 43.5°, which is approximately 90° in the centre of mass frame for the proton recoils from Compton scattering. At this angle, the cross-section was measured with 210, 230, 250, 273, 285 and 290 MeV bremsstrahlung. Later, one more point was measured with the magnet at 55° and with 250 MeV bremsstrahlung.

Parallel with the Compton experiments, a programme was set up to measure the cross-section of neutral pion production. The neutral pion runs were distributed between the Compton runs. Since the counting rate was much larger

and the cross-section is fairly well known ([20]), these neutral pion runs served in checking the performance and general stability of the equipment.

The second run in 1958 was taken with the proton aperture at an angle of 20° in the laboratory corresponding to a centre of mass photon scattering angle around 139°. Data were obtained at betatron energies of 120, 140, 163 184, 200 and 226 MeV.

For each case of the Compton runs, extreme care was taken in determining the settings of the angular and the momentum apertures and also of the magnet current, so that any possibility of observing the neutral pion production was removed. A further check was made by rotating the Čerenkov counter by plus and minus 20° from the correct Compton angle, and by observing that all good events disappeared.

In most of the neutral pion runs, and in some of the Compton runs, the energies of the recoil protons were too low to reach the $P2$ crystal. In such cases, the ($P1$, $P2$) coincidence system had to be abandoned. However, since the energy loss of the protons in the $P1$ crystal was now much larger, one could identify good protons on the basis of $P1$ pulse heights. The $P1$ counter was moved behind the momentum aperture, and the $P2$ counter was placed further back. In order to ease the switching between the $P1$-single and the ($P1$, $P2$) coincidence arrangements, and in order to minimize the chance of making a mistake, all electronic connections were left unchanged. The $P2$ channel of the coincidence circuit was biased off, so that the $P1$ singles passed as coincidences through the coincidence circuit.

3·2. *Empty target runs.* – A certain portion of the machine time was spent in measurement with the appendix emptied. The single count rates of all three counters were greatly reduced. The number of good protons (identified as big pulses on the pen recorder) remained practically unchanged. This was expected, since protons with an energy comparable with or even higher than that of the Compton recoils could be produced only by the photodisintegration of carbon and oxygen nuclei present in the appendix wall (those due to photodisintegration of deuterons which exist in the liquid hydrogen as impurity were too few). These protons outnumbered the Compton recoils by a ratio of ten to one, and they remained with the empty target runs. (These protons are, however, not in coincidence with photons).

On the other hand, both outputs of the master coincidence circuits (one with a resolving time of $2 \cdot 10^{-7}$ s and the other of $5 \cdot 10^{-8}$ s) were greatly reduced in number. These two numbers turned out to be proportional to

([20]) K. M. Watson, J. C. Keck, A. V. Tollestrup and R. L. Walker: *Phys. Rev.*, **101**, 1159 (1956).

their respective resolving times, indicating that they were all accidental. Film analysis showed that none of them had good proton pulses.

Actually, a small amount of hydrogen was still present in the empty target runs in the form of hydrogen gas and a constituent of mylar polyester foil. But the former amounted to only $\frac{1}{7}$% and the latter to 0.2% of the total hydrogen when the target was full. The effects of these were too small to be considered for the statistics obtained in the present experiment.

3·3. *Film analysis.* – Of the three pulses displayed on the oscilloscope traces, the photon and $P1$ pulses were delayed by 150 and 300 ns respectively, with respect to the $P2$ pulse. Thus, for a good proton γ coincidence the $P2$, γ and $P1$ pulses were equally spaced on the oscilloscope sweep. The γ pulse was of the opposite polarity to those of $P2$ and $P1$ to permit simple identification. Since the resolving time of the ($P1$, $P2$) coincidence circuit was 16 ns, the separation of $P2$ and $P1$ on the oscilloscope screen was always about the same. On the other hand, the resolving time of the master coincidence circuit was 200 ns so that the photon pulse could be anywhere within that time interval, sandwiched between two proton pulses. The time selection for good events was left to the film analysis. In this way one could measure both good and accidentally coincident events.

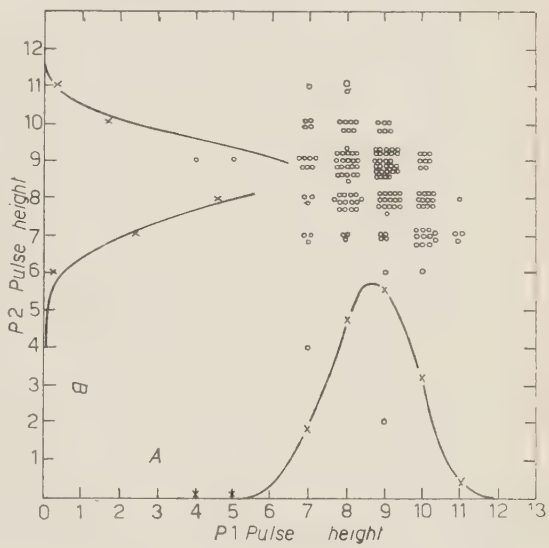

Fig. 6. - Pulse height correlation between $P1$ and $P2$. π^0 run at $\theta_p = 25°$, $\theta_\gamma = 105°$ lab. betatron 250 MeV.

Typical $P1$ and $P2$ pulse-height distributions and their correlations are shown in Fig. 6. They were selected on the basis of good timing between the $P2$ and photon pulses. The observed pulse-height distributions were mainly due to the variation of ionization loss in the crystals, which was expected since the momentum aperture accepted a finite energy band. The minimum pulse heights required on $P1$ and $P2$ to trigger the oscilloscope are indicated as A and B in the figure. It is evident that a small drift in the gain of the system could not eliminate any of the good events.

Since in most runs there existed a marked difference in height between

proton pulses due to a good proton and those due to a background count, film traces were classified into two groups by this criterion. Each event was then plotted on a graph against the separation (time) between $P2$ and photon pulses. Fig. 7 is an example of such graphs. It was taken from a 250 MeV Compton run at the proton angle of 43.5°. Traces with good proton pulses were plotted

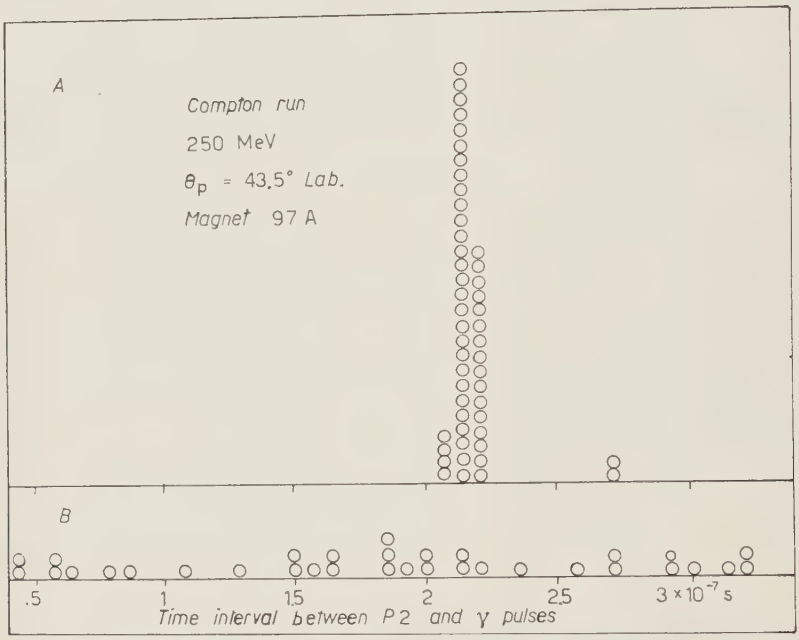

Fig. 7. – Number of counts versus the separation between the $P2$ and photon pulses on the oscilloscope trace. A) Both $P1$ and $P2$ pulse heights are above one half the average height. B) One is below one half of the average pulse height for that counter.

in (A), and those with poor ones in (B). In all runs, it was found that the plots in (B) form a uniform distribution indicating that they were entirely accidental. On the other hand, the plots in (A) were found to concentrate within a short time interval. In most runs, the accidentals in (A) were negligibly few. In a few runs, in which the betatron was run at highest energies, the plots (A) were accompanied by some backgrounds which distributed uniformly. In such cases, a subtraction was made to obtain the true count rate.

Fig. 8 shows the distribution of the photon pulse heights in these two groups. Those accompanied by good proton pulses demonstrated a peaked distribution, while those accompanied by poor proton pulses showed a rapidly decreasing distribution which indicated again that they were accidental in nature. Fig. 8 also shows that the discrimination level of the photon trigger circuit was set low enough to free good events from the effect of the gain drift.

Film analyses of the runs done with the single counter arrangements were performed in a similar way. In such cases, good protons had to be identified by the pulse height of $P1$ only, but the additional requirements of time correlation and the photon pulse height served to eliminate most background events.

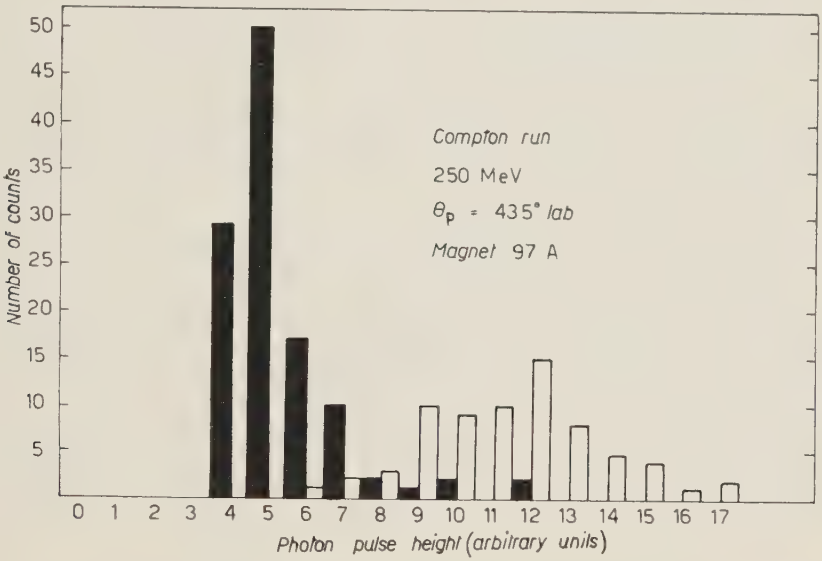

Fig. 8. – Pulse height distribution of the photon pulses. White: those accompanied by good proton pulses. Black: those accompanied by poor proton pulses.

There remained, however, a number of events with proton and photon pulses in the acceptable range which had poor time correlation. These would be treated as a background to be subtracted from the acceptable counts, such as those shown in the centre group of Fig. 7-*A*.

3·4. *Betatron energy and yield measurements.* – The energy of the betatron was determined by an integrating circuit which had been calibrated by a measurement of the peak magnetic field at the electron orbit of the machine.

The accuracy of the calibration was estimated to be around 0.2% at the time, but a subsequent recalibration in 1959, made by photomeson thresholds measurements, indicated energies higher by about 2%. An increase of the photon energy by 2% would increase the effective number of photons by about 10% and would, therefore, decrease the cross-sections by a corresponding amount. Below 260 MeV the betatron could produce X-rays for about 300 μs centered at 90° of the 60 cycle sinusoidal wave-form of the betatron current. For this type of operation, the spread of the maximum energy of the brems-

strahlung was estimated to be about 0.1%. Above 260 MeV, 90° operation was not possible due to radiation loss and the limitation on the maximum expander flux available. Therefore, the X-ray yield had to come out at an earlier phase angle as the energy of the betatron was raised. At 285 MeV, this phase angle was 75°. In order to keep the spread of the maximum energy small, the yield pulse was shortened as the betatron energy was raised. The spread remained always less than 1%.

The integrated beam intensity was measured by a thick-walled copper ion chamber which was placed at 8 metres from the betatron target. This ion chamber was periodically calibrated against a standard ion chamber which had been calibrated against a calorimeter. Accuracy of the calorimetric measurement was estimated to be 3%.

Knowledge of the shape of the photon spectrum from the betatron is very important in evaluating the cross-section. The spectrum used was that given by L. I. SCHIFF for the forward bremsstrahlung from a very thin target. Applicability of this formula to the actual betatron spectrum was tested, especially for the upper part of the spectrum, by J. E. LEISS, A. O. HANSON and T. YAMAGATA, who measured the betatron photon spectrum with a simple magnetic pair spectrometer. Good agreement between the formula and the experimental results was observed at two betatron energies, 243 MeV and 193 MeV.

4. – Efficiency calculations.

In order to evaluate the cross-section from the raw data obtained from the experiment, careful examination of the several factors which determine the « effective photon spectrum » is important. This is the spectrum of incident photons which could produce the proton-photon pairs such as are detectable by the particular setting of the counter system.

Since the aperture of the Čerenkov counter was made large, and the minimum requirement of the photon pulse height was small, both the solid angle and energy interval of the measurement was defined by the recoil proton detection system.

When the energy and angle of the recoil proton are specified, the energy of the incident photon is uniquely determined by a kinematical relationship. Therefore, if one has a counter system which detects mono-energetic protons emitted from a point target into an infinitesimal solid angle, the effective photon spectrum should be a δ-function multiplied by the incoming bremsstrahlung spectrum.

In reality, however, a measurement is always made with a system which detects protons emitted into a finite solid angle, with energies within a certain

energy interval. Furthermore, since the target is of finite dimensions, the limits of the solid angle and energy interval are smeared out. Therefore, the δ-function has to be replaced by a finite bell-shaped function whose exact shape is to be determined by the structure of the detector system. This function pill be called the « efficiency function ». It tells what fraction of the incident photons of a certain energy are eligible to produce events in the measurement. In other words, it is the efficiency of the detector system for photons of that energy.

Consider a small volume element in the target ΔV_i at a position specified as (x_i, y_i, z_i). The number of recoil protons produced in ΔV_i per unit yield of photons which are counted by the detection system can be written in general terms as

$$\Delta N_{p_i} = \varrho_H \frac{\Delta V_i}{A} \iiint n_\gamma(E_\gamma) \left(\frac{d\sigma}{d\Omega}\right) \cos\varphi \, d\vartheta \, d\varphi \, dE_\gamma \, (*) ,$$

where: ϱ_H = number of hydrogen atoms per unit volume;

$n_\gamma(E_\gamma)dE_\gamma$ = number of photons with energies between E_γ and $E_\gamma + dE_\gamma$ present in the incident X-ray beam per unit yield;

$d\sigma/d\Omega$ = differential cross-section of proton Compton effect;

$d\vartheta$, $d\varphi$ = horizontal and vertical angle elements of the recoil proton solid angle;

and A = cross-sectional area of the X-ray beam.

The limits of integration remain to be determined for each source point.

The limits for the vertical angle are well defined by the vertical aperture Φ_0 which was taken as the angle subtended by the aperture at the centre of the Φ_0. The maximum deviation was 2.3 % which was neglected. Since the maximum value of φ was around 2°, $\cos\varphi$ was taken as one.

The limiting horizontal angles in general are not those determined by the aperture alone, but depend as well on the range of proton energies accepted by the magnetic analyser. In order to determine these limits, a plot is made of the photon energies (E_γ) against Θ, such as that in Fig. 9*a*, for two proton energies E_{p1} and E_{p2}.

These energies correspond to the minimum and maximum proton energies from the volume V_i which are accepted by the momentum aperture of the magnetic analyser. The photon energies are obtained from the proton energies by adding the energy loss of the protons from the target into the magnetic analyser, and computing the photon energy which would give the corrected energy at that angle.

(*) One may note that the differential solid angle is written here in an unconventional way.

The efficiency function for this volume element $f_i(E_\gamma)$ at a particular photon energy is taken as the ratio of this effective aperture $\Theta_i(E_\gamma)$ to the geometric aperture Θ_0 at the centre of the target, as it is shown in Fig. 9*b*.

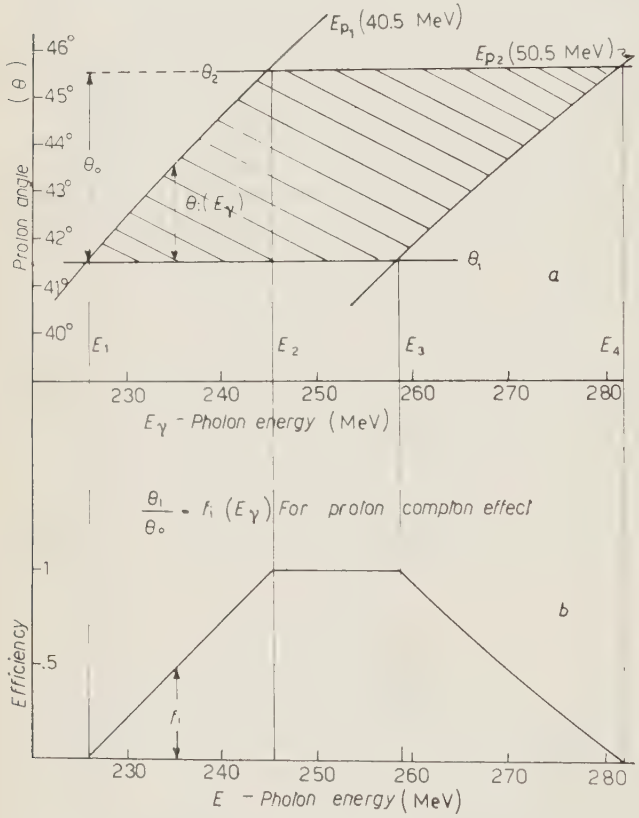

← Fig. 9*a*. – Parallelogram defined by the angular and momentum apertures of the analysing magnet in the E_γ-Θ_p plane.

← Fig. 9*b*. – The efficiency of the proton detector as a function of the photon energy as determined by the parallelogram of Fig. 9*a*: $f_i(E_\gamma) = \Theta_i/\Theta_0$.

In order to calculate the total number of protons expected from the target in terms of the cross-section, the number of protons must be evaluated for each small target volume and summed over the entire target volume. The relations may be written as

$$N_p = \sum_i \Delta N_{pi} = \frac{\varrho_H}{A} \frac{\overline{d\sigma}}{d\Omega} \Omega_0 V_0 \int n(E_\gamma) F(E_\gamma) \, dE_\gamma = \frac{N_H}{A} \frac{\overline{d\sigma}}{d\Omega} \Omega_0 N_\gamma ,$$

where: $\Omega_0 = \Theta_0 \Phi_0$ is the central solid angle;

$F(E_\gamma) = \dfrac{\sum_i f_i(E_\gamma) \, \Delta V_i}{V_0}$ is the average efficiency of the detector for photons of energy E_γ;

and N_H/A is the average number of hydrogen atoms per unit area in the irradiated target volume;

N_γ represents the total number of effective photons through the target area and is simply the integral $\int_0^{E_{max}} n(E_\gamma) F(E_\gamma) \, dE_\gamma$.

The cross-section in the centre of mass system, which is the quantity generally discussed, is obtained from the laboratory cross-section by multiplying by the calculated ratio of the two solid angles. Hence

$$\frac{d\sigma}{d\Omega^*} = \frac{N_p A}{N_H N_\gamma \Omega_0} \frac{d\Omega}{d\Omega^*}.$$

The computation of the efficiency function was done with the aid of the « ILLIAC », the University of Illinois' electronic digital computer. An example of an efficiency function calculated by the computer programme for a Compton scattering run at a betatron energy of 250 MeV is shown in Fig. 10.

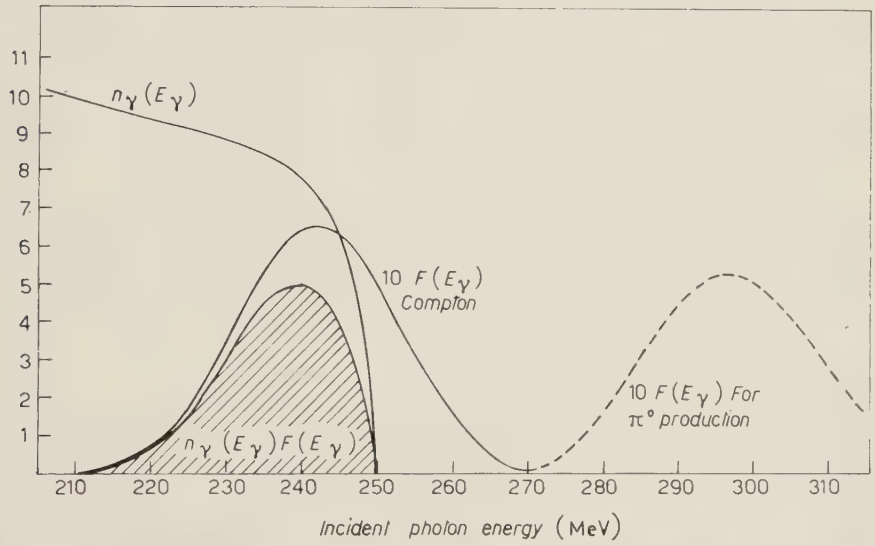

Fig. 10. - The bremsstrahlung spectrum $n_\gamma(E_\gamma)$, the efficiency function $F(E_\gamma)$ and the effective photon spectrum $n_\gamma(E_\gamma)F(E_\gamma)$ for the Compton effect measurement. The efficiency function of the neutral pion production for the same magnet setting is shown as a broken line, indicating that the neutral pion production cannot disturb the measurement of Compton effect. 250 MeV Compton run.

In this case the efficiency extends past the limits of the bremsstrahlung spectrum $n_\gamma(E_\gamma)$ and is well below the limits for detecting π^0 recoil protons, shown as a broken curve. The shaded area represents N_γ, the total number of effective photons per erg of incident bremsstrahlung flux at 250 MeV.

In the measurement of the neutral pion photoproduction, the geometrical efficiency of the photon counter for detecting the decay photons must be taken into account and multiplied by the efficiency for detecting the proton. The efficiency depends on the energy of the π^0 and its direction with respect to the axis of the photon counter. This efficiency is given for a few energies and angles in Table I for a circular aperture subtending 30° at the target.

TABLE I. – *Geometrical efficiency of the Čerenkov counter as a π^0 detector.*

E_{π^0} (MeV) \ α (°)	0°	6°	12°	18°	24°	30°
0	0.0341	0.0341	0.0341	0.0341	0.0341	0.0341
20	0.0970	0.0960	0.0933	0.0890	0.0835	0.0772
40	0.1452	0.1428	0.1359	0.1254	0.1127	0.0991
60	0.1944	0.1899	0.1772	0.1585	0.1369	0.1150
80	0.2452	0.2379	0.2177	0.1891	0.1572	0.1265
100	0.2974	0.2867	0.2576	0.2172	0.1741	0.1346
120	0.3505	0.3359	0.2965	0.2431	0.1880	0.1399
140	0.4043	0.3853	0.3343	0.2667	0.1993	0.1429
160	0.4583	0.4345	0.3710	0.2883	0.2083	0.1443
180	0.5121	0.4832	0.4064	0.3078	0.2154	0.1442
200	0.5655	0.5312	0.4406	0.3255	0.2206	0.1431

E_{π^0} is the kinetic energy of a neutral pion and α is the angle between the axis of the Čerenkov counter and the direction of the neutral pion motion.

The half-apex angle subtended by the circular aperture of the Čerenkov counter is 15°.

5. – Summary of results.

5·1. *Compton scattering cross-sections.* – The experimental cross-sections for the Compton runs are summarized in Table II, together with the experimental conditions. The errors listed are standard deviations due to counting statistics and do not include other systematic errors mentioned earlier, which may accumulate to about 10%. These values are about 3% larger than those first reported due to a re-evaluation of the acceptance solid angle of the proton magnet.

The cross-sections are shown as functions of the energy in Figs. 11 and 12 except for two high values with poor statistics. The cross-sections are plotted against the incident photon energy for centre of mass angles of 90° and 139° in Figs. 11 and 12. The effective photon spectrum associated with some of the points is indicated at the base of the figures.

The earlier measurements corresponding to photons scattered by 129° are included in Fig. 12. These values should be increased by about 10% if they

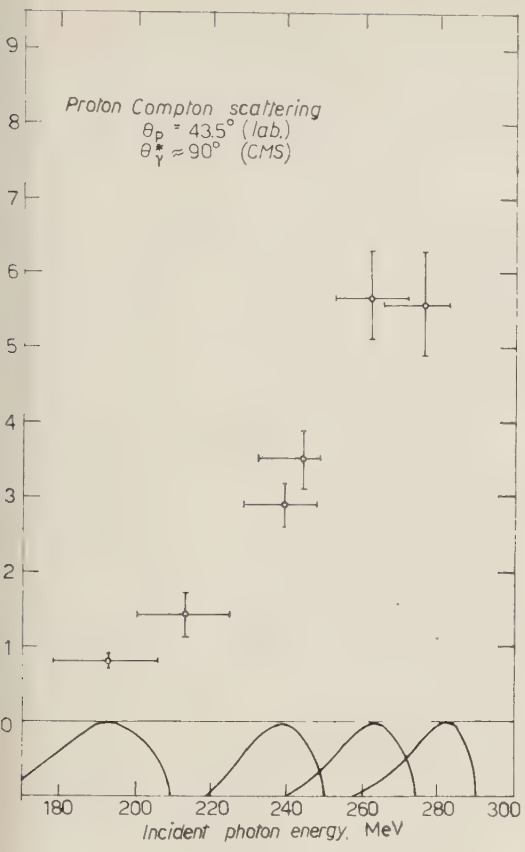

Fig. 11. – Differential cross-sections in the C.M. system for the elastic scattering of photons by protons by about 90° in the C.M. system. The cross-sections are given in Thomson units of $2.35 \cdot 10^{-32}$ cm²/sr. Vertical lines represent the standard error as determined by the number of counts. The horizontal lines do not represent errors but the energy limits corresponding to the half heights of the effective photon spectra shown below.

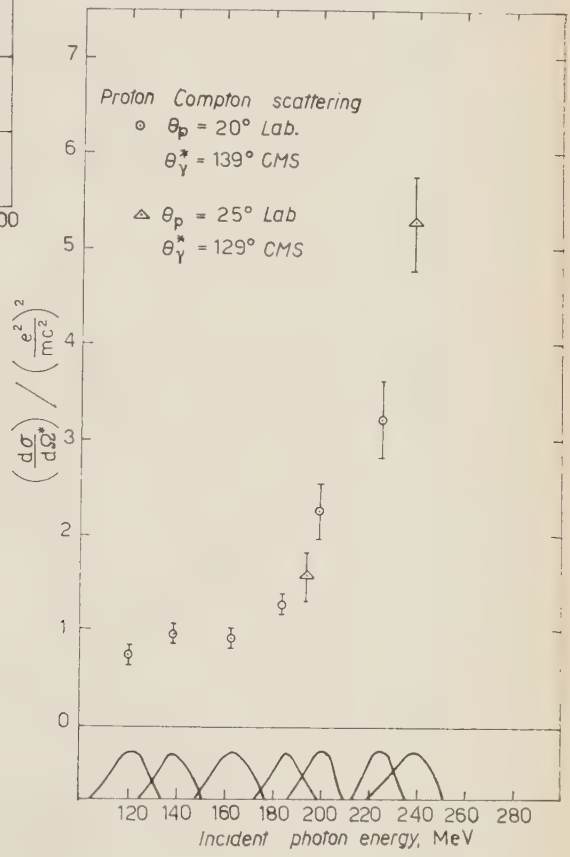

12. – Differential cross-sections in the system for the scattering of photons by 129° and 139° in the C.M. system.

TABLE II. – *Proton Compton effect cross-section.*

Betatron energy (MeV)	Photon counter angle (Lab)	Proton angle	Proton magnet energy limits (point source) (MeV)	Photon energies at half height (MeV)	Photon angle limits (c.m.s.)	Effective photon energy (MeV)	$d\sigma/d\Omega^*$ $2.35 \cdot 10^{-32}$ (cm^2/sr) (c.m.s.)
210	82°	43.5	21.5÷29.1	178÷206	86.1÷ 98.1	193	0.82±0.1
230	81°	43.5	27.7÷33.9	220 ÷225	88.0÷ 96.0	213	1.44±0.3
250	80.5°	43.5	36.4÷41.6	228÷248	87.7÷ 95.8	239	2.89±0.3
250	80.5°	43.5	38.2÷52.8	232÷248	85.7÷ 97.8	244	3.51±0.4
273	79°	43.5	43.9÷48.5	252÷272	87.6÷ 95.6	262	5.69±0.6
273	79°	43.5	46.3÷56.5	257÷272	87.6÷ 95.6	267	7.35±1.8
285	79°	43.5	48.2÷53.2	265÷283	87.5÷ 95.5	276	5.59±0.7
290	79°	43.5	50.4÷55.8	271÷288	87.4÷ 95.4	282	7.66±2.0
250	59°	55	16.9÷20.7	206÷24δ	65.1÷ 72.9	230	2.27±0.2
210	130°	25	40.2÷49.2	186÷206	125.5÷133.5	197	1.55±0.4
250	130°	25	59.1÷74.0	230÷248	125.0÷133.1	239	5.26±0.5
145	133°	20	20.8÷24.6	112÷127	136.0÷144.0	120	0.75±0.1
150	133°	20	22.7÷27.0	132÷144	135.8÷143.8	139	0.97±0.1
180	133°	20	31.7÷37.1	156÷170	135.7÷143.7	163	0.92±0.1
200	133°	20	39.2÷46.8	176÷193	135.6÷143.6	184	1.27±0.1
210	133°	20	47.5÷57.3	192÷208	135.5÷143.5	200	2.25±0.3
240	133°	20	61 ÷65.3	220÷233	135.3÷143.3	226	3.22±0.4

are to be compared with the other points, since it is clear that there is an increase in the scattering at larger angles.

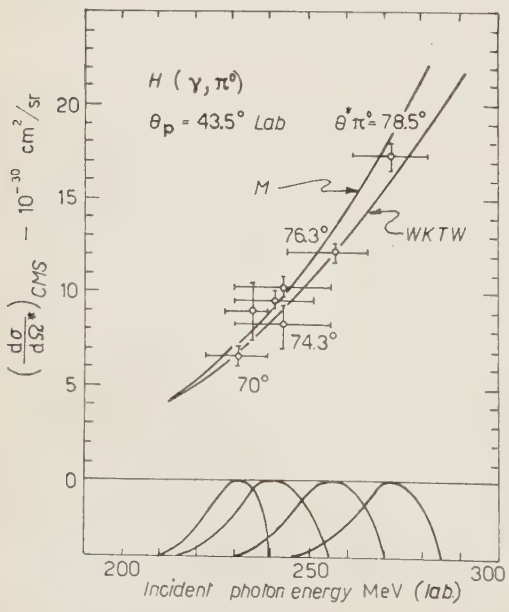

Fig. 13. – Differential cross-sections in the c.m.s. for neutral pion photoproduction at a proton angle of 43.5° lab.

The cross-sections are expressed in units of

$$(e^2/M)^2 = 2.35 \cdot 10^{-32} \text{ cm}^2/\text{sr} .$$

This is the classical Thomson scattering differential cross-section at 0°. The Klein-Nishina cross-section takes on the same value at 0° for all incident photon energies.

5·2. *Neutral pion photoproduction cross-sections.* – The experimental conditions and the final cross-sections obtained for neutral pion photoproduction are tabulated in Table III. The cross-sec-

TABLE III. – *Neutral pion photoproduction cross-section.*

Betatron energy (MeV)	Photon counter angle (Lab)	Proton magnet angle	Proton magnet energy limits (point source) (MeV)	Photon energies at half height (MeV)	Neutral pion angle limits (c.m.s.)	Effective photon energy (MeV)	$d\sigma/d\Omega^*$ 10^{32} (cm^2/sr) (c.m.s.)
240	60°	43.5	13.8÷18.6	222÷238	63.3÷ 76.5	231	6.8±0.5
240	60°	43.5	16.2÷21.9	227÷239	65.3÷ 77.9	234	9.2±1.6
255	60°	43.5	16.2÷21.9	230÷252	67.0÷ 79.1	241	9.9±0.5
270	60°	43.5	16.2÷21.9	230÷256	68.5÷ 80.1	243	10.6±0.6
285	60°	43.5	16.2÷21.9	230÷256	68.5÷ 80.1	243	8.5±1.2
270	60°	43.5	22.0÷28.0	244÷266	70.8÷ 81.7	257	12.4±0.5
285	63°	43.5	28.2÷34.4	271÷282	73 3÷ 83.6	272	17.8±0.8
210	99°	25	27.3÷33.3	200÷209	111.1÷121.9	205	3.0±0.7
250	105°	25	41.5÷51.5	230÷247	116.4÷126.0	238	5.2±0.5
200	116°	20	22.7÷27.0	182÷192	118.6÷130.4	186	1.1±0.2
230	116°	20	31.7÷37.1	200÷212	124.4÷134.5	206	2.7±0.2
250	116°	20	39.2÷46.8	215÷230	126.4÷136.3	222	3.3±0.3
250	116°	20	47.5÷57.3	231÷247	128.4÷137.8	240	7.1±0.6

tions are plotted against the incident photon energy in Fig. 13 ($\Theta_p = 43.5°$ lab) and Fig. 14 ($\Theta_p = 20°$ lab). Since the transformation from the laboratory to the c.m. system is dependent on the photon energy, the neutral pion angle is indicated for each point on the graphs.

These results should be compared with the values measured at other laboratories. For that purpose, the cross-section adopted by WATSON *et al.* ([20]) is drawn on the graphs as a solid line. The line marked by *M* represents the π^0 cross-section as deduced from single γ-ray measurements by MODESITT ([21]).

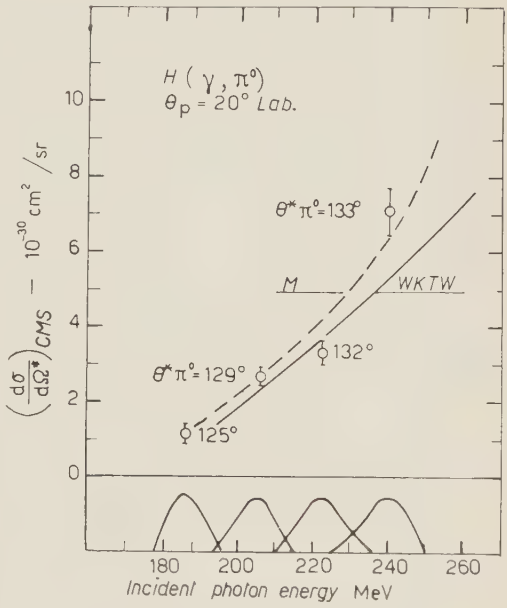

Fig. 14. – Differential cross-section in the c.m.s. for neutral pion photoproduction measured at a proton angle of 20° lab.

([21]) G. E. MODESITT: *Ph. D. Thesis, Photoproduction of neutral pions in hydrogen* (Universty of Illinois, 1958).

The photo-pion cross-sections can be seen to agree reasonably well with other measurements and serve to demonstrate their reproducibility as well as to indicate that the detector system was operating satisfactorily.

6. Comparison with the theory.

As was mentioned in the Introduction, the experimental results can be compared either with a more or less elaborated model, or with the predictions of the dispersion relations.

In all models the Thomson scattering, due to the static electromagnetic property of the nucleon, is superimposed upon a Rayleigh scattering due to the dynamic polarizability of the nucleon itself. The differences between one model and another lie mainly in the manner in which the Rayleigh scattering is pictured.

The Thomson scattering, or better, the $\omega \to 0$ limit of the photon-nucleon scattering which was discussed by LOW ([11]), and independently by GELL-MANN and GOLDBERGER ([22]) in two well-known papers, can be rigorously described on very general grounds, *i.e.* as a consequence of gauge and relativistic invariance.

Up to terms linear in the (incident) photon energy (momentum) $= \boldsymbol{k}$, the scattering amplitude for a transition between the initial state

$$\begin{cases} \text{photon} & (\boldsymbol{k}, \omega, \boldsymbol{\epsilon}) \quad \boldsymbol{\epsilon}\cdot\boldsymbol{k} = 0 \,, \\ \text{nucleon spinor} & \Psi_i = \begin{vmatrix} u \\ 0 \end{vmatrix} , \end{cases}$$

and the final state

$$\begin{cases} \text{photon} & (\boldsymbol{k}', \omega', \boldsymbol{\epsilon}') \quad \boldsymbol{\epsilon}'\cdot\boldsymbol{k}' = 0 \,, \\ & \\ \text{nucleon spinor} & \Psi_f = \begin{vmatrix} -\boldsymbol{\sigma}\cdot(\boldsymbol{k}-\boldsymbol{k}')\dfrac{v}{2M} \\ v \end{vmatrix} , \end{cases}$$

is given in terms of the two-component Pauli spinors by $a_k = v^* f u$, where

$$(1) \qquad f = -\frac{e^2}{M}(\boldsymbol{\epsilon}'\cdot\boldsymbol{\epsilon}) - 2i\mu^2 k\boldsymbol{\sigma}\cdot[(\boldsymbol{n}'\times\boldsymbol{\epsilon}')\times(\boldsymbol{n}\times\boldsymbol{\epsilon})] -$$
$$-\frac{ie\mu}{M}k\left|\boldsymbol{\sigma}\cdot\left\{\frac{\boldsymbol{n}(\boldsymbol{n}\times\boldsymbol{\epsilon})+(\boldsymbol{n}\times\boldsymbol{\epsilon})\boldsymbol{n}}{2}\right\}\cdot\boldsymbol{\epsilon}'-\right.$$
$$\left.-\boldsymbol{\sigma}\left\{\frac{\boldsymbol{n}'(\boldsymbol{n}'\times\boldsymbol{\epsilon}')+(\boldsymbol{n}'\times\boldsymbol{\epsilon}')\boldsymbol{n}'}{2}\right\}\cdot\boldsymbol{\epsilon}\right| - \frac{ie\mu_A}{M}k\boldsymbol{\sigma}\cdot(\boldsymbol{\epsilon}\times\boldsymbol{\epsilon}') \,.$$

([22]) M. GELL-MANN and M. L. GOLDBERGER: *Phys. Rev.*, **96**, 1433 (1954).

Here: $\hbar = c = 1$ and $e^2/4\pi = 1/137$;
M = nucleon mass;
μ, μ_A = total *and* anomalous magnetic moments of proton;
$\boldsymbol{n} = \boldsymbol{k}/k$, $\boldsymbol{n}' = \boldsymbol{k}'/k'$.

The above amplitude is a generalization of the Thomson formula. It says that up to the first order in k, all virtual states due to several coupling of the (bare) source are expressed by the static properties of the nucleon.

The scattering amplitude (1) is in the c.m. The transition to the laboratory frame is made, multiplying this amplitude by the factor k'/k. As is known, this is the factor which takes into account the change of frequency with respect to the nucleon initially at rest and then recoiling.

The amplitude (1) was written here in full to convey a better feeling of what follows. Compton scattering of a proton at high energies is a quite complicated process. However, a fairly good understanding of it can be reached if one makes clear first the meaning of the many transitions involved.

GELL-MANN and GOLDBERGER have shown that amplitude (1) can be interpreted term by term in *classic* (*non-quantized*) *manner*. The first term is the Thomson amplitude. The second is a magnetic dipole-magnetic dipole transition due to precession of $\boldsymbol{\mu}$ around $\boldsymbol{\mu} \times \boldsymbol{H}$. The others, due to the induced motion of the source, may be considered recoiling terms and are less important. The last one is an electric dipole-electric dipole transition. It is due to the currents inside the source and a similar term will be found later as a part due to the pion cloud.

The Rayleigh scattering amplitude, to be added to eq. (1), is due to the terms in powers higher than k, which are neglected in eq. (1). Any model faces the difficulty of making an appropriate distinction between terms which might be important and terms which one may neglect. The distinction depends, of course, on the value of k. Obviously, in the region between photo-meson threshold $\omega \simeq \mu$ and $\omega \simeq 3\mu$, the amplitude due to the pion-nucleon isobar state $T = \frac{3}{2}$, $J = \frac{3}{2}$, should be overwhelming. AUSTERN ([23]) has calculated this amplitude using a single resonance formula. In a crude, simple model, one may consider this resonant Rayleigh scattering as the only one to be added to the dominant term in eq. (1), *i.e.* to the Thomson amplitude.

As expected, this very crude model reproduces fairly well up to energies around $\omega \simeq 3\mu$, the main characteristic of the observed photon-proton scattering. This model was first discussed by YAMAGUCHI ([24]) as an extreme approximation of a more complex result obtained by a Chew-Low fixed nucleon

([23]) N. AUSTERN: *Phys. Rev.*, **100**, 1522 (1955).
([24]) Y. YAMAGUCHI: University of Illinois Report (1955), unpublished.

model. Of all possible terms, YAMAGUCHI retained only the Thomson amplitude a_T and the $(\frac{3}{2}, \frac{3}{2})$ resonant amplitude a_{33}.

This last can be written as a two-step transition from the initial state $|\Psi_0\rangle = |\boldsymbol{k}, \Psi_0\rangle$ (Ψ_0 is the physical nucleon) to the intermediate state $\langle\Psi_{33}|$ fol-

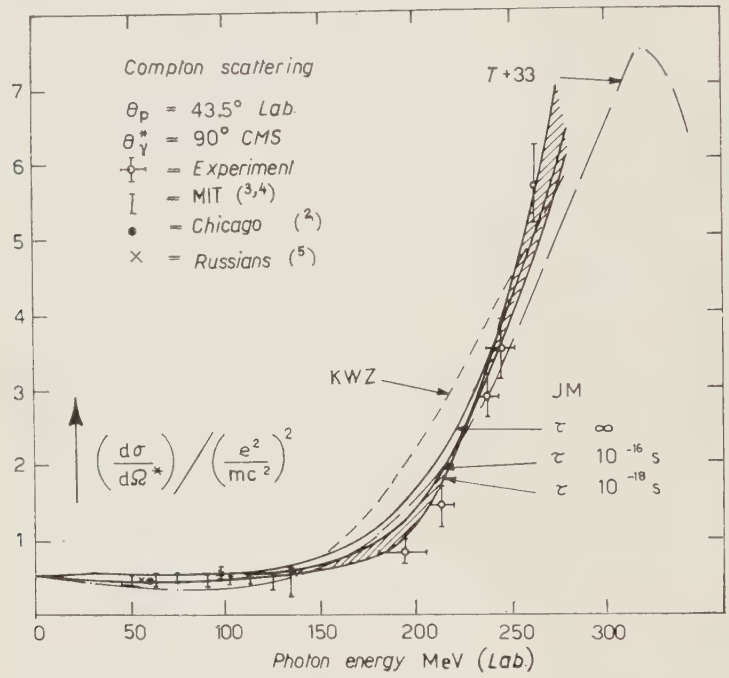

Fig. 15. – Comparison of the measured 90° scattering cross-section with those calculated. The $T+33$ represents the values from eq. (3), KWZ that of KARZAS, WATSON and ZACHARIASEN. JM represent the calculations of JACOB and MATHEWS for π^0 lifetimes of 10^{-16} s, 10^{-18} s, and infinity, the dashed area indicating the region defined by $10^{-18} < \tau < 10^{-16}$.

lowed by the return to the ground state of nucleon with emission of the scattered photon $\boldsymbol{k}'$. Hence, the matrix elements are directly derived from the matrix elements of photon-pion production. So one can express a_{33} by the magnetic moments of the nucleon ([10]) and by the δ_{33} phase-shift as follows:

$$(2) \quad a_{33} = \frac{2}{3}\left(\frac{\mu_n - \mu_p}{2}\right)^2 \frac{k^2}{\eta^3 f} \mu \sin\delta_{33} \exp[i\delta_{33}] \{2(\boldsymbol{n}'\times\boldsymbol{\epsilon}')\cdot(\boldsymbol{n}\times\boldsymbol{\epsilon}) - i\sigma\cdot(\boldsymbol{n}'\times\boldsymbol{\epsilon}')\times(\boldsymbol{n}\times\boldsymbol{\epsilon})\}.$$

Near the meson threshold the pion momentum η can be eliminated by the effective range approximation

$$\sin\delta_{33} \simeq \frac{4}{3}\frac{f^2}{k}\frac{\eta^3}{(1 - k/\omega_r)},$$

where ω_r is the resonant energy.

Both the non-spin flipping and the spin flipping parts of this magnetic dipole transition are taken into account in eq. (2). The electric quadrupole part is very small ([11]) and neglected. The addition of a_T with a_{33} ends in a

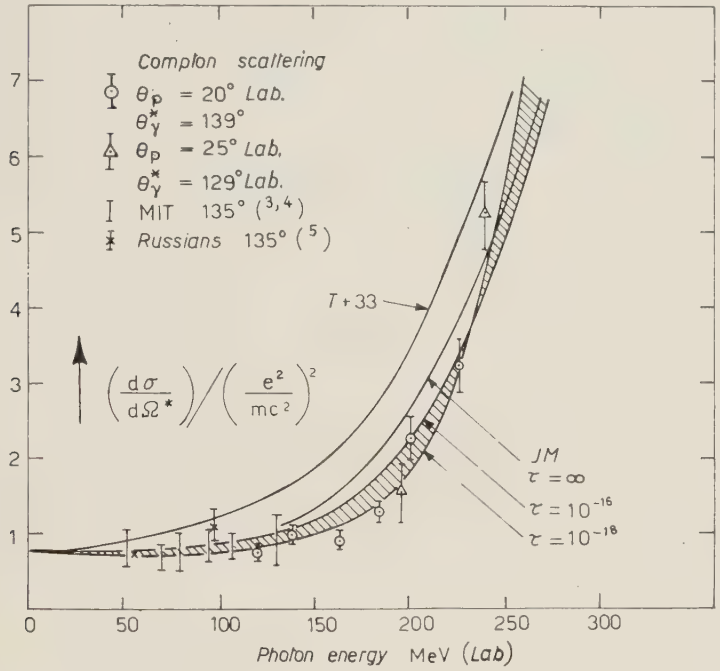

Fig. 16. – Comparison of measured and calculated cross-sections for photons scattered by about 135°. $T+33$ represents the values from eq. (3). While the lower curves are those of JACOB and MATHEWS for π^0 lifetimes of 10^{-16} s, 10^{-18} s, and infinity. The dashed area indicates the region defined by $10^{-18} < \tau < 10^{-16}$.

rather simple expression for the differential cross-section. This is the following

$$\frac{d\sigma}{d\Omega} = \left(\frac{e^2}{M}\right)^2 \left[\frac{1+\cos^2\vartheta}{2} - 2a\cos\vartheta\cos\delta_{33} + a^2\frac{7+3\cos^2\vartheta}{8}\right], \tag{3}$$

where ϑ is the scattering angle (c.m. = lab. in this approximation) and a is the part of a_{33} which is independent of angle.

FELD ([25]), making use of the one-level resonance formula on purely phenomenological grounds, obtained the same eq. (3). A plot of eq. (3) is presented in Figs. 15 and 16 as $T+33$.

Equation (3) is, of course, extremely crude. However, as it is seen in these figures, it reproduces qualitatively the experimental features of the total cross-

([25]) B. T. FELD: *Ann. Phys.*, **4**, 189 (1958).

section and also those of the angular distributions. They are characterized by the interference term proportional to $\cos \delta_{33}$, which is negative at energies below resonance. This model mainly fails at energies around photo-pion threshold.

Other much more complicated models have been elaborated by several authors, either with the fixed nucleon approximation of CHEW and LOW ([24-26]), or phenomenologically as an extension of the Feld atom-like model ([3,4,27]) Probably the most elaborated of them is that due to KARZAS *et al.* ([26]) which, aiming to settle the threshold difficulty, takes particularly into account the contribution due to the several electric dipole transitions.

Apart from the Thomson amplitude, these transitions consist of the diagram

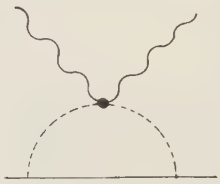

coming from the coupling $A^2\Phi^2$ of the Klein-Gordon equation and by all others, as for instance

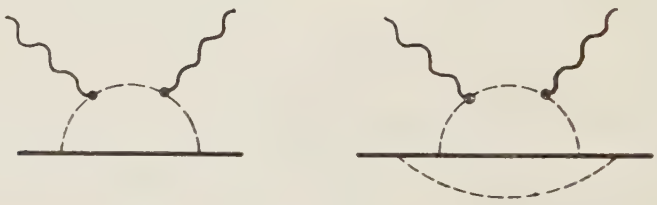

The first diagram can be calculated (in the static model approach) with the method used by FUBINI ([28]) to evaluate the nucleon form factors. The second, etc., diagrams can also be calculated by noticing that in the static limit a pion and a nucleon interact only in a P-state. To conserve parity an $E_1 \rightarrow E_1$ Rayleigh amplitude is reducible to an integral over the P scattering states. They correspond in the above sketched diagrams to the pion-nucleon states which absorb and emit the photon via the pion-current alone.

It is quite significant that the addition of the now-mentioned contributions to amplitudes a_T and a_{33} makes the agreement with the experiment better at

([26]) W. J. KARZAS, W. K. R. WATSON and F. ZACHARIASEN: *Phys. Rev.*, **110**, 253 (1958).

([27]) L. G. HYMAN: *MIT, Ph. D. Thesis* (1959).

([28]) S. FUBINI: *Nuovo Cimento*, **3**, 1425 (1956).

energies $\omega \leqslant \mu$, but definitively poorer than that obtained with the crude formula (3), at energies $\mu \leqslant \omega \leqslant 2\mu$. This is shown in Fig. 15 as a broken line. Between photo-pion threshold and $\omega = 2\mu$, the theoretical curve stands too high (about a factor of two or more) with respect to the experimental points. This fact is understood when one looks at the behaviour of the added terms and their interference effects.

As was already mentioned in the Introduction, only recently a quite plausible explanation of this difficulty has been found and the discrepancy removed. Simultaneously, another and better lower limit to the π^0 mean life has been found. Actually, it has been shown by JACOB and MATHEWS ([12]) and by HYMAN *et al.* ([4]) that the agreement with the experimental data becomes excellent when, to the several amplitudes previously mentioned, one adds that due to the diagram originated by the finite mean life of the π^0 as shown in Fig. 17.

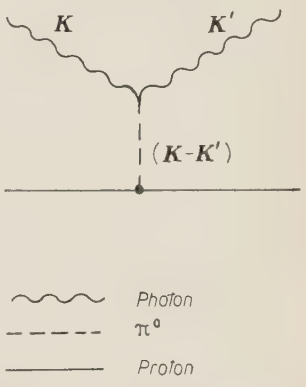

Fig. 17. – Low's diagram.

The possibility that this diagram could contribute appreciably to the Compton scattering was first suggested by Low ([11]). The amplitude corresponding to Low's diagram is:

$$a_L \propto \frac{i\boldsymbol{\sigma}\cdot(\boldsymbol{k}-\boldsymbol{k}')}{\{(\boldsymbol{k}-\boldsymbol{k}')^2+\mu^2\}}\,(\boldsymbol{\epsilon}\times\boldsymbol{\epsilon}')\cdot(\boldsymbol{k}-\boldsymbol{k}')\,\frac{ef}{\sqrt{\tau}}\,, \tag{4}$$

where τ is the lifetime of π^0.

In the model elaborated by HYMAN *et al.* ([4]), the amplitude corresponding to Low's diagram was included, in addition to a_T, a_{33}. Also the tail of the amplitude a_{13} ($T=\frac{1}{2}$, $J=\frac{3}{2}$), due to the second resonant state, was added to improve at $\vartheta = 90°$ the fit to the experimental points. As is known ([29]) the pion-nucleon state corresponding to a_{13} is a $D_{\frac{3}{2}}$, and the corresponding photo-pion transition is $E_1 D_{\frac{3}{2}}$. In analogy with a_{33}, the corresponding Compton scattering is an electric dipole-electric dipole scattering which interferes with a_T.

The Hyman *et al.* model gives very satisfactory agreement with experimental results for $d\sigma/d\Omega$ at 90°, but fails to give the right angular distribution. This might not be surprising. As the formally analogous direct photoelectric term, the amplitude (4) contributes mainly by interference effects. So the good agreement obtained by HYMAN and others at 90° seems to be somewhat fortuitous and due mainly to the fact that of all electric dipole terms

([29]) P. C. STEIN: *Bull. Am. Phys. Soc.*, **4**, 24 (1959).

only a_T and a_{13} were retained. KARZAS *et al.* do somewhat the opposite. They neglect a_L and a_{13} and keep the electric dipole terms, due to the internal currents of the nucleon. The complete picture is that between the terms arising by the interferences of these dipole amplitudes and that due to the interference of a_T and a_{13}, there is, at $\vartheta = 90°$, a partial cancellation. The agreement starts to be poor at other angles, where the interference effects of the Low's term become more complicated.

The conclusion is then reached that it might be practically impossible to disentangle by models all the different processes involved in the scattering of a photon by a proton. Actually, in treating this phenomenon, the use of the dispersion relations (as originally emphasized by GELL-MANN *et al.* [1]) seems much more powerful than one would have expected, even apart from the well-known general arguments in their favour.

The main reason is the following. There are three significant processes which occur when a high-energy photon strikes a proton: i) the electron pair production (*); ii) all photo-meson processes; iii) the elastic scattering. The first is associated with a diffraction scattering (Delbruck scattering), which is negligible but for extreme forward scattering. The third is about two orders of magnitude smaller than the second one. Thus, only the second contributes appreciably to the imaginary part of the amplitudes, so that it is a reasonable approximation to neglect all absorptive effects except those due to photomesons. This is equivalent to neglecting in the cross-section all terms of order e^4 and higher.

This fact allows us to write down directly the real part of the scattering amplitude as integrals over the imaginary part. The situation is, for instance, quite different for pion scattering, where the dispersion relations become integral equations for the scattering amplitude.

In a quite recent paper [12], JACOB and MATHEWS applied the dispersion relations quite successfully to the Compton effect. An attempt in this direction was also made by CAPPS [30], whose approach was slightly different from that of JACOB and MATHEWS. CAPPS used the two forward dispersion relations and then he extended them to other angles by considering the multipole amplitudes expected to dominate the scattering. With respect to the more recent paper of JACOB and MATHEWS, the main difference lies in the fact that Low's diagram is not included. However, JACOB and MATHEWS write the real part of the amplitude in a way which is more independent of any par-

(*) It was pointed out to us by Dr. GOLD'ANSKIJ that an electron pair can simulate a Compton scattering when one electron suffers a subsequent wide angle scattering in a target proton. A calculation shows that this effect is less than 10^{-3} with respect to the measured cross-sections.

(30) R. H. CAPPS: *Phys. Rev.*, **106**, 1631 (1957); **108**, 1032 (1957).

ticular multipole analysis, which is also an advantage. Precisely, the Compton scattering matrix is formally written by them, assembling all possible invariant combinations of the four vectors $\boldsymbol{\epsilon}$, $\boldsymbol{k}$; $\boldsymbol{\epsilon}'$, $\boldsymbol{k}'$ and of the pseudovector $\boldsymbol{\sigma}$ up to terms in e^2. It can be shown ([31]) that, apart from the matrix element given in eq. (4), this is equivalent to introducing E_1 and M_1 for $J=\frac{1}{2}$, and E_1, M_2, E_1-M_2, E_2, M_1, and E_2-M_1 for the scattering in $J=\frac{3}{2}$.

As already mentioned, the imaginary part is practically only due, to the photo-meson production. JACOB and MATHEWS assumed that up to $\omega \leqslant 500$ MeV, only $E_1(\frac{1}{2})$ and $M_1(\frac{3}{2})$ contribute appreciably. Beyond $\omega \simeq 500$ MeV they considered that the only contributing amplitudes are due to (charged and neutral) $E_1(\frac{3}{2})$. They have also shown that the influence of $E_1(\frac{3}{2})$ in the region of interest for this experiment is negligible.

In a recent paper of LAPIDUS and CHOU ([32]), the influence of $E_1(\frac{1}{2})$ imaginary part near the photo-meson production threshold is thoroughly discussed. The peculiar energy dependence of this gauge-invariance term has been expressed by

$$|E_1|^2 \simeq |E_1^+|^2 = 0.54 \frac{e^2}{M} \frac{\sqrt{\omega^2-1}}{\omega} .$$

Its contribution in the dispersion integral leads to a cusp in the real amplitude corresponding to E_1 at the photo-meson threshold. This cusp is practically imperceptible in the over-all cross-section. But it also brings down the cross-section near the threshold appreciably, as already found by KARZAS *et al.* Beside the Low diagram, which is essential but was neglected by LAPIDUS and CHOU, this effect due to E_1 is necessary to improve the agreement with the experiment.

In the JACOB and MATHEWS paper, the matrix element (4), which can be written as

$$M = \frac{i\boldsymbol{\sigma}\boldsymbol{A}(k_1 \cos\vartheta)}{\sqrt{\tau(q^2-\mu^2)}} = \frac{i\boldsymbol{\sigma}\boldsymbol{A}(k_1 \cos\vartheta)}{\sqrt{\tau}\{\cos\vartheta - (1+\mu^2/2k^2)\}} , \tag{4'}$$

is simply added to the spin-flipping part of the scattering amplitude. The procedure is equivalent to introducing in the real part some values of J which are neglected in the imaginary part, *i.e.* in the photo-meson absorption. It is also equivalent to ignoring the form factors, due to the fact that Low's diagram deals with virtual pions (*). They also neglect automatically the contribution of the higher order multipoles of the $A^2\Phi^2$ term. But, as shown by

([31]) J. MATHEWS: *Ph. D. Thesis* (California Institute of Technology, (1957).

([32]) L. I. LAPIDUS and CHOU KUANG-CHAO: *Žurn. Éksp. Theor. Fiz.*, **37**, 1714 (1959); **38**, 201 (1960).

(*) Concerning this relevant point, see a discussion in the JACOB and MATHEWS ([12]).

KARZAS *et al.*, higher order poles are not relevant in the region and at the angle so far investigated.

This is correct at least as long as the influence of a π-π interaction is neglected. The validity of this assumption depends, of course, from the position of the pole due to the possible π-π isobar. However, if this is $y_b \simeq 1+2\mu^2/k^2$, according to the Chew's criterion [33], most of the Illinois values at energies $\omega \simeq \mu$ are in the « useful region »

$$\cos\vartheta - y_0 < y_0 - y_b ,$$

where $y_0 = 1 + \mu^2/2k^2$ and $y_b = 1 + 2\mu^2/k^2$ is the nearest dangerous pole. Hence, for $0 \leqslant \omega \lesssim 2\mu$ all these approximations seem to be well justified.

The comparison with the first part of this discussion, where we went from one model to another, increasing complications and completeness, shows that very likely, in the formal and general approach followed by JACOB and MATHEWS, all more relevant virtual states previously discussed are included in this energy interval. In the energy region explored by this experiment a good quantitative agreement with the experimental results depends mainly on the introduction of Low's diagram. Its influence is much larger than one would expect glancing at the order of magnitude of

$$M^2 \simeq -\frac{g^2 m_\pi^3 \hbar}{4c^2}\left(\frac{\hbar}{M_p c}\right)^2 \frac{1}{\tau(q^2 - m_\pi^2)^2} ,$$

mainly via interference effects (*). This is clear if one makes a mulitpole analysis of the amplitude written by JACOB and MATHEWS. The spin flipping term M will interfere with terms such as those due to $M_1(\frac{3}{2}) \to M_1(\frac{3}{2})$ or $E_1(\frac{1}{2}) \to E_1(\frac{1}{2})$, etc., transitions, which are preponderant in the region of interest.

The agreement with the available experimental data is shown in Figs. 15, 16 and 18, where the M.I.T. Russian and our results are compared with the curves calculated by JACOB and MATHEWS. Without reproducing the other significant curves already given by JACOB and MATHEWS, we may say that the use of all available data on Compton scattering by protons allows one to locate with great confidence the limits of the π^0 mean life as follows

$$10^{-18} < \tau \lesssim 10^{-16} \ (**) .$$

(*) This point seems to be lost in the paper by S. C. FRAUTSCHI: *Progr. Theor. Phys.*, **22**, 544 (1959).

[33] G. F. CHEW: *Phys. Rev.*, **112**, 1380 (1958).

(**) These limits are still not very sharp. However, they are immune from the complications arising in the method suggested by PRIMAKOFF, which means that they are immune from « coherent » production of π^0 by nuclear matter.

Regarding this point, see OSBORNE *et al.*, MORPURGO (private communication), FERNELL and FLASER (private communication).

The lower limit is better established than the higher. Actually the influence of the Low diagram is more critical towards the shorter values of τ. However, as is shown in Fig. 18, the upper limit can also be considered with confidence. Fig. 18 will point out a value of τ very near to 10^{-17}. This should not be over-

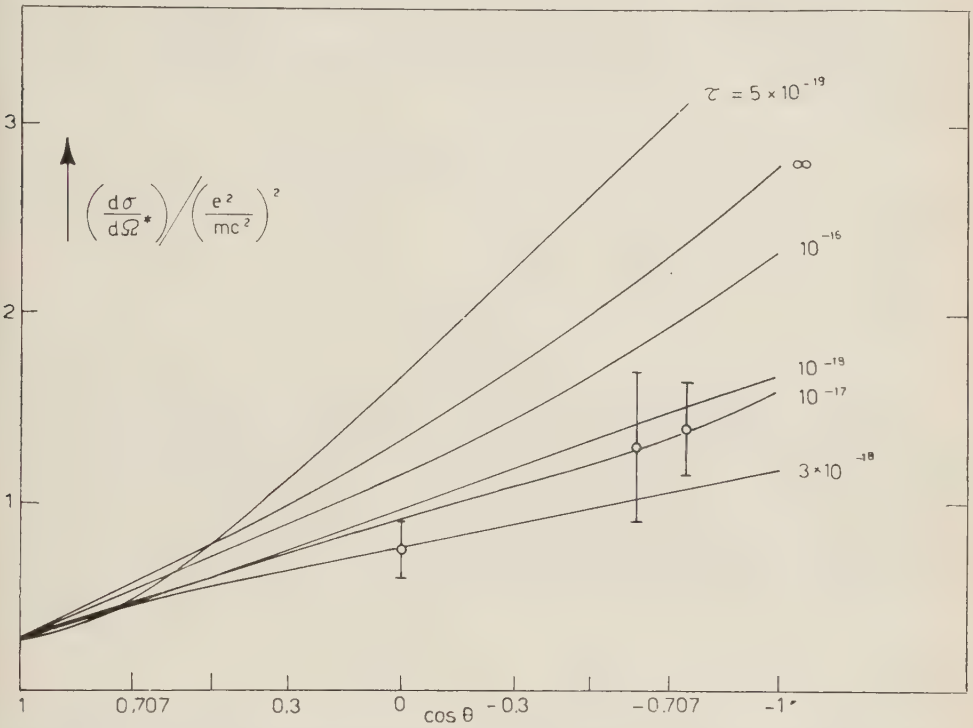

Fig. 18. - Experimental angular distribution at 190 MeV compared with calculations by Jacob and Mathews with various values of π^0 lifetime.

stated. Apart from the uncertainties implied in the approximation of Jacob and Mathews (previously discussed), other purely experimental uncertainties (for instance, in the calibration of betatron energy) can well displace the experimental points in the region between the $\tau = 10^{-16}$ and $\tau = 10^{-18}$ curves. Simultaneously, we may say that now the Compton scattering by protons goes among the several phenomena which are consistently picturing the properties of the physical nucleon at energies below the double pion production.

* * *

The authors are indebted to many individuals who have assisted with some parts of this work. In particular, we are indebted to Dorothy Carlson-Lee for her help with the liquid hydrogen target, to Paul Goldan for his work

with the Čerenkov counter, and to MEGUMU YOSHIMINE for work with the electronic digital computer. In addition, we would like to thank the operating staff of the betatron and others who assisted in some phase of the work, CHI HAN SAH, THOMAS BAKER, CHARLES HEBEL, STANLEY ENGELBERG, CHARLES REINHARDT and EDWARD GRAY.

The authors are also indebted to Professors G. F. CHEW and F. E. LOW for helpful discussions, and to Professor YOSHIO YAMAGUCHI for help with the interpretation of the theory.

RIASSUNTO

La diffusione elastica dei fotoni da protoni è stata misurata con fotoni tra 100 e 290 MeV agli angoli di 90° e 139° c.m. È stato osservato l'aumento previsto della sezione d'urto alle energie prossime a quella della risonanza $(\frac{3}{2}, \frac{3}{2})$ del sistema pione-nucleone. La diffusione si può spiegare qualitativamente con la combinazione dell'ampiezza Thomson con quella della risonanza $(\frac{3}{2}, \frac{3}{2})$. Uno studio più dettagliato nella regione immediatamente al di sopra della soglia di fotoproduzione ha mostrato che la sezione d'urto è sensibile all'accoppiamento del mesone π^0 con i fotoni. Dai dati sperimentali si può concludere che la vita media del π^0 deve essere compresa fra 10^{-16} e 10^{-18} s.

IL NUOVO CIMENTO Vol. XVIII, N. 6 16 Dicembre 1960

Pion-Pion Interaction from π Production in $\pi.N$ Collision.

F. Bonsignori, V. Bortolani and A. Stanghellini

Istituto di Fisica dell'Università - Bologna
Istituto Nazionale di Fisica Nucleare - Sezione di Bologna

(ricevuto il 3 Ottobre 1960)

Summary. — The Chew and Low model for the determination of the $\pi\pi$ cross section is used for the analysis of an experiment of pion production by pions. The one-pion-exchange model and the possible $\pi\pi$ resonances are discussed.

1. – Introduction.

Recently many theoreticians (1) have realized that the $\pi\pi$ interaction is fundamental for the construction of a theory of strong interacting particles.

Several attempts were made to find some evidence for this interaction and if possible, its charge and energy behaviour, studying different processes such as nucleon charge structure, τ-decay spectra, pion-nucleon scattering (2), etc.

It was thought that the most suitable process for the study of $\pi\pi$ interaction is the π production in pion-nucleon collision. Chew and Low (3) have suggested an unambigous method to determine the pion-pion scattering cross-section from an extrapolation of the $\pi.N \to \pi\pi.N$ final nucleon laboratory kinetic energy distribution.

(1) G. F. Chew: *Kiev Conference; Ann. Rev. of Nucl. Sci.*, **9**, 29 (1959); G. F. Chew and S. Mandelstam: *Theory of the low-energy pion-pion interaction*, UCRL 8728 (April 1959).

(2) W. R. Frazer and J. R. Fulco: *Phys. Rev. Lett.*, **2**, 365 (1959); J. Bowcock, W. N. Cottingham and D. Lurié: *Nuovo Cimento*, **16**, 918 (1960).

(3) G. F. Chew and F. E. Low: *Phys. Rev.*, **113**, 1640 (1959).

In this work we shall apply the method to the experiment made in Bologna by ALLES BORELLI *et al.* (*) at 960 MeV incident pion kinetic energy.

It will clearly result that the method is very delicate in the actual application and that the present statistics are by no means sufficient to give any positive reply.

2. – The Chew and Low extrapolation.

Let us review the Chew and Low method. They consider the contribution to the π production in which the incoming π takes out one pion from the nucleon cloud.

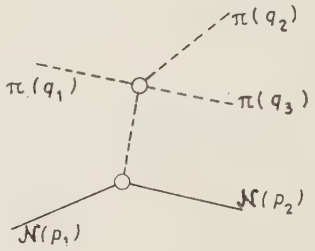

In the physical region for the π production the intermediate π is outside the mass shell with mass

$$\Delta^2 = (p_2 - p_1)^2 ,$$

If one takes the limit for $\Delta^2 \to -\mu^2$ the pion becomes real and one has the proper $\pi\pi$ cross-section for a definite energy in the $\pi\pi$ center of mass $w^2 = (q_2 + q_3)^2$, namely

$$\lim_{\Delta^2 \to -\mu^2} \frac{\partial^2 \sigma}{\partial \Delta^2 \, \partial w^2} \to \frac{f^2}{2\pi q_{1L}^2 \mu^2} \frac{\Delta^2}{(\Delta^2 + \mu^2)^2} w \sqrt{\frac{w^2}{4} - \mu^2} \, \sigma_{\pi\pi}(w) , \tag{1}$$

for $\pi^- + p \to \pi^- + \pi^0 + p$ and twice for $\pi^- + p \to \pi^- + \pi^+ + n$. The very crucial point in the method is that at $\Delta^2 = -\mu^2$ this term is the only singular one and so it dominates the nearest regions of Δ^2. By dividing the available region in various strips of w and using the relation $\Delta^2 = 2MT_L$, (T_L recoiling nuc-

(*) We thank V. ALLES BORELLI and P. WALOSCHEK for having allowed us to use their experimental results and for useful discussion.

leon laboratory kinetic energy) we obtain

$$\lim_{T_L \to -10\ \mathrm{MeV}} \frac{\mathrm{d}\sigma}{\mathrm{d}T_L} = A \frac{T_L}{(T_L - 10)^2}, \tag{2}$$

where

$$A = \frac{f^2}{2\pi q_{1L}^2 \mu^2} \int_{w_1}^{w_2} w \sqrt{\frac{w^2}{4} - \mu^2}\, \sigma_{\pi\pi}(w)\, \mathrm{d}w^2 .$$

In general A depends in a rather involved manner on T_L, due to the fact that the limits of the phase space are functions of T_L, but one can choose square limits and so all complications disappear.

We consider the actual expression for the production differential cross-section when the π term is present,

$$\frac{\mathrm{d}\sigma}{\mathrm{d}T_L} = \frac{AT_L}{(T_L + 10)^2} + \frac{B(T_L)}{T_L + 10} + C(T_L) ,$$

where $C(T_L)$ are all the contributions not singular at $T_L = -10$ MeV, namely those coming from the core production or from a modification of the one-pion effects. $B(T_L)$ is an interference term which has obviously a first order pole at $T_L = -10$ MeV.

One multiplicates $\mathrm{d}\sigma/\mathrm{d}T_L$ by $(T_L+10)^2$ and obtains

$$f(T_L) = (T_L + 10)^2 \frac{\mathrm{d}\sigma}{\mathrm{d}T_L} = AT_L + B(T_L)(T_L + 10) + C(T_L)(T_L + 10)^2 , \tag{3}$$

and fits $f(T_L)$ in the physical region by a polynomial. Taking the limit for $T_L \to -10$ MeV one obtains

$$\lim_{T_L \to -10\mathrm{MeV}} f(T_L) = -10A , \tag{4}$$

the other terms disappearing because they have a factor (T_L+10) at least.

In this manner one obtains a mean value of the $\pi\pi$ scattering cross-section in the w region considered. If this region is sufficiently small one can take the $\sigma_{\pi\pi}(w)$ out of the integral and obtains

$$A = \frac{f^2}{2\pi q_{1L}^2 \mu^2} \bar{\sigma}_{\pi\pi} \int_{w_1}^{w_2} w \sqrt{\frac{w^2}{4} - \mu^2}\, \mathrm{d}w^2 . \tag{5}$$

The main point for the success of the method is the determination of the polynomial to use as extrapolating function.

A priori no limit is imposed on the order of the polynomial but a statistical analysis of the experimental errors has to fix it [4].

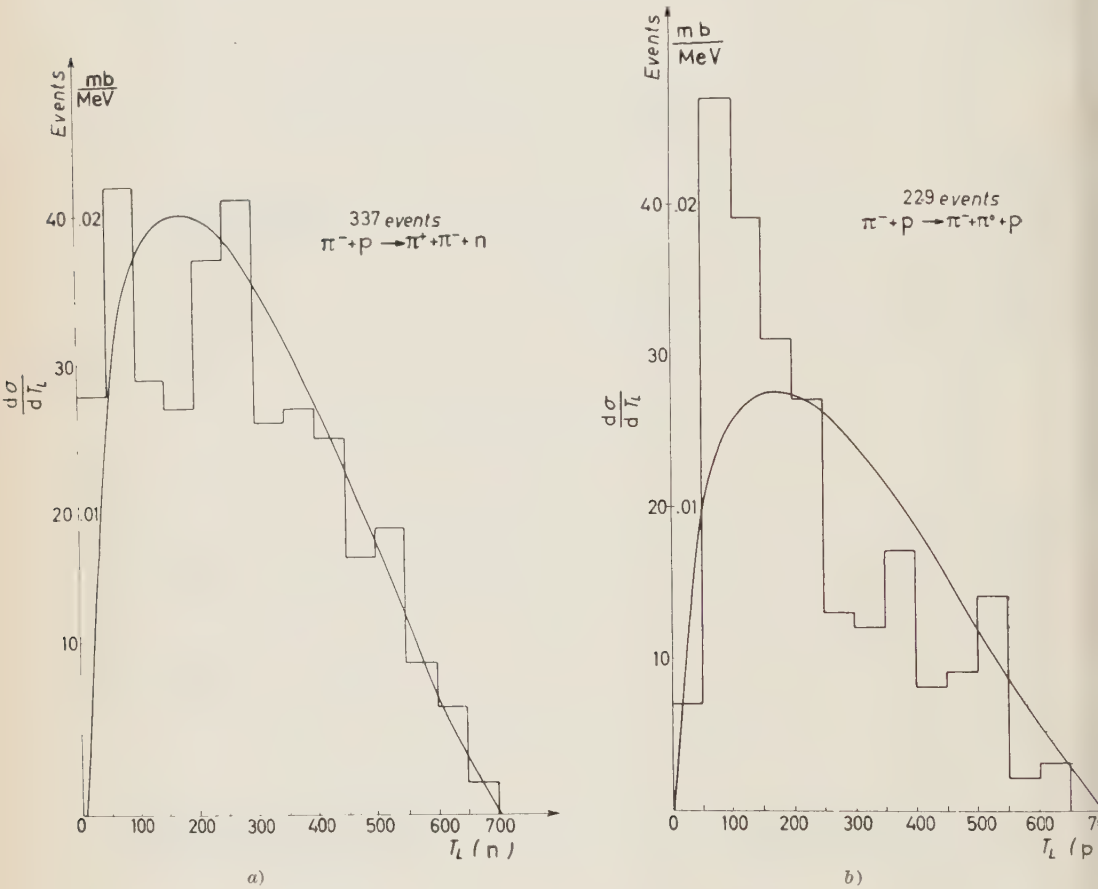

Fig. 1. - 1*a*, *b*. – Recoiling nucleon lab. kinetic energy distribution compared with a statistical spectrum.

Let us return to the experiment. We have plotted in Fig. 1*a* and 1*b* the differential cross-section against T_L for the two reactions.

We have devided the permitted region for w which runs from 2 to 5.6 μ in 4 equal intervals form 2 to 2.9; 2.9 to 3.8; 3.8 to 4.7; 4.7 to 5.6 and plotted in Fig. 2 (*a* and *b*), Fig. 3 (*a* and *b*) the corresponding distributions.

(4) P. Cziffra and M. J. Moravcsik: University of California Radiation Laboratory Report UCRL 8523 (1958, unpublished).

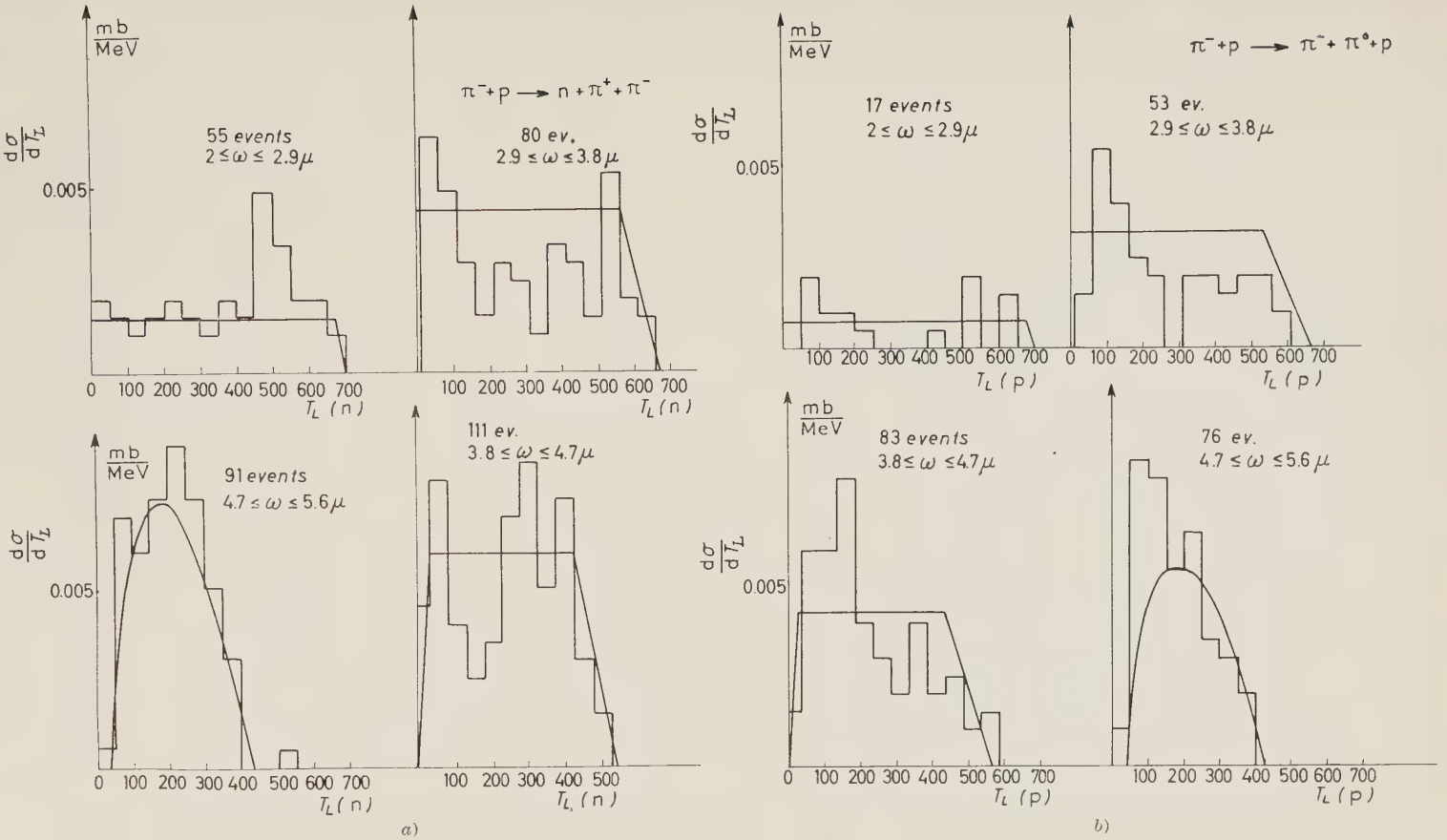

Fig. 2*a*, *b*. – Recoiling nucleon laboratory kinetic energy distribution for several intervals of w (two-pion total energy in their c.m.) compared with statistical spectra.

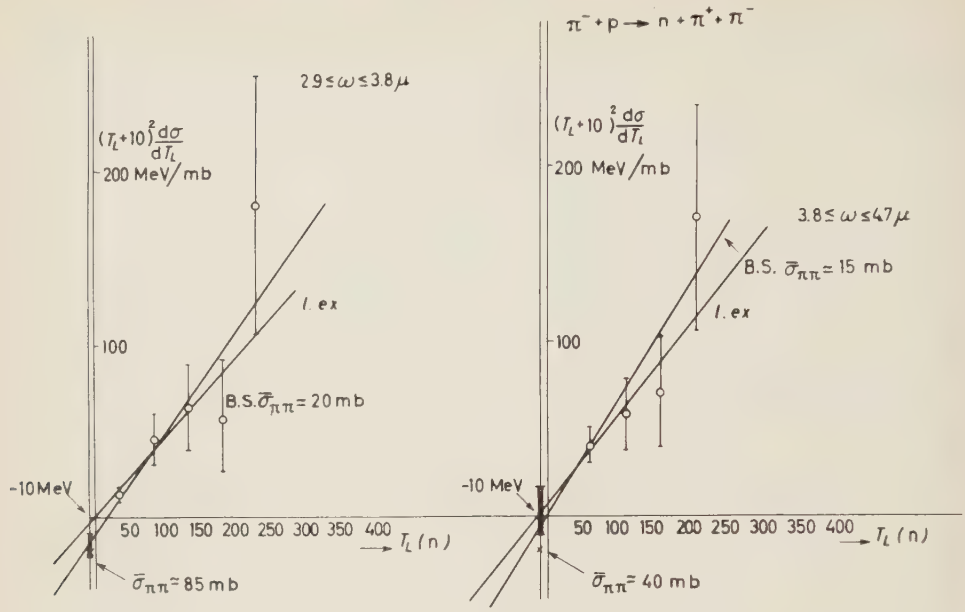

Fig. 3*a*, *b*. – Linear extrapolation to $T_1 = -10$ MeV and B.S. model for $\pi^- + p \rightarrow n + \pi^+ + \pi^-$ reaction.

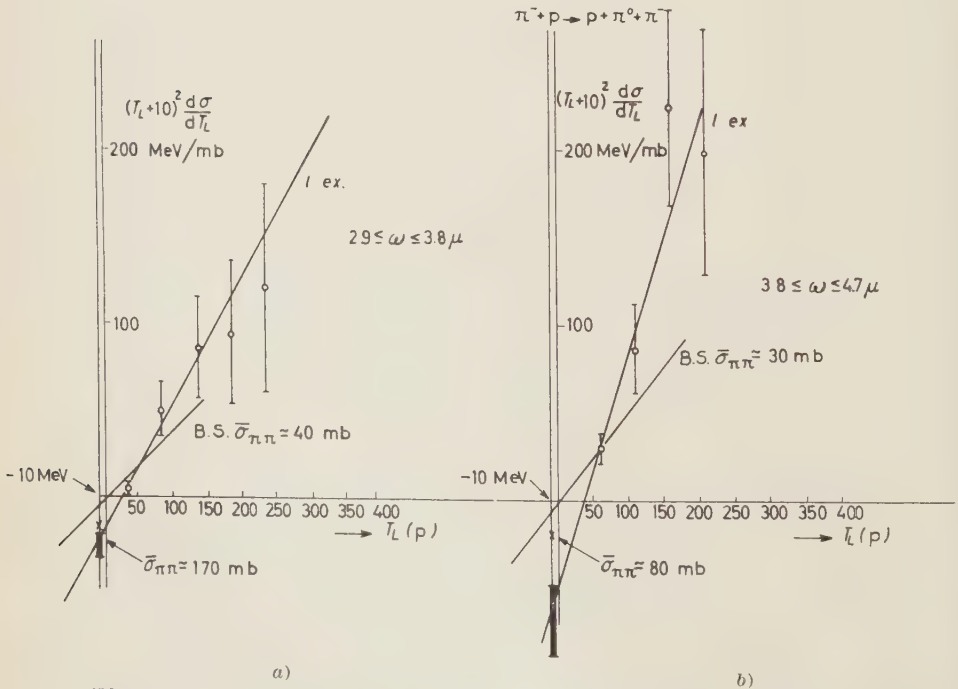

Fig. 4*a*, *b*. – Linear extrapolation to $T_1 = -10$ MeV and B.S. model for $\pi^- + p \rightarrow p + \pi^0 + \pi^-$ reaction.

For comparison we drew the statistical theory distribution in each histogram.

The two intermediate intervals from 2.9 to 3.8 μ and from 3.8 to 4.7 μ were used to perform the extrapolations (Fig. 4).

The first interval is too poor of events to be used.

The last one has a complicated phase-space and is far from small T_L so that the π term cannot dominate.

We have performed the linear extrapolation and the results are reported in each figure. The parabolic one was tried unsuccesfully, the error in the coefficients being comparable with the coefficients itselves.

This means that the present situation is so meagre, that nothing can be done better than a linear extrapolation.

We wish to note that the linear extrapolation tends to give negative cross-section in the physical region for very small T_L. This must be interpreted in the sense that a more complicated extrapolation is necessary.

If one has to give any confidence to the results, one has a general positive reply.

The $\pi\pi$ cross-sections turn out to be in general very large with a big error.

We wish to make several remarks on the difficulty in the practical application of the method.

1) The experimental points have a poor energy resolution (of the order of 20 MeV or more for T_L).

2) We cannot collect events in smaller intervals because there are too few.

3) The experimental points have a natural lower limit in T_L (as a function of w) and the most interesting region near $T_L = -10$ is forbidden.

4) If pion-pion interaction does not exist the extrapolating curves have to pass through zero at $T_L = -10$ MeV.

5) A quite sizable $\pi\pi$ cross-section of the order of 20 mb is very near to this point. This means that a discrimination between these two cases, impossible at present, will certainly be very difficult in the future.

If one has to plan an experiment for the determination of the $\pi\pi$ cross-section, one should think of collecting at least $(10 \div 100)$ times as many events as those analysed in the present experiment.

It would be better to go to higher energies to amplify the phase space at low T_L.

On the other hand the residue A (which is proportional to $\sigma_{\pi\pi}$) contains in the denominator the square of the incident pion momenta and so it rapidly becomes small as the energy increases.

3. – The one pion exchange model (O.P.E.M.).

We now wish to discuss a model proposed by BONSIGNORI and SELLERI [5]. They suggest that the evident deviation from the statistical spectra, or from the isobaric model spectra which is similar to the former (*), is imputable to the pion-pion interaction.

The factor $T/(T+10)^2$ is responsible for the shifting of the statistical maximum to low values of T_L.

This fact becomes more evident if one considers the partial distribution for the various intervals of w.

The statistical distribution is practically constant and the $\pi\pi$ term has $\sim 1\ T_L$ behaviour, the maximum at $T_L = 10$ MeV of the function $T/(T+10)^2$ being out of the permitted region or mediate in the large interval of T_L.

This fact was accepted by B. and S. as an evidence for $\pi\pi$ interaction. They suppose that the lower region of T_L (less than 85 MeV) was dominated by the one pion term and they find a $\sigma_{\pi\pi}$ of the order of $(20 \div 40)$ mb.

We wish to show what this hypothesis means in term of the C. and L. method.

If the lower region of T is dominated by the one-pion term the function $f(T_L) = (T+10)^2\,\mathrm{d}\sigma/\mathrm{d}T_L$ becomes AT_L simply.

So one is forced to make a linear extrapolation which passes through $T_L = 0$, and the constant A is determined by the first points (under 85 MeV). These lines are drawn in Fig. 3 and 4.

The values of the $\sigma_{\pi\pi}$ obtained in this manner are very similar to those of B and S. It might be that a « future » extrapolation will be very near to the B. and S. line at low T_L and hence confirm their hypothesis.

We wish to show what is the contribution of a resonant $J=1$, $T=1$ cross-section on the w distribution,

$$\frac{\mathrm{d}\sigma}{\mathrm{d}w} = \frac{f^2}{\pi q_{1L}^2 \mu^2} \sqrt{\frac{w^2}{4} - 1}\; w^2\, \sigma_{\pi\pi}(w) \int_{T_1(w)}^{T_2(w)} \frac{T_L\,\mathrm{d}T_L}{(T_L+10)^2}\,. \tag{6}$$

The pion pion cross-section is given by

$$\sigma_{\pi^0\pi^-} = \sigma_{\pi^+\pi^-} = \frac{60\pi}{(w^2/4) - 1} \sin^2 \delta_{11} \quad \text{mb}\,.$$

We shall consider the maximum value

$$\sigma_{\max} = \frac{60\pi}{(w^2/4) - 1} \quad \text{mb}\,. \tag{7}$$

(5) F. BONSIGNORI and F. SELLERI: *Nuovo Cimento*, **15**, 465 (1956).

(*) Practically any theory not strongly dependent on T_L has the same T_L distribution.

In Fig. 5 (*a* and *b*) this maximum value contribution is plotted with the experimental $d\sigma/dw$ against w.

As one sees, this term gives a large contribution.

One cannot trust the above calculation for several reasons:

1) The one-pion exchange cannot dominate all the T_L permitted region. It is better to consider a limited region of Δ^2. This limit may be chosen considering that the 3 π exchange starts at $\Delta^2 = -(3\,\mu)^2 (T_1 \simeq -100$ MeV).

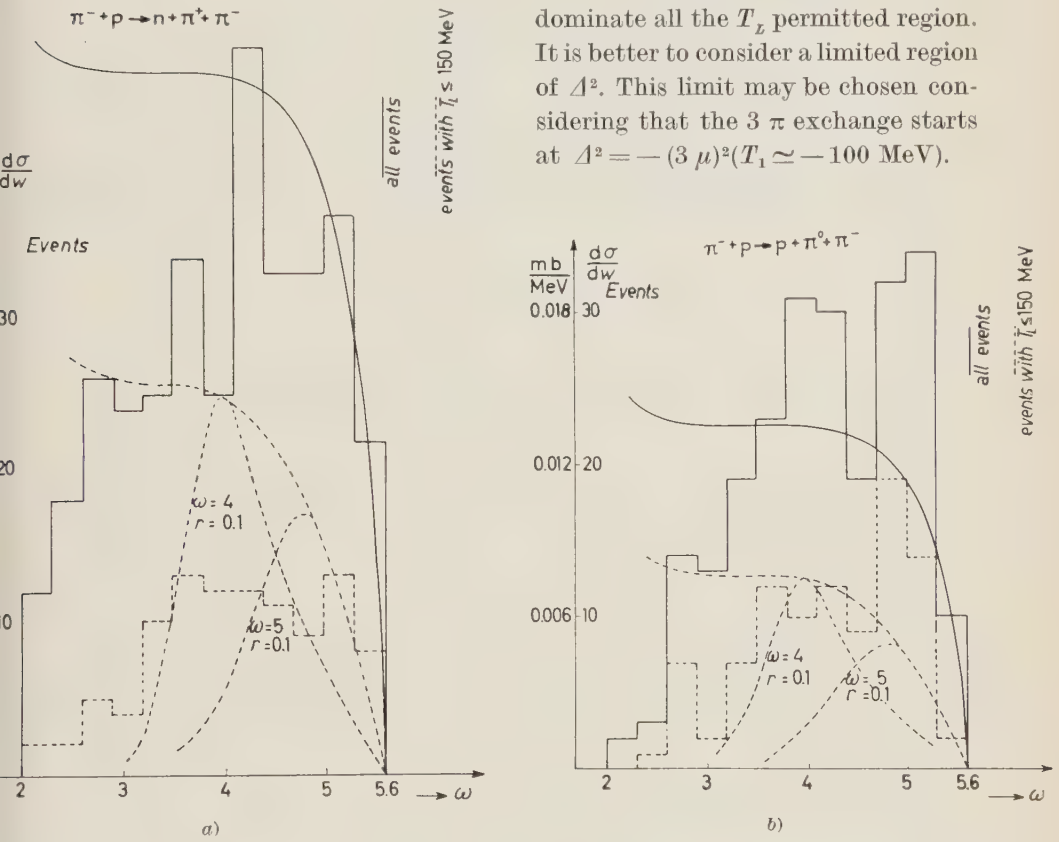

Fig. 5*a*, *b*. – w distributions compared with the resonant ($T=1$, $J=1$) one-pion-exchange contribution.

2) We calculate the one pion exchange term out of the pole at $T_1 = -10$ MeV. Probably some natural cut-off modifies the value we obtain. So the value we obtain is to be considered a maximum value also in this sense.

3) The OPEM is coherent with other contributions and interference effect might spoil partly its behaviour.

Having those points in mind we have performed the w distribution for $T_L \leq 150$ MeV (Fig. 5*a* and 5*b*). We have calculated besides the maximum

contribution, two resonance behaviours for the OPEM at $w = 4\,\mu$ and $w = 5\,\mu$ with a $\Gamma \simeq 0.1\,\mu$.

As one sees, we can exclude resonances in the low w region ($w < 3\,\mu$). Moreover we notice:

a) A rapid increase of the distribution up to $w \sim 4\,\mu$.

b) A pronounced peack in the $\pi^- + \mathrm{p} \to \pi^0 + \pi^- + \mathrm{p}$ around $w \sim 5\,\mu$.

These two behaviours are not in agreement with a statistical spectrum.

It is very difficult to think to a $T = 1$, $J = 1$ resonance. In this case the $\pi^- + \mathrm{p} \to \mathcal{N} + \pi^+ + \pi^-$ reaction has to be favoured by a factor two.

If this resonance is present, it may be spoiled in this reaction by the predominance of the final interaction between the neutron and the negative pion.

* * *

We thank Dr. F. SELLERI for useful discussions.

APPENDIX

We give the maximum contribution to $\mathrm{d}\sigma/\mathrm{d}w$ for different isotopic and angular momentum resonant states.

$$\sigma_\mathrm{n} = \sigma(\pi^- + \mathrm{p} \to \mathrm{n} + \pi^+ + \pi^-)$$

$$\sigma_\mathrm{p} = \sigma(\pi^- + \mathrm{p} \to \mathrm{p} + \pi^0 + \pi^-)$$

	$T=0;\ J=0$	$T=1;\ J=1$	$T=2;\ J=0$	$T=0;\ J=2$	$T=2;\ J=2$
$\frac{\mathrm{d}\sigma_\mathrm{n}\,\max}{\mathrm{d}w}$	$\frac{2}{9}c$	$\frac{6}{4}c$	$\frac{2}{36}c$	$\frac{10}{9}c$	$\frac{10}{36}c$
$\frac{\mathrm{d}\sigma_\mathrm{p}\,\max}{\mathrm{d}w}$	0	$\frac{3}{4}c$	$\frac{1}{4}c$	0	$\frac{5}{4}c$

RIASSUNTO

Il metodo di Chew e Low per la determinazione della sezione d'urto pione-pione viene usato per l'analisi di un esperimento di produzione di pioni da pioni. Si discute il modello in cui si tiene conto dello scambio di un pione e la possibile esistenza di risonanze pione-pione.

IL NUOVO CIMENTO Vol. XVIII, N. 6 16 Dicembre 1960

Energy Gap in the Spectrum of Free Quasi-Particles in Nuclear Matter.

G. Fano and A. Tomasini

Istituto di Fisica dell'Università - Bologna
Istituto Nazionale di Fisica Nucleare - Sezione di Bologna

(ricevuto il 31 Ottobre 1960)

Summary. - A sufficient condition is given for the existence of an energy gap in the spectrum of free quasi-particles in nuclear matter, assuming a finite repulsive potential inside the core.

1. – Introduction.

It has been shown that a difficulty arises in the theory of the Fermion systems (in reality it has been proved only in the case of the dilute Fermi gas [1]), due to the breakdown of the conditions of applicability of the Goldstone expansion.

This difficulty is connected with the possible existence of a superfluid state of the system in the sense that this difficulty is probably due to the bound state discovered by Cooper [2]. However at the present state of our knowledge the two problems should be regarded as separated: the first one is a mathematical problem of elimination of the vanishing denominators in the expansion of Bruckner's t matrix; the second one is the problem of the existence of a superfluid state of the system.

It is very likely that the first problem can be solved [3] if one performs first the Bogoljubov-Valatin canonical transformation, and then a perturbation expansion, taking as the unperturbed Hamiltonian the term describing free

[1] L. Van Hove: *Physica*, **25**, 849 (1959).
[2] L. N. Cooper: *Phys. Rev.*, **104**, 1189 (1956).
[3] See ref. [1] and G. Fano: *Nuovo Cimento*, **15**, 959 (1960).

« quasi particles ». No vanishing denominators can appear in the perturbation theory if the excitation spectrum of the « quasi particles » has an energy gap.

The aim of this paper is to see if there is an energy gap in the spectrum of the quasi particles in the case of nuclear matter, in spite of the existence of the repulsive core.

We notice that the energy of a quasi particle is $E_k \simeq \sqrt{\xi_k^2 + \Delta^2}$, where Δ is the gap and ξ_k is a well defined expression which is practically the Hartree energy.

Let us now consider the second problem: COOPER and co-workers [1] have found a condition for the superfluidity of nuclear matter.

Following their point of view one should solve an equation very similar to the one that we have examined in order to solve the first problem (*), but now ξ_k has the meaning of single particle energy in the nuclear matter (without considering the interaction between pairs of total momentum zero). This single particle energy must be determined assuming a model.

We will consider here only the first problem.

In Section 2 the canonical transformation is performed. We have chosen a superposition of states with the same projection of the isotopic spin for the following reasons.

The « dangerous » denominators appear when we consider two particles of momenta $\boldsymbol{k}$ and $-\boldsymbol{k}$ near the Fermi surface. Actually in heavy nuclei the Fermi momentum is different for protons and neutrons since their density is different. Therefore the « Cooper effect » is impossible between neutrons and protons, and we have considered n-n and p-p correlations only (**).

An integral equation is obtained which is very similar to the equation found by BOGOLJUBOV, TOLMACHEV and SHIRKOV [6] and it is solved by an iteration method.

In Section 3 the calculations are carried out with a potential including a repulsive core and exchanges forces.

The potential V_1 inside the core is taken large but finite; in fact a poten-

[1] L. N. COOPER, R. L. MILLS and A. M. SESSLER: *Phys. Rev.*, **114**, 1377 (1959); R. L. MILLS, A. M. SESSLER, S. A. MOSZKOWSKI and D. G. SHANKLAND: *Phys. Rev. Lett.*, **3**, 381 (1959).

(*) After this work was performed, we read a paper of EMERY and SESSLER [5], which solves the problem of the superfluidity in nuclear matter using indipendently a mathematical method showing some similarity with ours (in the case of an infinite potential inside the core).

[5] V. J. EMERY and A. M. SESSLER: *Phys. Rev.*, **109**, 248 (1960).

(**) In reality one should consider also the Coulomb forces (neglected in our Hamiltonian) which are responsible for the difference of the densities. But the consideration of the Coulomb forces hardly changes the results.

[6] N. N. BOGOLJUBOV, V. V. TOLMACHEV and A. V. SHIRKOV: *A New Method in the Theory of Superconductivity* (New York, 1959).

tial higher than the mass of the nucleon would render the use of a potential theory meaningless.

V_1 has been considered as a parameter, and its maximum value insuring the convergence of the perturbation expansion is established.

In Section **4** the numerical results are given.

2. – Formalism.

Consider the Hamiltonian

$$H = T + V \,, \tag{1}$$

with

$$T = \sum_{k,s,\tau} (\varepsilon_k - \lambda) a^+_{ks\tau} a_{ks\tau} \,, \tag{2}$$

$$V = \frac{1}{4} \sum_{\substack{k_1 k_2 k_3 k_4 \\ s_1 s_2 s_3 s_4 \\ \tau_1 \tau_2 \tau_3 \tau_4}} a^+_{k_1 s_1 \tau_1} a^+_{k_2 s_2 \tau_2} \langle k_1 s_1 \tau_1,\, k_2 s_2 \tau_2 | V | k_3 s_3 \tau_3,\, k_4 s_4 \tau_4 \rangle a_{k_3 s_3 \tau_3} a_{k_4 s_4 \tau_4} \,, \tag{3}$$

where the indices k, s, τ indicate the momenta, the spin and the isotopic spin of the particles. The matrix element appearing in V is related to the two body potential W by

$$\langle k_1 s_1 \tau_1,\, k_2 s_2 \tau_2 | V | k_3 s_3 \tau_3,\, k_4 s_4 \tau_4 \rangle = \langle \varphi_{k_1 s_1 \tau_1, k_2 s_2 \tau_2} | W | \varphi_{k_4 s_4 \tau_4, k_3 s_3 \tau_3} \rangle \,, \tag{4}$$

where the φ's are antisymmetrized two particle states and W is a potential including exchange forces in the following way:

$$W = V(r) \left[\frac{1+\beta}{2} + \frac{1-\beta}{2} P_M \right] , \tag{5}$$

(P_M is the Maiorana exchange operator).

The canonical transformation is ($u_k^2 + v_k^2 = 1$)

$$a_{ks\tau} = u_k \eta_{ks\tau} + v_{ks} \eta^+_{-k,-s,\tau} \,, \tag{6}$$

where $v_{k\uparrow} = v_k$, $v_{k\downarrow} = -v_k$ and the η's are the destruction operators of the quasi particles.

As usual ([6-8]), we determine the canonical transformation minimizing the

([7]) J. G. Valatin: *Nuovo Cimento*, **7**, 843 (1958).

([8]) J. Bardeen, L. Cooper and J. R. Schrieffer: *Phys. Rev.*, **108**, 1175 (1957).

expectation value U of H in the « vacuum » $|\psi_0\rangle$ defined by

$$\eta_{ks\tau}|\psi_0\rangle = 0 \,. \tag{7}$$

As expected, we find the condition

$$2\xi_k u_k v_k - \Delta_k(u_k^2 - v_k^2) = 0 \,, \tag{8}$$

where

$$\xi_k = \varepsilon_k - \lambda + \int \mathrm{d}^3k' \, v_{k'}^2 \left[\frac{3+5\beta}{2} V_0 + \frac{3-5\beta}{2} V_{|\boldsymbol{k}-\boldsymbol{k}'|}\right], \tag{9}$$

$$V_k = \left(\frac{1}{2\pi}\right)^3 \int \mathrm{d}^3r \, \exp\left[i\,\boldsymbol{k}\cdot\boldsymbol{r}\right] V(r) \,, \tag{10}$$

$$\Delta_k = -\int \mathrm{d}^3k' \, V_{|\boldsymbol{k}-\boldsymbol{k}'|} u_{k'} v_{k'} \,. \tag{11}$$

From eq. (8), (11) the following non-linear integral equations can be derived:

$$\Delta_k = -\frac{1}{2} \int \mathrm{d}^3k' \, V_{|k-k'|} \frac{\Delta_{k'}}{\sqrt{\xi_{k'}^2 + \Delta_{k'}^2}} \,. \tag{12}$$

We are interested in finding the spherically symmetrical solutions of eq. (12). Therefore we perform the integration over the solid angle; putting

$$K(k, k') = -\frac{1}{2} \int \mathrm{d}\Omega_{k'} V_{|\boldsymbol{k}-\boldsymbol{k}'|} \,, \tag{13}$$

eq. (12) becomes

$$\Delta_k = \int_0^\infty \mathrm{d}k' \, k'^2 K(k, k') \frac{\Delta_{k'}}{\sqrt{\xi_{k'}^2 + \Delta_{k'}^2}} \,. \tag{14}$$

The kernel $K(k, k')$ can be simply expressed as an integral in the configuration space:

$$K(k, k') = -\frac{1}{\pi k k'} \int_0^\infty \mathrm{d}r \, V(r) \sin kr \sin k'r \,. \tag{15}$$

We now make the assumption that

$$\Delta_k \ll E_F \,, \tag{16}$$

where E_F is the Fermi energy.

As in the limit $\Delta_k \to 0$ v_k^2 becomes simply

$$v_k^2 = \frac{1}{2}\left(1 - \frac{\xi_k}{|\xi_k|}\right) = \begin{cases} 1 & \text{for } k < k_F, \\ 0 & \text{for } k > k_F, \end{cases} \tag{17}$$

we make the approximation of substituting this step-function into the expression (9).

So doing ξ_k becomes equal to the one particle energy calculated with a Hartree method.

Choosing our units in such a way that $k_F = 1$, we get (M is the mass of a nucleon)

$$\xi_k = \frac{k^2}{2M} - \lambda + \int_{k'<1} \mathrm{d}^3k' \left[\frac{3+5\beta}{2} V_0 + \frac{3-5\beta}{2} V_{|k-k'|}\right]. \tag{18}$$

Obviously $\xi_k = 0$, for $k = 1$.

Therefore in the r.h.s. of eq. (14) the most important part of the integrand is near $k' = 1$. So we divide the range of integration in two parts

$$\Delta_k = \int_{1-l}^{1+l} \mathrm{d}k'\, k'^2 \frac{K(k,k')\,\Delta_{k'}}{\sqrt{\xi_{k'}^2 + \Delta_{k'}^2}} + \int_{\text{out}} \mathrm{d}k'\, \frac{k'^2 K(k,k')\,\Delta_{k'}}{\sqrt{\xi_{k'}^2 + \Delta_{k'}^2}}, \tag{19}$$

where

$$\int_{\text{out}} \mathrm{d}k' = \int_0^{1-l} \mathrm{d}k' + \int_{1+l}^{\infty} \mathrm{d}k',$$

and l is a quantity chosen in such a way that:

1) l is small enough for the function $k'K(k,k')\Delta_{k'}$ to be approximated with the constant $K(k,1)\Delta_1$ in the interval $1-l < k' < 1+l$;

2) l is large enough for the function $\sqrt{\xi_{k'}^2 + \Delta_{k'}^2}$ to be approximated with $|\xi_{k'}|$ in the two intervals $0 < k' < 1-l$ and $1+l < k' < +\infty$.

If the assumption (16) holds, it is very plausible that a value of l can be found satisfying the requirements 1 and 2).

Therefore we replace eq. (19) with the approximate equation

$$\Delta_k = K(k,1)\,\Delta_1 \int_{1-l}^{1+l} \mathrm{d}k'\, \frac{k'}{\sqrt{\xi_{k'}^2 + \Delta_1^2}} + \int_{\text{out}} \mathrm{d}k'\, k'^2 \frac{K(k,k')\,\Delta_{k'}}{|\xi_{k'}|}. \tag{20}$$

Putting

$$\left(\frac{\mathrm{d}\xi_k}{\mathrm{d}k}\right)_{k=1} = \xi' \,, \tag{21}$$

we can further approximate $\xi_{k'}$ in the interval $1-l<k'<1+l$ with the function

$$\xi_{k'} = \xi'(k'-1) \,. \tag{22}$$

Substituting this expression in the $\int_{1-l}^{1+l}\mathrm{d}k'$ appearing in eq. (20), we easily obtain

$$\Delta_k = \frac{2\,K(k,1)\,\Delta_1}{\xi'} \sinh^{-1}\frac{\xi' l}{\Delta_1} + \int_{\text{out}} \mathrm{d}k'\, k'^2 \frac{K(k,k')\,\Delta_{k'}}{|\xi_{k'}|} \,. \tag{23}$$

This equation is very similar to eq. (6.11) of Bogoljubov, Tolmachev and Shirkov ([6]).

It is useful to introduce a new function,

$$f(k) = \frac{\Delta_k \xi'}{2\,\Delta_1 \sinh^{-1}(\xi' l/\Delta_1)} \,. \tag{24}$$

The equation for $f(k)$ is

$$f(k) = K(k,1) + \int_{\text{out}} \mathrm{d}k'\, k'^2 \frac{K(k,k')}{|\xi_{k'}|} f(k') \,. \tag{25}$$

The « energy gap » Δ_1 can be obtained from eq. (24)

$$\Delta_1 = \frac{\xi' l}{\sinh\left(\xi'/2f(1)\right)} \,. \tag{26}$$

Therefore we must consider the equation (25) which determines $f(1)$. This equation is linear and can be solved in a Neumann series

$$f(1) = K(1,1) + \int_{\text{out}} \mathrm{d}k' \frac{K(1,k')k'^2 K(k',1)}{|\xi_{k'}|} + \tag{27}$$

$$+ \int_{\text{out}} \mathrm{d}k' \int_{\text{out}} \mathrm{d}k'' \frac{K(1,k'')k''^2 K(k'',k')k'^2 K(k',1)}{|\xi_{k''}|\,|\xi_{k'}|} + \ldots \,.$$

A sufficient condition for the convergence of this expansion is (9)

$$L^2 = \int_{\text{out}} \mathrm{d}k \int_{\text{out}} \mathrm{d}k' \, |L(k, k')|^2 < 1 \,, \tag{28}$$

where

$$L(k, k') = \frac{k\, K(k, k') k'}{\sqrt{\xi_k \xi_{k'}}} \,.$$

3. – A particular case: a finite potential inside the core.

We now give a particular form to the function $V(r)$ appearing in eq. (5). We will use the potential

$$V(r) = V_1(r) + V_2(r) \,, \tag{29}$$

where

$$V_1(r) = \begin{cases} V_1 & \text{for } r < r_c \,, \\ 0 & \text{for } r > r_c \,, \end{cases} \tag{30}$$

$$V_2(r) = -V_2 \exp[-\alpha r] \,, \tag{31}$$

$$\left| \begin{array}{l} r_c = 0.592\, k_F^{-1} \,, \\ \alpha = 0.368\, k_F \,, \\ k_F = 1.48 \cdot 10^{13} \text{ cm}^{-1} \,, \\ V_2 = 33 \text{ MeV} \,, \end{array} \right. \tag{32}$$

and the potential V_1 inside the core is left as a parameter.

The condition (28) for the convergence of the perturbative expansion will establish an upper limit to the value of V_1.

We will calculate the first two terms of the expansion (27) and we will discuss the condition (28).

From formulae (15), (29), one has

$$K(k, k') k k' = -\frac{V_1}{2\pi} f_1(k, k') + \frac{V_2 \alpha}{2\pi} f_2(k, k') \,, \tag{33}$$

(9) E. Goursat: *Cours d'Analyse Mathématique*, tome III (Paris, 1942), p. 348.

where

$$(34)\qquad \begin{cases} f_1(k,k') = \dfrac{\sin(k-k')r_c}{k-k'} - \dfrac{\sin(k+k')r_c}{k+k'}\,, \\ f_2(k,k') = \dfrac{1}{\alpha^2+(k-k')^2} - \dfrac{1}{\alpha^2+(k+k')^2}\,. \end{cases}$$

Let us now work out the expression of ξ_k in this particular case. Eq. (18) can be written as

$$(35)\qquad \xi_k = \frac{k^2-1}{2M} + \frac{3-5\beta}{2}\left[A(k) - A(1)\right],$$

where

$$(36)\qquad A(k) = \int_{k'<1} \mathrm{d}^3k'\; V_{|k-k'|} = -2\int_0^1 \mathrm{d}k'\, k'^2\, K(k,k')\,.$$

The integration can be easily carried out; so one can verify that for values of V_1 up to 1000 MeV, the contribution of the term depending on V_1 to the r.h.s. of eq. (35) is only a small percentage and can be neglected. So we are left with the term depending on V_2

$$(37)\qquad A(k) = -\frac{V_2\alpha}{\pi}\left[\frac{1}{2k}\ln\frac{\alpha^2+(1-k)^2}{\alpha^2+(1+k)^2} + \frac{1}{\alpha}\left(\mathrm{tg}^{-1}\frac{1-k}{\alpha} + \mathrm{tg}^{-1}\frac{1+k}{\alpha}\right)\right].$$

In order to compute the « energy gap » it is necessary to know ξ' (see formulae (21), (26)). The term depending on V_1 can be neglected also in this case and one gets

$$(38)\qquad \xi' = \frac{1}{M} + \left(\frac{3-5\beta}{2\pi}\right)V_2\alpha\left[\frac{1}{2}\ln\frac{\alpha^2}{\alpha^2+4} + \frac{1}{\alpha^2+4} + \frac{1}{\alpha^2}\right].$$

Let us now compute the first two terms of the expansion (27). We have

$$(39)\qquad f(1) = f^{(1)}(1) + f^{(2)}(1) + f^{(3)}(1) + \dots\,,$$

$$(40)\qquad f^{(1)}(1) = K(1,1) = -\frac{V_1}{2\pi}f_1(1,1) + \frac{V_2\alpha}{2\pi}f_2(1,1)\,,$$

$$(41)\qquad f^{(2)}(1) = \int_{\mathrm{out}} \mathrm{d}k' \frac{\left[k'\,K(1,k')\right]^2}{|\xi_{k'}|} = \left(\frac{1}{2\pi}\right)^2\left[a_{11}V_1^2 - 2a_{12}V_1V_2\alpha + a_{22}V_2^2\alpha^2\right],$$

where

$$a_{ik} = \int_{\text{out}} \mathrm{d}k' \, \frac{f_i(1, k') \, f_k(1, k')}{|\xi_{k'}|} , \qquad (i, k = 1, 2). \tag{42}$$

The condition (28) for the convergence of the expansion becomes

$$1 > \left(\frac{1}{2\pi}\right)^2 \left[b_{11} V_1^2 - 2 b_{12} V_1 V_2 \alpha + b_{22} V_2^2 \alpha^2\right] , \tag{43}$$

where

$$b_{il} = \int_{\text{out}} \mathrm{d}k \int_{\text{out}} \mathrm{d}k' \, \frac{f_i(k, k') \, f_l(k, k')}{|\xi_k \xi_{k'}|} , \qquad (i, l = 1, 2). \tag{44}$$

We must now choose a value of l satisfying the two conditions discussed in the previous section (*). A good choice seems to be $l = 0, 1$.

In order to symplify the computations we use the reduced mass approximation; *i.e.* we make an expansion of $A(k)$ in powers of k^2 and we keep only the first two terms

$$A(k) = A(0) + \frac{8 \alpha V_2}{3\pi(1 + \alpha^2)^3} k^2 + \dots . \tag{45}$$

Therefore

$$\xi_k = \frac{k^2 - 1}{2M^*} , \tag{46}$$

where

$$\frac{1}{2M^*} = \frac{1}{2M} + \frac{4(3 - 5\beta)}{3\pi(1 + \alpha^2)^3} V_2 \alpha , \tag{47}$$

$$\begin{cases} M^* = 0.79 \, M & \text{for } \beta = \ \ 0 , \\ M^* = 0.70 \, M & \text{for } \beta = -0.4 . \end{cases} \tag{48}$$

We define

$$\begin{cases} a'_{ik} = \dfrac{1}{2M^*} \, a_{ik} , \\ b'_{ik} = \left(\dfrac{1}{2M^*}\right)^2 b_{ik} . \end{cases} \tag{49}$$

(*) It should be noticed that if the two conditions allow l to be inside a certain range $l_1 < l < l_2$, the best choice in order to have a better convergence of the perturbation expansion is $l = l_2$.

4. – Numerical results and conclusions.

The quantities a'_{ik}, b'_{ik} have been calculated substituting for ξ_k its simplified expression (46), and making use of an electronic computer. They are equal to

$$a'_{11} = 0.0631\,, \qquad a'_{12} = 1.127\,, \qquad a'_{22} = 43.12\,,$$

$$b'_{11} = 0.2648\,, \qquad b'_{12} = 2.366\,, \qquad b'_{22} = 82.96\,.$$

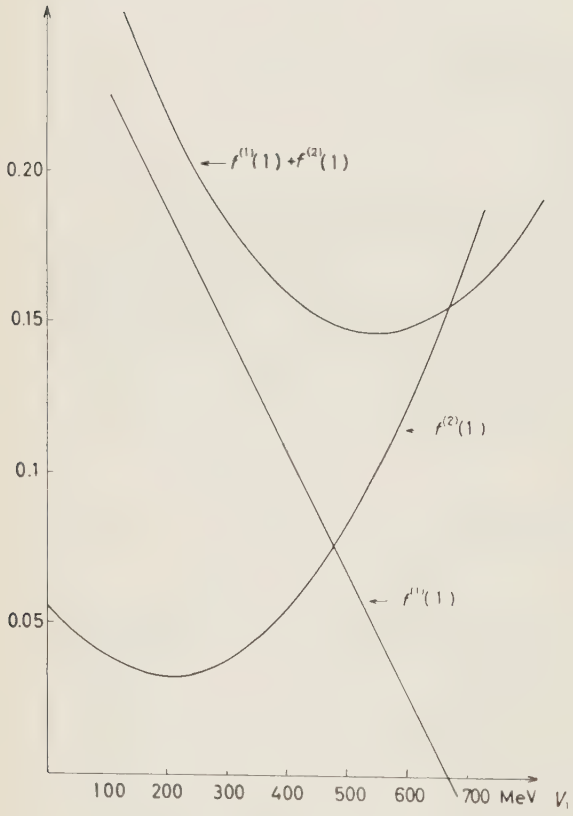

Fig. 1.

The final results are shown in Fig. 1, where the terms $f^{(1)}(1)$ and $f^{(2)}(1)$ are plotted against V_1. The condition (43) becomes

$$V_1 < 729 \text{ MeV} \quad \text{for } \beta = \quad 0\,,$$

$$V_1 < 811 \text{ MeV} \quad \text{for } \beta = -0.4.$$

The n-th term of the expansion (39) can be majorized ([9]) in the following way (see eq. (28) for the definition of L):

$$(50) \qquad |f^{(n)}(1)| \leqslant f^{(2)}(1) L^{n-2}\,.$$

Therefore it is easy to deduce that for V_1 less than about 500 MeV the sum of the series (39) is certainly positive (both for $\beta = 0$ and $\beta = -0.4$), and a finite gap exists in the energy spectrum of the « quasi-particles » (*).

For $V_1 \simeq 500$ MeV, eq. (26) gives $\Delta_1 \simeq 0.015$ MeV. But we cannot be sure that this result is of the right order of magnitude, as Δ_1 depends exponentially on $f(1)$.

For instance, with $f(1)$ twice as large, one gets $\Delta_1 \simeq 0.6$ MeV.

(*) It must be noticed that in making this estimate we have chosen the worst possible case: *i.e.* the case in which all terms $f^{(n)}(1)$, for $n > 2$, are negative.

From the above results one can conclude that a sufficient condition for the existence of a gap in the spectrum of the free quasi-particles, is that the potential inside the core is lower than 500 MeV (a condition which probably is too stringent).

Therefore we think that in nuclear matter if one makes the Bogoljubov-Valatin canonical transformation and writes down the Hamiltonian in terms of the quasi-particles, one can eliminate the difficulties in the Goldstone expansion arising from the vanishing denominators.

* * *

We wish to thank Prof. B. Ferretti for useful discussions; we are also indebted to Dr. C. Lolli and Dr. S. Giambuzzi for assistance in numerical calculations with the I.B.M. 650 of the University of Bologna.

RIASSUNTO

Viene data una condizione sufficiente per l'esistenza di un « gap » nello spettro energetico delle quasi-particelle nella materia nucleare, assumendo un potenziale repulsivo finito nel core.

Relation between π-N Scattering and Nucleon Structure through $\pi\pi$ Interaction.

A. Stanghellini

Istituto di Fisica dell'Università - Bologna
Istituto Nazionale di Fisica Nucleare - Sezione di Bologna

(ricevuto il 9 Novembre 1960)

Summary. — The relation between long range effects in pion-nucleon scattering and nucleon structure through pion-pion interaction in $T=1$, $J=1$ state is analysed by means of different models.

Introduction.

The problem of including $\pi\pi$ interaction in the solution of the dispersion relations for π-N scattering has been faced by several authors ([1,2]), by making semi-phenomenological approximations in the framework of Mandelstam representation.

The main assumption underlying those investigations is the existence of a $T=1$, $J=1$ $\pi\pi$ resonance.

Parameters such as the position, width and couplings of this resonance with the nucleon are found to be the same as that appearing in the vector part of the nucleon structure if the two pion intermediate states are taken into account.

([1]) *a)* J. Bowcock, W. N. Cottingham and D. Lurié (B.C.L.): *Nuovo Cimento*, **16**, 918 (1960); *b) Effect of a pion-pion scattering resonance on low energy pion-nucleon scattering* - II (CERN preprint); *c) $\pi\pi$ scattering, nucleon structure and π-N scattering* (CERN preprint).

([2]) S. C. Frantschi and J. D. Walecka: CERN preprint; S. C. Frantschi: *Phys. Rev. Lett.*, **5**, 159 (1960).

In this work we wish to show that the relation between $\pi.\mathcal{N}$ scattering and nucleon structure through $(T=1, J=1)$ $\pi\pi$ interaction can be understood physically in a simple manner, without passing through the integral representation of the nucleon form factors and the Mandelstam representation of $\pi.\mathcal{N}$ scattering, and is mainly due to the symmetries of the problem.

We shall show that two models, which start from different physical hypotheses, lead to the same relation.

1. – The « local » model.

Let us select the following from the many contributions to $\pi.\mathcal{N}$ scattering through $\pi\pi$ interaction:

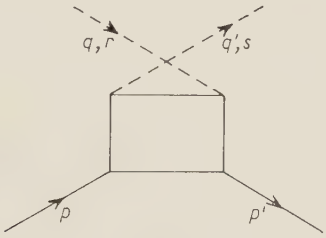

Fig. 1.

in which the two external pions are absorbed at the same point by two internal pions. The rest of the interaction is described by the box.

We define a phenomenological interaction between the four pions, in which two pions are emitted or absorbed in an antisymmetric state $(T=1)$,

$$H_{4\pi}(x) = \lambda \sum_{\alpha'\beta'} \sum_{\alpha\beta ki} \frac{\partial \varphi^{\alpha'}(x)}{\partial x_i} \varphi^{\beta'}(x)\, \varepsilon_{\alpha'\beta' k} \frac{\partial \varphi^{\alpha}(x)}{\partial x_i} \varphi^{\beta}(x)\, \varepsilon_{\alpha\beta k}. \tag{1.1}$$

The contribution to the T matrix for $\pi.\mathcal{N}$ scattering coming from Fig. 1 is

$$\langle p', q' \,|\, T^{\pi\pi} \,|\, p, q \rangle = \int \mathrm{d}^4x \, \langle p'q' \,|\, O(x)\, H_{4\pi}(x) \,|\, pq \rangle = \tag{1.2}$$

$$= \frac{\lambda}{\sqrt{4\omega\omega'}} \sum_{\alpha'\beta' ki} \int \mathrm{d}^4x \exp\left[i(q'-q)x \right] \bar{u}^{\beta'}(p') O(x) \frac{\partial \varphi^{\alpha'}(x)}{\partial x_i} \varphi^{\beta'}(x)\, \varepsilon_{\alpha'\beta' k}\, u^{\beta}(p')\, (q'+q)_i\, i\, \varepsilon_{srk},$$

where $O(x)$ is an operator representing the box.

We now consider the following contribution to nucleon structure,

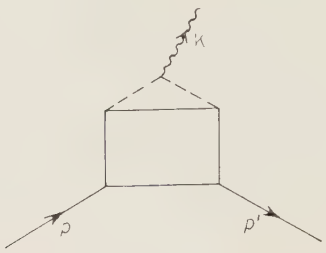

Fig. 2.

It is evident that the box is equal to that previously considered.

We have

$$(1.3) \qquad p'\,\gamma' p \qquad \frac{e}{\sqrt{2k}} \sum_{\alpha'\beta'} \sum_{i} \int \mathrm{d}^4x \exp\left[ikx\right] \langle p' \mid O(x) \frac{\partial \varphi^{\alpha'}(x)}{\partial x_i} q^{\beta'}(x) \varepsilon_{\gamma'\beta'3} \mid p \rangle \, \epsilon_i \,,$$

ϵ_i being the photon polarization.

Comparing (1.2) and (1.3) we see that the same matrix element appears in the two cases. So we can write, taking the appropriate normalization,

$$(1.4) \qquad \overline{u}(p') T^{\pi\pi}_{sr} u(p) = \frac{\lambda}{e}\, i \sum_{ki} \varepsilon_{srk}\, \overline{u}(p') \tau_k J^{\pi}_i u(p) (q' + q)_i \,.$$

The relation (1.4) is the one we were looking for, which connects $\pi\pi$ effects in $\pi\mathcal{N}$ scattering to part of the nucleon structure.

J^{π}_i contributes to the vector part of the nucleon structure.

Let us make the hypothesis that the main deviation from the point charge and magnetic moment of the nucleon is given by the pion current (for not too large a value of the momentum transfer $t = k^2$).

This hypothesis is clear from a physical point of view and is the same as that made in the dispersive approach.

So we can write

$$(1.5) \qquad \frac{1}{e}\, \overline{u}(p') J^{\pi}_i u(p) \cdot \left[F^{v}_1(t) - \frac{\alpha_1}{2} \right] \overline{u}(p') \gamma_i u(p) \, -$$

$$- i \left[F^{v}_2(t) - \frac{g}{2M} \alpha_2 \right] \overline{u}(p')\, \sigma_{ij} (p' - p)_j u(p) \qquad F^{v}_1(0) = \frac{M}{g} F^{v}_2(0) = \frac{1}{2},$$

where α_1 and α_2 represent the fractions of charge and magnetic moment contained in the « core » (not due to the two pions exchange).

In effect these subtraction constant terms are also supported by the fact that there may be some « direct » interaction between the two external pions with the nucleon due to higher mass states.

These interactions give contributions of the same form as the subtraction terms with unknown coefficients.

Collecting our results in term of the pion nucleon amplitude we obtain

$$(1.6)\qquad \begin{cases} T^{\pm} = -A^{\pm} + i\gamma Q B^{\pm}, \quad Q = \dfrac{q'+q}{2}, \\ A^{-}_{\pi\pi} = \lambda(p'+p)(q'+q)\left[F_2^v(t) - \dfrac{g}{2M}\alpha_2\right], \\ B^{-}_{\pi\pi} = 2\lambda\left[F_1^v(t) - \dfrac{\alpha_1}{2} + 2M F_2^v(t) - g\alpha_2\right], \end{cases}$$

and 0 for the A^{+}, B^{+} amplitude due to the presence of the $i\tau_k\varepsilon_{srk}$ operator.

Let us pass to the c.m. variable and write the f_1 and f_2 amplitudes in the static approximation,

$$(1.7)\qquad \begin{cases} f_1^{-} = \dfrac{2\lambda}{4\pi}\dfrac{M}{W}\left[-q^2\cos\theta\left(F_2^v(t) - \dfrac{g}{2M}\alpha_2\right) + \omega\left(F_1^v(t) - \dfrac{\alpha_1}{2}\right)\right], \\ f_2^{-} = \dfrac{2\lambda}{4\pi}\dfrac{M}{W}q^2\left[\dfrac{1}{2M}\left(F_1^v(t) - \dfrac{\alpha_1}{2}\right) + \left(F_2^v(t) - \dfrac{g}{2M}\alpha_2\right)\right]. \end{cases}$$

The result given by formulae (1.7) has to be compared with the equivalent one obtained by J. Bowcock *et al.* [1] (eq. 5.6 of their paper).

The structure of (1.7) comes from the symmetries imposed to the problem. It is confirmed that the charge distribution alone contributes to the no spin-flip amplitudes, and the total magnetic moment structure to the spin-flip amplitudes.

Evidently one can use the experimental form factors to pass from F_1 and F_2 to the phase-shifts. But let us use the Clementel and Villi [3] model in order to make a clear comparison with the results of BCL.

Apart from normalization constants the two results are completely equivalent.

In fact we have

$$F_1(t) - \frac{\alpha_1}{2} + \beta_1 = \lambda\left(f(0) + \frac{at}{t_r - t}\right),$$

which has to be compared with something proportional to

$$f(t) = C_1 + \frac{a}{t_r - t} = f(0) + \frac{at}{t_r - t},$$

where $f(0) = C_1 + (a/t_r)$.

[3] E. Clementel and C. Villi: *Nuovo Cimento*, **4**, 1207 (1958).

β_i are the constants that we have to add in order to take into account the two pion nucleon « contact » effect due to higher masses.

2. – The « bipion model » (4).

Let us suppose that the interaction between pions is resonating in the $T=1$, $J=1$ state. This resonance can be simulated by a particle with those symmetries.

The interactions of this particle with pions, nucleon and photon are given by:

« bipion » – two pions vertex $\quad i\lambda\pi\pi_{\mu,k}(q'+q)_\mu \varepsilon_{srk}$,

« bipion » – nucleons vertex $\quad \pi\pi_{\mu,k}\{C_1\overline{u}(p')\gamma_\mu\tau_k u(p) - iC_2\overline{u}(p')\tau_k\sigma_{\mu\nu}t_\nu u(p)\}$,

« bipion » – photon vertex $\quad \pi\pi_{\mu,3}\epsilon_\mu$

and finally the bipion propagator:

$$f(t)\left[\delta_{\mu\nu} - \frac{t_\mu t_\nu}{t}\right],$$

where t_μ is the quadrimomentum of the « bipion ».

For deriving the relation between $\pi.N$ scattering and nucleon structure we don't need to have an explicit form of the propagator.

The lowest order calculation of $\pi.N$ scattering and nucleon structure through the « bipion » represented in Fig. 3 gives:

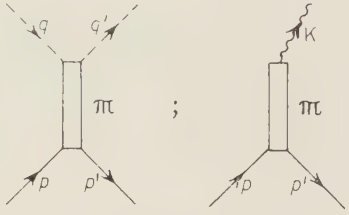

Fig. 3.

$$\overline{u}(p')\,T^{\pi\pi}_{sr}\,u(p) = i\lambda\varepsilon_{srk}(q'+q)_\mu f(t)[C_1\overline{u}(p')\gamma_\mu\tau_k u(p) - iC_2\overline{u}(p')\tau_k\sigma_{\mu\nu}t_\nu u(p)] \,, \tag{2.1}$$

$$\epsilon_\mu\,\overline{u}(p')J^{\pi\pi}_\mu u(p) = \epsilon\epsilon_\mu f(t)[C_1\overline{u}(p')\gamma_\mu\tau_3 u(p) - iC_2\overline{u}(p')\tau_3\sigma_{\mu\nu}t_\nu u(p)] \,, \tag{2.2}$$

(4) M. Gourdin, D. Lurié and A. Martin (CERN preprint) used this model for a short derivation of the solution of the Mandelstam representation for the isoscalar part of photo-pion production.

from which we obtain the relation:

$$\overline{u}(p')\,T^{\pi\pi}_{sr}\,u(p) = \frac{\lambda}{e}\,i\varepsilon_{srk}(q'+q)_\mu\,\overline{u}(p')\,J^{\pi\pi}_\mu\tau_k\,u(p)\,, \tag{2.3}$$

which is equal to (1.4).

The model we have just considered is evidently the direct parent of the hypothesis used by J. Bowcock [1] for the solution of the Mandelstam representation for $\pi\mathcal{N}$ scattering.

But it is evident from our analysis that the relation between $\pi\mathcal{N}$ scattering and nucleon structure through $\pi\pi$ interaction is more general and is also true if no $J=1$, $T=1$ $\pi\pi$ resonance is present.

The selection from the two types of interactions can be obtain only from the analysis of the nucleon structure itself. The present situation seems to favour the resonant model. In fact by the only hypothesis that the spectral functions of the form factors are big for a definite value of the momentum transfer (corresponding to the « bipion » mass), Bowcock *et al.* [1] were able to derive the Clementel and Villi model which fits sufficiently well the experimental form factors.

3. – Conclusion.

It is quite interesting that a simple model gives predictions similar to the Mandelstam approach.

We suggest to apply the same procedure to other processes in which the machinery of solving the integral equations is even more complicated.

In particular we suggest to apply the same method to $\mathcal{N}\mathcal{N}$ scattering, in which will appear the product of two form factors, (with the same constants as those used in $\mathcal{N}\mathcal{N}$ scattering), to pion photoproduction and to Compton scattering.

This simplified version may be very useful for a first insight into these problems.

Instead of discussing the above-mentioned processes, we wish to spend some words about K$\mathcal{N}$ scattering which is practically similar to $\pi\mathcal{N}$ scattering. Using a phenomenological interaction of the form

$$H(x) = -\,i\lambda'\,\frac{\partial\varphi^*(x)}{\partial x_i}\,\tau_k\varphi(x)\,\frac{\partial}{\partial x_i}\,\varphi^\alpha(x)\,\varphi^\beta\varepsilon_{\alpha\beta k} + \text{h. c.} \tag{3.1}$$

where φ is the K field, one obtains

$$\frac{1}{\lambda'}\,\overline{u}(p')T_{\mathrm{K}\mathcal{N}}\,u(p) = \frac{1}{e}\,\overline{u}(p')\,\boldsymbol{\tau}_{\mathrm{K}}\cdot\boldsymbol{\tau}_{\mathcal{N}}\,J_\mu u(p)(k'+k)_\mu\,. \tag{3.2}$$

The isotopic dependence is -3 for the $T=0$ K$\mathcal{N}$-state and 1 for the $T=1$ state.

The same effect is present for $\bar{\mathrm{K}}\mathcal{N}$ scattering with the opposite sign.

From (3.2) one may expect a behaviour of the K$\mathcal{N}$ phase shift similar to the corresponding ones for $\pi\mathcal{N}$ scattering.

* * *

I wish to thank Prof. S. Fubini for useful discussions.

RIASSUNTO

Si usano differenti modelli per mostrare che l'interazione pione-pione nello stato $T=1$, $J=1$ pone una relazione tra lo scattering pione-nucleone e la struttura del nucleone.

LETTERE ALLA REDAZIONE

(La responsabilità scientifica degli scritti inseriti in questa rubrica è completamente lasciata dalla Direzione del periodico ai singoli autori)

Preliminary Results of a Measurement of the Differential Cross Section for Single π^0 Meson Photoproduction in Hydrogen.

G. Cortellessa and A. Reale

Istituto Superiore di Sanità - Roma

(ricevuto il 6 Giugno 1960)

The differential cross section for single π^0-meson photoproduction in hydrogen between the threshold and 1200 MeV has been extensively measured during the last eight years. The detailed shape of the differential and total cross section has been investigated with different experimental apparatus. A general picture now is possible: the total cross section shows definite evidence for three « peaks » at 320 MeV, (700 ÷ ÷800) MeV, (1000 ÷ 1100) MeV photon laboratory energy. The first region of energy, between the threshold and 500 MeV, has been extensively studied and the agreement between the various experimenters is good.

The second « resonance » has been studied, from 500 to 900 MeV incident photon laboratory energy, by many experimenters, with some discrepancies among the data. These differences are more pronounced for the backward and forward c.m.s. angles for the meson. Experimental data for the third energy region, between 900 and 1100 MeV, are very few. It is possible, nevertheless, to speak of a third « resonance » also in π^0-meson photoproduction.

Our aim has been to try to establish whether the discrepancies at the second resonance are due to lack of angular and energy resolution in the previous measurements.

The detection of single π^0-meson photoproduction is performed in our experiment through a coincidence between the recoil proton from the reaction and one of the γ-rays coming from the decay of the π^0-meson. A telescope built with five scintillation counters, with absorbers in-between the counters, defines a proton event.

The counters have a thickness of 5 mm, and an area of (15×15) cm^2 except the first one that has an area of (10×10) cm^2. The telescope subtends a laboratory angle of $\pm 1°$ at 58° from the beam. Electronically the five counters are connected as a fourfold coincidence among the first four counters anticoincided by the last counter:

$$1 + 2 + 3 + 4 - 5 .$$

The coincidence circuitry is double: slow and fast pulses are treated differently. Slow pulses derived by the last dynode of the 6810A photomultipliers are amplified, discriminated, shaped, sent to the coincidence circuit. Fast pulses taken from the anode of the photo-

multipliers are shaped at a length of 15 ns and sent to a fast coincidence circuit. Slow and fast coincidences are mixed together and with the signal from the γ-ray telescope.

The γ-ray telescope is made of a Čerenkov counter with a lead glass radiator. A scintillation counter, connected in anticoincidence, in front of the Čerenkov counter eliminates the charged particles contribution.

The energy resolution of the system is ± 30 MeV of the laboratory energy of the incoming γ-ray. This energy resolution has been obtained, in spite of the angular aperture of the telescope, by shaping properly the copper absorbers between counter 1 and 2 and counter 4 and 5.

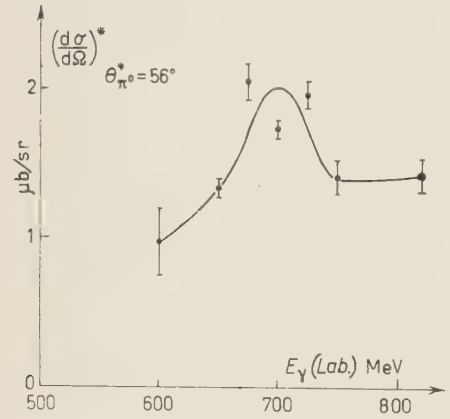

Fig. 1.

The experimental results are summarized in Fig. 1 and correspond to a 56° c.m.s. angle for the π^0-meson. It is possible to see that the three points at 675, 700, 725 MeV laboratory energy for the γ-ray are higher than the others. The first conclusion that we draw is that the peak of the differential cross-section at 56° c.m.s. angle is at a laboratory energy of about 700 MeV and that the width of the resonance is of the order of 50 MeV.

The errors quoted in the drawing are statistical. We have analyzed elsewhere [1] the possibility of contamination due to other reactions. We have found that the contribution of the Compton effect on protons cannot be larger than 10% at most for the 600 MeV point and less for the others.

A complete analysis of the width and position of the second peak in the total cross-section will be possible when we shall have completed our measurements for other c.m.s. angles.

We think now that there is some evidence, also from these preliminary data, that the resonance is quite narrow and centered at the same energy as the resonance for single π^+-meson photoproduction.

We think that our experimental results are not in contrast with the previous determinations of the differential cross section for single π^0-meson photoproduction. The present measurement has been made with a resolution, both in γ-ray energy and π^0-meson c.m.s. angle, two or three times better than previous measurement. A confirmation of this steep variation of the differential cross-section with the energy, together with the already known steep variation with the angle in some regions of the angular distribution, gives support to the idea that the whole angular distribution is to be measured again with the highest practical resolution.

A further reason for following these lines is given by the more recent theoretical views [2] that present a more complex picture of the second and third « resonance » and require a deeper experimental investigation.

We are accordingly extending, with the present experimental arrangement, our measurements to different c.m.s. angles for the π^0-meson.

[1] G. CORTELLESSA and A. REALE: *Scient. Rep. of the Istituto Superiore di Sanità* (to be published).

[2] P. CARRUTHERS and H. A. BETHE: *Phys, Rev. Lett.*, **4**, 536 (1960).

IL NUOVO CIMENTO Vol. XVIII, N. 6 16 Dicembre 1960

A Note on the Fermi-Teller « Z-Law ».

A. Astbury, P. M. Hattersley, M. Hussain, M. A. R. Kemp and H. Muirhead
Chadwick Laboratory, University of Liverpool - Liverpool

(ricevuto il 1° Agosto 1960)

During a recent experiment [1] data were obtained which are relevant to the Fermi-Teller « Z-law ». This law [2] suggests that when negative muons are brought to rest in a compound, the atomic capture probability for an element of charge Z and N atoms per cm^3 should be proportional to the product NZ.

Conflicting experimental evidence [3] has been obtained as to whether the capture follows this law, or is simply proportional to the atomic concentration N.

If M mesons stop in an element the number of decay electrons appearing between times t and $t+\mathrm{d}t$ is given by the expression

$$n(t) = \lambda_D \exp[-\lambda_T t]\,\mathrm{d}t\,, \tag{1}$$

where λ_D represents the electronic decay rate, and λ_T the total disappearance rate (decay plus capture). Thus if the mesons stop in a compound of two elements the decay electrons will have the following distribution in time

$$n(t) = M(C_1\lambda_{D1}\exp[-\lambda_{T1}t] + C_2\lambda_{D2}\exp[-\lambda_{T2}t])\,\mathrm{d}t, \tag{2}$$

where C_1 and C_2 represent atomic capture probabilities in elements 1 and 2.

At time $t=0$, we obtain

$$\frac{n_1}{n_2} = \frac{C_1\lambda_{D1}}{C_2\lambda_{D2}}\,. \tag{3}$$

In our experiment negative muons from the Liverpool synchrocyclotron were brought to rest in lead fluoride (PbF_2). The number of electrons appearing as a function of time was registered on the screen of a kicksorter [1]. After subtraction of background the composite curve given in eq. (2) was analysed and a result

$$n_{\mathrm{Lead}}/n_{\mathrm{Fluorine}} = 1.62 \pm 0.15\,.$$

was obtained.

[1] A. Astbury, M. Hussain, M. A. R. Kemp, H. Muirhead and T. Woodhead: to be published.

[2] E. Fermi and E. Teller: *Phys. Rev.*, **72**, 399 (1947).

[3] J. F. Lathrop, R. A. Lundy, R. A. Swanson, V. L. Telegdi and D. D. Yovanovitch: *Nuovo Cimento*, **15**, 831 (1960).

The work of YOVANOVITCH [4] suggests that

$$\lambda_{D\,\mathrm{Lead}}/\lambda_{D\,\mathrm{Fluorine}} = 0.34 \pm 0.03 ,$$

thus we find

$$C_{\mathrm{Lead}}/C_{\mathrm{Fluorine}} = 4.8 \pm 0.7 .$$

The Fermi-Teller « Z-law » predicts a value of 4.5 for this ratio; if the capture probability varied according to atomic concentration a figure of 0.5 would be expected.

[4] D. D. YOVANOVITCH: *Phys. Rev.*, **117** 1580 (1960).

IL NUOVO CIMENTO Vol. XVIII, N. 6 16 Dicembre 1960

On a Model for Ξ-Decays.

A. P. Balachandran (*) and N. R. Ranganathan (**)
University of Madras - Madras

(ricevuto il 20 Agosto 1960)

Recently in an attempt to explain some of the observed features of Σ-decays Barshay and Schwartz [1] considered a model in which the Σ-hyperon is considered as a bound state of a Λ^0 and a pion. In view of the apparant success of this model, it becomes of interest to consider a similar model for the Ξ-particle *i.e.* we treat the Ξ-hyperon as a bound state of a Λ^0 and a $\overline{K}$ [2]. In this note we will discuss the consequences of such an assumption on the decay modes of the Ξ-particle. In a later contribution we hope to deal with the strong interactions of the Ξ-particle using this model.

We first consider the case where the parity of the $(\Lambda^0 K)$ system relative to the Ξ-hyperon is even. In such a case the bound state will be an S-state. We may also assume that the parity of Λ^0 relative to a system consisting of a nucleon and a $\overline{K}$ is odd. Then the decay of the Ξ-particle will proceed by the Λ^0 within the Ξ decaying into a pion and a nucleon and the nucleon subsequently absorbing the $\overline{K}$ in a P-state relative to it. Let us denote by A and $\pm A$, the amplitudes for Λ^0 decaying into an S and a P-wave pion-nucleon system respectively. Similarly let B be the amplitude for the nucleon absorbing a K-meson via a P-wave interaction. Then we obtain

$$(1)\qquad \Xi^- = (\Lambda^0 K^-)_S \to A K_S^- \cdot \left(-\sqrt{\frac{2}{3}}\,(\pi^- p) + \frac{1}{\sqrt{3}}\,(\pi^0 n)\right)_S \pm \pm A K_S^- \left(-\sqrt{\frac{2}{3}}\,(\pi^- p) + \frac{1}{\sqrt{3}}\,(\pi^0 n)\right)_P \cdot \to -\frac{1}{\sqrt{3}}\,AB(\Lambda^0\pi^-)_P \mp \frac{1}{\sqrt{3}}\,AB(\Lambda^0\pi^-)_S ,$$

where the notation is the same as in reference [1]. It follows that the asymmetry parameters α_Λ and α_Ξ for the Λ^0 and Ξ-decays have to be equal, *i.e.* $\alpha_\Lambda = \alpha_\Xi$. It is easily seen that this result holds irrespective of the signs of the relative parities $P(\Lambda^0\overline{K}\Xi)$ and $P(N\overline{K}\Lambda^0)$.

It is to be noted that the decay mechanism of the Ξ cannot be via the decay of the $\overline{K}$ into two pions since the Λ^0 cannot subsequently absorb a

(*) Research Fellow of the University of Madras.

(**) Senior Research Fellow of the Atomic Energy Commission.

[1] S. Barshay and M. Schwartz: *Phys. Rev. Lett.*, **4**, 618 (1960).

[2] N. Dallaporta: *Nuovo Cimento*, **7** 200 (1959); P. Budini, N. Dallaporta and L. Fonda: *Nuovo Cimento*, **9**, 316 (1958).

pion because of isotopic spin conservation. Also the process $\pi+\pi\to\pi$ is in general not possible because of G-conservation. However the process $\overline{\mathrm{K}}\to\pi+\pi+\pi$ with $\pi+\pi+\pi\to\pi$ is possible. This will modify the S-wave amplitude in the Ξ-decay.

Incidentally it may be remarked that Goldhaber's model [3] is not capable of explaining the decay features of the composite particle since the basic weak interaction is the decay of $\overline{\mathrm{K}}$ into pions.

Considerations analogous to those in reference [1] also show that the $\Delta S/\Delta Q=1$ rule is satisfied for the Ξ-decay if all weak interactions are to proceed only through four-fermion couplings. For instance the decay mode $\Xi^0\to\Sigma^-+\mathrm{e}^+ +\nu$ is forbidden since this has to proceed through $\Lambda^0\to\mathrm{n}+\pi^-+\mathrm{e}^+ +\nu$ which is forbidden by our assumption.

* * *

We wish to thank Professor Alladi Ramakrishnan and Mr. K. Venkatesan for helpful discussions.

[3] S. Goldhaber: *Phys. Rev.*, **101**, 433 (1956); G. Györgyi: *Žurn. Éksp. Teor. Fiz.*, **32**, 152 (1957).

Example of Two Mesons' Production in K^- Stars at Rest.

S. Mora

Istituto di Fisica dell'Università - Parma

(ricevuto il 7 Settembre 1960)

During an analysis of about 4 500 K^--stars at rest originated in an emulsion stack exposed to the Heckman K^- beam of the Bevatron, an event with two identified mesons of opposite charge has been found.

In addition to these tracks a proton and a recoil 3 μm long, opposite to the proton track, are present.

The event is shown in Fig. 1 where (*a*) and (*b*) are the mesonic tracks and (*c*) is the protonic one; (*r*) is the recoil and K^- is the primary track.

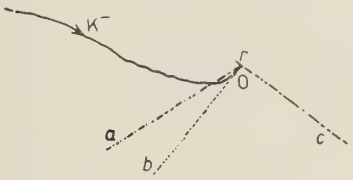

Fig. 1. – Sketch of the event.

The angle between (*a*) and (*b*) is of 18° degrees. These tracks have been followed until the end of their ranges and $\pi \to \mu$ decay for (*a*), σ star for (*b*) have been found. The range measurements give for (*a*) an emission kinetic energy of 10.3 MeV and for (*b*) a value of 17.4 MeV. In addition (*c*) track has been followed until the end of the range and a value of 80.1 MeV has been found for the energy.

Ionization measurements prove that this track was produced by a proton. The (*a*) track clearly comes out from the point *O*; the (*b*) track is superimposed in the first few microns to the K^- track.

The hypothesis that (*b*) originates before the point *O*, shifting the K^- interaction, is ruled out owing to the impossibility to interpret as hyperfragment or Σ^- star the close event in which a meson is associated with a proton of 80 MeV kinetic energy.

However, if a $\Sigma^\pm$ escapes from the nucleus and travels a very short distance (< 1 μm) it does not decay into a meson of observed energy; if a Λ^0 escapes from the nucleus and decays in flight after a very short time, one can easily compute from the observed energies of the proton and of the π^--meson and from the angle between the emission direction of these particles, a *Q* of the Λ^0 equal to 20 MeV, rather far from the known value of 37.2 MeV [1].

A first interpretation of the event is consistent with that one observes if one assumes that both the mesons are emitted

[1] W. E. Slater: *Suppl. Nuovo Cimento*, **10**, 1 (1958).

in a fast process following the reaction

$$(1) \quad K^- + p \to \pi^+ + \pi^- + \Lambda^0 + 38 \text{ MeV},$$

where 38 MeV is the Q of the reaction.

In our case the proton is bound to the nucleus and therefore the Q of this reaction includes the kinetic energy of the reaction products, the binding energy of the proton and the excitation energy of the nucleus ([2]).

The presence of a proton of 80 MeV kinetic energy can be explained by a non mesic decay of the Λ^0 trapped in the nucleus ($Z > 3$).

The last hypothesis is justified by the low energy spectrum of the Λ^0 in the reaction (1), which should highly increase the trapping probability of the Λ^0 in the nucleus.

However this hypothesis is in part confirmed by the energy difference between the Q of the reaction (1) and the total measured kinetic energy of the two mesons.

In effect such a difference could be reasonably attributed to the excitation energy of the nucleus taking the binding energy of the Λ^0 equal to the binding energy of the proton.

The reaction (1) can be rewritten in the form:

$$(2) \quad K^- + \langle p \rangle - B_p = \pi^+ + \pi^- + \Lambda^0 + B_{\Lambda^0} + E_{ex} + T_{\pi^+} + T_{\pi^-},$$

where the dashes indicate that the proton and the Λ^0 are bound; B_p and B_{ex} are the binding energies of the proton and of the Λ^0, E_{ex} is the excitation energy of the nucleus, T_{π^+} and T_{π^-} are the kinetic energies of the two mesons.

Even if all experimental data support this very simple interpretation, owing to the rarity of the event, one cannot rule out another possibility although a chain of different and sometimes very infrequent processes are to be assumed.

This second interpretation is based on the assumption that the two mesons are emitted successively with two different processes: a fast one and a slow one ([3]).

The reactions involved in these processes can occur following the successive steps:

(*a*) a π^+-meson and a Σ^- hyperon rise in the K^- absorption on a proton, bound in a nucleus;

(*b*) the Σ^-, absorbed in the nucleus gives rise to a Λ^0 hyperon which remains, trapped in the nucleus ([4]);

(*c*) the high energy proton originates after the Σ^- absorption;

(*d*) the π^--meson is the product of the mesonic decay of the Λ^0 in the nucleus ($Z > 3$).

The events (*c*) ([5-6]) and (*d*) ([7]) are very infrequent. If we consider that only a few per cent of all K^- absorptions satisfy the condition (*b*), we can say that the occurrence of the (*b*), (*c*), (*d*) fenomena in the same event is to be considered very improbable.

Experimental evidence of the reaction (1), already postulated by the Gell-Mann-Nishijima scheme, has been recently given ([8]).

In that work 12 events of this type have been found in about 10 000 K^- absorptions at rest on free protons using a

([2]) F. C. GILBERT, C. E. VIOLET and R. S. WHITE: *Phys. Rev.*, **107**, 228 (1957).

([3]) G. QUARENI, A. QUARENI VIGNUDELLI, G. DASCOLA and S. MORA: *Suppl. Nuovo Cimento*, **16**, 140 (1960).

([4]) J. HORNBOSTEL and G. T. ZORN: *Phys. Rev.*, **109**, 165 (1958).

([5]) K⁻ COLLABORATION: *Nuovo Cimento*, **13**, 690 (1959).

([6]) M. NIKOLIĆ, Y. EISENBERG, W. KOCH, M. SCHNEEBERGER and H. WINZELER: *Helv. Phys. Acta*, **33**, 221 (1959).

([7]) E. M. SILVERSTEIN: *Suppl. Nuovo Cimento*, **10**, 41 (1958).

([8]) L. W. ALVAREZ: Communication at the Kiev Congress (1959).

hydrogen bubble chamber; this ratio is not in disagreement with the present data if one takes into account that about 30% of all K^- absorptions from emulsion nuclei are multinucleon absorptions and that about 50% of the remaining events are K^- absorptions on neutrons ([6,9]).

([9]) K^- COLLABORATION: *Nuovo Cimento*, **14**, 315 (1959).

However events of this type, where the Λ^0 remains trapped in the nucleus, can be utilized in order to have an indication on the binding energy of the Λ^0 in a nucleus, with $Z > 3$.

* * *

I wish to thank Prof. CECCARELLI and Prof. QUARENI of the Institute of Physics of the Bologna University for the very helpful discussions had with them.

The Most Probable Path of a Scattered Particle.

N. C. Barford

Physics Department, Imperial College - London

(ricevuto il 3 Ottobre 1960)

A graphical method has been described which gives the most probable path of a particle through a plate of scattering material, when only the initial and final positions and directions of the path are known (1). A generalization of the theory on which this is based makes it possible to obtain a more complete solution and to determine the path length without any need for graphical construction.

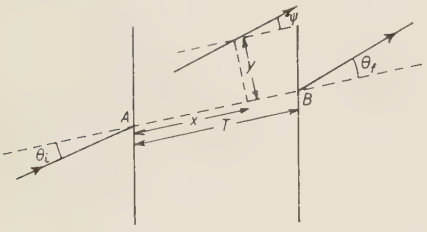

Fig. 1.

Suppose the particle enters the plate at a point A in the direction θ_i and leaves it at B in the direction θ_f, and that at an intermediate point of its path, (x, y), it has the direction ψ. The angles are measured relative to AB and are projections on a convenient plane; x is the abscissa measured along AB and y is the projected ordinate in the same plane, as shown in Fig. 1. Then, following the methods already developed (1,2), the probability that the particle passes through A, (x, y) and B in the directions mentioned has the differential form

$$P = F[x, y - x\theta_i, \psi - \theta_i] F[T - x, -\{y + (T - x)\psi\}, \theta_f - \psi],$$

where

$$F(t, l, \theta) = \frac{\sqrt{3}\omega^2}{2\pi t^2} \exp\left[-\omega^2\left(\frac{\theta^2}{t} - \frac{3l\theta}{t^2} + \frac{3l^2}{t^3}\right)\right], \tag{1}$$

and T is the distance AB.

(1) N. C. Barford and G. T. Reynolds: *Nuovo Cimento*, **4**, 929 (1956).
(2) B. Rossi and K. Greisen: *Rev. Mod. Phys.*, **13**, 240 (1941).

The most probable path is then that for which

$$\frac{\partial P}{\partial y} = \frac{\partial P}{\partial \psi} = 0 .$$

On solving these simultaneous equations in y and ψ we obtain the following equivalent equations for the most probable path:

$$(2) \qquad \begin{cases} y = [\theta_i x(T-x)^2 - \theta_f x^2(T-x)]/T^2 , \\ \psi = [\theta_i(T-x)(T-3x) + \theta_f x(3x-2T)]/T^2 . \end{cases}$$

Provided θ_i and θ_f are both small compared with unity so that the most probable path does not deviate much from the line AB, we may make the following approximation for the path length:

$$(3) \qquad s = \int_A^B (1+\psi^2)^{\frac{1}{2}}\,\mathrm{d}x ,$$

$$\simeq \int_A^B 1 + \frac{1}{2}\psi^2\,\mathrm{d}x .$$

Eq. (2) and (3) now give

$$(4) \qquad s = T[1 + (2\theta_i^2 - \theta_i\theta_f + 2\theta_f^2)/30] .$$

This result takes account of scattering in one plane only. If the initial and final directions of the path, projected on two orthogonal planes through AB, are θ_i', θ_f' and θ_i'', θ_f'' respectively, the general result is

$$(5) \qquad s = T[1 + \{2(\theta_i'^2 + \theta_i''^2) - (\theta_i'\theta_f' + \theta_i''\theta_f'') + 2(\theta_f'^2 + \theta_f''^2)\}/30] .$$

It has been pointed out that in some cases only the initial and final directions of the track can be considered fixed [1]. Thus, dealing firstly with the two-dimensional case, the directions φ_i, φ_f relative to the normals at the plate boundaries would be known, but not the relative positions of the ends of the path A and B, see Fig. 2.

To deal with this situation we return to eq. (1) and note that if θ and t are fixed, then the most probable displacement, l, is determined by

$$\frac{\partial F}{\partial l} = \frac{\sqrt{3}\omega^4}{2\pi t^2}\left(\frac{3\theta}{t^2} - \frac{6l}{t^3}\right)\exp\left[-\omega^2\left\{\frac{\theta^2}{t} - \frac{3l\theta}{t^2} + \frac{3l^2}{t^3}\right\}\right] = 0 ,$$

which gives

$$l/t = \theta/2 .$$

This does not correspond exactly to the case under consideration because a variation in the final position, B, gives rise to variations in both the displacement, l, and the thickness traversed, t. However, provided that the scattering, $(\varphi_f - \varphi_i)$, is small, we shall neglect the variation in t because it is small compared with the thickness of plate that the particle would have traversed had it not been scattered. Then, since

$$\theta = \varphi_f - \varphi_i ,$$

the most probable position of B will be that which makes the line AB lie at equal inclinations to both the initial and final directions, *i.e.*,

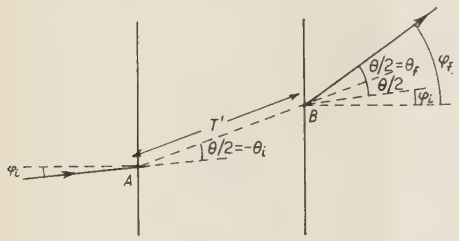

Fig. 2.

$$\theta_i = (\varphi_i - \varphi_f)/2 = -\theta_f , \tag{6}$$

as shown in Fig. 2. Applying this in two orthogonal planes will determine the most probable position of B relative to A.

If T' is the distance AB for this most probable position, eq. (4), (5) and (6) determine the most probable path length,

$$s = T'[1 + (\varphi_i - \varphi_f)^2/24]$$

for scattering in one plane only, and

$$s = T'[1 + (\varphi_i' - \varphi_f')^2/24 + (\varphi_i'' - \varphi_f'')^2/24] ,$$

where φ_i', φ_f'; φ_i'', φ_f'' are the projected angles of the initial and final directions of the track on two orthogonal planes through AB.

Behaviour of Ions in Mass Spectrometers under Pulsed Repeller Voltage Conditions.

A. Galli, A. Giardini-Guidoni and G. G. Volpi

Laboratorio di Spettrometria di Massa del C.N.E.N. - Roma
Istituto di Chimica Generale ed Inorganica dell'Università - Roma

(ricevuto il 7 Ottobre 1960)

In an attempt to analyse the behaviour of ions in the source of our mass spectrometer we have pulsed by means of a square wave the repeller voltage between positive and negative values with respect to the exit slit of the source. If a suitable frequency range is used one would expect to be able to follow the kinetics of approach to steady state conditions of the ionic current corresponding to the positive and negative values of the repeller voltage. From the kinetic parameters useful informations can be obtained on the behaviour of ions and on the conditions of the source. By overimposing the square wave to a negative d.c. potential, it was experimentally found that the ion current recorded, at given frequency, was dependent only on the positive value of V_{rep}, if the negative values were lower than -2.5 V. To evaluate the contribution of the negative part of the wave, we can note that if a d.c. potential is used for the repeller electrode the ion current collected at $V_{rep} = -2.5$ V was 1% of that corresponding to the maximum efficiency ($V_{rep} = 0$). The contribution is therefore negligible and even more so at more negative values of V_{rep}. In our experimental conditions we are therefore observing ions formed during the positive semiperiod only. The frequency interval used was $(0.002 \div 2)$ MHz and the rise time of the wave was about 0.1 μs. Other relevant features of our mass spectrometer have already been published [1].

Representative data are reported in Fig. 1. The experimental results seem to obey an equation of the type:

$$(1) \quad i_T/i_{T\to\infty} = 1 + (\exp[-\alpha T] - 1)/\alpha T,$$

where i_T is the « peak » height at given frequency and $i_{T\to\infty}$ is its extrapolation at zero frequency, *i.e.*, the « peak » height in stationary conditions. Eq. (1) is represented in Fig. 1 as solid lines and the parameter α was chosen so as to give the best fit. The parameter α is found to be dependent on the repeller voltage, on the energy of ionizing electrons and the nature of the gases. At high values of

[1] A. Giardini-Guidoni and G. G. Volpi: *Nuovo Cimento*, **17**, 919 (1960).

ionizing current (89 μA) it appears to increase strongly with the pressure while this dependence desappears at low values (13 μA).

quires the absence of a voltage gradient in the source and it is therefore not readily acceptable in pratice at values of V_{rep} above $+(1 \div 2)$ V. In addition

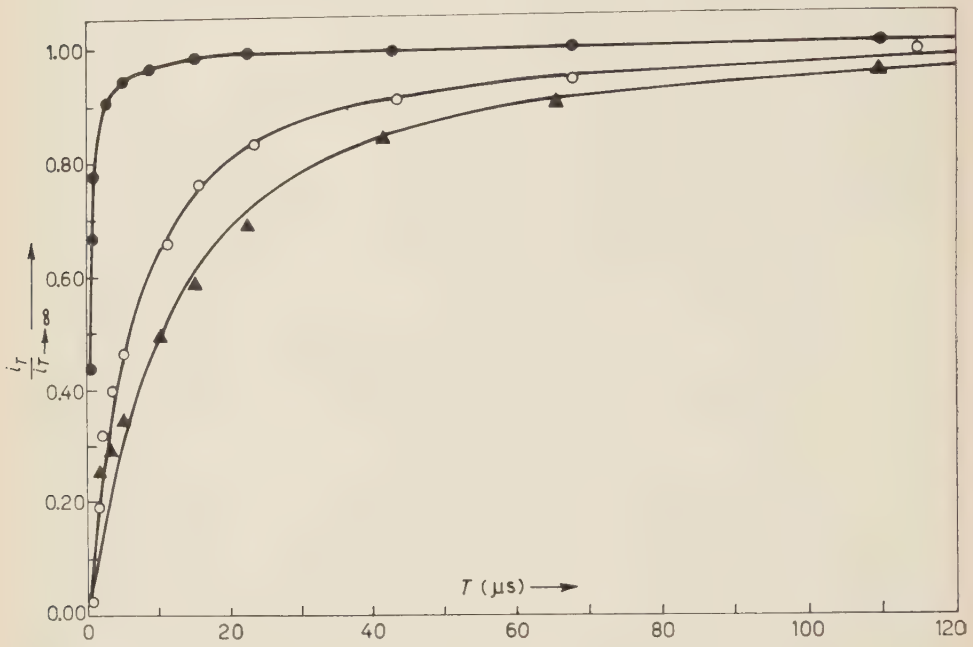

Fig. 1. – Comparison of experimentaldata with eq. (1). Ionizing electron current 89 μA, electron energy 80 eV. ● Argon: pressure in source $4.5 \cdot 10^{-5}$ mm Hg; V_{rep} d.c. $= -1.5$ V, square wave voltage $= \pm$ 10 V; $\alpha = 3 \cdot 10^6\ s^{-1}$. ○ Argon: press. in source $1.5 \cdot 10^{-5}$ mm Hg; V_{rep} d.c. $= -1.5$ V, square wave voltage $= \pm$ 4.0V; $\alpha = 2.5 \cdot 10^5\ s^{-1}$. ▲ Neon: press. in source $2.1 \cdot 10^{-5}$ mm Hg; V_{rep} d.c. $= -1.5$ V, square wave voltage $= \pm$ 4.0 V; $\alpha = 1.5 \cdot 10^5\ s^{-1}$.

Having shown the possibility of following the kinetics of approach to the steady state, we now wish to discuss the above results briefly. Eq. (1) can be obtained if the time dependence of ions in the source obeys the expression:

$$(2) \qquad dn^+/dt = A - \alpha n^+ ,$$

and if the averaging effect of the detector of ions is taken into account. Eq. (2) corresponds to the physical model of a homogeneous concentration of ions throughtout the source. In this model $1/\alpha$ is the average life-time of ions in the source. The model, however, re-

it is difficult to conciliate the simple kinetic expression (2) with the complex dependence of α, as discussed above. When V_{rep} is higher than $+(4 \div 5)$ V, eq. (1) is not the only one to fit the experimental points. These can be equally well fitted by the expression

$$(3) \qquad i_T/i_{T\to\infty} = 1 - 1/\alpha T .$$

It is interesting to note that such an expression can be obtained from a model in which ions produced at the ionization plane are subjected to a constant voltage gradient throughout the source. In practice these conditions should be experi-

mentally approached when V_{rep}, applied externally, is strong enough to render the space charge effect negligible (2). In this case $1/\alpha$ would be the time of direct flight of ions from the formation point to the exit slit.

It is possible that the true kinetic expression is in fact more complicated than shown by eq. (1) or (3), which may represent limiting cases. Unfortunately the averaging effect of the detector makes the experimental data insensitive to the models chosen. Elimination of such a smoothing effect should be of help in the determination of the kinetic equation leading to the steady state and should give us a direct mean to study the behaviour of ions in mass spectrometer sources. Work in this direction is in progress.

(2) W. M. BRUBAKER: *Journ. Appl. Phys.*, **26**, 1007 (1955).

Electroproduction of Schizons.

P. Budini and G. Furlan

Istituto di Fisica dell'Università - Trieste
Istituto Nazionale di Fisica Nucleare - Sottosezione di Trieste

(ricevuto il 10 Ottobre 1960)

The definitive answer to the problem of the existence of an intermediate boson field as a transmitter of the weak interactions will undoubtedly come from experiments.

Thus it is of interest to study the processes which present the most favourable situation for clear-cut answer experiments.

We think that one of these might be the electroproduction of so called schizons and in particular that of negative ones.

The mass of the intermediary boson m_W has to be $> m_K$ mass of the K-meson [1]. If further

$$m_W > m_K + m_\pi \,, \tag{1}$$

then the W-meson can decay in $K+\pi$ and in electron-nucleon collisions one could obtain the apparent process

$$e^- + \mathcal{N} \to K^- + \pi^0 + \mathcal{N} + \nu \,. \tag{2}$$

The competitive process via strong interactions is the production of K pairs; thus if

$$m_K + m_\pi < m_W < 2m_K \,, \tag{3}$$

one could work below the threshold of K pairs production, in this case electroproduction of one single K^- would prove the existence of W^- and constitute a rough measurement of its mass (*).

(1) T. D. Lee and C. N. Yang: in press.

(*) A process based on the same mechanism could also be the apparent K^--production by π^- against a nucleus under the treshold of $K\text{-}\overline{K}$ production via strong interaction. The cross-section turns out to be 10^4 times larger than the one considered in the note. This was suggested to us by professor Dallaporta.

The leptonic decay mode of W^-, especially important when (1) is not satisfied, would give the process

$$e^- + \mathcal{N} \to W^- + \mathcal{N} + \nu \to \mu^- + \tilde{\nu} + \nu + \mathcal{N} . \tag{4}$$

Not far from the threshold of W^- production, μ^- is practically monochromatic ($p_\mu \simeq m_W/2$). The possibility to separate these meson from the continuous spectrum of μ^-, produced via electromagnetic and strong interactions, might depend from experimental possibilities. (If the target is H, then μ^- are produced via strong interactions only after double pion production.)

We have calculated the cross-section for the electroproduction of a negative W-meson in an external electrostatic field

$$A_\mu(q) = \frac{1}{(2\pi)^{\frac{3}{2}}} \frac{n_\mu}{|\bar{q}|^2} F(|\bar{q}|^2) , \qquad n^2 = -1, \tag{5}$$

where $F(|\bar{q}|^2)$ represents the form factor of the source of the external field (*).

The cross-section obtained is rather long to be written down. One has to take care of the sums over the three independent polarizations of the W^- and to this end the general formula can be used

$$\sum_{\alpha=1,2,3} (\varepsilon_\mu^\alpha p_\mu)(\varepsilon_\nu^\alpha q_\nu) = \boldsymbol{p}\cdot\boldsymbol{q} + \frac{(\boldsymbol{k}\cdot\boldsymbol{p})(\boldsymbol{k}\cdot\boldsymbol{q})}{m_W^2} + \frac{1}{m_W^2}(p_0 q_0\, \boldsymbol{k}\cdot\boldsymbol{k} + q_0 k_0\, \boldsymbol{k}\cdot\boldsymbol{p} + p_0 k_0\, \boldsymbol{k}\cdot\boldsymbol{q}) . \tag{6}$$

Considering that the case of interest is only that one near the threshold (when K pairs cannot be produced via strong interactions), we have developed the cross-section in powers of $|k|/m_W$ keeping only the first term. We obtain

$$\begin{aligned} \mathrm{d}\sigma = {} & \frac{\alpha^2}{4\pi^3} \cdot \frac{g_{e\nu}^2}{m_W^2} \frac{k\varepsilon'^2}{|\bar{q}|^4} |F|^2 \,\mathrm{d}\omega\, \mathrm{d}\Omega\, \mathrm{d}\Omega' \left\{ \frac{1}{\left[m_W - 2\varepsilon'((k/m_W)\cos\theta' - 1)\right]^2} \cdot \right. \\ & \cdot \Big\langle \cos\psi(6\varepsilon\varepsilon' - \varepsilon^2 - \varepsilon'^2) + \cos\vartheta(6\varepsilon - 2\varepsilon') + k\cos\vartheta'(6\varepsilon' - 2\varepsilon) + 3\varepsilon^2 + 3\varepsilon'^2 - 2\varepsilon\varepsilon' + \\ & + 2\frac{k}{m_W}(\varepsilon + \varepsilon')(2\varepsilon'\cos\vartheta'\cos\psi + m_W\cos\vartheta + (\varepsilon + \varepsilon')\cos\vartheta') \Big\rangle - \\ & - \frac{4}{\left[m_W - 2\varepsilon'((k/m_W)\cos\vartheta' - 1)\right]\left[1 - (2\varepsilon\varepsilon'/m_W^2)(\cos\psi - 1)\right]} \Big\langle 3(\varepsilon + \varepsilon')\cos\psi + \\ & + k(3\cos\vartheta - \cos\vartheta') - 9\varepsilon - \varepsilon' - \frac{2k}{m_W}\left[3\varepsilon(\cos\vartheta + \cos\vartheta') - \varepsilon'\cos\vartheta'(1 + \cos\psi)\right] \Big\rangle + \\ & \left. + \frac{4}{\left[1 - (2\varepsilon\varepsilon'/m_W^2)(\cos\psi - 1)\right]^2} \Big\langle 3 - \cos\psi + \frac{2k}{m_W}(\cos\vartheta + \cos\vartheta') \Big\rangle \right\} , \end{aligned} \tag{7}$$

(*) Considering that the three dimensional transmitted impulse $|\bar{q}|$ is $\gtrsim m_W$ one should introduce also the form-factor of W^- in the graph where the W^- interacts with the external fied, the same applies also to the inverse process with incoming neutrino (2).

(2) T. D. Lee and C. N. Yang: *Phys. Rev. Lett.*, **4**, 307 (1960).

where p, p', k are the momenta of the electron, neutrino and meson respectively and ψ is the angle between $\boldsymbol{p}$ and $\boldsymbol{p}'$, ϑ the angle between $\boldsymbol{p}$ and $\boldsymbol{k}$, and ϑ' that between $\boldsymbol{p}'$ and $\boldsymbol{k}$.

If we integrate over the angles and over the energy of the emitted « schizon », we obtain for the total cross-section

$$\left.\begin{aligned} \sigma_{\text{tot}} &\simeq 1.2\cdot 10^{-38}\ \text{cm}^2 \times |F(\tilde{q}^2)|^2\,, \\ &\simeq 4.3\cdot 10^{-38}\ \text{cm}^2 \times |F(\tilde{q}^2)|^2\,, \end{aligned}\right\} \tag{8}$$

assuming $\varepsilon = 1$ GeV, $m_{\text{W}} = 0.5$ GeV and $k/m_{\text{W}} = \frac{1}{5}$, $\frac{1}{3}$ respectively. $\tilde{q}$ represents the mean transmitted impulse.

For a complex (*light*) nucleus and coherent scattering one could substitute

$$|F(\tilde{q}^2)|^2 \to Z^2\,|F_z(q^2)|^2\,. \tag{9}$$

So doing, with $Z = 26$ and $F = 1$, we obtain a relatively high cross-section $\sigma_{\text{tot}} \sim \sim 10^{-35}$ cm^2, which is of the same order of magnitude as the cross-section for W production in neutrino capture experiments ([2]). But considering that the minimum value of $|\bar{q}|$ ranges from m_{W} to $\frac{3}{2}m_{\text{W}}$ $\left(|\bar{q}|\ \text{min} = m_{\text{W}}\left((2m_{\mathcal{N}} - m_{\text{W}})/2(m_{\mathcal{N}} - m_{\text{W}})\right)\right)$ depending from the masses m_{W} of the W-meson and $m_{\mathcal{N}}$ of the target, the nucleus will in most cases undergo strongly inelastic scattering and the nucleons of the nucleus will behave in the process as if they were free. (The same applies also, in our opinion, to the inverse process.) Further, since at these values of $|\bar{q}|$ one has from electron-nucleon elastic scattering experiments ([3]) $\sigma_{\text{n}} \sim \sigma_{\text{p}}$, we will take for complex nuclei, the total cross-section

$$\sigma = A\,|F(\tilde{q}^2)|^2 \sigma_{\mathcal{N}}\,, \tag{10}$$

that is, for $A = 200$ and $|F|^2 \simeq \frac{1}{10}$ (see (3)),

$$\sigma_{\text{tot}} \simeq 2\cdot 10^{-37}\ \text{cm}^2\,,$$

$$\simeq 0.86\cdot 10^{-36}\ \text{cm}^2\,.$$

This cross-section should be considered as a lower limit to the true one. In fact we have taken into account only the static contribution of the nuclear electromagnetic field. If the magnetic moment contribution should be of the same order of magnitude as in the elastic scattering processes one should multiply the cross-section by a factor greater then five at the values of q^2 considered.

In order to obtain the cross-section for K^-- and μ^--production one has to take into account the decay rates of the W-meson, this means that one should still multiply (10) by a factor smaller than $\frac{1}{5}$, depending on the mass of the W-meson, for the process (2) and of the order of magnitude of $\frac{1}{5}$ of the process (4).

([3]) R. HOFSTADTER: *Ann. Rev. of Nucl. Sci.* (1957).

Search for Electrons from Muon Capture.

M. Conversi, L. di Lella, A. Egidi, C. Rubbia (*) and M. Toller

Istituto di Fisica dell'Università - Roma
Istituto Nazionale di Fisica Nucleare - Sezione di Roma

(ricevuto il 10 Ottobre 1960)

In spite of their occurrence not being incompatible with any of the well-established conservation laws, none of the processes $\mu \to e+\gamma$ (1); $\mu \to 3e$ (2); and $\mu^-+p \to p+e^-$ or $\mu^-+n \to n+e^-$ (3) has been observed as yet. Upper limits of the order of 10^{-6} and 10^{-5} respectively have been reported for the branching ratios of (1) [1] and (2) [2] relative to ordinary muon decay. Processes (3) have been searched for by letting μ^--mesons be captured in a Cu target [3]. An upper limit of $5 \cdot 10^{-4}$ has been reported for the branching ratio

$$(4) \qquad R = \frac{\text{Rate of } \mu^-+\text{Cu} \to \text{Cu}+e^-}{\text{Rate of } \mu^-+\text{Cu} \to \text{Ni}+\nu} .$$

A closer investigation of the degree of « forbiddeness » of processes (3) seemed desirable in view of the following arguments: *a*) the present status of the theory of weak interactions demands a close examination of all possible decay and capture modes of the muon; *b*) it has been shown on theoretical grounds [4] that independently of any specific model (such as the hypothesis of a charged vector boson responsible for the transmission of the weak interaction), processes (3) might occur even if (1) is somehow completely forbidden; *c*) the possibility that μ^- nuclear absorption occurs coherently [4] makes an experiment of this kind far more sensitive as a test of a possible μ-e-γ interaction than one would otherwise expect.

With this in mind we have performed an experiment capable of showing the existence of processes (3), if the branching ratio (4) were larger than a few times 10^{-6}. The experiment has been carried out with the low-energy muon beam recently developed at CERN [5]. About 95% of the particles of this beam are muons of

(*) Now at CERN, Geneva, Switzerland.

(1) J. Ashkin, T. Fazzini, G. Fidecaro, N. H. Lipman, A. W. Merrison and H. Paul: *Nuovo Cimento*, **14**, 1266 (1959); D. Berley, J. Lee and M. Bardon: *Phys. Rev. Lett.*, **2**, 357 (1959); also for previous work.

(2) J. Lee and N. P. Samios: *Phys. Rev. Lett.*, **3**, 55 (1959).

(3) J. Steinberger and H. B. Wolfe: *Phys. Rev.*, **100**, 1490 (1955); also for previous work.

(4) S. Weinberg and G. Feinberg: *Phys. Rev. Lett.*, **3**, 111, 244 (1959); N. Cabibbo and R. Gatto: *Phys. Rev.*, **116**, 1334 (1959).

(5) A. Citron *et al.*: *Berkeley Meeting* (September 1960). We wish to acknowledge the co-operation of all members of the Citron group who have developed this beam.

energy around 60 MeV. After going through a bending magnet and a Pb collimator, the beam crosses a graphite moderator (Fig. 1) experimentally chosen to get a maximum for μ^--stops ($\sim 3\,700$ stops/s) in the target T. This is a 0.5 cm thick Cu sheet (at 45° to the beam direction) in which a fraction $f=0.92$ of the stopped μ^--mesons are captured ([6]). Furthermore, for Cu coherent capture is expected to be at least six times more probable than incoherent capture ([4]), so that the energy spectrum of the « capture electrons » should be sharply peaked slightly above 100 MeV.

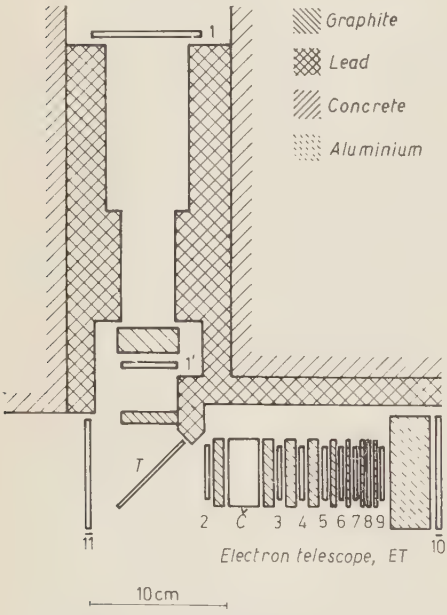

Fig. 1. – Experimental set-up. T is a Cu sheet 0.5 cm thick. For protection against cosmic ray showers, another plastic scintillator (counter 12, not shown in the figure) was placed horizontally above ET, separated from the latter by 2 cm of Pb.

Counters 1, 1′, 2, 3, ..., 11, 12 (12 is not shown in Fig. 1) are plastic scintillators; $\check{C}$ is a Čerenkov counter made of lucite. All but the two monitoring counters 1, 1′ and the « guard counter » 12, belong to what we shall call the electron telescope, ET, containing eight graphite absorbers (total thickness 20.4 g/cm²) and protected all around by thick walls of heavy concrete. Coincidences among the first three, five, six, ..., nine counters of the ET (counted starting from counter 2) are scaled, if in anticoincidence with counters 1, 11 and if occurring during the ~ 400 μs long machine bursts. The 7-fold coincidences also trigger the sweep of an oscilloscope, 1 μs long, on which pulses from counters 7, 8, 9, 10, 12 and the coincidence pulses 1.1′ are displayed with appropriate delays. For an 8-fold or a 9-fold coincidence to be classified as « good » and recorded as a possible capture electron, the presence on the sweep of a pulse $1\cdot1'$ is required, and the absence of pulses from counters 10 and 12. Furthermore, the position of pulse $1\cdot1'$ on the picture of the oscilloscope trace must correspond to a μ^--stop followed by electron emission within the time interval from ~ 15 to 500 ns. For a μ^- lifetime in Cu of 160 ns ([6]), only a fraction $\alpha=0.87$ of events are thus accepted.

If emitted from T within the solid angle of acceptance of ET ($\omega=0.07$ sr for 8-fold coincidences), a capture electron would, in general, cross most of the counters from 2 to 9 and stop in the 8 cm thick Al absorber placed between counters 9 and 10. In order to determine the detection efficiency of ET for such high-energy electrons, $\bar{\varepsilon}$, its efficiency for monochromatic electrons of various energies from 70 to 110 MeV has been measured ([7]). Energy losses in T have been taken into account making measurements with Cu sheets of different thicknesses in front of ET.

([6]) J. C. SENS: *Phys. Rev.*, **113**, 679 (1959).

([7]) Thanks are due to Dr. R. C. HANNA for his help in the preparation of the electron beam used in these measurements.

The most significant results are shown in Fig. 2, from which we get $\bar{\varepsilon}=0.14$ for 8-fold coincidences.

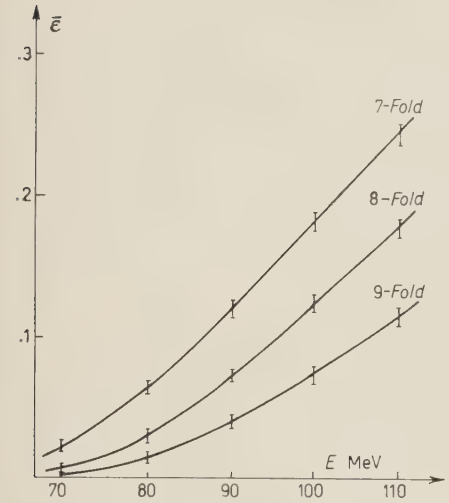

Fig. 2. – Detection efficiency of ET for electrons of various energies emerging from a Cu sheet of thickness 3.5 mm, equivalent to half the effective thickness of T. E is the energy of the electrons incident on the Cu sheet.

On the other hand, the efficiency of ET for decay electrons of μ^--mesons which have escaped nuclear absorption in Cu is very low (less than 10^{-5} for electrons which cross all counters from 2 to 7 included) and exhibits experimentally a fast decrease with increasing telescope thickness. Thus ET enables an extremely sharp distinction between capture electrons (energies around 100 MeV) and decay electrons (maximum energy ~ 53 MeV, apart from second order effects due to the motion of the μ^--meson in the Bohr orbit).

The results of 47 runs of 1 h each are summarized in Table I. The performance of the whole apparatus was frequently checked through measurements without graphite absorbers in ET. Under these conditions large numbers of coincidences due to decay electrons were recorded. In particular, from 3-fold coincidences $2.\check{C}.3$ measured with and without a C target equivalent to the Cu target T, and from the total number of monitors $1\cdot 1'$ recorded in the above-mentioned 47 runs, the total number, N, of muons stopped in T was found to be $N=6.26\cdot 10^8$, No « good » 8-fold coincidence has been correspondingly recorded.

If $m(R)$ is the average number of 8-fold coincidences expected for a given value R of the branching ratio (4), then the probability of this negative result depends on R as $\exp[-m(R)]$ if a Poisson distribution is assumed. An explicit expression of $m(R)$ is clearly

$$m(R)=Nf\alpha(\omega/4\pi)\bar{\varepsilon}R+\bar{b}=3.91\cdot 10^5\,R+\bar{b}\,,$$

where $\bar{b}$ represents the total expected background (estimated to be of the order of 1 event) due both to decay

TABLE I. – *Results of* ~ 47 h *of measurements taken with the* Cu *target* T (Fig. 1). All n-fold coincidences ($n=3, 5, 6, \ldots 9$) are recorded when in anticoincidence with counters 1 and 11 and if occurring during the machine bursts, ~ 400 μs long. « Good coincidences » are those in which no pulse from counters 10 and 12 appears on the oscilloscope trace while a pulse $1\cdot 1'$ is present there in a position corresponding to a μ^- stop followed by electron emission within the time interval from ~ 15 to 500 ns.

Type of event	$1\cdot 1'$	3-fold	5-fold	6-fold	7-fold	8-fold	9-fold
Total number	$1.56\cdot 10^9$	207 305	695	62	33	18	7
Number of « good coincidences »			—	—	5	0	0

electrons capable of giving an 8-fold coincidence and to random 8-fold events. If no attempt is made to take into account this background we conclude that

$$R < 5.9 \cdot 10^{-6},$$

with 90% confidence level (*).

This conclusion holds for a mixture 6 to 1 of coherent and incoherent captures (4) to which the value $\bar{\varepsilon} = 0.14$ refers. In the case of purely incoherent capture the result depends on the energy left to the nucleus. Assuming 15 MeV of average nuclear excitation we find $\bar{\varepsilon} = 0.06$ and therefore $R < 1.4 \cdot 10^{-5}$.

Our result is quite consistent with that very recently found by SARD *et al.* (8) who, using a different technique in an experiment of comparable sensitivity, have recorded, however, three events of the type searched for, whereas the total expected background is estimated to be 0.23 ± 0.04.

(*) For a comparison with the result of STEINBERGER and WOLFE (3) we should derive the upper limit R^* of R from the condition $\exp[-m(R - R^*)] \approx 0.27 \exp[-m(R = 0)]$, which yields

$$R \quad 3.1 \cdot 10^{-6}.$$

(8) R. D. SARD, K. M. CROWE and H. KRUGER: (to be published).

K-Conversion Coefficients of $E2$ Transitions (*).

M. K. Ramaswamy

Department of Physics, Ohio State University - Columbus, O.

(ricevuto il 10 Ottobre 1960)

Recently Subba Rao (1) has collected and analyzed the data on the K-conversion coefficients of pure $E2$ transitions from the first excited state to the ground state of even-even nuclei (2^+-0^+). Plotting the ratio $R(\alpha_K)$ of the α_K (experimental) to α_K (theory) as a function of the mass number A, he concluded that the K-conversion coefficients may possibly depend on the deformation of the nucleus.

There is known to exist another class of pure $E2$ transitions of the type 0^+-2^+ in even-even nuclei. In this note we carry out an analysis similar to that done by Subba Rao (1) for 0^+-2^+ transitions. Table I lists all the nuclei for which α_K has been measured. There are other cases, namely, ^{12}C, ^{42}Ca, ^{70}Ge and ^{214}Po for which no experimental data on α_K exist.

In Table I, the first column lists the nucleus, the second the energy of the $E2$ transition, the third column the measured value of α_K, the fourth column the theoretical values of α_K taken from

Table I. – 0^+-2^+ $E2$ *transitions.*

Nucleus	Energy of $E2$ transition (keV)	α_K (exp)	α_K (theory)	$R(\alpha_K)=\frac{(\alpha_K)\,\mathrm{exp}}{(\alpha_K)\,\mathrm{theory}}$	β	$R(\alpha_K)$ for 2^+-0^+
^{106}Pd	621	$19.1\cdot10^{-4}$ (*a*) (*)	$27.9\cdot10^{-4}$	0.68 ± 0.14	—	—
^{152}Sm	563	$(9\pm2)\cdot10^{-3}$ (*b*)	$7.8\cdot10^{-3}$	1.15 ± 0.26	0.28	1.08 ± 0.16
^{152}Gd	271	$(50\pm20)\cdot10^{3}$ (*b*)	$62\cdot10^{-3}$	0.81 ± 0.32	0.2	0.84 ± 0.21
^{166}Er	1 379	$17\cdot10^{-4}$ (*a*) (*)	$14.6\cdot10^{-4}$	1.17 ± 0.23	0.33	1.18 ± 0.12

(*) A 20 % error has been assigned arbitrarily in plotting on Fig. 1.

(*a*) Nuclear data sheets, National Research Council, Washington, D.C.: for ^{106}Pd α_K has been calculated from the total β-branching.

(*b*) I. Marklund, O. Nathan and O. B. Nielsen: *Nucl. Phys.*, **15**, 199 (1960).

(*) Supported by the U. S. Atomic Energy Commission.

(1) B. N. Subba Rao: *Nuovo Cimento*, **17**, 189 (1960).

Sliv and Band (2), the fifth column the ratio $R(\alpha_K)$ and the sixth column the deformation parameter β and the last column the value of $R(\alpha_K)$ for 2^+-0^+ transition in the same nucleus taken from Subba Rao (1).

Fig. 1 is a plot of $R(\alpha_K)$ as a function of mass number A for the four cases

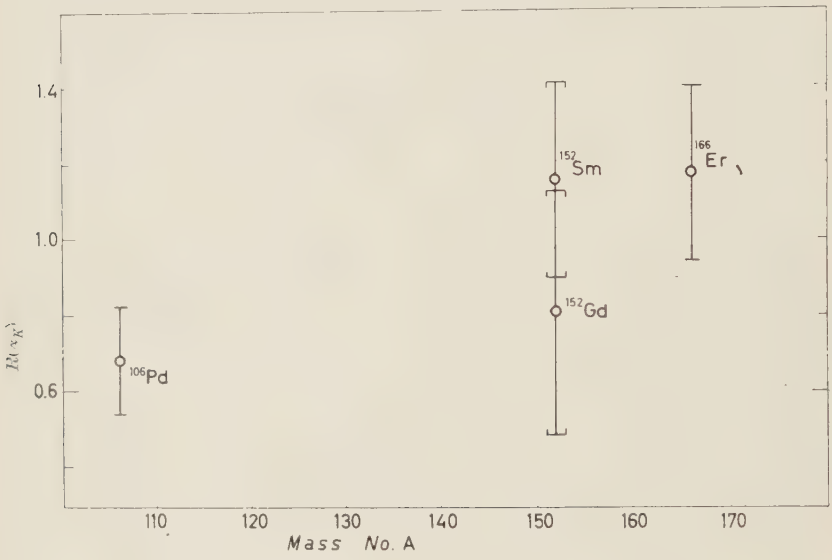

Fig. 1. – Plot of $R(\alpha_K)$ as a function of mass number A.

listed in Table I. For ^{106}Pd and ^{166}Er a 20% error has been assigned for α_K.

(2) L. A. Sliv and I. M. Band: Leningrad Physico-Technical Institute Report (1956) (translation: University of Illinois Report 57ICCKI, unpublished).

We may make the following observations:

1) One needs more cases with better statistics.

2) The ratios for 2^+-0^+ and 0^+-2^+ transitions in the same nucleus are consistent within the statistical errors assigned.

3) For ^{106}Pd the ratio falls below unity which is compatible with other spherical nuclei listed by Subba Rao.

In conclusion it may be remarked that the dependence of α_K on deformation may be real and it will be interesting to find a theoretical explanation.

A Note Concerning the Magnetic Moment of the Muon (*).

N. Byers and F. Zachariasen (**)

Institute of Theoretical Physics, Department of Physics, Stanford University - Stanford, Cal.

(ricevuto il 17 Ottobre 1960)

In view of the recent interest in the existence of a vector boson (χ) intermediary for the weak interactions, we should like to report a calculation of the effect of such a particle on the magnetic moment of the muon. If a charged vector field mediates in μ-decay, a contribution to the magnetic moment of the muon much larger than that due to the Fermi interaction occurs (it is proportional to G, the Fermi coupling constant, rather than G^2).

The calculation was performed using a dispersion relation for the vertex $\gamma \to \mu^+ + \mu^-$ which is the interesting quantity. The only relevant intermediate state, to lowest order in the weak interactions, is the $\chi^+\chi^-$ state. In computing the absorptive part of the vertex function, the amplitudes $\gamma \to \chi^+ + \chi^-$ and $\chi^+ + \chi^- \to \mu^+ + \mu^-$ were replaced by their perturbation theory values. This, of course, yields the same answer as ordinary perturbation theory. An unsubtracted dispersion relation must be used to compute the anomalous moment; the unsubtracted dispersion integral diverges logarithmically in agreement with the usual perturbation theory result.

If the same neutrinos are emitted in β-decay and μ-decay, the process $\mu \to e + \gamma$ is also described by basically the same vertex. It then follows that there is a relation between the anomalous moment due to the χ-particle (μ_χ) and the $\mu \to e + \chi$ decay rate ($1/\tau_\gamma$) which is independent of the divergent integral. If $M_\chi^2 \gg m_\mu^2$, one has

$$\mu_\chi = \sqrt{(8\pi^2/m_\mu^2)(1/\tau_\gamma)} \,. \tag{1}$$

Apart from this relation, it is necessary to cut off the integral in order to obtain a finite result for either μ_χ or $1/\tau_\gamma$ [1]. The moment and rate then depend on the value of the cut-off. It is amusing, though hardly of significance, to note that the dispersion method of calculation requires that the cut-off Λ be greater than $2M_\chi$, since $4M_\chi^2$ is the lower limit of the dispersion integral. The $\mu \to e + \gamma$ decay rate is, if the dispersion method of calculation is taken seriously, iden-

(*) Supported in part by the United States Air Force through the Air Force Office of Scientific Research.

(**) Present address: Department of Physics, California Institute of Technology, Pasadena, Cal.

(1) G. Feinberg: *Phys. Rev.*, **110**, 1482 (1958); M. E. Ebel and F. J. Ernst: *Nuovo Cimento*, **15**, 173 (1960); taking $I \approx 1$, we obtain $\varrho \approx 10^{-3}$ from equation 2 and 3.

tically equal to zero if Λ is precisely $2M_\chi$. By choosing Λ sufficiently close to $2M_\chi$, $1/\tau_\gamma$ can be made as small as one desires.

Numerically, the following results were obtained. First, if the neutrinos in β-decay and μ-decay are identical, eq. (1) yields

$$\mu_\chi = (e/2m_\mu)\sqrt{\varrho}\,8.4\cdot 10^{-8}\,, \tag{2}$$

where ϱ is the branching ratio for $\mu \to e+\gamma$. If the experimental upper limit for ϱ is used ($\varrho < 10^{-6}$), one then has $\mu_\chi < 3\cdot 10^{-10} e/2m_\mu$. Our calculated value of ϱ agrees with the earlier results [1].

If the $\mu \to e+\gamma$ decay is forbidden because the neutrino in β-decay is not identical to that in μ-decay, our calculation of μ_χ is

$$\mu_\chi = (e/2m_\mu)(gm_\mu/M_\chi)^2(I/32\pi^2)\,, \tag{3}$$

where I is the divergent integral which, if cut off at Λ^2, is approximately equal to $\ln(\Lambda/2M_\chi)$ if $\Lambda^2 \gg m_\mu^2$; g is the $\chi\mu\nu$ coupling constant ($G=g^2/M_\chi^2$). Taking $I=1$, we find $\mu_\chi \approx 10^{-9} e/2m_\mu$. As is only to be expected, this is much too small to be seen at present; it is of the order of the sixth-order electromagnetic moment contribution.

Remarks on a Paper by Bialynicki-Birula on Some Properties of Green's Functions.

E. R. Caianiello

Scuola di Perfezionamento in Fisica Teorica e Nucleare - Napoli

(ricevuto il 3 Novembre 1960)

In a recent work (1) I. Bialynicki-Birula demonstrates that some equations among propagation kernels, or Green's functions, of field theory, derived several years ago (2) by this writer and used since in a series of mathematical works (3) aiming at a rigorous formulation of field-theoretical questions, can be obtained quite trivially by means of functional methods.

The purpose of this note is not to comment upon this fact, which is trivial indeed, and as such was referred to several times (4). In the literature of the early fifties there is no shortage of formal derivations of similar results (*e.g.*, a good deal of attention was given also to the functional derivatives of $\lg \langle S \rangle_0$, instead of $\langle S \rangle_0$). Explicit indications were also given in ref. (2), Sect. **4** and **4**-*b*), as a side remark, on the possible use for this purpose of a functional technique which may be at times advantageous, because it involves differentiation with respect to free modes or propagators rather than to external sources.

Our purpose is rather to point out once more, in the hope of avoiding future misunderstandings, that, while the formal derivation of any such equation does certainly reduce to a straightforward exercise (for which a good variety of methods are available!), things stand quite differently when the aim is mathematical rigor as well as simplicity. Notation becomes then a matter of importance, and the relevant things are, first the choice of the quantities which are best suited to the quantitative investigations of interest, and thereafter the precise formulation and study of the difficulties which are met thereby.

There is a far cry, for instance, from hyperbolic differential equations to the « corresponding » integral equations, nor do the first alone suffice at all to define kernels, or Green's functions, correctly (5); when something wrong is done in the

(1) I. Bialynicki-Birula: *Nuovo Cimento*, **17**, 951 (1960).

(2) E. R. Caianiello: *Nuovo Cimento*, **11**, 492 (1954).

(3) E. R. Caianiello: *Nuovo Cimento*, *passim*, from 1954 on.

(4) E. R. Caianiello: *Nuovo Cimento*, **11**, 492 (1954); **10**, 739 (1957); *Collôque sur les Problèmes Mathématiques de la Théorie Quantique des Champs* (Lille, June 1957).

(5) E. R. Caianiello: *Nuovo Cimento*, **14**, 185 (1959).

transition, hosts of troubles appear, which it would be hardly fair to blame exclusively on the physics. For all such purposes, functional methods are definitely inadequate, at least in their present shape.

To our knowledge, the first complete and explicit connection between the kernels defined in ref. [2] and standard functional derivatives is due to D. J. CANDLIN [6], who gave, besides all the results of ref. [1], also elegant remarks on some other points discussed in ref. [2].

[6] D. J. CANDLIN: *Nuovo Cimento*, **12**, 380 (1954).

The Frascati Storage Ring.

C. Bernardini, G. F. Corazza, G. Ghigo
Laboratori Nazionali del CNEN - Frascati

B. Touschek
Istituto di Fisica dell'Università - Roma
Istituto Nazionale di Fisica Nucleare - Sezione di Roma

(ricevuto il 7 Novembre 1960)

It was decided in a program meeting held in February 1960 in Frascati to study the possibility of a colliding beam experiment with electrons and positrons. The discussion of this proposal led to the design of the machine, which we want to describe briefly in this letter.

Electrons and positrons of 250 MeV each are stored in a DC weak focussing magnet. The electrons and positrons circulate on the same orbit (this is guaranteed by the *TCP* theorem) meeting in the gap of the radio frequency and in the neighbourhood of three other points spaced along the orbit at 90° from one another. The particles are produced by converting the γ-rays of the Frascati electron synchrotron on two targets placed inside the acceleration chamber and alternately exposed to the beam.

The magnet (which weights about 8 tons) as well as the arrangement of the acceleration chamber are shown in the figures. The orbit contains four « quasi-straight » (weak field) sections, 18 cm in length, accommodating respectively the radiofrequency, injection ports and the « experimental section » in which about one quarter of all the interactions between electrons and positrons should become observable. The doughnut is made of stainless steel and it is intended to evacuate to about 10^{-10} mm giving a lifetime of 250 h to either beam.

The magnet which at the moment is being assembled at Terni is scheduled to arrive at Frascati in November 1960. Magnetic measurements will be carried out in December and work on the beam should start by the middle of January. In the first period of operation we intend to study the process of injection with the purpose of finding an optimal target arrangement. Electrons and positrons will be registered by observing their synchrotron radiation.

Application of a statistical theory of the injection process shows that only about 5 electrons/s should be accumulated in the ring. This means that in 100 h of charging one should be able to accumulate about $1.8 \cdot 10^6$ electrons. To observe 1 pulse per minute of the mon-

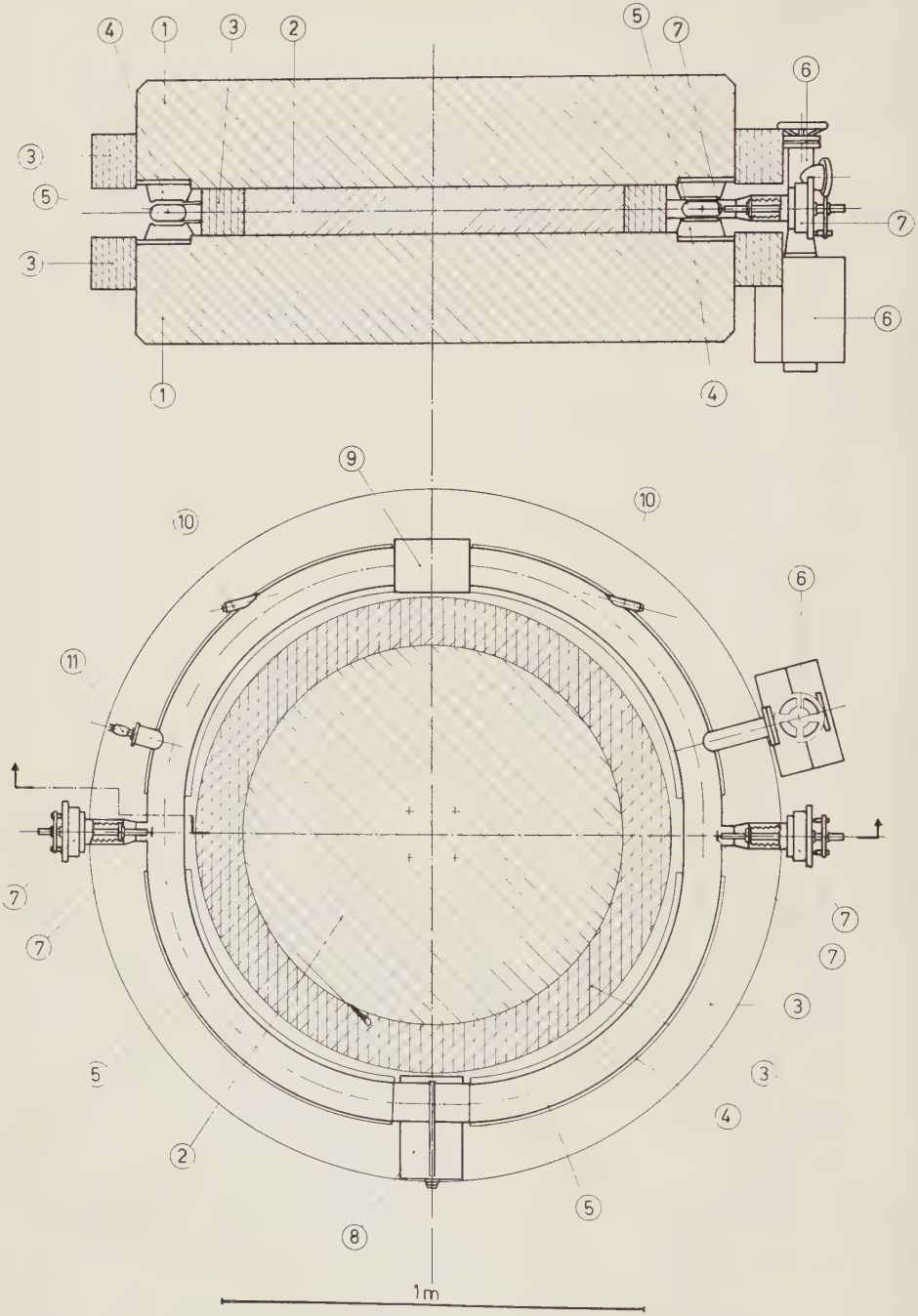

Fig. 1. – Elevation and plan section of the Frascati Storage Ring (anello di accumulazione = AdA): 1) magnet yoke; 2) magnet core; 3) coils; 4) polepieces; 5) doughnut; 6) titanium pump; 7) injection ports; 8) RF cavity; 9) experimental section; 10) windows for the observation of the synchrotron radiation; 11) vacuum gauge.

itoring reaction

$$e^+ + e^- \to 2\gamma ,$$

one has to accumulate about 10^8 particles of either kind. Defining as a « successful » ring one which gives more than 1 pulse per minute of the monitoring reaction it is seen that according to the statistical theory the machine should not be successful by a factor of about 50. To bridge this gap it is hoped that we can profit from some of the following factors:

Distance synchrotron — storage ring	5
Non linear injection effects	10
Target improvements	20
Improved synchrotron intensity . .	4

With a successful machine a study of the pion-pion interaction in the process

$$e^+ + e^- \to \pi^+ + \pi^- ,$$

seems possible and feasible — provided that this interaction is strong enough —; the production of muon pairs in an experiment intended as a check of quantum electrodynamics will require a higher intensity (by about a factor 10). If such an intensity can be achieved the measurement of the π^0 lifetime by means of the reaction

$$e^+ + e^- \to \pi^0 + \gamma ,$$

does not seem completely impossible.

The following is a list of data concerning the beams circulating in the ring:

Length of orbit	408	cm
Radio frequency ($k=2$)	147	MHz
Radio voltage	10	kV
Length of bunches . . .	16.7	cm
Radial width of bunches	.22	cm
Height of bunches (at 10^{-10} mm)	$5.6 \cdot 10^{-4}$	cm
Radiation loss/revolution	580	eV
Lifetime of beam at 10^{-10} mm	250	h

* * *

It is a pleasure to give our thanks for valuable help in the planning and execution of the project to the staff of the National Physical Laboratories in Frascati and in particular to Dr. Sacerdoti for the design of the magnet and to Dr. Puglisi for his work on the radio-frequency.

Determination of the Hyperfine Structure of Atomic Nitrogen by Continuous Optical Orientation (*).

W. W. Holloway jr. and E. Lüscher

Department of Physics, University of Illinois - Urbana, Ill.

(ricevuto il 9 Novembre 1960)

Several experiments have been reported [1-4] in which the hyperfine structure of atomic nitrogen has been determined by optical orientation with spin-exchange. The production of atomic nitrogen in these experiments was accomplished by a pulsed r.f. discharge. The discharge dissociated the molecular nitrogen which was used as a buffer gas in the resonance bulb. In an effort to improve the experimental accuracy by avoiding the large transients associated with this method, an arrangement for providing a continuous supply of atomic nitrogen has been used. Certain of the experimental results are consistent with the computation by Das and Mukherjee [5] of the magnetic interaction constant of atomic nitrogen.

The experimental technique of atomic orientation by optical pumping with spin-exchange and the monitoring of the orientation by the transmission method has been described elsewhere [1,2] and will not be repeated here. Important departures from the previous experiments include a smaller resonance bulb (250 cm^3) to reduce the effect of inhomogeneities in the magnetic environment, the use of Cesium as the optical pumping agent, and the arrangement for supplying atomic nitrogen to the resonance bulb continuously. To supply the atomic nitrogen, tubing from the resonance bulb was connected to a Welch Duo-Seal vacuum pump, which served to circulate N_2 gas at a pressure of 1 cm Hg. The molecular N_2 was used both as a buffer gas and as a source of atomic nitrogen. An air-cooled r.f. electrodeless discharge some 20 cm from the resonance bulb dissociated an appreciable fraction of the molecular nitrogen and the atomic nitrogen was carried into the resonance bulb by the flow of gases.

(*) This research was supported in part by the Office of Naval Research and by the National Science Foundation.

This letter is based upon a dissertation submitted by one of us (W.W.H.) in partial fulfilment of the requirements for the Ph. D. degree at the University of Illinois.

(1) W. W. Holloway jr. and R. Novick: *Phys. Rev. Lett.*, **1**, 367 (1958).

(2) L. W. Anderson, F. M. Pipkin and J. C. Baird jr.: *Phys. Rev.*, **116**, 87 (1959).

(3) N. Knable, W. W. Holloway jr. and R. Novick: *Bull. Am. Phys. Soc.*, **4**, 259 (1959).

(4) W. W. Holloway jr., N. Knable and R. Novick: *Proc. of the Ann Arbor Conference on Optical Pumping* (June 1959), p. 13.

(5) T. P. Das and A. Mukherjee: to be published in the *Journ. Chem. Phys.*

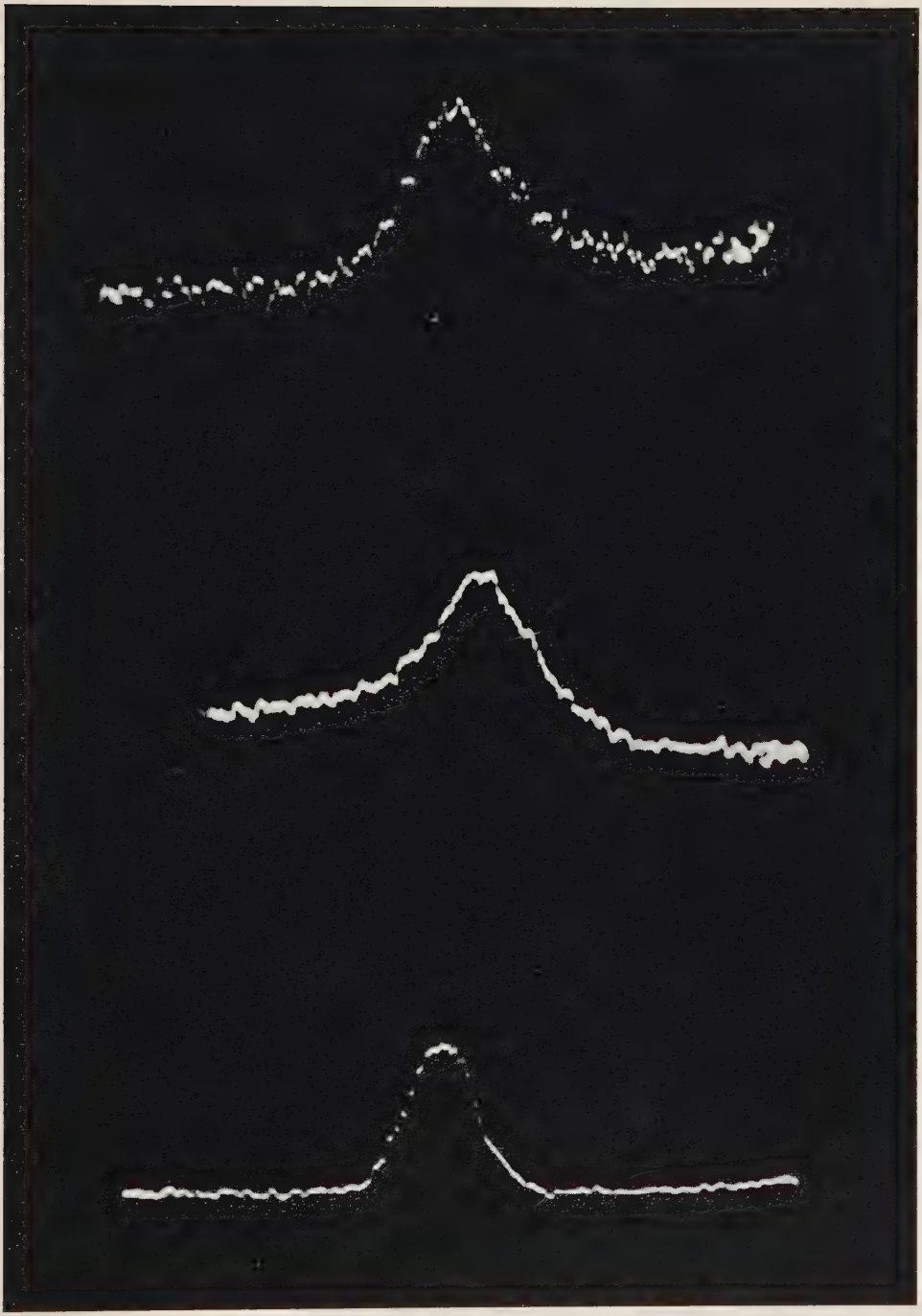

Fig. 1. – Resonances observed in atomic nitrogen at a magnetic field of 12 mOe. The time-scale of one trace is 1.5 s. Upper trace: unresolved Zeeman resonances of the $F = \frac{5}{2}$ state of ^{14}N. Middle trace: hyperfine transition between the $(\frac{5}{2}; \frac{5}{2})$ and the $(\frac{3}{2}; \frac{3}{2})$ states of ^{14}N. Bottom trace: hyperfine transition between the (2, 1) and the (1, 0) states of ^{15}N.

The ground state of ^{14}N ($I=1$, $J=\frac{3}{2}$) consists of three hyperfine levels having total angular momentum values of $F=\frac{5}{2}$, $\frac{3}{2}$ and $\frac{1}{2}$, while the ground state of ^{15}N ($I=\frac{1}{2}$, $J=\frac{3}{2}$) has two hyperfine levels with the total angular momentum values of $F=2$ and $F=1$. All of the Zeeman transitions ($\Delta F=0$ and $\Delta M_F=\pm 1$) and all of the σ-hyperfine transitions ($\Delta F=\pm 1$ and $\Delta M_F=\pm 1$) were observed with characteristic resonances shown in Fig. 1.

The line width is apparently limited by inhomogeneities in the magnetic field with a variation of approximately 1 mOe over the volume of the bulb.

The zero-field splitting, found by correcting the measured transition frequencies for the magnetic field are:
for ^{14}N

$$\nu(\tfrac{5}{2}\text{-}\tfrac{3}{2}) = (26\,127\,325 \pm 125)\ \text{Hz}\,,$$

$$\nu(\tfrac{3}{2}\text{-}\tfrac{1}{2}) = (15\,676\,380 \pm 75)\ \text{Hz}\,,$$

and for ^{15}N

$$\nu(2\text{-}1) = (29\,290\,950 \pm 100)\ \text{Hz}\,.$$

No pressure shift was observed in ^{14}N; the estimated limit is less than 60 Hz per cm Hg. The error quoted above for the transition frequencies is two times the standard deviation.

With these experimental results, the hyperfine structure constants can be calculated as follows:

^{14}N: $|A(14)| = (10\,450\,928 \pm 45)$ Hz,

for the magnetic h.f.s. coupling constant,

$$|B(14)| = (5 \pm 35)\ \text{Hz}\,,$$

for the quadrupole coupling constant,

^{15}N: $|A(15)| = (14\,645\,475 \pm 50)$ Hz,

for the magnetic h.f.s. coupling constant. The hyperfine structure anomaly Δ is defined by

$$1 + \Delta = \frac{A(14)\,g(15)}{A(15)\,g(14)}\,.$$

Using the value for $g(14)$ and $g(15)$ from ANDERSON *et al.* [2], we get the numerical value of Δ:

$$\Delta = (1.000 \pm 0.006) \cdot 10^{-3}\,.$$

In the classical theory the hyperfine structure constant A and the quadrupole coupling constant B for the $^4S_{\frac{3}{2}}$ ground state of nitrogen vanish. The variational computation of DAS and MUKHERJEE [5] yields an A-value for ^{14}N of 7.3 MHz. Their paper indicates that the interaction occurs between the nucleus and the electron-function with s-wave character. Because of the spherical symmetry one does not expect to observe a quadrupole interaction.

The s-wave character of the electron wave function at the nucleus suggests that the hyperfine anomaly may be due to the finite nuclear volume. However, more complete data on the ^{15}N-nuclear charge distribution are required to determine whether or not nuclear size effects are a major contribution to the anomaly.

* * *

We are indebted to Dr. R. NOVICK for many suggestions and for help in the beginning stages of the present experiment. We thank Dr. T. P. DAS for communicating his results to us prior to publication; and we thank Dr. C. P. SLICHTER, Dr. D. G. RAVENHALL and Dr. H. FRAUENFELDER for several helpful discussions.

Note on the Photoparticles' Angular Distribution.

A. Molinari

Istituto di Fisica dell'Università - Torino

(ricevuto il 9 Novembre 1960)

The aim of the present note is to underline a remarkable difference between the nuclear reactions' and photo-reactions' angular distributions.

When many energy levels of a compound nuclear state are involved in the reaction so that the statistical assumptions can be considered valid, the phase relations between the matrix elements of the transitions to and from the compound states are, as is well known, randomly distributed, so that it becomes possible to disregard all the interference terms, which cannot give rise therefore to any anisotropy.

The anisotropy may still arise because of the general conservation theorems, in particular for the angular momentum conservation, and it can be calculated in a classical approximation with results in good agreement with those deduced using a more correct quantum mechanical approach [1].

For the nucleus-photon interaction the angular momentum conservation requires that the nucleus, after it has captured the incident photon, turns about the incidence direction. It follows that particles which are moving in the equatorial plane will have greater probability to evaporate overcoming the nuclear barrier than the others, giving rise to a maximum of the differential cross-section at 90° (or 270°), while in the other types of nuclear reactions the differential cross-sections present a maximum at 0° (or 180°).

In all cases, it must be noted, that the symmetry of the differential cross section about 90° is strictly preserved and it is not possible to explain with those arguments any forward-backward asymmetry.

Actual calculations shows nevertheless that, in the photonuclear case, the anisotropic term is too small, to be in agreement with experiments, differently from the case *e.g.* of (p, n), (α, n) ... reactions where these same calculations give a reasonable agreement with the experimental values.

In fact, in the limit of the classical approximation, the differential cross section for the emission of a particle of energy E_2 in the direction $\boldsymbol{n}$ from a compound

[1] T. Ericson and V. Strutinski: *Nucl. Phys.*, **8**, 284 (1958).

nucleus of total angular momentum I, formed by photon absorption, can be written

$$\sigma(\boldsymbol{n}, E_2) = \sigma_I \frac{1}{2\pi} \int \mathrm{d}\varphi \int \mathrm{d}^3 l \, \frac{\Gamma(l, \boldsymbol{n}, E_2)}{\Gamma_I} , \tag{1}$$

if the target nucleus and the outgoing particle are spinless. Here σ_I is the cross section for the formation of the compound nucleus, φ is the azimuthal angle and l is the orbital angular momentum of the outgoing particle.

Conveniently acting on (1) and assuming a definite dependence (which will affect appreciably the results) from the spin of the final states of the system, we reach the following expression for the angular distribution [2]:

$$W(\boldsymbol{n}, E_2) = \mathrm{const} \int_0^\infty l T_2(l) \, \frac{\exp\left[\alpha_i I^2 - \alpha_f (l^2 + I^2)\right]}{\Gamma_I} J_0(i\, 2\alpha_f I l \sin\vartheta) \, \mathrm{d}l , \tag{2}$$

where $T_2(l)$ is the transmission coefficient of the residual nucleus.

Let us now consider the particular case of electric dipole transitions — for instance the electromagnetic absorption in the region of the giant resonance — determined by photon absorption in a spinless nucleus (even mass number).

Here the total angular momentum of the compound nucleus will be $I = \pm 1$.

We find therefore (for instance in the case of $I = +1$)

$$W(\boldsymbol{n}, E_2) = \mathrm{const} \int l T_2(l) \, \frac{\exp\left[\alpha_i - \alpha_f (1 + l^2)\right]}{\Gamma_I} J_0(2i\alpha_f l \sin\vartheta) \, \mathrm{d}l = \tag{3}$$

$$= \mathrm{const} \int l T_2(l) \exp\left[-\alpha_f l^2\right] J_0(2i\alpha_f l \sin\vartheta) \, \mathrm{d}l .$$

Hence by applying the Bessel functions expansion, it is possible to deduce easily the angular distribution which will be given by the expression

$$A = 1 + \frac{\alpha_f^2 \sin^2\vartheta \int_0^\infty l^3 T_2(l) \exp\left[-\alpha_f l^2\right] \mathrm{d}l}{\int_0^\infty l T_2(l) \exp\left[-\alpha_f l^2\right] \mathrm{d}l} + \dots . \tag{4}$$

We may now assume a definite expression for the penetrability $T_2(l)$: in the « sharp cut-off approximation » $T_2(l)$ is one in the classically permitted region, zero outside, while a less crude value of $T_2(l)$ can be, for instance, the expression

$$T_2(l) = 1 - \frac{l(l+1)\hbar^2}{2MR^2} \frac{1}{E} .$$

[2] For the symbols and deductions of (2) see ref. [1]. V. Strutinski: *Congrès International de Physique Nucléaire* (Paris, 1958).

(obviously the calculation will be valid only for neutrons). With such a hypothesis we obtain respectively

$$A \simeq 1 + \alpha_f \sin^2 \vartheta \qquad \text{and} \qquad A \simeq 1 + 2\alpha_f \sin^2 \vartheta \,, \tag{5}$$

the constant α_f being given by

$$\alpha_f = \frac{\hbar^2}{2\mathscr{J}T} \,,$$

where $\mathscr{J}$ is the momentum of inertia of the nucleus considered as a rigid sphere and T is the nuclear temperature [3].

For a heavy nucleus ($A = 200$) and a nuclear temperature of the order of 1 MeV we obtain for the angular distribution

$$A \simeq 1 + \quad 10^{-2} \sin^2 \vartheta \,,$$

$$A \simeq 1 + 2 \cdot 10^{-2} \sin^2 \vartheta \,,$$

which is in agreement with the experiments if we limit ourselves to consider the low energy photoneutrons while, for the high energy photoparticles, the anisotropic term is quite too small to be in agreement with experiments.

* * *

I wish to thank Prof. R. Malvano for the suggestions and discussions concerning this work.

[3] See ref. [1]. It is interesting to observe that with this value of the constant we obtain an inferior limit for the anisotropy. A less crude picture of the nucleus will lead to a reduction of the momentum of inertia, increasing consequently the anisotropic term. See ref. [2].

The Excited Hyperon and Pion-Hyperon Resonances (*).

S. F. Tuan

Department of Physics, Brown University - Providence, R.I.

(ricevuto il 12 Novembre 1960)

Sometime back, it was suggested [1,3] that by examining the correlations between outgoing pions and hyperons in strange particle reactions like $K^- + p \to Y + \pi + \pi$, we can obtain information on possible pion-hyperon resonances even in the unphysical region relative to the K^--p threshold. Recently Good [4] reports from the study of momentum spectra for π^+ and π^- in the reaction $K^- + p \to \Lambda + \pi^+ + \pi^-$ at K^- lab. momentum 1.15 GeV/c, the existence of an excited hyperon Y* in the $I=1$ state, strongly produced, and of mass (1370 ± 25) MeV. Interpreted as a resonance in π-Λ scattering, Y* has Q value of about 115 MeV (corresponding to a relative momentum $P' \sim 190$ MeV/c for the decay particles of the strong decay $Y^* \to \pi + \Lambda$) and a full width at the bottom of the order of 100 MeV.

At the present moment, there is no compelling evidence for a strong contribution from the process $K + K^- \to \pi + \pi$ to our current understanding of the K^-p system [5,6] at least in an energy region of the order of the K^-p threshold. In addition, interpretation of the data presented at Kiev [7], that K^--p nuclear-Coulomb interference is constructive, is still open to question [6]. Since the « Good » resonance lies in the unphysical region at about (60 ± 25) MeV below the K^-p threshold, we would like to discuss qualitatively this resonance in terms of zero effective range theory [1-3]

(*) This work was supported by the U. S. Atomic Energy Commission.

(1) R. H. Dalitz and S. F. Tuan: *Ann. Phys.*, **8**, 100 (1959).

(2) R. H. Dalitz and S. F. Tuan: *Phys. Rev. Lett.*, **2**, 425 (1959).

(3) R. H. Dalitz and S. F. Tuan: *Ann. Phys.*, **10**, 307 (1960).

(4) M. Alston *et al.*: *Proc. of the Intern. Rochester Conference on High-Energy Physics* (1960, to be published). Also private communication from Prof. Good.

(5) While the effective range of an interaction like $(K\bar{K}) \to (\pi\pi) \to (p\bar{p})$ can in general be much larger than $1/2m_\pi$ (~ 0.7 fermi), corresponding to the exchange of an intermediate system of mass $2m_\pi$; the recent phenomenological analysis of Rodberg and Thaler [*Phys. Rev., Lett.*, **4**, 372 (1960)] on the effective range of K^+-p [which shares common features with the K^--p system on the matter of $(K\bar{K}\pi\pi)$ interaction] yields a range value of only 0.5 fermi. This is indicative that $(K\bar{K}\pi\pi)$ interaction may not be dominant in the energy range under consideration. For further details, see ref. (3).

(6) P. T. Matthews: *Proc. of the Intern. Conference on High-Energy Physics* (1960, to be published).

(7) L. W. Alvarez: *Proc. of the Intern. Kiev Conference on High-Energy Physics* (1959, to be published).

or the so called scattering length approximation.

JACKSON and WYLD (8) pointed out that an adequate explanation of the dip in ($\bar{K}\mathcal{N}$) elastic and charge exchange cross sections just *above* threshold can be understood in terms of « repulsive » (9) $K\mathcal{N}$ interaction. This then obviates the necessity of introducing a resonance (10) to explain the peak; such a resonance would in any case be very broad and lead to an unreasonably large effective range (2-5) ($\sim 7/m_K$). In terms of the scattering length approximation, JACKSON and WYLD's proposal corresponds to the Dalitz solutions (*a*-) and (*b*-). Subsequent analysis (1-3) on the basis of unitarity and analyticity of the scattering amplitude below K^--p threshold points strongly to the possibility of a ($\pi\Lambda$) and ($\pi\Sigma$) resonance in the $I=1$ state for solution (*a*-) (and a corresponding $I=0$ ($\pi\Sigma$) resonance, should (*b*-) be the appropriate solution). Such a π-Y scattering resonance (Y = Λ, Σ) arises primarily from the *important* K-interactions, being a consequence of the properties of *S*-wave K-$\mathcal{N}$ scattering; it is in the $S_{\frac{1}{2}}$ state for odd (KY) parity and $P_{\frac{1}{2}}$ state for even (KY) parity. The location of the resonance (2,3) is peaked around about (20 ÷ 30) MeV below the K^--p (c.m.) threshold energy, which is perhaps a little uncomfortable for easy identification with the experimental ($\pi\Lambda$) $I=1$ resonance (4), centered around (60 ± 25) MeV below $K\mathcal{N}$ threshold. However the position and width of the theoretically deduced resonance depend sensitively on the assumed value for pion-hyperon scattering phase shift at K^--p threshold, thus the possibility of a wider resonance in this region need not be excluded. We note in addition that low energy K^--p scattering data favor (*a*) type solutions ($I=1$ resonance) over (*b*) type solutions ($I=0$ resonance).

Since determination of K-parity [assuming (Λ, Σ) parity to be even] from double subtracted K-$\mathcal{N}$ dispersion relations depends only on the sign of the contribution to the scattering amplitude f from the unphysical region (for the favored pseudo-scalar case, Im $f > 0$ will suffice), positive resonances below K^--p threshold may actually lend greater effectiveness to the method. Results like: Im $f_I^{(J,l)}$ (I, l are the isospin and orbital momentum for the K^--p system) has the sign $(-1)^l$ throughout the unphysical range $M_\Lambda + m_\pi \leqslant E \leqslant M + m_K$, derived from the K-matrix formalism (3), can then be used to good advantage since f is a weighted sum of amplitudes $f_I^{(l,J)}$ for individual scattering states. However the correlation between « repulsion » (*a*-) and scalar K-parity is now very much weakened (11).

Attempts have been made recently to reconcile the excited hyperon Y* with pion-hyperon resonances proposed on theoretical grounds, in particular the global symmetry model of Gell-Mann (12) and the vector theory of strong interactions of SAKURAI (13). The probable large phase shift difference (3) ($\sim \pm 60°$) between the $I=1$ and $I=0$ $\pi\Sigma$ states at energies of the order of K^--p threshold, however suggests that global symmetry (requiring small phase shift difference)

(8) J. D. JACKSON and H. W. WYLD: *Phys. Rev. Lett.*, **2**, 355 (1959).

(9) We wish to emphasize again that « attraction » and « repulsion » in our terminology imply nothing further than that the real part of the forward scattering amplitude is positive (or negative), corresponding to constructive (or destructive) Coulomb-nuclear interference. The question whether a « repulsive » interaction is true repulsion or strong attraction can be decided only by higher energy behaviour. See in this connection, KARPLUS *et al.* [*Phys. Rev. Lett.*, **2**, 510 (1959)].

(10) P. T. MATTHEWS and A. SALAM: *Phys. Rev. Lett.*, **2**, 266 (1959).

(11) S. F. TUAN: EFINS-59-40 (1959), unpublished.

(12) M. GELL-MANN: *Phys. Rev.*, **106**, 1296 (1957).

(13) J. J. SAKURAI: *Ann. Phys.*, **11**, 1 (1960).

is inconsistent with the data in this region. We wish to emphasize that whereas it is physically sensible to compare the strong decay relative momentum P'_Y for the excited hyperon Y* with that of the 3-3 resonance in pion-nucleon scattering ($P_{33} \sim 230$ MeV/c), it is far from clear, in drawing an analogy with global symmetry (which ignores the Σ-Λ mass difference), whether comparison should be made between P_{33} and P'_Λ (~ 190 MeV/c) or with P'_Σ (~ 105 MeV/c) corresponding to $Y^* \to \pi + \Sigma$. For a mean mass value $(m_\Sigma + m_\Lambda)/2$, the associated decay momentum for Y* is 150 MeV/c — rather low for a convincing comparison with a global symmetry resonance, which should have a strong decay momentum comparable to P_{33}. A perhaps more plausible hypothesis would be to associate Gell-Mann's p-wave ($J = \frac{3}{2}$, $I = 1$) pion-hyperon resonance with a possible resonance indicated by the rapid variation in elastic angular distribution between 300 MeV/c and 400 MeV/c for the K^--p system; this corresponds to π-Σ c.m. momentum of between 200 and 270 MeV/c. The vector theory ([13]) on the other hand favors a strongly attractive $I = 0$ state for π-Σ S-wave scattering, with the distinct possibility of a resonant state at energies of the order of (K^-p) threshold ([14]). However the π-Σ phase shift for the $I = 1$ state (though attractive) is expected to be small; in addition we expect $K^- + p \to \Sigma + \pi$ to be much less frequent than $K^- + p \to \Sigma + n\pi$, with $n > 1$ in the GeV region. We must emphasize also that whereas the zero effective range resonance is a direct consequence of the strong K-baryon coupling on the pion-hyperon system, both global symmetry and the vector meson theory type resonances are derived on the assumption of a relatively weak influence of K-meson interactions on this system at least in the low energy region.

([14]) It is uncertain whether such a resonance is peaked above or below K^-p threshold.

There then remains the question of the role the (K K$\pi\pi$) interaction plays in low-energy K^--p scattering ([5]). From the prevailing viewpoint ([15]), the major effect of such an interaction would probably arise from an energy region corresponding to exchange of a pair of resonating pions between the K-meson and the nucleon. This implies that the major contributions arise in the K$\mathcal{N}$ channel for c.m. energy

$$E^* = \sqrt{(M^2 - \omega^2/4)} + \sqrt{(m_K^2 - \omega^2/4)}\,,$$

where ω denotes the c.m. energy of the π-π system at resonance ($\sim 4.7 m_\pi$). The energy E^* would then be about 190 MeV below the physical threshold, and its influence on low-energy scattering parameters woud be large only if the K K$\pi\pi$ coupling parameter were unreasonably large. We believe that the suggested enormous corrections ([16]) to the phenomenological determined zero range scattering lengths, contradict the basic premise of effective range theory. It is conceivable however that in a complete dynamical calculation, where $K\bar{K} \to$ resonating pions $\to \mathcal{N}\mathcal{N}$, π-Y scattering, and K-p scattering and absorption are interconnected by unitarity through the Mandelstam representation, the comprehensive contributions from Born approximation poles, intermediate two pion (and three pion) resonance effect due to the « double-cross » cut from K-$\bar{K}$, and pion-hyperon resonances (like the excited hyperon Y*) below $\bar{K}\mathcal{N}$ threshold, may offer surprising cancellations such as to leave unaltered the gross features of the current purely phenomenological scattering length approach ([17]). It is expected also that resonance phenomena like boson bound system $K^* \leftrightarrow K + \pi$,

([15]) J. Bowcock, W. N. Cottingham and D. Lurié: *Phys. Rev. Lett.*, **5**, 386 (1960).

([16]) F. Ferrari, G. Frye and M. Pusterla: *Phys. Rev. Rev.*, **4**, 615 (1960).

([17]) I would like to thank Dr. R. C. Hwa for an interesting discussion. A detailed study by Dr. Hwa is in progress.

interacting with K, may well dominate our thinking in explaining such anomalies as the persistent backward asymmetry in the angular distributions $\pi^- + p \to \Lambda^0 + K^0$.

In conclusion, we would like to point out a few experiments which would clarify considerably the current confused situation:

(*a*) Clear cut study to determine conclusively whether low energy K^--p nuclear-Coulomb interference is destructive or constructive.

(*b*) Aside from such obvious necessities as the determination of the spin of Y* ($\frac{1}{2}$ or $\frac{3}{2}$) from an angular distribution study ([18]), it will be very instructive to obtain information about a possible $I=1$, $\pi^{\pm}$-Σ^+ resonance, predicted by zero range theory at roughly the same energy as Y*. This can best be obtained from

$$K^- + p \to \pi^0 + \Sigma^+ + \pi^-,$$

though at 1.15 GeV/c the filtering out of

$$K^- + p \to \Sigma^{\pm} + \pi^{\mp},$$

$$K^- + p \to \Sigma^{\pm} + \pi^+ + \pi^0 + \pi^0,$$

may pose quite a problem (a lower energy run at $0 < p_K < 700$ MeV/c will probably give more clear cut information). On the other hand a run at energy higher than 1.15 GeV/c (once the separation difficulty is resolved) may yield useful information about a possible π-Σ resonance (c.m. momentum ~ 250 MeV/c) suggested by the K^--p angular distribution at 400 MeV/c.

(*c*) The study of (1) correlations between outgoing pions and hyperons in associated productions $\pi + p \to \pi + Y + K$, (2) distribution of π-Σ Q-values in K^--d capture reactions, and (3) inelastic Y-$\mathcal{N}$ scattering $Y + p \to Y + \pi + p$, should be prosecuted vigorously for independent evidence of pion-hyperon resonances (See reference [2]) for details).

* * *

It is a pleasure to thank Professor M. L. Good for a very instructive communication. Conversations with Professors P. T. Matthews and J. J. Sakurai have been most helpful.

([18]) Preliminary data suggest that $J = \frac{3}{2}$ is somewhat more likely (private communication from Prof. H. K. Tiho). In view of its importance to theoretical understanding, we would like to encourage a very accurate determination for this spin.

IL NUOVO CIMENTO Vol. XVIII, N. 6 16 Dicembre 1960

Relativistic Deuteron Wave Function - II.

M. Gourdin

Faculté des Sciences - Orsay
Faculté des Sciences - Bordeaux

J. Tran Thanh Van

Faculté des Sciences - Orsay

(*Nuovo Cimento*, **18**, 443 (1960))

On page 449, line 11, the formula instead of

$$E_0(p) = \frac{2}{(p^2+\gamma^2)\{(p^2+\gamma^2)^2+4p^2M^2\}^{\frac{1}{2}}},$$

should read

$$E_0(p) = \frac{2}{(p^2+\gamma^2)\{(p^2+\gamma^2)+[(p^2+\gamma^2)^2+4p^2M^2]^{\frac{1}{2}}\}}.$$

Some Properties of Single Loop Diagrams in Perturbation Theory.

M. Fowler, P. V. Landshoff and R. W. Lardner

St. John's College - Cambridge

(*Nuovo Cimento*, **17**, 956 (1960))

Figure 1(*b*) is wrongly orientated and should be rotated clockwise through 90°.

IL NUOVO CIMENTO Vol. XVIII, N. 6 16 Dicembre 1960

An Experiment on Nuclear Interactions of High Energy ((10 ÷ 100) GeV).

E. R. T. Awunor-Renner, L. Blaskovitch, B. R. French, C. Ghesquière, I. B. de Minville-Devaux, W. W. Neale, C. Pelletier, P. Rivet, A. B. Sahiar and I. O. Skillicorn

Imperial College - London
Ecole Polytechnique - Paris

(*Nuovo Cimento*, **17**, 134 (1960))

In Fig. 15 (page 153) instead of $I > I_0$, and $I = I_0$ read

$$I > 2\,I_0 \quad \text{and} \quad I < 2\,I_0\,.$$

Appendix II. Page 164, third line from the bottom, the equation should read

$$1.5 \sum (U - p_l) + (U - p_l) \text{ degraded primary} = M_N - (U - p_l) \text{ recoil.}$$

In paragraph 4·9 we should have mentioned that the introduction of the quantity $\sum (U - p_l)$ is due to S. N. Vernov and that the considerations we make had already been made by our Soviet Colleagues (see, for instance, N. G. Birger and Yu. A. Smorodin: *Žurn. Éksper. Teoret. Fiz.*, **36** (9), 823 (1959)). We would like to apologize to them for not having referred to their very valuable work in our paper.

LIBRI RICEVUTI E RECENSIONI

P. R. Aigrain, R. J. Coelho e G. Accarelli – *Electronic Processes in Solids*. The Technology Press and J. Wiley Inc., New York, 1960, pp. 67, prezzo $ 4.

Si tratta di un libretto che riassume le lezioni di Aigrain al M.I.T. a cura dei due giovani collaboratori. La parte più interessante è la trattazione relativa ai fenomeni di trasporto, esposta in modo elegante e nuovo, e che include i risultati più recenti sugli elettroni veloci nei semiconduttori. Questa parte è preceduta da un certo numero di capitoletti sulla teoria elettronica dei solidi, che ci sembrano troppo concentrati e laconici per essere utili ad uno studente e che forse possono servire come richiamo ai fisici più adulti. Ad esempio, la meccanica statistica degli elettroni nei solidi è esposta solo in una pagina e mezza. La bibliografia è pure assai scarsa.

G. Careri

T. L. Hill – *Introduction to Statistical Thermodynamics*. Addison-Wesley Inc., London, 1960, pagine 508, prezzo $ 9.75.

Si tratta di un libro di testo per studenti di chimica e fisica al livello del nostro quarto anno. La scelta degli argomenti è molto ampia, specialmente per i sistemi di molecole in interazione, e veramente aggiornata agli ultimi sviluppi. Così viene bene presentata la funzione di distribuzione nei fluidi classici e la teoria delle soluzioni di polimeri e dei geli, mentre è troppo concisa la presentazione delle statistiche quantistiche e dei fondamenti della meccanica statistica. Perciò il libro ci sembra certo pregevole, ma destinato più ai chimici che ai fisici.

G. Careri

Progress in Cryogenics, a cura di K. Mendelssohn. Ed. Heywood & Co. Ltd., London.
I vol.: pp. VIII-259; prezzo 63 s.
II vol.: pp. VIII-280; prezzo 63 s.

Anche la tecnica delle basse temperature hanno i loro «Progress»: questa serie, curata da K. Mendelssohn, è dedicata ai metodi sperimentali ed alle tecniche, ma investe, almeno marginalmente, dato il suo ampio respiro, anche molti problemi scientifici.

Le rassegne presentate in questi primi due volumi sono opera di ricercatori specializzati, per la maggior parte inglesi e americani, ma anche di altre nazioni, in particolare Russia e Olanda, dove si trovano laboratori assai progrediti nel campo delle basse temperature. Gli argomenti trattati spaziano dalle questioni tecniche di interesse generale ai metodi studiati per la soluzione di particolarissimi problemi sperimentali e danno modo al lettore di farsi un'idea di alcuni nuovi campi che si stanno aprendo alla ricerca scientifica ed alla pratica applicazione.

La costruzione dei recipienti termicamente isolati, per il trasporto di gas liquefatti, sta subendo, ad esempio, una piccola rivoluzione, dato che qualcosa di nuovo si sta affiancando al classico vaso di Dewar; si tratta dell'impiego di pol-

veri (o fibre) nel vuoto e di schermi intermedi per arrestare la radiazione, che è una importante fonte di perdite nel vaso Dewar. Si veda a questo proposito il lavoro di M. M. Fulk nel primo volume e l'articolo di G. H. Zenner nel secondo, dove si tratta in generale di apparecchiature per conservare e trasferire gas liquefatti.

Tra le tecniche speciali si parla di raffreddamento termoelettrico che già trova qualche applicazione ma che più promette per il futuro con lo sviluppo di nuovi materiali (D. A. Wright) e delle macchine per refrigerazione a gas (J. W. L. Köhler). Tra i metodi impiegati per ricerche particolari sono descritti quelli per la misura di grandezze meccaniche a bassa temperatura (H. M. Rosenberg), e quelli per lo studio della attenuazione delle onde ultrasonore dovuta a interazioni elettroniche nei metalli (R. W. Morse); su questo problema è anche data una interessante discussione generale. Altri importanti aspetti dell'applicazione delle basse temperature nella ricerca scientifica sono il « congelamento » di radicali liberi (G. J. Minkoff), la camera a bolle a idrogeno liquido (N. C. Barford), ed i metodi di orientazione nucleare (E. Ambler).

Termometria e calorimetria sono, naturalmente, argomenti importanti, per i particolarissimi problemi che presentano quando ci si avvicina allo zero assoluto. Si tratta qui della determinazione delle scale di temperatura, ed in particolare di quella raccomandata per uso internazionale nel 1958 (H. Van Dijk), della costruzione di termometri a resistenza (C. R. Barber), di misure calorimetriche a bassa temperatura (R. W. Hill) e della determinazione di calori specifici col metodo delle onde termiche (N. V. Zavaritsky).

Alcune tra le più interessanti applicazioni derivano poi certamente dallo sviluppo dei processi di distillazione (B. R. Brown) che permettono, tra l'altro, la separazione del deuterio su scala industriale (M. P. Malkov *et al.*), e dai nuovi sviluppi nella tecnica dei circuiti ad elementi superconduttori (D. R. Young) e dall'impiego in elettronica della risonanza in sistemi microfisici (E. O. Schulz-Du Bois).

È dunque chiaro che gli argomenti trattati sono assai vari e di grande interesse ed è altrettanto evidente che rimangono molte importanti zone da esplorare, che forniranno materia, probabilmente, per le prossime rassegne di questa serie.

F. A. Levi

Les Traceurs Radiactifs en Métallurgie Physique di C. Leymonie et P. Locombe. Dunod, Paris, 1960.

Questo libro di C. Leymonie è una rassegna abbastanza completa delle applicazioni che la tecnica dei traccianti radiattivi ha trovato nella fisica dello stato solido ed in metallurgia. Dopo un'esposizione assai elementare dei fondamenti della radioattività e dei metodi di rivelazione delle radiazioni si passa alla trattazione dei vari problemi che possono essere studiati proficuamente mediante l'uso dei radioisotopi.

Gran parte del libro è dedicata alla « diffusione » che infatti ha beneficiato in maniera pressochè fondamentale dell'uso dei traccianti. Gli altri capitoli sono dedicati alla segregazione, alle reazioni superficiali e agli equilibri vapore-fase condensata.

È indubbio che tutti gli argomenti trattati sono di viva attualità e che avere riunita ed ordinata in un volume una ricca bibliografia rappresenta di per sè un titolo di merito per l'autore. Ci si permette tuttavia di notare che il libro manifesta degli squilibri nel senso che si è voluto fare il punto della situazione (o almeno se ne ha l'impressione) limitandosi in genere ad un'elencazione

dei risultati pubblicati, alcuni dei quali in notevole contrasto fra di loro, senza sottoporli ad un'analisi critica sia pure dal solo punto di vista dell'accuratezza delle misure se non della ragionevolezza delle deduzioni.

Tuttavia il libro resta un'opera in complesso utile soprattutto come opera di prima consultazione per coloro che intendono iniziare l'uso di traccianti radioattivi nelle proprie esperienze.

A. Paoletti

R. H. Bube – *Photoconductivity of Solids*. J. Wiley & Sons, New York, 1960, pp. xv-461.

Questo libro, ad opera di un autorevole esponente scientifico dei Laboratori RCA, è la prima monografia sistematica sulla vasta gamma di fenomeni pertinenti alla fotoconducibilità dei solidi cristallini. Si può subito aggiungere che, per l'ampiezza della rassegna e per la sicurezza critica, esso sarà di utilissima lettura non solo agli specialisti del campo, ma a tutti coloro che sono interessati, in generale, allo studio delle caratteristiche di materiali isolanti o semiconduttori.

Il libro tratta soprattutto gli aspetti specifici della fotoconducibilità nei solidi; tuttavia non manca di analizzare tutti quei fenomeni che sono collegati con la creazione, il trasporto, e la ricombinazione di « carriers » liberi entro la struttura a bande di un solido non-metallico. In questo senso il libro è particolarmente pregevole, poichè pone in rilievo, con una vasta documentazione, gli aspetti complementari di alcune importanti proprietà (assorbimento ottico, fotoconducibilità, luminescenza).

Il libro ha carattere composito, dovendo riunire la trattazione dei fondamenti fisici, l'interpretazione modellistica, e la rassegna del ricchissimo materiale teorico e sperimentale. Inoltre, per esigenze di compattezza, la trattazione evita le questioni teoriche più generali. Tuttavia l'autorità del Bube (il quale è un noto specialista dei problemi in esame) ha modo di rivelarsi pienamente nell'eccellente sintesi critica e nella chiarezza di esposizione.

Una prima parte del libro è dedicata alle generalità chimico-fisiche sui materiali fotoconduttori e all'interpretazione fenomenologica. Viene poi sviluppata l'analisi modellistica, che si ricollega a pochi elementi di teoria delle bande, e alla nozione di livelli singolari come centri di cattura o di ricombinazione per elettroni e « buche ». Introdotti alcuni parametri convenienti, la fotoconducibilità viene trattata secondo un ben noto modello statistico, in termini dei livelli di Fermi generalizzati e delle condizioni di equilibrio microscopico. Tale descrizione viene usata per definire le caratteristiche di risposta di un generico fotoconduttore (efficienza, sensibilità, dipendenza dalla temperatura e dalla intensità di eccitazione, cinetica di decadimento, ecc.). L'analisi è completata dalla discussione di numerosi problemi particolari, specialmente importanti per ragioni tecniche o di principio. Un intero capitolo è poi dedicato ai contatti metallo-semiconduttore e ai problemi di polarizzazione. Il quadro informativo si chiude con una rassegna delle tecniche di preparazione dei materiali.

La seconda parte del libro è rivolta agli aspetti più propriamente fisici. Un capitolo è dedicato al ruolo delle impurezze e delle imperfezioni reticolari nella fotoconduzione « estrinseca ». In esso vengono ampiamente descritti gli effetti di centri singolari di vario tipo sulle caratteristiche elettriche ed ottiche. Speciale attenzione è rivolta alla funzione di impurezze donatrici o accettatrici, in rapporto con le loro proprietà atomiche; sono pure trattati gli effetti di attivazione compensata, l'azione di impurezze di ossigeno, il ruolo dei difetti puntiformi, ecc.

Un altro capitolo riguarda i problemi connessi con la fotoconducibilità « intrinseca ». Vengono discussi la struttura a bande di isolanti e semiconduttori, i varii tipi di transizioni elettroniche, i processi di assorbimento della radiazione. Le transizioni dirette e indirette fra bande di valenza e banda di conduzione sono trattate con un certo dettaglio, allo scopo di precisare il concetto di « banda proibita ». Sono pure descritti gli altri meccanismi di eccitazione (transizioni fra bande di valenza, assorbimento proprio di carriers liberi, accoppiamento con modi vibrazionali, formazione di eccitoni) che hanno una certa importanza nel quadro generale.

In successivi capitoli si espongono le conoscenze attuali sui meccanismi di scattering di elettroni e buche da parte di vibrazioni reticolari, impurezze cariche, e imperfezioni. Inoltre viene discussa la natura dei centri di cattura e di ricombinazione, con un'analisi dettagliata della complessa fenomenologia cui essi danno luogo. Alla fine, viene fatta una rassegna delle teorie modellistiche più complete, e si riprende l'analisi formale — ad illustrazione di altri importanti fenomeni, quali il quenching ottico e termico della fotoconducibilità e della luminescenza, la risposta non lineare di certi materiali, ecc.

Alcune sezioni aggiuntive descrivono le principali applicazioni dei fotoconduttori, e trattano in sintesi numerosi fenomeni collegati con la fotoconducibilità, con speciale riguardo per gli effetti fotovoltaici.

La documentazione fornita dal libro è molto ricca. La bibliografia comprende più di mille voci, ed è aggiornata in parte al 1959. L'esemplificazione sui vari tipi di materiali è continua e sistematica essa copre (oltre ai semiconduttori elementari) tutti i composti inorganici — polari o covalenti — di un certo interesse. Infine il libro è corredato di abbondanti illustrazioni.

P. Camagni

R. Dugas – *La théorie physique au sens de Boltzmann et ses prolongements modernes*. Préface de L. de Broglie. Éditions du Griffon, Neuchâtel (Suisse), pp. 308.

Il Dugas (uno storico francese della scienza scomparso nel 1957) ha cercato di ricostruire in questo libro l'evoluzione del pensiero di Ludovico Boltzmann, sia per quanto riguarda questioni di fisica che questioni più propriamente epistemologiche.

Particolarmente interessante è la parte seconda dell'opera, nella quale viene narrata la storia del teorema *H* e delle polemiche, talvolta violente, che Boltzmann dovette sostenere con diversi oppositori (Loschmidt, Zermelo, Burbury, Culverwell, ...). La storia di questi contrasti rivela quello che vorrei chiamare « l'esprit de finesse » di Boltzmann, il quale riusciva a superare obbiezioni come l'« Umkehreinwand » e il « Wiederkehreinwand » che parevano dover scuotere fin dalle fondamenta l'edificio della meccanica statistica.

Nell'articolo della *Encyklopädie* sui fondamenti della meccanica statistica Paul e Tatjana Ehrenfest hanno esposto in maniera ineguagliabile, ma sintetica, l'evoluzione della concezione boltzmanniana. Invece il presente libro ci mostra dettagliatamente come questa concezione si sia a poco a poco sviluppata attraverso un processo continuo di interazione col pensiero degli oppositori e come alla fine Boltzmann sia riuscito ad incorporare in una sintesi superiore quel che c'era di valido nelle loro critiche.

Assai poco persuasivo riesce invece l'Autore quando asserisce che il contrasto tra l'atomista Boltzmann e la scuola degli energetisti trova la sua esatta controparte ai nostri giorni nel contrasto tra la scuola di Copenaghen e i realisti alla de Broglie-Bohm. È troppo facile obbiettare al Dugas che vi è una differenza essenziale tra la posizione di Boltz-

mann e quella degli avversari della scuola di Copenaghen: BOLTZMANN combatteva gli energetisti *da fisico*, costruendo la teoria cinetica dei gas e la meccanica statistica, mentre i realisti suddetti non sono finora andati al di là di un complesso di osservazioni aventi un interesse essenzialmente epistemologico. Mi sembra pertanto che sarebbe meglio evitare certi paralleli storici, i quali denotano oltretutto uno scarso senso delle proporzioni. Questi appunti non vogliono tuttavia togliere valore al libro che, come si è accennato, è sotto vari aspetti veramente notevole e ricco di notizie interessanti sull'opera e sulla vita di Ludovico Boltzmann. Ricorderò qui, per terminare, la predilezione del grande scienziato per Beethoven e per Schiller e la massima che egli pose all'inizio delle sue lezioni sui principi della meccanica: « Bring' vor, was wahr ist - Schreib' so, dass es klar ist - Und verficht's bis es mit dir gar ist! ».

A. LOINGER

Vistas in Astronomy, vol. III. Edited by A. BEER. Pergamon Press, Oxford, 1960, pp. 345, con numerose figure nel testo e fuori testo.

Arthur BEER, astronomo dell'Osservatorio di Cambridge, dopo l'ottimo successo dei primi due volumi di *Vistas in Astronomy* ha curato ora l'edizione di un terzo volume, concepito sulla stessa linea dei primi due e come quelli inteso a dare una visione d'insieme degli ultimi progressi in campo astronomico.

L'opera ha i medesimi pregi e difetti dei precedenti due volumi. I difetti si riducono in sostanza alla frammentarietà, dovuta al gran numero degli autori che vi hanno collaborato; cosicchè più che un'esposizione armonica ed equilibrata di certi argomenti si ritrova, anche in questo terzo volume, un insieme di note diverse, legate tra loro soltanto da un tenue filo. Per contro, tutte queste note che avrebbero potuto figurare benissimo nelle riviste specializzate, presentano questioni di notevolissimo interesse, e segnaliamo per i fisici quelle sulla relatività (determinazione della deflessione della luce in campo gravitazionale; paradosso dell'orologio), sull'osservazione di satelliti artificiali, e le varie comunicazioni che trattano la formazione delle stelle in campi magnetici, la loro evoluzione ed il loro stato fisico.

L'edizione, come le precedenti, è eccellente, su carta patinata e ricca di illustrazioni.

L. ROSINO

LEVINGER – *Nuclear Photodisintegration*. Oxford University Press, 1960.

Nell'esteso dominio della fisica nucleare l'argomento delle fotoreazioni occupa un posto a sé stante, sia per il tipo particolare di interazione che interviene nel problema, sia per le tecniche sperimentali usate in questo campo, che risulta ancora uno dei più attivi per gli interrogativi sia teorici che sperimentali che restano insoddisfatti pur dopo molti anni di ricerche e di discussioni.

Il presente volumetto di LEVINGER cerca di trattare il complesso argomento, ancora in pieno stadio di sviluppo, ponendo tuttavia l'accento più sull'aspetto teorico che su quello sperimentale del problema.

L'autore, le cui importanti ricerche sul fotoeffetto nucleare iniziarono nel 1949, si occupa anzitutto della interazione delle particelle cariche (del nucleo) con la radiazione seguendo lo schema ben noto di considerare il nucleo come sistema quantistico mentre il campo di radiazione è trattato classicamente.

Esamina così separatamente le transizioni di tipo E_1, E_2 e M_1 con relative regole di selezione.

Successivamente passa ad applicare la teoria svolta al caso più semplice, il deutone.

L'abbondanza di risultati teorici e sperimentali, fino ai più recenti presi in esame in questo capitolo può costituire un utile mezzo di aggiornamento su quello che costituisce uno dei problemi fondamentali della fisica nucleare, per coloro che non si occupano specificamente del problema.

Ma dove il libro presenta il suo aspetto più interessante è nel capitolo sulle regole della somma: i risultati forniti dalla teoria classica, dalla teoria quantistica con i vari operatori di scambio, dalla teoria dispersiva per il calcolo della sezione d'urto integrata e dei vari « momenti » vengono esposti con cura e l'intero capitolo permette di farsi una visione abbastanza chiara delle informazioni che le regole della somma ci possono dare e dei loro limiti. Appare infatti chiaro, dalla trattazione del Levinger, che pur essendo le regole della somma utilissime in quanto possono fornire non solo le principali proprietà della sezione d'urto del fotoeffetto, ma aiutare a capire fin dove un risultato derivato da un particolare modello è peculiare di quel modello, tuttavia in esse è contenuta una certa arbitrarietà dovuta in definitiva al fatto che non si conosce adeguatamente la funzione d'onda dello stato fondamentale del nucleo.

La seconda parte del libro è dedicata alla modellistica fotonucleare: viene dedotto quanto i vari modelli possono dire sulla sezione d'urto totale di assorbimento, sui prodotti delle fotoreazioni nucleari. I modelli vengono sistemati nei « range » di energia in cui hanno meglio dimostrata la loro validità: modello collettivo e modello a shell (Wilkinson) per le basse energie (regione della risonanza gigante essenzialmente), e modello a quasi-deutone per gli effetti ad alte energie.

Giustamente l'autore fa rilevare che ciò che manca è un modello capace di spiegare contemporaneamente ciò che succede alle basse ed alle alte energie.

Come considerazione generale si può affermare che si sarebbe desiderata in qualche caso una minore brevità nella esposizione dei metodi di calcolo utilizzati nei vari modelli. Inoltre il lettore ha qua e là l'impressione che venga affastellata una grande copia di dati sui quali è detto troppo poco per potersi fare un'idea un po' precisa del problema.

La ricca bibliografia di cui è corredato il volumetto, riesce però in parte ad ovviare a questo inconveniente.

Oltre a costituire una prima ed utilissima messa a punto di ciò che si sa oggi sulle fotoreazioni nucleari, il libro del Levinger, che spesso si preoccupa di richiamare l'attenzione su quelli che sono i problemi ancora aperti in tale campo di ricerche, può costituire un'utile base di partenza per ulteriori sviluppi.

R. Malvano

J. M. Ziman – *Electrons and Phonons*, Oxford University Press, 1960, pp. 554, prezzo 84 scellini.

Il volume è un trattato sulla teoria dei fenomeni di trasporto nei solidi, destinato ai ricercatori ed agli specialisti ed anche agli studenti più avanzati. È un libro di teoria, che desidera gettare le basi e costruire tutti i fatti più importanti di questa parte della fisica, ed in questo senso è un libro riuscito. Non è un libro di facile consultazione, nel senso che per capirlo bisogna mettersi nel punto di vista dell'autore, cioè bisogna conoscerlo dal principio.

La bibliografia è molto estesa, ma ci sembra che alcuni importanti argomenti dei semiconduttori (quale ad esempio il comportamento degli elettroni « caldi ») non siano sviluppati. Le que-

stioni fondamentali sono invece trattate a fondo, e spesso in modo fresco ed efficace.

G. Careri

F. G. Tricomi: *Integral equations* Interscience Publishers Inc., New York e London, 1957, VIII + 238 pp. , $ 7.00.

Nella prefazione a questa sua più recente opera, l'Autore così si esprime: « le equazioni integrali furono uno dei primissimi soggetti matematici ad attrarre la mia attenzione, eppure questo libro appare dopo tutta una serie di altri. Come mai? La ragione è, che lo scrivere un libro sulle equazioni integrali costituisce un compito al cui svolgimento sono necessari molti anni di meditazione.

Infatti una tale opera deve soddisfare a due requisiti, che non è facile conciliare. Deve presentare i risultati essenziali della teoria con adatta generalità, sul metro del moderno rigore matematico, e ciò per facilitare la ricerca pura nello studio dei teoremi di esistenza. D'altra parte, non deve essere scritto in modo così astratto da allontanare il fisico, l'ingegnere ed il tecnico, che certamente hanno bisogno di questo strumento matematico, e lo meritano ».

Che l'Autore sia mirabilmente riuscito nel suo intento, apparirà senz'altro evidente a chiunque avrà dedicato uno studio, attento ma non faticoso, a questa utilissima opera.

Il primo capitolo è dedicato alle equazioni integrali di Volterra, lineari (§ 1.1-1.12) e non lineari (§ 1.13). Quelle lineari sono considerate per nuclei di classe L_2 (di quadrato integrabile secondo Lebesgue), e le non lineari, della forma

$$\varphi(x) = f(x) + \int_0^x F[x, y, \varphi(y)]\,dy$$

sotto certe ipotesi meno restrittive di quelle che vengono poste di consueto.

Riveste particolare interesse la descrizione di un procedimento, che risale a Fubini, e di cui l'Autore ha mostrato in numerose occasioni la grande importanza, mediante il quale si ottengono sviluppi asintotici delle funzioni di Bessel, per elevati valori dell'argomento, e si tratta altresì il caso più complicato della valutazione asintotica di funzioni di Bessel con ordine ed argomento uguali. Non si può fare a meno di trovare « affascinanti » (vedi nota a pag. 38) le espressioni asintotiche per il minimo zero di $J_\nu(x)$ e $N_\nu(x)$.

Nella bibliografia sulle equazioni non lineari, avremmo visto con piacere una indicazione della lucida nota di Tonelli pubblicata su *Mem. Acc. Bologna*, (8), **5**, 17-22 (1928).

Il secondo capitolo tratta le equazioni di Fredholm. Viene tra l'altro esteso il teorema fondamentale di tale Autore al caso di nuclei di classe L_2, facendo uso di un metodo di Schmidt, ritrovato e generalizzato da Picone (vedi *Appunti di Analisi Superiore*, Napoli, 1940, p. 582 e seguenti). Un paragrafo (2.6) è dedicato ad un rapidissimo cenno a metodi numerici, fra i quali uno di Lanczos (vi è una svista nello scriverne il nome a p. 76 e 236). Chiude il capitolo una trattazione del problema di Dirichlet mediante il metodo di Fredholm.

Il terzo capitolo, dal titolo « nuclei simmetrici e sistemi ortogonali di funzioni » ha inizio con una concisa esposizione di classici risultati sull'approssimazione in media, e sulla chiusura e completezza di certi sistemi di funzioni. Come applicazione al calcolo numerico, si descrive un procedimento di Enskog (1926) per la risoluzione numerica delle equazioni integrali lineari di Fredholm di 2ª specie. Seguono teoremi generali sullo spettro di un nucleo simmetrico, proprietà estremali e delimitazioni per gli autovalori. Si accenna al metodo di Ritz per il loro calcolo con un esempio.

Viene ampiamente sviluppato lo studio, dal punto di vista sia teorico che numerico, delle velocità critiche di un albero in rotazione e delle oscillazioni trasversali di una trave (cfr. TRICOMI: *Ricerche di Ingegneria*, Roma, **4**, 47-53, 1936). Completa il capitolo lo studio delle equazioni di Fredholm di prima specie, a nucleo simmetrico o simmetrizzabile, dei sistemi di tali equazioni e delle vibrazioni di una membrana.

Equazioni integrali singolari ed alcuni tipi di equazioni integrali non lineari costituiscono l'argomento del quarto capitolo, l'ultimo del libro. L'autore elenca i principali fenomeni che si presentano, quali la presenza di spettri continui, di autovalori con una infinità di corrispondenti autosoluzioni, di punti di biforcazione. La trasformazione finita di Hilbert è studiata in dettaglio, in vista delle sue applicazioni a problemi di aerodinamica, sulla base di recenti lavori dell'Autore (1951), e così l'equazione di Carleman (*Ark. f. Mat. Astr. Fys.*, **16**, 1922), cui è dedicata una nota dell'Autore del 1955 (*Ann. di Mat.*, (4), **39**, 1955). Infine il problema delle oscillazioni forzate, di ampiezza finita, di un pendolo, dà lo spunto a una trattazione completa e concisa delle equazioni di Hammerstein.

Completano il volume due appendici ed una raccolta di 32 esercizi. Nella prima appendice si richiamano alcuni risultati elementari sui sistemi di equazioni lineari algebriche, e nell'altra è riportata una dimostrazione del teorema di Hadamard sui determinanti. Gli esercizi, tutti di notevole interesse, sono di varia difficoltà; alcuni elementari, altri oggetto di vere e proprie ricerche.

E. APARO

W. C. SANGREN – *Digital computers and nuclear reactor calculations*. pp. XI+208, J. Wiley and Sons, Inc. (1960), $ 8,50.

Finalmente un libro che in maniera chiara e brillante riesca a spiegare come dalle equazioni che descrivono un problema fisico si arrivi alla formulazione adatta per i calcolatori elettronici. Giustamente l'autore ha preferito, alla discussione di problemi a carattere generale, affrontare direttamente l'equazione di criticità, l'equazione della teoria dell'età, le equazioni del trasporto e quelle della cinetica del reattore e mostrare come il problema si evolve e si modifica per acquistare quella forma che consenta una immediata traduzione nel linguaggio delle macchine calcolatrici.

Di particolare interesse, anche per altri campi di ricerca, è il capitolo sulla soluzione delle equazioni del trasporto col metodo di Montecarlo. I calcoli nucleari sono esposti in quattro capitoli che formano la seconda metà del libro. I primi quattro capitoli sono un'introduzione ai calcolatori digitali, ai metodi di programmazione ed all'analisi numerica.

Certamente questo libro sarà apprezzato da tutti coloro che usano i calcolatori elettronici come mezzo per la ricerca scientifica.

E. CLEMENTEL